MECHANISMS OF MULTIPLE INFRARED PHOTON ABSORPTION AND DISSOCIATION

by

CHRISTOPHER REISER

B.A., Lawrence University
(1976)

SUBMITTED IN PARTIAL FULFILLMENT
OF THE REQUIREMENTS FOR THE
DEGREE OF

DOCTOR OF PHILOSOPHY

at the

MASSACHUSETTS INSTITUTE OF TECHNOLOGY

June 1980

Signature of Author Signature redacted
Department of Chemistry
May 23, 1980

Certified by Signature redacted
Jeffrey I. Steinfeld
Thesis Supervisor

Accepted by Signature redacted
Glenn A. Berchtold
Chairman, Departmental Graduate Committee

This doctoral thesis has been examined by a Committee of the Department of Chemistry as follows:

Professor F. Read McFeely Signature redacted
Chairman

Professor Jeffrey I. Steinfeld Signature redacted
Thesis Supervisor

Professor James L. Kinsey Signature redacted

MECHANISMS OF MULTIPLE INFRARED PHOTON ABSORPTION AND DISSOCIATION

by

Christopher Reiser

Submitted to the Department of Chemistry
on May 23, 1980 in partial fulfillment of the
requirements for the Degree of Doctor of Philosophy

ABSTRACT

The infrared laser induced multiple photon reactions of olefins of the type $R_2C{=}CHCl$ have been investigated. In all cases, the dominant mode of reaction is elimination of HCl, although free rotation around the double bond may precede elimination. Clear evidence for the formation of the vinylidene carbene $F_2C{=}C{:}$ from $F_2C{=}CHCl$ was shown although the case for the corresponding dimethyl species $(CH_3)_2C{=}C{:}$ is not as convincing. The experimental results for the vinyl chloride system can be represented with a kinetic model with rates calculated from RRKM theory, which assumes an unhindered flow of energy amongst the vibrational modes prior to reaction.

Spectroscopic studies of species undergoing multiple infrared photon absorption was begun with infrared laser double resonance spectroscopy in the ν_3 band of SF_6, using a CO_2 laser pump and a tunable diode laser probe. Effects of saturation and dynamic Stark shifting are clearly seen in 2-level and folded 3-level spectra. No mixings via the molecular vibration-rotation Hamiltonian sufficiently strong to influence the spectra were found. K-changing collisions were invoked to explain the apparent disparity between the observed spectra and the spectra predicted from lineshape theories derived from 2-level and 3-level Bloch equations. From the decay of the double resonance signals, we measured relaxation times $P\tau = 24 \pm 3$ nsec·Torr for 2-level signals and $P\tau = 43 \pm 11$ nsec·Torr for 3-level signals.

Thesis Supervisor: Dr. Jeffrey I. Steinfeld

Title: Professor of Chemistry

To my family and to Libby

PREFACE

Since most of this work has been word-processed on a MINC computer, some stylistic conventions have been adopted to accomodate the LA34 DECWRITER IV printer. This device is not capable of typing subscripts, superscripts or Greek symbols; where appropriate, these symbols have been inserted after the printing of the manuscript by the computer. References have been denoted in the text not as superscripts but as a number enclosed in square brackets, e. g. [X.Y], where X is the Chapter (or Appendix) identifier and Y indexes references within each chapter. In all other matters, the guidlines outlined in the MIT Archives booklet, "Specifications for Thesis Preparation" (1979) have been observed.

ACKNOWLEDGMENTS

Many members of the Basement Executive Council deserve my thanks for lasting friendship and tutoring. B. D. Green first taught me to align a laser; Fran Lussier introduced me to the joys of DeKhotinskii cement. Craig Jensen deserves special mention as a fast friend who provided stimulation in many areas of chemistry; he remains the only man in my memory whose callouses cannot be shown in public. Long nights were spent slaving over DILDOR with Tom Anderson, who renewed my interest in drinking after the departure of C. Jensen. Other Council members must be acknowledged for stimulating discussions, including Tom Quelly (the skies are safe), Jim Long (still finding a tube with no hole), Mark "Maypo" Spencer, Bobbi Roop and Dave Harradine. Joe Francisco merits honorable mention as the most difficult case I have yet encountered in a Chinaman.

Other basement rats should also be noted; Ed Murphy, for one, always provided timely excuses for adjourning to the Muddy. I am indebted to Mike McClellan, Rick Gottscho and my ex-roomies Lou Nucci, Gary Hattery, Steve "Gobble" Koch and Jeff de Roulet for muchly appreciated comaraderie. My best wishes go to Graham Arnold.

Of the faculty, my advisor Jeff Steinfeld deserves my deep gratitude for his generous support and continuously challenging banter. While it is not true that we have stolen his key to the lab, we have found that independent thinking is of paramount importance in practical situations. Bob Field the Boy Wonder came to my aid many times, and I hope he never forecloses on the FF100 I may still owe him. F. "Bombay

Slums" Read McFeely, Purveyor of Pandemonium and Keeper of the Screw, deserves anything he gets. Bob Silbey, on the other hand, has escaped capital punishment only by disguising himself as a theoretical professor; in reality he is the great-great-great grandfather of the Klingon race.

Special thanks go to Vera Spanos for shelter from the madness, to Raphie Levine for a very pleasant ascent of Pike's Peak, and to Libby Huggins for keeping me sane.

I am indebted to Will Gilbert of Prof. Petsko's group for taking the time to print the final version of this work on the line printer of their PDP 11/60 computer system.

TABLE OF CONTENTS

Title Page 1

Abstract 2

Acknowledgements 6

Chapter 1. Background 12

Chapter 2. Laser Induced Chemistry: Results

2.1 Introduction 22

2.2 Kinetic model for CH_2CDCl 23

2.3 LID of other halogenated olefins . . 31

Chapter 3. Laser Induced Chemistry: Discussion

3.1 Chemical mechanisms 38

3.2 Kinetic effects 40

3.3 Energy disposal in fragments . . 46

Chapter 4. Gaussian Beam Deconvolution

4.1 Basic method 54

4.2 Experimental difficulties 57

Chapter 5. Diode-Infrared Laser DOuble Resonance

5.1 Introduction 61

5.2 Experimental details 63

5.3 Additional discussion 68

5.4 DILDOR in NH_3 73

5.5 Improvements for future experiments . . 80

Chapter 6. Analysis of SF_6 Double Resonance Spectra

6.1 Introduction 83

6.2 Lineshape expressions 84

6.3 Results 93

6.4 Discussion 102

Chapter 7. Conclusions 106

References 113

Appendices:

A. "Infrared Photochemistry of Halogenated Ethylenes" 119

B. "Formation of vinylidenecarbene intermediates..." 128

Appendices (cont'd)

C. Synthesis of C_2H_2DCl . . . 130

D. "Energy deposition in molecules..." . . 134

E. "Infrared double resonance in SF_6..." . 143

F. Biomation 820 interfaces . . . 154

G. Program listings 167

H. Consideration of the SF_6 Hamiltonian . . 181

I. Gizmos 187

J. "Studies of SiH_4..." . . . 195

Biographical Note 207

LIST OF FIGURES

2-1. LID of CH_2CDCl 27

3-1. Flowchart for LID 47

3-2. Densities of states for vinylidenecarbenes . 52

4-1. Minimum volumes versus precision . . 60

5-1. Q-switched laser triggers . . . 67

5-2. SF_6 spectrum near 946 cm^{-1} . . . 69

5-3. N_2O laser DILDOR schematic . . . 74

5-4. NH_3 absorption feature . . . 76

5-5. NH_3 DILDOR spectra 77

6-1. Calculated 2LDR in SF_6 . . . 89

6-2. Calculated absorption spectrum of SF_6 near 946 cm^{-1} 91

6-3. Calculated 2LDR lineshape for background lines . 94

6-4. Calculated vs. observed 2LDR SF_6 spectra . 96

6-5. Deviation of calculated 2LDR spectra . . 97

6-6. Calculated vs. observed 3LDR SF_6 spectrum . 99

6-7. Deviation of calculated 3LDR spectra . . 101

F-1. Biomation 820 interface block diagram . . 155

F-2. MINC interface 157

F-3. MINC interface timing . . . 160

F-4. 8/L interface 162

F-5. 8/L interface timing . . . 163

I-1. 8/L to MINC cable 191

I-2. TAC II pulse counter schematic . . 193

J-1. Schematic for LID on SiH_4 . . . 198

J-2. Apparatus for c.w. absorption measurements . 199

J-3. Stabilized CO_2 laser . . . 200

LIST OF TABLES

2-1. Vibrational frequencies of CH_2CDCl . . 26

2-2. Summary of LID on isocrotyl chloride . . 29

2-3. Summary of LID products from isocrotyl chloride . 30

2-4. Summary of LID on CF_2CHCl . . . 34

3-1. Distribution of energy in nascent CF_2 . . 49

3-2. Vibrational frequencies for vinylidenecarbenes . 53

J-1. TEA laser experiments on SiH_4 . . 203

J-2. Absorption coefficients for SiH_4 and NH_3 . 204

Although photochemistry has been actively studied for many decades, the advent of continuously improving laser technology has caused a renaissance of interest in the use of light in chemistry. A particular laser induced process may take advantage of any of the various properties unique to laser radiation, such as high spectral intensity, narrow linewidth, short pulse duration or facile beam directability. Applications have ranged from gross laser heating and pyrolysis, such as in thermal diffusion columns [1.1] or the production of sinterable powders [1.2], to state-selective excitations, such as vibrational energy enhancement of the bimolecular HCl + K reaction rate [1.3].

Laser induced and laser enhanced chemistry has blossomed in the past several years into a full-scale discipline whose central theme is influencing chemical events by coupling energy, via laser radiation, into the various molecular degrees of freedom. The discipline is so broad that we must restrict our scrutiny from the start to a small subset of laser induced chemical processes. In this thesis, this subtopic involves the intimate chemical and physical processes incurred in the megawatt infrared laser induced dissociation of small molecules.

Multiple infrared photon absorption (MIRPA) is a relatively new area of research. The first observation of MIRPA may be ascribed to Isenor et. al. [1.4], who employed a CO_2 TEA laser to irradiate low pressure samples of SiF_4, NH_3 and other molecules at intensities of up to 10^9 W/cm^2. Visible fluorescence emitted from the samples was attributed to emission from highly excited parent molecules or photofragments. The authors' interpretation stated that sufficient energy was absorbed into the near resonant molecular vibrations to cause direct collisionless dissociation, since the emission followed the 200 ns laser pulse in temporal and geometric shape. Absorption of multiple photons presumably occured through a series of discrete overtone vibrational states until the density of vibrational states, or number of vibrational states per unit energy, became a "quasi-continuum", thus providing a facile pathway for the absorption of energy from the laser field. In this manner, the absorption of 20-40 photons was envisioned.

Within the next several years, Ambartzumian et. al. [1.5] and Lyman et. al. [1.6] reported isotopically selective laser induced dissociations of SF_6. In these experiments, gas samples of SF_6 with a natural abundance of sulfur isotopes were enriched in either ^{32}S or ^{34}S. The enriched isotope could be chosen by tuning the CO TEA laser used to irradiate the samples to the ν_3 band frequency of the unwanted isotope, thereby preferentially dissociating unwanted isotopic molecules. The large ν_3 dipole moment, high

isotopic shift of the ν_3 fundamental frequency, coincidence with CO_2 laser frequencies and spectroscopic similarity to UF_6 made SF_6 an "ideal" candidate for studying MIRPA and laser induced dissociation (LID).

In his dissertation, Jensen [1.7] gives a sweeping tour of the experiments and interpretations of the MIRPA process in SF_6. This process is not restricted to hexafluorides, but in fact has become a general process occurring in a wide range of molecular sizes and types [1.8]. Several recent review articles attest to the popularity of the field [1.9] and provide specific details for the interested reader.

Usually LID experiments are carried out at pressures ranging from a few microns to tens of Torrs of parent molecules. In some cases, inert or scavenger buffer gas may be added. To achieve the intensities required to force MIRPA to occur, the TEA laser output is focused into the sample cell so that peak intensities fall in the 10^6 to 10^9 W/cm^2 range. The net chemistry is inferred, after a suitable number of laser pulses, by IR spectrophotometry, gas chromatography, mass spectrometry and other means. In some cases [1.10] in situ analysis techniques have been employed to determine the identity of the primary photofragments. For the most part, however, the photochemist has been left the often tedious chore of determining the primary photochemistry from the net chemical products.

The value of the MIRPA approach to photochemical reactions lies ultimately in the ability to choose what the primary fragments will be. Initially it was hoped [1.11] that mode specific chemistry could be achieved, wherein reactions involving specific bonds could be forced by exciting appropriate vibrational modes. This would be a "chemist's dream", that is, to obtain the ability to perform a specific reaction seemingly at will. As we shall see in Chapters 2 and 3, however, the criteria necessary to achieve mode selective behavior appear to be particularly elusive in the laboratory.

Lack of mode selectivity or specificity does not imply uselessness, however. As mentioned above, isotopic enrichment continues to be a major application of megawatt infrared photolysis; isotopes of C, H, S, Cl, and B have been separated, just to name a few. Creation by LID of high local densities of exotic species has been used by King and Stephenson [1.12] in their spectroscopic studies of CF_2. In a similar manner, Steinfeld et. al. [1.13] used high local concentrations of reactive radicals produced by LID to etch an SiO_2 surface placed close to (but not in) the TEA laser beam. Although no LID process has actually been applied in a commercial enterprise, the projected cost of some LID processes, such as deuterium enrichment, have begun to approach the cost effectiveness of currently used techniques [1.14].

Perhaps the greatest stumbling block to further

applications of LID is a lack of understanding of the rates and mechanisms of fundamental physical processes which contribute in concert to the observed net chemistry. Only a limited understanding of the intimate details of the dynamical process can be had from analysis of chemical evidence after the event is completed. Despite a growing mass of elegant experimental evidence, large gaps in our understanding still exist. Specifically, experimental efforts should be aimed at four interleaved questions:

1) How does a molecule absorb multiple photons? This question cannot be answered by bulk chemical methods. It requires a detailed understanding of the interaction of very intense infrared fields with molecules having near resonant vibrational modes. Spectroscopic parameters specific to each example molecule must play an important role, so that effects of sample pressure, laser frequency and laser intensity (or fluence) are adequately describable.

2) How does the vibrational energy distribute in the molecule? Once energy has been absorbed, collisional or spontaneous intramolecular energy relaxation will tend to distribute energy in modes other than the mode which was originally resonant. The speed of intramolecular vibrational relaxation (IVR) is evidenced in many LID experiments, for example [1.15] in the LID of CF_3Br,

$$CF_3Br \xrightarrow{nh\nu} CF_3 + Br \qquad (1\text{-}1)$$

energy is placed initially in CF stretches although it is the bromine bond which breaks. Presumably the speed and extent of IVR influences the chances of observing mode specific chemical behavior and of using models of unimolecular reaction rates based on a statistical distribution of energy amongst the vibrational modes, such as the RRKM method [1.16].

3) What kinds of exotic reactions can be expected? To answer this question we must understand how laser excitation differs from simple heating (which is the key to question (2)) and what unimolecular kinetics the molecules follow given that excitation. Since using a laser to produce chemistry that can be done by more conventional techniques is at best uneconomical [1.14], reaction mechanisms unique to this form of excitation must be elucidated before LID can find significant applications in experimental and commercial technology.

4) Can a simple model be used to predict LID phenomena? Presumably once a resonably complete set of absorption, relaxation and reaction rates are known for a particular system, a sufficiently large computer code could model the system behavior. In many cases, however, the ability to predict chemical behavior with a simpler, analytical model would be of greater use in applying MIRPA to a particular chemical problem.

The experimental approach we have used over the past several years has been designed to illuminate various portions

of the complex set of problems outlined above. In many cases the work done in our laboratory has complemented that done elsewhere, and the combination of experimental results has greatly improved the scope of our understanding. Thus our work, and the work reported in this thesis, does not comprise an exhaustive series of experiments on the subjects involved in MIRPA, but has been chosen as our knowledge progressed to attack a few key points where our understanding of the LID process was particularly thin.

Originally the data collected were chemical in nature, aimed at answering question (3) above. F. M. Lussier [1.17] initiated work on the infrared photolysis of vinyl chloride, which was considerably extended to include a host of halogenated olefins. This work is contained in Chapters 2 and 3 and in Appendices A, B and C.

Net LID chemistry of the type described in Appendix A showed what experimental parameters play significant roles in influencing various stages of the LID process. Sample pressure, laser beam geometry, pulse intensity or fluence and other more subtle factors were found to influence greatly the total amount of energy deposited in the molecules. The simple kinetic schemes we used to model our LID results in the vinyl chloride system showed that the average energy absorbed per molecule $\langle E \rangle$ is strongly dependent on experimental conditions such as initial gas sample pressure, the presence of cold diluents which tend to deactivate excited molecules,

and beam geometry (which we review in Chapter 4 and Appendix D).

When a model for a LID process is constructed, a reliable estimate of the internal energy-dependent reaction rates much be obtined. In all kinetic models of LID with which the author is familiar, RRKM unimolecular reaction rate theory [1.16] has been used to describe the microscopic rates of reaction quantitatively. The success of the RRKM method in modeling dissociation rates over a wide variety of LID conditions and reactions (such as isomerization, cyclic molecular elimination and simple bond scission) has been remarkable. The implications of the success of RRKM rates for answering question (2) above will be discussed in Chapters 3 and 7.

One question which has not been resolved experimentally involves the quantitative observation of the distribution of molecules over energy created by MIRPA. Theoretical [1.18] and semi-empirical [1.19,1.20] models have "predicted" various distributions which in turn "predict" a variety of experimental data, but to date no direct measurement of a MIRPA distribution has been made. As Jensen [1.7] pointed out, a distribution is not uniquely determined by chemical evidence alone. Direct observation, involving interrogation of individual species undergoing MIRPA, is necessary for direct comparison with existing dynamical theories.

Spectroscopic investigations of this nature have proven to be difficult to carry out. In molecules possessing no easily accessable excited electronic state, the lack of resonant excitation makes the usefulness of visible probe radiation very limited. We have chosen to use a tunable infrared diode laser to probe the vibrational bands themselves as they are being pumped by intense CO_2 laser fields. This work, Diode Infrared Laser DOuble Resonance (DILDOR), was begun by Jensen several years ago; in his thesis [1.7] he reported preliminary results in SF_6. Since that time our efforts at answering question (1), how SF_6 molecules interact with very intense resonant infrared fields, have been considerably extended, being included in Chapters 5 and 6 and in Appendix E.

In the DILDOR experiments accomplished thus far, the effects of power broadening, saturation, dynamic Stark shifting and collisional rotational relaxation have been studied in SF_6 for pump intensities up to 11 kW/cm^2. The limit of pump laser intensity and temporal resolution of the observed signals has been reached for the Q-switched laser pulses used in the currently existing apparatus. Moulton and Mooradian [1.21] have extended this work in SF_6 to higher pulse intensities but not to other molecules. A high repetition rate CO_2 TEA laser currently being constructed by Dave Harradine will enable these experiments to be extended to the intensities generally required for LID. The shorter length of the TEA laser pulse may also be valuable in studies

of collisional deactivation. Further improvements in the existing apparatus will be discussed in Chapter 6.

Chapter 2. Laser Induced Chemistry: Results

2.1 Introduction

As was pointed out in Chapter 1, a detailed understanding of the multiple infrared photon absorption (MIRPA) process necessitates interrogation of individual molecules. The gross behavior of an ensemble of molecules can then be "predicted" by a suitable average over the microscopic behavior obtained by these interrogations. Often, however, the experimentalist is faced with the reverse problem, that is, having information about an ensemble without knowing microscopic details. This is currently the case in the understanding of MIRPA and the chemistry it produces.

The clever chemist can, however, recover certain details of the microscopic dynamics of multiple infrared photon laser induced dissociations (LID) by using the chemical behavior of molecules as his method of interrogation. In chemical systems whose internal energy dependent reaction rates are well characterized, the known microscopic rates of dissociation become a valuable internal "yardstick" of internal energy content. By comparing the observed rates of reaction to the microscopic rates of reaction, the chemist can begin to make quantitative statements about the MIRPA process.

We have used this technique to study the LID of halogenated ethylenes, $\begin{matrix} X \\ H \end{matrix}\!\!>\!C\!=\!C\!<\!\!\begin{matrix} Y \\ Cl \end{matrix}$; X = H, H, D, H, Cl, Cl
Y = H, D, H, Cl, H, Cl

The report of these experiments has been published (J. Am. Chem. Soc. 101, 350 (1979)) and is included in this thesis as Appendix A. The reader is encouraged to peruse Appendix A before reading this chapter, so that he may be famaliarized with the experimental method and results of the photolyses reported therein. The remainder of this chapter is devoted to experimental results not specifically reported in Appendix A but which nevertheless have aided our understanding of the MIRPA process and laser induced chemical reactions.

Some of the chemistry noted below has been published in a short note, included as Appendix B. The abbreviated account of the method of synthesizing the isotopically labelled molecules CHDCHCl and CH_2CDCl found in Appendix A has been expanded into much greater detail in Appendix C.

2.2 Kinetic model for CH_2CDCl

In Appendix A, the LID of CH_2CDCl was reported. The percent of α,α elimination of DCl versus α,β elimination of HCl was determined by GC/MS analysis of the acetylenes C_2HD and C_2H_2 produced. These data are reproduced in Fig. 2-1b.

Although it was claimed in Appendix A that these data are consistent with the RRKM picture presented for the more complicated system CHDCHCl, the details were not presented. For completeness, they will be included here.

The kinetic model for CH_2CDCl is similar to that used for

CHDCHCl and is constrained by the same assumptions as those put forth in Appendix A to qualify the use of this approach. In this case, the model is somewhat simpler, because isomerization need not be considered. Only two reactions occur,

$$CH_2CDCl \xrightarrow{k_1} C_2H_2 + DCl \quad (78\%)$$
$$CH_2CDCl \xrightarrow{k_2} C_2HD + HCl \quad (32\%) \qquad (2\text{-}1)$$

where

$$k_1 = k_{gem}$$
$$k_2 = k_{cis} + k_{trans} \doteq k_{cis} \qquad (2\text{-}2)$$

In this model, trans elimination has been neglected, as in the model for CHDCHCl.

Using Eqns. (2-1), one can write immediately

$$dA/dt = -[k_1' + k_2']A \qquad (2\text{-}3)$$

$$d[C_2H_2]/dt = k_1' A$$
$$d[C_2HD]/dt = k_2' A \qquad (2\text{-}4)$$

where A is convenient notation for $[CH_2CDCl]$ and

$$k_i' = fk_i \; ; \quad f = 5 \times 10^{-5} \qquad (2\text{-}5)$$

The constant f is the approximate ratio of the volume interacting with the laser to the total volume of the reaction cell. Variations of ~50% of f change the net results by only 1 or 2%.

Equations (2-3) and (2-4) can be integrated, using the boundary conditions of unit concentration of A and null concentration of acetylenes at t=0:

$$A(t) = A(0)\exp(-[k_1' + k_2']t) \quad (2\text{-}6)$$

$$[C_2H_2](t) = k_1A(0)[1 - \exp(-[k_1' + k_2']t)]/k_1+k_2 \quad (2\text{-}7)$$

$$[C_2HD](t) = k_2\,[C_2H_2](t)/k_1$$

To find xC_2HD, Equations (2-7) need be evaluated at some appropriate time, taken to be 10^-7 reaction-seconds/pulse x 1500 pulses = 150 microseconds, as is done in Appendix A.

The constants k_i' must be calculated from the RRKM microscopic reaction rates, $k^{RRKM}(E)$, by the same formula as prescribed in Equations (16)-(21) of Appendix A. These equations calculate the ensemble-averaged dissociation rates for two ensembles of molecules, one having a Poisson distribution f(E) of molecules over energy and the other having a maximum entropy distribution. Constants used in the calculation of the $k^{RRKM}(E)$ are listed in Table 2-1.

The results of using Equations (2-7) are shown in Fig. 2-1 for energies of activation E_a identical to those which produced best results for the CHDCHCl system. For the maximum entropy distribution, a slightly different set of E_a renders a far superior fit. These adjustments are not much larger than the 1-2 Kcal/mole uncertainties of the values for the E_a. This point will be discussed in the next chapter; for

Table 2-1. Vibrational frequencies of CH_2CDCl and transition state configurations (cm^{-1}).

	mode[a]	molecule	β-elim.	α-elim.
(a')	1	2305	2250	2200
	2	3125	3100	3100
	3	3030	2500	2500
	4	1595	1800	1800
	5	1355	1340	1350
	6	911	900	860
	7	1110	750	r.c.
	8	710	r.c.	590
	9	394	290	280
(a")	10	805	1500	1500
	11	895	850	820
	12	590	590	590

a. listed in accordance with standard assignment; see Ref. [2.1] and [2.2]

r.c. = reaction coordinate

Figure 2-1. Effective branching ratios for HCl/DCl elimination in the LID of CH_2CDCl. a) observed; ■ = P(38) laser line, ▲ = P(32). b) calculated; o = Poisson distribution with E_a = 70 and 69; Δ = maximum entropy distribution with E_a = 69 and 73; + = maximum entropy distribution with E_a = 70 and 69 Kcal/mole for cis- and gem-elimination respectively. Solid curve drawn in a) has been included in b) for comparison.

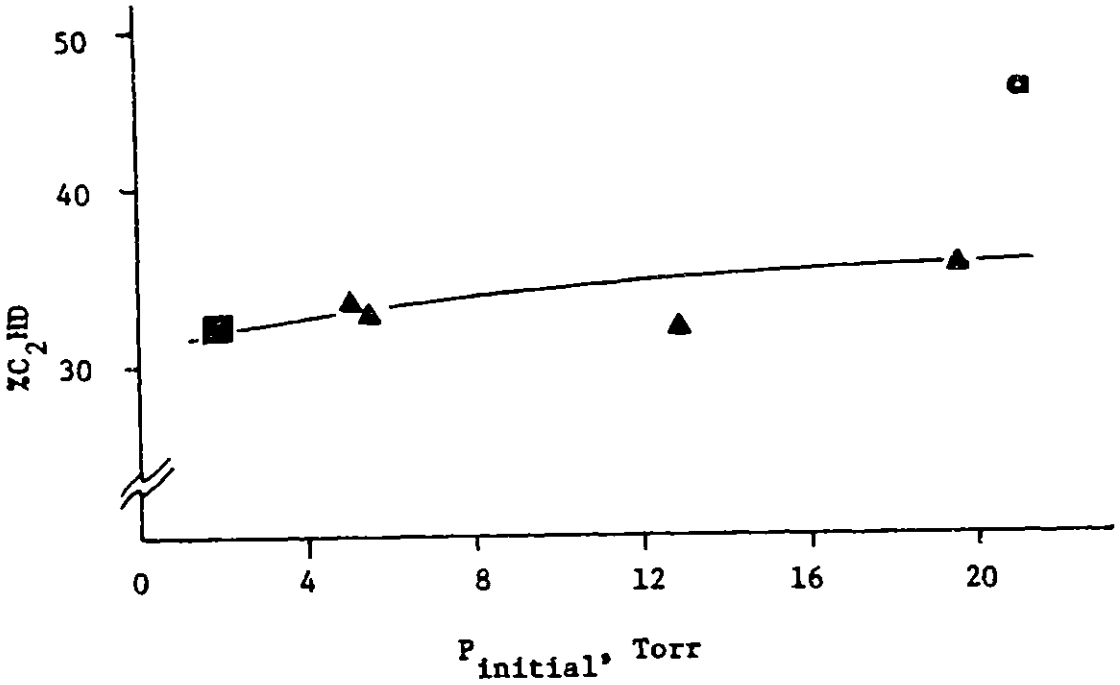
a
50
40
30
$\%C_2HD$
0
4
8
12
16
20
$P_{initial}$, Torr

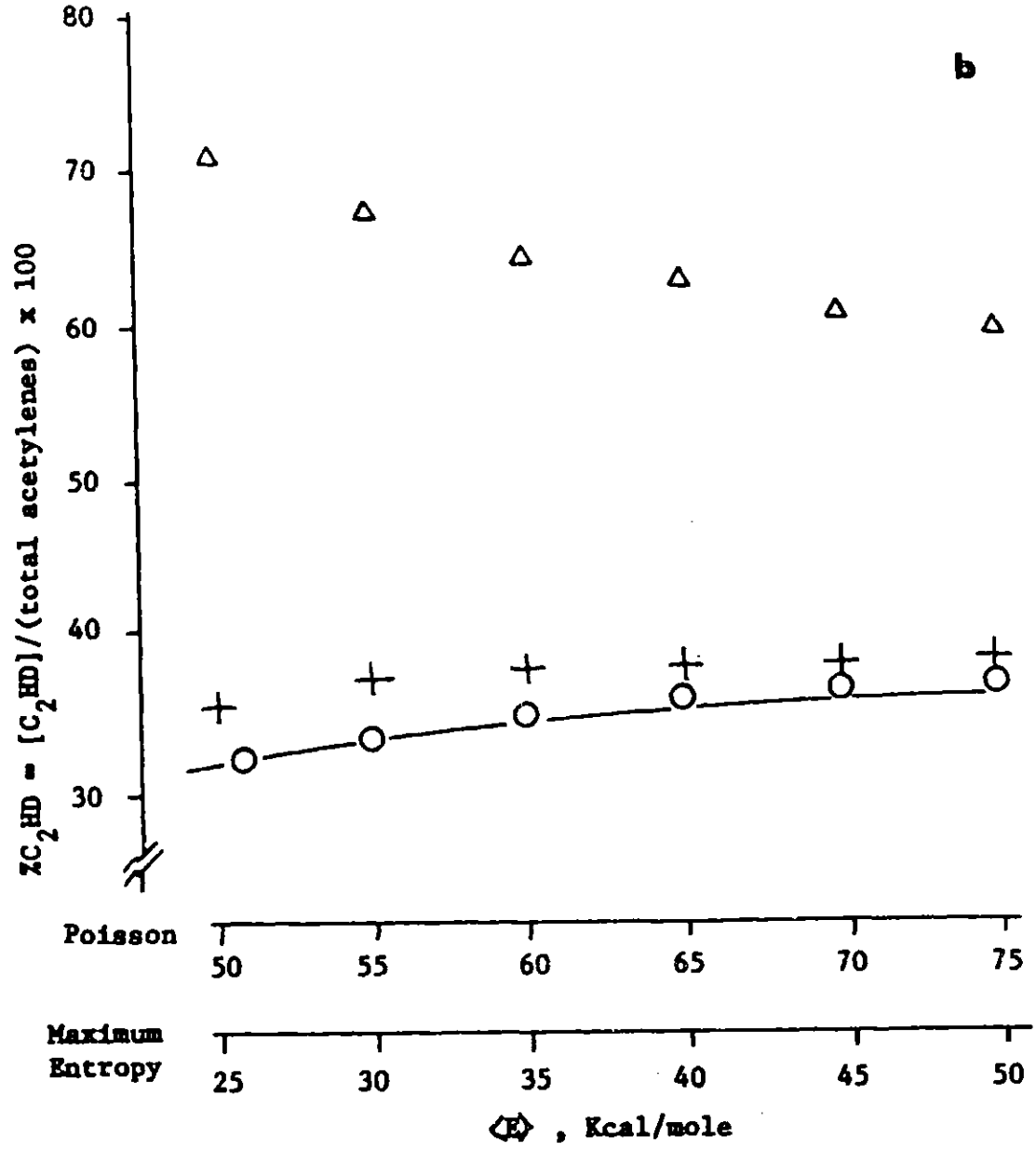
b
80
70
60
50
40
30
$\%C_2HD = [C_2HD]/(\text{total acetylenes}) \times 100$
Poisson
50
55
60
65
70
75
Maximum Entropy
25
30
35
40
45
50
$\langle E \rangle$, Kcal/mole

Table 2-2. Summary of LID experiments on isocrotyl chloride.

Date	notebook II page	p(I) Torr	p(buffer) Torr	# shots	line 9.6μ	Remarks
10/10/78	5W	0	4.8 MeOH	1500	P(16)	only product in IR spectrum = C_2H_2
"	5Y	4.2	0	"	"	many peaks--some impurities
10/11	6Y	1	10 MeOH	"	"	acetylenes formed
10/12	7W	1.25	10.6 MeOH	1300	"	"
"	"	0	11 MeOH	1500	"	"
10/13	7Y	5	22.1 H_2O	1500	"	no reaction
10/16	8W	0	32.3 NH_3	500	P(18)	no changes
"	"	10?	" "	1000	"	white soot; great attenuation; very slight fluorescence
10/18	"	9.4	0	2500	"	submitted for GCMS analysis
10/30	9Y	3.2	29.8 H_2S	1500	"	IR weak; GC looks like blast of II alone
11/6	11W	4.9	48.3 H_2S	1500	"	same as last entry
11/7	11Y	8.6	13.9 H_2S	121	"	brilliant flashes; white soot; new peaks in IR plainly seen
3/8/79	25Y	4.25	14.4 D_2S	1500	"	no fluorescence; for GCMS analysis
"	"	4.45	0	"	"	" "
"	"	4.2	14.1 H_2S	"	"	" " ; no soot

Table 2-3. Summary of products seen in the infrared photolysis of isocrotyl chloride.

GC peak #	rel. strength	ident.	Reasoning
1	3	allene	boiling point is lowest; mass peak 19.5 is unique to allene*
2	10	1,3-butadiene	mass peak 39 is very strong*
3	2	butadiyne plus 1-butyne or 1,2-butadiene	butadiyne is indicated by strong mass peak at 50; others must be included to account for a large mass peak at 54; bp's are very close for all three
4	3	2-butyne	bp is highest of those listed here; MS agrees with library

*library MS data have been taken from "Eight Peak Index of Mass Spectra" 1st ed., Vol. 1 and 2 (Mass Spectrometry Data Centre, Reading, 1970)

now we need to conclude only that the agreement between the observed and calculated points can be very good for either distribution f(E). As was found in the CHDCHCl system, the mean energy <E> required to fit the data with the Poisson distribution is considerably higher than the <E> needed for the maximum entropy distribution.

2.3 LID of other halogenated olefins

2.3.2 Isocrotyl chloride, $(CH_3)_2C=CHCl$

The large fraction of gem elimination seen in the vinyl chloride system suggests that a radical of the type $R_2C=C$: may be formed. In the vinyl chloride system, reaction products that one would expect from this species were never detected, presumably because hydrogen migration occurs much too quickly. If the groups on the β carbon were inhibited from migrating, however, the proposed intermediate might possess a sufficiently long lifetime to form bimolecular reaction products with added buffer gases. For this reason, the infrared photolysis of two additional molecules, 1-chloro-2-methyl propene (isocrotyl chloride, I) and 1,1-difluoro-2-chloroethene (II) was investigated.

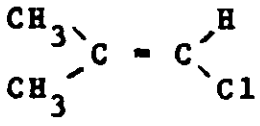

I

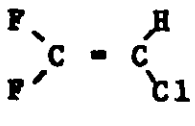

II

For the photolysis of I, a single Ge 11.1" (28 cm) focal length lense was used to focus the TEA laser beam into a 50 cm

Pyrex cell. The cell was fitted with a removable cold finger with a stopcock, a sidearm for cooling with LN_2 and a gas inlet for in situ evacuation and filling. For a typical run, the cell was filled to the desired pressure of I, which was then frozen into the removable cold finger and the stopcock closed. A known pressure of buffer gas was then admitted to the cell. The buffer gas and isocrotyl chloride was cryopumped into the sidearm. In this manner, mixing of the two gases was assured upon sublimation from the sidearm into the cell.

A summary of infrared photolyses done on the isocrotyl chloride system is shown in Table 2-2. Some difficulty was encountered during GC analysis of the reaction products; apparently certain GC columns reacted with the starting materials. From the IR spectra and GCMS results, however, it was determined that the reaction products of photolyses with added buffer gases did not differ significantly from photolyses with no buffer gas. Particularly significant is the lack of deuterium in the MS of products formed in photolyses with D_2S as the buffer gas.

Products that were formed comprise a host of C4 hydrocarbons. Although the cracking patterns of many of these olefins and alkynes are very similar, the GC peaks can be ordered by boiling point and elemental composition assigned by the mass of the most intense MS peaks. In this manner, the products are assigned according to Table 2-3. By far the most

abundant product is 1,3-butadiene, the most stable hydrocarbon with composition C_4H_6. This is the expected composition of the organic fragment arising from the dehydrohalogenation of I.

2.3.2 1,1-difluoro-2-chloroethene (II)

Photolyses of II were performed with the same technique used for I. Various pressures of II with a variety of buffer gases were photolyzed by focussing the approximately 0.4 J laserpulse with the 11.1" (28 cm) Ge lens. A summary of experiments on II is tabulated in Table 2-4.

One interesting feature of this system is the blue fluorescence observed around the focus of the beam. We have observed this effect in other vinyl halide systems; it has also been reported [2.3] in the MIRPA of chromyl chloride. In the latter system, the observed luminescence was attributed to excitation of a low-lying excited singlet state followed by fluorescence back to the ground state. In the olefin systems studied here, the lowest excited singlet states lie in the UV. The observed luminescence may come from highly excited fragments, but this conjecture has not been tested.

From the GCMS of several reaction mixtures, the products of the photolysis of II were identified. When II was photolyzed at 4.0 Torr with no added gas, the principal products were C_2F_4 (67%) and C_2F_3H (33%). A small amount of $C_2F_2H_2$ was also detected, but no C_2F_2 was found. When 14 Torr

Table 2-4. Summary of LID experiments on difluorovinyl chloride. All experiments were performed with the R(18) 10.6 laser line, 28 cm f.l. lens.

Date	notebook #II page	p(II) Torr	p(buffer) Torr	# shots	Observations
11/22/78	13W	10	0	1000	bright flashes; soot; HCl formed, other products
11/24	"	1.8	0	1000	IR show products; no flashes
11/27	13Y	1.95	16.1 H_2S	1000	no flashes; GC taken, ambiguous results
12/4	14Y	2.15	9.0 "	1500	very slight powder
"	"	2.25	6.2 NH_3	500	slight luminescence; white soot
"	"	2.2	4.1 MeOH	1500	blue fluorescence; problems with GC
"	15W	5.1	15.1 H_2S	"	very slight powder; large energy deposition
"	"	5.05	14.3 MeOH	2000	tremendous attenuation of beam; fluorescence; GC shows massive peak in Rxn mixture
12/6	15Y	5.1	0	1000	same massive peak here too
12/20	16Y	4.15	13.1 H_2S	1500	white powder; GCMS done
"	"	4.0	0	1000	intense fluorescence; visible brown powder; GCMS
"	"	4.0	14.0 MeOH	1500	very slight powder; GCMS done
3/8/79	25W	4.25	14.35 D_2S	1500	thin blue fluorescence; audible signal; GCMS done

of methanol was added, however, the products $C_2F_2H_2$, C_2F_3H and C_2F_4 were observed in ratios of 1:0.15:0.07 respectively. A very similar product mixture was observed when 13 Torr of H_2S was used as a buffer.

The abundance of $C_2F_2H_2$ suggests that CF_2C: formed in the dehydrohalogenation of II leaches hydrogen from the buffer gas. As a test of this hypothesis, D_2S was used as the buffer gas. Amongst the reaction products was seen undeniable evidence of $C_2F_2D_2$. The mass spectrum did not reveal which isomer of $C_2F_2D_2$ was detected, but it is believed to be CF_2CD_2 from the weight of previous evidence.

2.3.3 1,1,1-trifluoro-2-iodoethane (III)

A few experiments on III were performed at pressures of 4 to 6 Torr with 0.4 J pulses of the 9.6 micrometer P(18) laser line. The experimental apparatus was the same as used above. In all experiments, copious amounts of iodine were formed, as evidenced by dark crystals which formed near the center of the cell, where the beam waist occurs. No products were observed when the beam was not focussed.

Unlike other systems we studied, the primary species formed, presumed to be $CF_3\dot{C}H_2$, undergoes considerable bimolecular addition to other fragments. The GC spectrum showed two close peaks, which, from MS analysis were shown to be $CF_3CH_2CH_2CF_3$ and $CF_3CH_2CF_2CFH_2$ or $CF_3CH_2CFHCF_2H$ respectively. The unambiguous identity of the component or

mixture in the second GC peak could not be determined because the cracking patterns of the two candidates listed above are almost indistinguishable. A possible mechanism which accounts for the observed products includes hydrogen and fluorine migration following the initial loss of iodine:

$$CF_3CH_2I \xrightarrow{nh\nu} \underset{IV}{CF_3\dot{C}H_2} + I$$

$$IV + IV \longrightarrow CF_3(CH_2)_2CF_3 \quad \text{(first gc peak)}$$

$$IV \longrightarrow \dot{C}F_2CFH_2 \quad (V)$$

$$IV + V \longrightarrow CF_3CH_2CF_2CFH_2$$

$$V \longrightarrow CF_2H\dot{C}FH \quad (VI)$$

$$IV + VI \longrightarrow CF_3CH_2CFHCF_2H$$

While it is possible to account for all the possible products in this way, further experiments would be necessary to verify the various steps of this mechanism.

Loss of HI following MIRPA would lead to the stable product CF_2CFH, which may undergo further LID during subsequent laser shots. No C2 species other than the parent molecule were detected in these experiments, but an analysis with greater sensitivity may detect them.

2.3.4 chlorocyclobutane (VII)

Under essentially the same conditions as used for III, VII was photolyzed with the P(18) 9.6 μ laser line. IR and GC spectra revealed four products: ethylene, acetylene, vinyl

chloride and 1,3-butadiene. These products are in concert with the results of King et al. [2.4] who observed two reaction channels in Very Low Pressure Pyrolysis (VLPP) of VII. One channel produces vinyl chloride and ethylene, and the other HCl and butadiene. The acetylene produced here presumably arises from photolysis of the primary photoproducts. Joseph S. Francisco is currently investigating this system in detail [2-5].

Chapter 3. Laser Induced Chemistry: Discussion

3.1 Chemical mechanisms

In the previous chapter and in Appendix A, the mechanisms by which vinyl chloride reacts were elucidated in fine detail. The principal mode of dissociation was found to be three centered molecular elimination of HCl. The data for α-d_1-vinyl chloride are unambiguous on this point. The results of trans-d_1-vinyl chloride photolyses are discussed in detail in Appendix A.

In all of the systems studied, by far the greatest amount of reaction was seen to occur through the reaction channel having the lowest activation energy E_a . For the vinyl chloride system, isomerization was seen to be many times faster than the elimination channels at all $\langle E \rangle$. Molecular elimination of HCl was preferred over the higher energy Cl bond scission channel in the photolysis of CF_2CHCl. Elimination of iodine from CF_3CH_2I occurs with such great efficiency that products which would result from the higher energy molecular elimination of HI were not seen at all. All evidence points to the conclusion that a reaction mechanism having lower activation energy barrier is favored over a mechanism having a higher energy barrier.

This, of course, is in concert with unimolecular reaction rate theory. As is evident from Fig. 3a in Appendix A, the

microscopic unimolecular reaction rates are very sensitive to their E_a , and only at extremely high internal energies E_v do the rates converge. To accept that this behavior will be followed is tantamount to admitting that for this type of laser induced chemistry, mode specific reactions may never be possible. By this method of excitation, a low activation energy reaction channel cannot be bypassed in favor of another at higher activation energy merely because the initial vibrational excitation began in a particular set of vibrational modes. This point will be discussed further in the next section.

Evidence for the formation of the long-lived intermediate $F_2C{=}C{:}$ is clear-cut, and is reviewed in Appendix B. As was shown there, evidence for the existence of its dimethyl counterpart $(CH_3)_2C{=}C{:}$ is not as convincing. Use of the cyclopropenyl intermediate seems to be necessary, especially since it leads to many of the observed products:

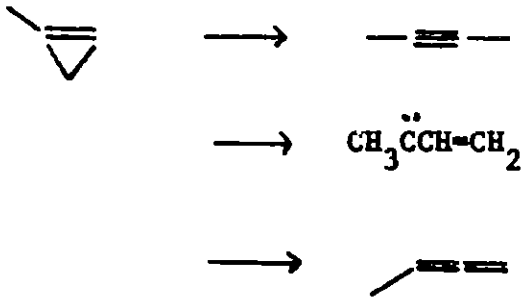

(3-1a)

$$\longrightarrow \quad CH_3\ddot{C}CH{=}CH_2 \longrightarrow H_2C{=}CHCH{=}CH_2 \qquad \text{(3-1b)}$$

(3-1c)

In (3-1c), H migration across the double bond is required, and can be expected to occur readily, as seen in the photolysis of vinyl chloride to make acetylene.

It must also be stressed here that all of the laser induced reactions reported in this thesis have been induced by other methods as well. Acetylene is formed in shock tube dissociation [3.1] of vinyl chloride; vinylidene carbene chemistry is well known in the liquid phase [3.2] and so on. No entirely new and exotic reactions have been performed using MIRPA. The reaction product mixtures may be different from those induced by other methods (such as by direct heating); this point will also be discussed in the next section.

3.2 Kinetic effects

3.2.1 Effects of the internal energy distribution

As Craig Jensen made clear in his thesis [3.3], first moments of a distribution do not uniquely determine that distribution. Specifically, the chemistry induced by a distribution of molecules over energy P(E) produced in a MIRPA experiment is, in itself, insufficient to specify P(E) uniquely. If the microscopic rates $k_i^{RRKM}(E)$ are well characterized for a system having i channels of reaction, then a LID experiment may render as many as i first moments:

$$k_i^{AVG} = \int_{E_{a_i}}^{\infty} P(E)\, k_i^{RRKM}(e)\, dE \qquad (3\text{-}2)$$

In the trans-d_1-vinyl chloride system, for example, three moments are determined, those being the average rates k_i^{AVG} for isomerization, cis-elimination and gem-elimination.

However, much of the information gained by these i

moments of P(E) is redundant. Since only "hot" molecules react, the average rates k_i^{AVG} determined by the net chemistry actually sample only the high energy portion of the distribution P(E). No information is gained for energies lower than the lowest E_a, because the k_i^{RRKM} (E) do not sample this portion of the distribution. When the E_a for simultaneous reactions are nearly equal, the k_i^{RRKM} (E) sample a nearly identical portion of P(E); in this case, knowing two k_i^{AVG} gains little more information than knowing only one k_i^{AVG}.

This is precisely the point of Fig. 4 of Appendix A. By using the chemical evidence alone we are not able to choose a particular form of the distribution. Both the Poisson and the maximum entropy distributions are capable of fitting the data. What is needed is an independent measurement of P(E), such as <E> (the average energy of the distribution), which is sensitive to the entire distribution, not merely its high energy shape. If <E> were known for the various conditions used in the photolysis of trans-d_1-vinyl chloride, this additional constraint would allow us to construct a distribution subject only to maximum entropy and the observed first moments <E> and k_i^{AVG}. In effect the energy centroid of the distribution would be dictated by <E> while the dispersion would be determined by the extent to which the distribution overlaps the k_i^{RRKM} (E).

Experimentally, the value of <E> may be very difficult to

measure. One technique [3.4] involves addition of a nonabsorbing "chemical thermometer" gas to the reaction cell. Since a very small fraction of the total distribution P(E) reacts, most of the energy contained in the pumped molecules under study thermalizes via collisional V→V,R,T relaxation. A small amount of gas not affected by the particular laser frequency would come to the same vibrational temperature as the directly pumped molecules, and hopefully would react before V→T deactivation occurs. The extent of reaction of the "thermometer" molecules is then compared to a thermal average rate, thus determining <E> for the total sample.

Since this method is inherently collisional, and occurs over the entire volume of the cell, it renders a value of <E> equivalent to the gross amount of energy absorbed averaged over the entire sample. In a given system, however, only a small portion of molecules in the cell are irradiated by the laser beam, and only a fraction of these molecules undergo MIRPA [3.5]. It is the <E> of this fraction which we would like to measure, since these are the molecules in the distribution prepared by the laser pulse. This method, if not corrected for these effects, can be expected to give consistently low values of <E>.

There is another method of determining <E> which at least in principle can determine <E> for an arbitrarily small volume of sample in the laser beam. This method is Gaussian deconvolution; it is discussed mathematically in Appendix D

and is applied to this particular problem in the following chapter. It should be noted that this method was not developed until roughly two years after the vinyl chloride work was completed.

3.2.2 Rates of laser pumping and intramolecular vibrational relaxation

To model a LID kinetic system completely, one must incorporate the full time evolution of the system rather than "freeze" it into a quasi-static state, as we have done with the vinyl chloride model. The time dependence of the MIRPA process during the laser pulse, energy flow into nonresonant vibrational modes, collisional activation/deactivation and other processes must be included in the total picture. Since so many distinct processes are involved in a typical MIRPA event, a model incorporating a great number of kinetic processes explicitly would easily require more rate constants than are available or even determinable for a given system. This extreme complexity may be worth less than a much simpler approach, such as the one we have used for vinyl chloride.

Several authors have investigated various methods of modelling the time dependence of the MIRPA-LID process. Lyman [3.6] and others [3.7] have approximated their systems with a Master Equation formalism. A harmonic energy grid is constructed which is resonant with the laser field. The rates of pumping population between successive levels are determined

by approximating the dipole matrix element in an astute fashion, by including collisional coupling between levels by V-V energy exchange, and by careful inclusion of the proper degeneracies of each level. Although these models can be adjusted to reproduce a variety of data, such as energy deposition as a function of pressure or laser intensity [3.6], the distribution predicted by the Master Equation approach never deviates appreciably from a Poisson. This may be a consequence of the harmonic grid necessitated by this method; coherently pumped harmonic oscillators produce a Poisson distribution analytically [3.8]. This model also neglects all rotational relaxation effects.

More complex models, which have included rotational hole burning and relaxation, have been demonstrated by Cantrell and coworkers [3.9] for SF_6. These models utilize the elegant angular momentum algebra of octahedrally symmetric molecules, and have addressed the frequency and intensity dependence of energy deposition and dissociation effeciency. Many other investigators have proposed models specific to SF_6; Jensen gives a sweeping review of these in his dissertation [3.3].

What would be of greater value to our understanding of LID as a general process is a model general enough to be applicable to any molecule yet simple enough to be useful with a minimum of spectroscopic and kinetic data. Ackerhalt and Galbraith [3.10] have introduced a model which, they claim, meets these expectations. It includes both coherent and

incoherent laser pumping, intramolecular vibrational relaxation into many separate vibrational ladders, unimolecular reaction kinetics and a minimum of empirically determinable parameters. It has been successfully applied to SF_6 (of course!) and the authors claim that it is flexible enough to accommodate many different types of molecules.

The situation remains, however, that for most molecules whose LID has been studied, even the few parameters needed for a model such as that of Ackerhalt and Galbraith are not known. Moreover, determining these parameters and calculating predictions with abandon may not be lucrative or meaningful. In many cases, a "rule of thumb" would suffice to understand and predict the qualitative response of a chemical system; a flowchart of this nature has been provided recently by Thiele, Goodman and Stone [3.11] and is depicted in Fig. 3-1.

The reasoning behind Fig. 3-1 is straightforward. If intramolecular vibrational relaxation (IVR) is faster than the laser pump rate (LPR), energy deposited in the molecule randomizes amongst all vibrational modes as quickly as it is absorbed. No mode selective chemistry can be expected. Similarly, if IVR is faster than the dissociation rate (DR), vibrational energy will be randomized before reaction will occur, and no selective chemistry will occur. If, however, IVR is slower than both LPR and DR, vibrational energy will not be able to leak out of the set of modes directly pumped by the laser before dissociation occurs. In this case,

selectivity is possible (but not guaranteed) because only a few modes contain relatively large amounts of excitation. If DR is faster than LPR, however, molecules will react as soon as they absorb sufficient energy to surmount the lowest E barrier. In this case the products will be very similar to those produced in thermal reactions. If LPR is faster than DR, molecules may absorb much more energy than the lowest E barriers, and higher energy channels normally never sampled by thermal reactions become available. A semi-selective, definitely nonthermal mixture of products would be seen in this case.

All of the laser induced chemistry reported here is consistent with this reasoning. The vinyl chloride work would seem to fall in the upper left hand box of Fig. 3-1, "NO SELECTIVITY." Other systems, such as the cyclobutyl chloride system mentioned in Chapter 2, have demonstrated a nonthermal distribution of products and thus fall in the lower right hand box. These systems are currently under continued study.

3.3 Energy disposal in fragments

Another consequence of falling into the lower right hand box in Fig. 3-1 is that when the molecule dissociates, an excess energy ΔE given by

$$\Delta E = E_v - \Delta H \qquad (3\text{-}3)$$

is partitioned amongst the degrees of freedom of the

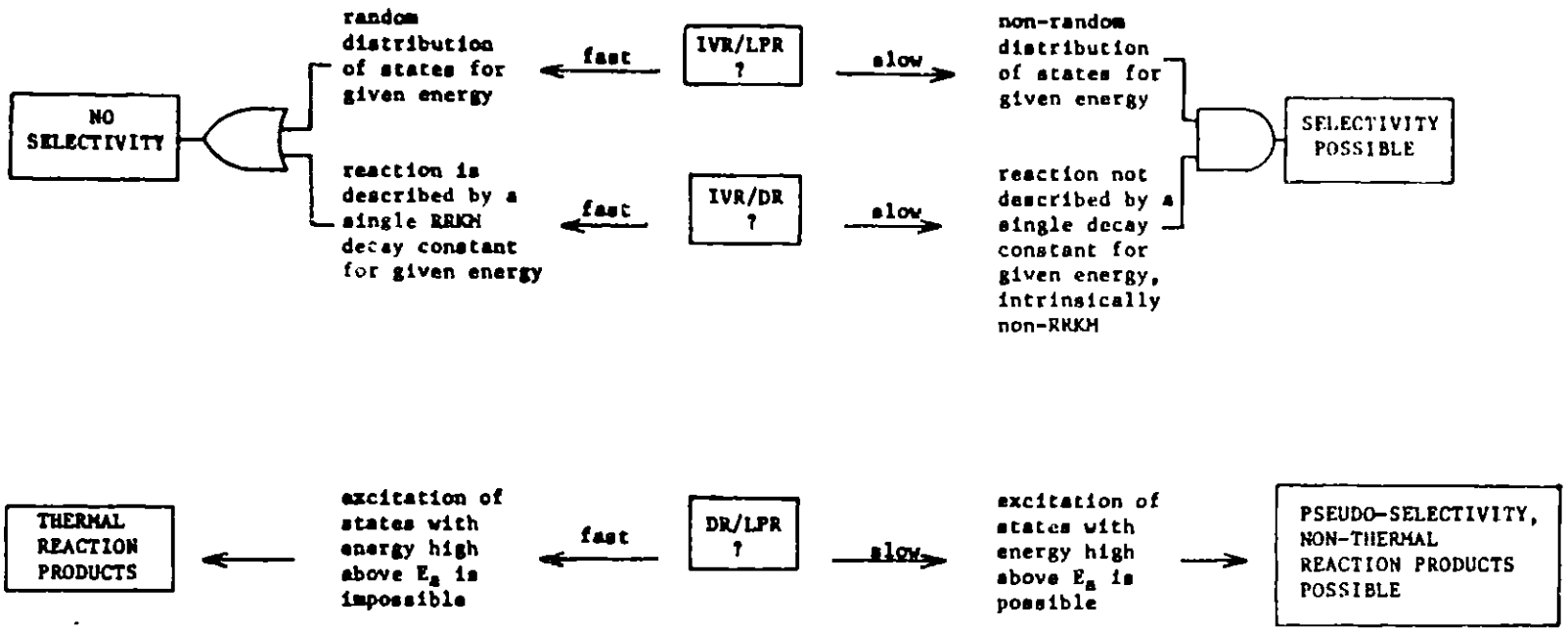

IVR = Intramolecular Vibrational Relaxation
DR = Decay Rate (reaction rate)
LPR = Laser Pump Rate

FROM: E. Thiele, M. F. Goodman and J. Stone, Opt. Eng. 19, 10 (1980)

Fig. 3-1. Flowchart for determining the roles played by various kinetic processes in determining the products seen in an LID experiment.

fragments. In Eqn. 3-3, E_v is the vibrational excitation forced into the molecule before it undergoes a reaction having net enthalpy ΔH. Fragments can be expected to be born vibrationally "hot" even for endothermic reactions; additional absorption of photons by these "hot" fragments and secondary reactions may also occur.

The precise partitioning of excess energy amongst the dissociation products has been studied for a few systems, such as for CF_2HCl [3.12]. This molecule dissociates into CF_2 and HCl; the internal energy content of the former species was measured spectroscopically by laser induced fluorescence. It was found that a considerable amount of energy was partitioned into translation (approximately 7 Kcal/mole) and that the distributions of vibrational and rotational energy could be described by a probability p(E) of the form

$$p(E) \cong \exp(-E_b/kT_b) \qquad (3\text{-}4)$$

where b is V for vibration or R for rotation. Typical average energies for this system are listed in Table 3-1. Similar behavior was observed for the LID of CF_2Br_2 and CF_2Cl_2 [3.12].

The energy partitioning into the CF_2 radicals described above suggests that partitioning of energy into the various degrees of freedom of the fragments of LID is statistical, that is, constrained only by the total energy available. If this is the case, one would expect that fragments of comparable vibrational and rotational complexity would be

Table 3-1. Distribution of energy in the nascent CF_2 fragment formed in the LID of CF_2HCl, CF_2Br_2 and CF_2Cl_2. Data are taken from J. C. Stephenson and D. S. King, J. Chem. Phys. 69, 1485 (1978)

	CF_2HCl	CF_2Br_2	CF_2Cl_2
T_V (K)	1160	790	1050
E_V (kcal/mole)	3.6	1.8	2.9
T_R (K)	2000	450	550
E_R (kcal/mole)	6.0	1.4	1.6
T_T (K)	2300	570	510
E_T (kcal/mole)	6.9	1.7	1.5
E_{avg} (kcal/mole)	16.5	4.9	6.0

awarded equivalent amounts of energy. A comparison of the average amounts of energy partitioned into the CF_2 fragments from CF_2Br_2 and CF_2Cl_2 shown in Table 3-1 is in concert with this assumption.

In Appendix B we comment on the effect of excess energy partitioning on the ability of fragments $R_2C{=}C{:}$ to rearrange. In the case of the hypothetical $H_2C{=}C{:}$, the barrier to rearrangement is only a few Kcal/mole [3.13]. The fragment is expected to contain a comparable amount of vibrational energy, and hence the rearrangement should occur easily. If the conjecture that energy partitioned into the vibrational degrees of freedom is proportional to the number of vibrational states available, then we would expect that the $F_2C{=}C{:}$ species would be born with a vibrational energy comparable to the $H_2C{=}C{:}$ species. Since the barrier to rearrangement for $F_2C{=}C{:}$ has been calculated [3.14] to be much greater than the few Kcal/mole needed for $H_2C{=}C{:}$, we concluded that the former species was born with a small amount of internal energy, insufficient to surmount the barrier for rearrangement.

The greater vibrational complexity of $(CH_3)_2C{=}C{:}$, compared to $H_2C{=}C{:}$ and $F_2C{=}C{:}$ should lead to a partitioning of a much greater fraction of the excess energy into the first-named species. This is graphically illustrated in Fig. 3-2, where the number of vibrational states available per Kcal/mole is plotted as a function of internal energy E_v. We

conclude from Fig. 3-2 that the enormous amount of "vibrational heat capacity" of $(CH_3)_2C{=}C{:}$ will sink much more excess energy than the other two vinylidene carbenes. What we observe chemically is that the dimethyl species sinks enough energy to surmount the barrier to rearrangement, which we estimate in Appendix B to be 10-15 Kcal/mole. From this we conclude that, in the absence of quantitative data to the contrary, energy partitioning amongst these LID products is consistent with simple statistical behavior.

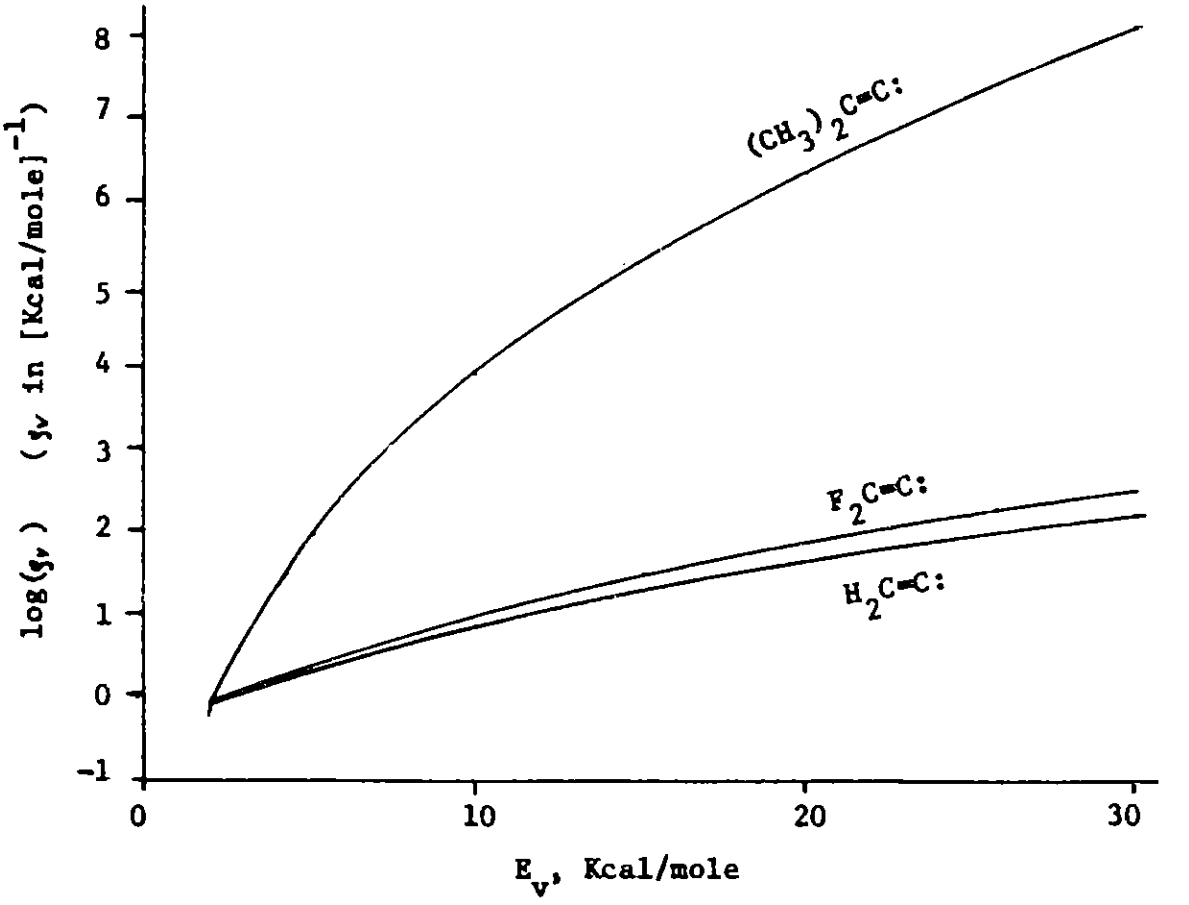

Fig. 3-2. Density of vibrational states per Kcal/mole as a function of the internal energy E_v. The expression for ρ_v used to calculate these curves is the same as that used in Appendix A:

$$\rho_v = \frac{(E_v + aE_z)^{s-1}}{(s-1)! \prod^{s} h\nu_i} \left[1 - \beta \frac{dW}{dE'}\right]$$

This is the Whitten-Rabinovitch density of states function*; the definitions of parameters E_z, E', a, β and W can be found in Appendix A; s is the number of vibrational modes having frequencies ν_i. The vibrational frequencies used in these calculations are contained in Table 3-2.

*G. Z. Whitten and B. S. Rabinovitch, J. Chem. Phys. 38, 2466 (1963)

Table 3-2. Vibrational frequencies used in the calculation of Fig. 3-2.

$H_2C{=}C$:	$F_2C{=}C$:	$(CH_3)_2C{=}C$:	parameter
3089	1795	1650	vibrational frequencies
3037	1680	420	
1612	1495	500	
1281	1410	1100	
1036	1205	1200	
897	840	1300	
		200	
		300	
		1150	
		1250	
		1450	
		200	
		1195	doubly degenerate vibrations
		1475	
		1471	
		1430	
		2964	
		2982	
1.0372	0.8753	1.2844	β
15.66	12.04	48.25	E_z, Kcal/mole
1.80 E19	6.43 E18	1.60 E73	$\pi\nu_i$, $(cm^{-1})^s$
6	6	24	s

These frequencies were obtained by reading absorption spectra of the parent molecule from standard IR spectra taken at MIT. Frequencies assigned to bands arising from =CCl-H and =C-Cl stretches and bends were then cast out.

4.1 Basic method

In the previous chapter we concluded that chemical evidence alone is insufficient to determine uniquely the distribution P(E) of molecules over energy produced in a MIRPA event. Additional experimental evidence, such as a determination of <E>, is required before quantitative statements can be made about the shape of P(E). In particular, a determination of <E> accurate to within a factor of two would be necessary to choose between Poisson and maximum entropy distributions for the trans-d_1-vinyl chloride system.

The difficulty of measuring <E> directly can be appreciated when one realizes where in the laser beam molecules that undergo transformation are located. In a weakly focused beam, intensities sufficiently high to cause MIRPA and consequent reaction are located at or near the focal point. The actual volume inside the beam which contains the reacting species may be very small [4.1] (typically 0.01 cm^3) compared to the total volume swept out by the beam inside the reaction cell (~100 cm^3). A measurement of the total energy deposited in the entire sample would not render a value of <E> for that small volume of reacting species because much of the energy is deposited in molecules in the lower intensity

portions of the beam and does not lead to LID.

What we seek is a method of determining the response of the system at particular fluences although our measuring technique renders the response over the entire fluence range intercepted by the sample. Since the intensity profile of a "TEM_{00}" Gaussian laser beam is known analytically for all points in the beam [4.2], it might be possible to deconvolute the data to reveal system response at discrete fluences (or intensities). The technique, in fact, has been elucidated by Kolodner et. al. [4.3] and by Reiser and Steinfeld (Appendix D) and has been used by Herman [4.4]. The reader is invited to read Appendix D to familiarize himself with Gaussian beam optics and to glean the salient mathematical details of the technique.

Basically, the deconvolution procedure relies on the fortuitously simple form of a Gaussian beam profile to unfold the response of the system analytically. Any given measurement using a Gaussian beam, for example, a measurement of total absorption, contains two kinds of information: that which determines the absorption at discrete fluences $\langle n \rangle(\phi)$ and the geometry of the fluence profile in the beam $\phi(x,y,z)$. By doing a series of experiments in which an appropriate parameter, such as the net energy per laser pulse, is systematically varied, the clever experimenter can effectively subtract the profile information $\phi(x,y,z)$ by taking the difference between adjacent points. The fortuitous nature of

the mathematical formalism allows us to use the local slope ∂(energy deposited)/ ∂(total pulse energy) and experimentally determinable constants to effect the "subtraction" of the Gaussian fluence profile. The simplicity of the procedure can be seen in the section entitled "Treatment of Experimental Data" in Appendix D.

Nearly any experimental effect which is fluence or intensity dependent can be studied with this technique, provided that the total response is detected over the entire portion of the laser beam intercepted by the sample. For determining $\langle n \rangle(\phi)$, transmission measurements may be difficult when the beam intensity is very large and energy deposition is small. Optoacoustic detection is a more appropriate method of measurement in this case, and has been used with Gaussian beam deconvolution of experimental data by Black et. al. [4.5].

Other effects can also be studied. The intensity dependence of multiple (visible) photon ionization could be determined by placing electrodes around the laser beam to measure net ionization current. Laser induced fluorescence or laser induced collisions could be studied provided that integrating optics are used to collect fluorescence from all portions of the beam. Nonlinear optical phenomena, such as frequency multiplying or mixing, could be studied in fine detail without the need to describe the input beam intensities by cross sectional averages.

4.2 Experimental difficulties

Since the deconvolution technique inherently relies on taking the slope of an experimentally determined curve, the precision of the deconvoluted data is severly affected by the precision of the original data. Small differences between large numbers can be quite noisy, and for this reason Black [4.5] fit his experimentally determined curve with a convenient algebraic function before taking the slope analytically. Generally a trick of this sort is always possible by fitting the observed data to an n-degree polynomial [4.6] which is guaranteed to have an easily determinable, continuous first derivative.

When the observed data are sparse, however, expermental precision ultimately limits the value of the deconvoluted data. As an example let us consider the energy depostion example used in Appendix D, i.e. multiple photon absorption in SF_6, when small uncertainties are imposed upon the "observed" data. In this case, a precision of a few percent in the measurement of the total energy deposited in the SF sample implies that deviations of a few percent from the observed value are statistically not meaningful. If a demon were to remove absorbing molecules from the focal point of the beam, where we are most interested in the absorption function $\langle n \rangle(\phi)$, such that the net energy deposited changed by only a few percent, our measurement would not be statistically different. In a qualitive way, then, we see that the

precision of the experimental determination limits the precision with which we determine $\langle n \rangle(\phi)$, which we translate into a geometrical volume. Uncertainty in the observed information implies uncertainty in the deconvoluted information.

We can use the numerical example of Appendix D to illustrate these statements graphically. Let us suppose that we performed an experiment using a 28 cm focal length lens to focus a pulsed CO_2 laser beam into a sample of SF_6, whose absorption is given by [4.5]

$$\begin{aligned} \langle n \rangle (\phi) &= 9.15\,\phi && 0 \leq \phi < 2.55 \\ &= 14.1(\phi + 0.084)^{1/2} + 0.51 && \phi \leq 2.55 \end{aligned} \qquad (4\text{-}1)$$

ϕ in J/cm^2

Using a simple convolution equation,

$$E_D \propto \int_{\phi_m}^{\phi_0} \langle n \rangle (\phi) \, v(\phi) \, d\phi \qquad (4\text{-}2)$$

where ϕ_m is a convenient lower bound of the fluence (taken to be 0.01 J/cm^2), ϕ_0 is the peak fluence (9.42 J/cm^2 for a pulse energy of 10 mJ) and $v(\phi)$ is given by Eqn. (24) of Appendix D appropriate for a 28 cm focal length lens, we can numerically compute the total energy deposited in the sample E_D. We then change the upper bound of Eqn. (4-2) so that the calculated energy deposited E_D' is, for example, 95% of E_D. This means that we have calculated the energy deposited throughout the beam except in the last small volume near the focal point. This volume $V(\phi')$ is easily calculated by Eqn. (16) of Appendix D; the energy deposited in this

volume $V(\phi')$ is equal to the precision of the determination of E_D . $V(\phi')$ is plotted against the precision in Fig. 4-1.

As we see in Fig. 4-1, if our "measurement" of E_D were infinitely precise, we could determine the $\langle n \rangle(\phi)$ for a vanishingly small volume of sample. As the precision degrades, however, the corresponding uncertainty in the geometrical information increases, so that the deconvoluted data will give the response $\langle n \rangle(\phi)$ averaged over the interval $\phi' \leq \phi \leq \phi_0$. Eventually this imprecision becomes unacceptable, for intance, when ϕ' reaches the threshhold fluence for dissociation, which is approximately 1 J/cm^2 for SF [4.7]. This point is marked with an arrow in Fig. 4-1. We conclude that only for highly precise measurements of E_D can the deconvolution technique be of value.

As is clearly stated in the "Treatment of Experimental Data" section of Appendix D, Gaussian beam deconvolution renders the average response $\langle n \rangle(\phi)$ over whatever distribution of molecules over absorbed energy $P(E; \phi)$ is formed when an ensemble of molecules is subjected to a uniform fluence ϕ . This technique can never give information about the shape of $P(E; \phi)$. The information obtained, such as $\langle n \rangle(\phi)$, must be combined with other data, such as data from LID experiments discussed in the previous two chapters, to obtain a clear understanding of the distribution P(E). Ideally one would like to measure P(E) directly, and for this we must turn to more elegant spectroscopic techniques, which

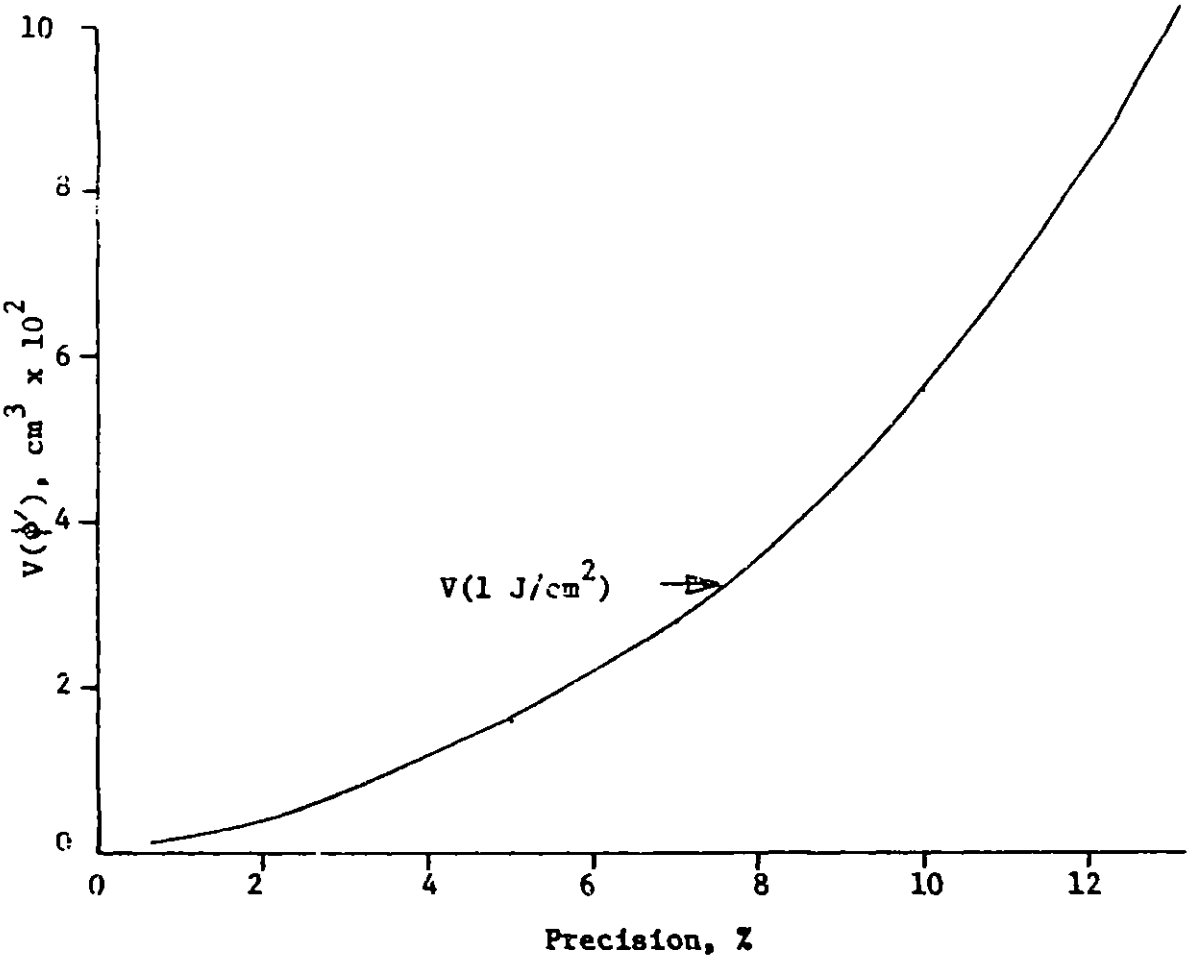

Fig. 4-1. Minimum volumes $V(\phi')$ discernable by deconvolution of a Gaussian beam for experiments of finite precision. Details of the calculation are given in the text.

we begin to discuss in the following chapter.

5.1 Introduction

Thus far in this thesis we have investigated MIRPA by studying net chemistry or net absorption in typical systems. The information obtained is necessarily an average over the range of fluence, intensity and time dependent processes which contribute to the net LID results. As we concluded in Chapter 3, chemical evidence alone is insufficient to elucidate the fine details of the dynamics of MIRPA events, even when aided by techniques such as Gaussian beam deconvolution.

Ideally we would like to understand the nature of the MIRPA phenomenon on a fundamental level. Specifically, we would like to answer such questions as by what route do the molecules absorb the first few photons, what roles are played by vibrational anharmonicity and by rotational compensation, how fast does rotational hole filling occur, at what energies does intramolecular vibrational relaxation become fast, and is there a good method of predicting pressure effects. Ultimately our goal would be the ability to predict the types of chemistry we expect from a particular system from fundamental spectroscopic evidence, given a reasonably general framework such as Fig. 3-1.

To answer the questions raised above one must directly interrogate molecules which are being subjected to the very

intense infrared laser fields used in MIRPA and LID experiments. This implies the use of a spectroscopic probe to monitor the molecular behavior during excitation by an intense pump field. Since in many systems used in LID experiments no easily accessible electronic states exist, visible probe radiation is of only limited usefulness. The technique of choice is infrared-infrared double resonance, wherein the infrared spectroscopic probe monitors vibrational populations affected by the application of the infrared pump field.

This technique was first used by Steinfeld and coworkers [5.1], who used two CO_2 lasers as pump and probe beams in SF_6. This work and that of others [5.2] was restricted to probing at the small number of discrete frequencies to which CO_2 lasers can be tuned. The use of a tunable narrow linewidth diode laser has vastly increased the spectroscopic information gained by the double resonance technique, as has been demonstrated by Moulton and Mooradian [5.3]. Our own work on diode-infrared laser double resonance (DILDOR) in SF_6, begun by Jensen [5.4], has been reported and is included in this thesis as Appendix E, which the reader is urged to peruse.

The present DILDOR experiments are designed to probe the absorption dynamics of the first one or two photons. The interaction of the pump field with individual absorption features can be easily monitored, and a wealth of dynamical information has been recovered. The salient features of the experimental apparatus, procedure, results and discussion are

contained in Appendix E. To avoid repetition, experimental details not mentioned in Appendix E, results on DILDOR in ammonia, and further discussion of a few details of data interpretation will form the bulk of this chapter.

5.2 Experimental details

Working with a diode laser can be a very tedious and aggravating experience. As is mentioned in Appendix E, diodes must be kept cold to insure their survival, although they must be warmed to room temperature periodically. As air leaks into the cold head vacuum jacket, a gradual temperature rise can be noticed over a period of weeks. When the temperature reaches 15-20 ^{o}K, the cold head must be warmed (to insure that moisture will be removed), evacuated and rechilled. Care must be taken to avoid backstreaming pump oil into the cold head.

Occasionally the cold head will "ratchet" upon startup, producing a grunting noise. This is an indication that a foreign substance, such as dust or moisture, has found its way into the helium flow and is lodged in the cold head. Replacing the helium in the cold head after disconnecting it from the refrigerator is the only known cure, short of having the cold head rebuilt.

To date no means of detecting the diode beam other than with a cryogenically cooled semiconductor detector has been found. If the diode beam is found, it must be traced around the table using apertures to reveal the beam position. A HeNe

laser beam can be superimposed on the diode beam to act as a tracer, but usually the diode beam must be traced with an iris after the first two mirror reflections. The HeNe beam can then be used to trace a path to the remaining mirrors, through the monochromator and onto the detector.

Once the diode beam is routed through the monochromator, a series of scans must be made to determine the frequencies over which the diode lases. This is a rather tedious operation; it involves systematically changing the diode temperature, while making a current scan with the monochromator slits wide (about 2 mm), moving to a different monochromator setting, scanning again, etc., for each temperature. A range of currents and temperatures can then be selected to determine if the laser has a mode at the precise frequency desired.

An important diagnostic at this point cannot be overlooked. It is mandatory that an etalon scan must be made when a mode is located at the correct frequency. Many times the mode is not "pure", that is, it contains two modes at nearly the same frequency which tune in unison. Often a mode may "hop", or jump to another frequency, so that a continuous current scan is not continuous in frequency. The etalon fringes are currently the only method we have to interpolate between reference frequency absorption lines.

A disturbing feature in the present system is the current ripple in the scanning current power supply, an Arthur D.

Little TDLS-II. This ripple was measured to be approximately 0.15 mA peak to peak. A typical diode mode tuning rate of 0.12 etalon fringes/mA (one fringe equals 0.05 cm^-1), the measured ripple implies a peak to peak frequency jitter in the diode mode of 26 MHz. This will be an important consideration in the following chapter.

Care must be taken to avoid grounding either of the recorder output jacks on the TDLS-II. For this reason, the variable dc offset voltage supply has been floated from ground. This supply is placed in series with the recorder output voltage. In this way, tuning ranges of a few hundred mA can be recorded using the entire useful X-scale range of the X-Y recorder. The variable dc voltage supply effectively extends the range of the "zero" knob on the recorder.

Several features of the Q-switched CO_2 laser must be noted. The optimum mixture of gases is approximately 4:1:1 for He, CO_2 and N_2 respectively, at a total pressure of 8 Torr. Dirt which collects on the ZnSe windows is most easily removed by applying water and Pex detergent with cotton. Effective c.w. power at a repetition rate of 125 Hz is typically 300 mW for the 10.6 micron P(18) line; we have measured a c.w. output on this line in excess of 30 Watts.

The diameter of the Q-switched beam is easily measured with a variable aperture. A power meter is placed behind an iris diaphragm mounted on an X-Y translation stage. The iris is placed over the center of the beam. The power transmitted

through the iris is then measured by the power meter as a function of the iris diameter. This function can be compared to the known [5.5] transmittance of a Gaussian beam of spotsize ω through an aperture of diameter d,

$$\text{fraction transmitted} = 1 - \exp(-d^2/2\,\omega^2) \qquad (5\text{-}1)$$

In this manner, the spotsize of the Q-switched beam was found to be 2.5 mm for the work reported in Appendix E.

It is possible to align the pump and probe beams so well that they cannot be separated at the cold head (see Fig. 1 of Appendix E). A 1° misalignment is sufficient to effect the required separation. A gold coated mirror is necessary to eject the Q-switched beam from the apparatus; mirrors of lower quality cause unwanted scattering. Stray reflections of the pump beam have caused serious frequency and intensity fluctuations in the diode beam; the amount of care required to minimize stray reflections cannot be overstressed. For example, the pump beam must strike mirrors in the center (which necessitates, in some cases, placing the probe beam near the mirror edges) to avoid reflections from the mirror edges and mounts.

Synchronization of the boxcar integrator with the laser pulse is accomplished with the circuit shown in Fig. 5-1. Trigger jitter is minimized when the negative-going trigger pulse occurs 15-30 μsec before the laser pulse. Generally it is impossible to keep this interval constant before 7 PM on

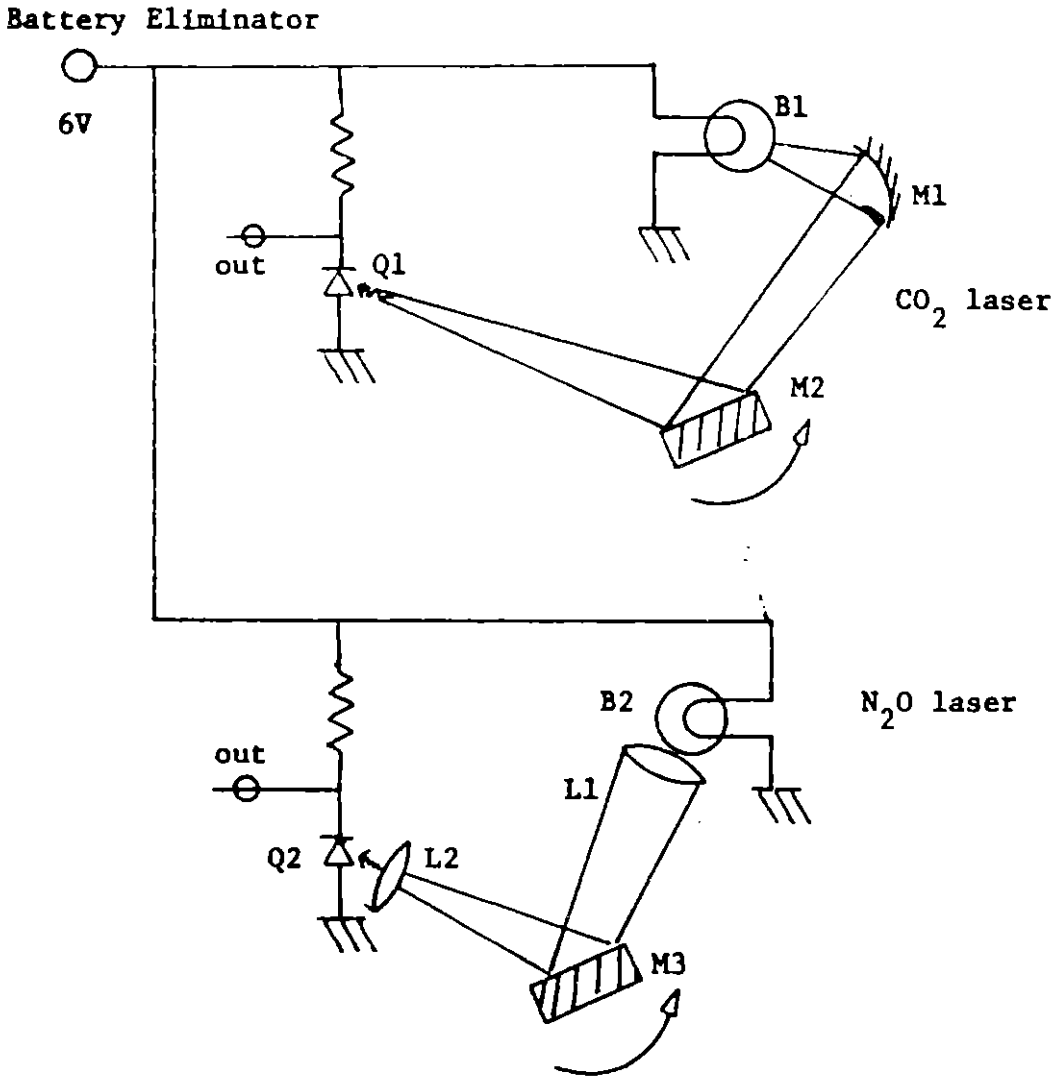

Fig. 5-1. Circuit diagram and optical configuration for Trigger pulses from the Q-switched CO_2 and N_2O lasers. Q1, Q2 - phototransistors; B1, B2 - 6V light bulbs; M1 - concave mirror; M2, M3 - rotating mirrors; L1, L2 - lenses.

weekdays. Apparently the speed of the mirror motor changes slightly with changes in wall socket voltage even though a massive voltage regulator is used to power the motor. Tweaking the grating alignment and minimizing the delay between trigger and laser pulses may help.

Brewster windows and grating lines insure that the pump field is horizontally polarized. Although polarization may not be the same for all diode lasers, diode beams are usually well polarized in the plane of the junction [5.6], or vertically polarized in the lab frame. This is not mentioned in Appendix E, and may have considerable impact on DILDOR signals. It will be discussed further in the following chapter.

5.3 Additional discussion

All of the SF_6 DILDOR spectra worthy of note are contained in the various figures of Appendix E. All spectra were taken with the same diode laser (now dead) in the same mode. This mode, the SF_6 spectrum inside it, and the assignments of the lines (courtesy of Dr. R. S. McDowell of the Los Alamos Scientific Laboratory) are exhibited in Fig. 5-2.

With the aid of hindsight, after completing the calculations to be presented in the following chapter, a few of the finer points of discussion in Appendix E should be reviewed. One of these points pertains to the field-induced

Fig. 5-2. Absorption spectrum of 0.08 Torr SF_6 in a 30 cm long cell. Top trace shows diode laser mode tuning curve (no cell in beam path). Lower trace shows etalon scan for a 1" Ge etalon (f.s.r. = 0.0499 cm^{-1}). Assignments courtesy of R. S. McDowell of Los Alamos. Frequency markers in cm^{-1} are shown at the bottom of the graph.

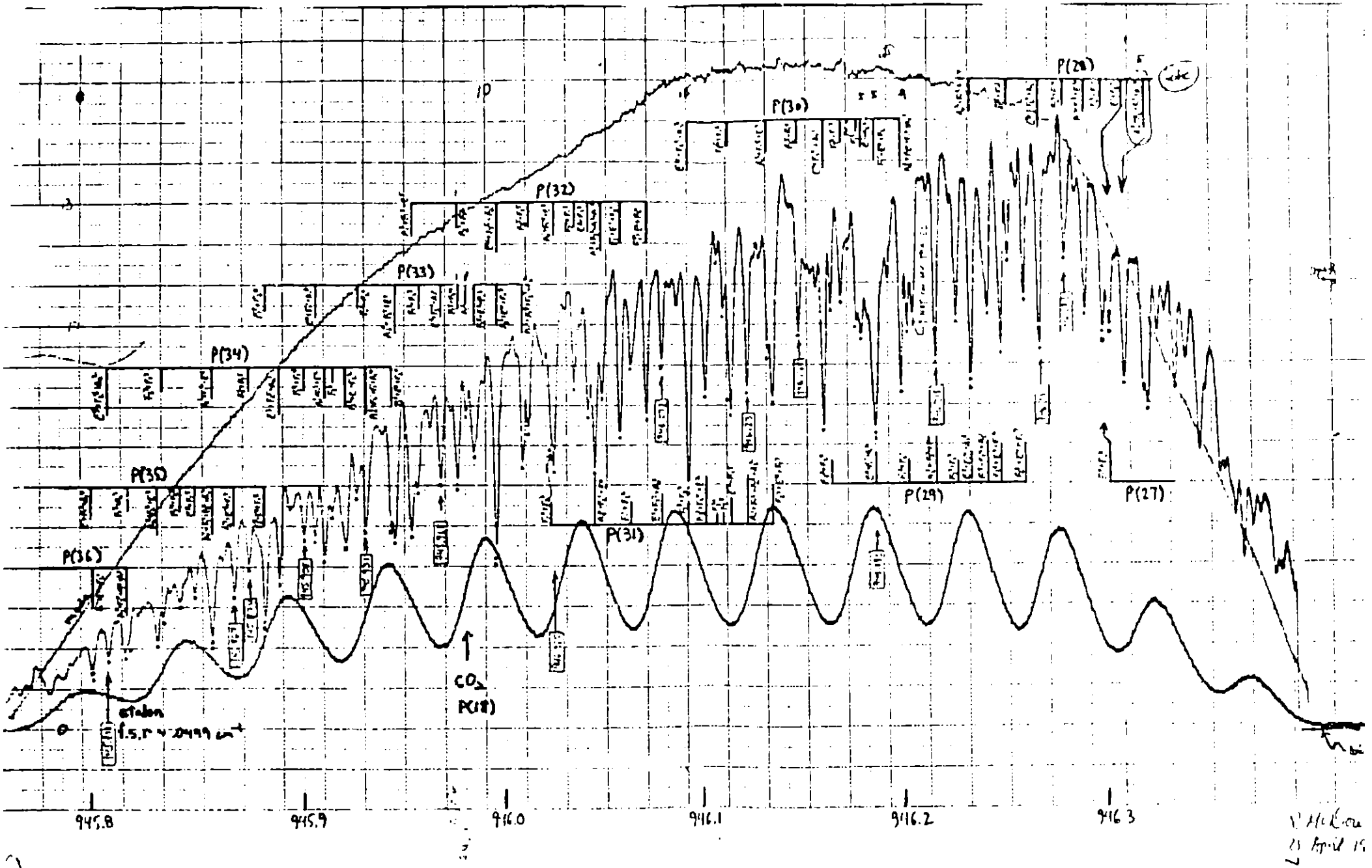
P(28)
P(30)
P(32)
P(33)
P(34)
P(35)
P(36)
P(31)
P(29)
P(27)
CO_2
P(18)
945.8
945.9
946.0
946.1
946.2
946.3

mixings which supposedly were responsible for the satellite structure around the main feature of the 2-level double resonance (2LDR) and 3-level double resonance (3LDR) spectra (see Figs. 2 and 7 respectively in Appendix E). As we will show in Chapter 6 and Appendix H, these mixings do not explain the satellite structure. The matrix elements which are responsible for the "weak transitions" in SF_6 [5.7] do not play the significant role originally believed in Appendix E. This will be placed on more quantitative footing in the following chapter.

Up to now, collisions were not thought to be important within the 0.5 μsec time scale of these experiments. This may not be entirely correct, given that the rotational relaxation time of the 3LDR signal, $\tau_{3\text{-level}}$, was measured to be 0.54 μsec. Since this represents the time required for a 1/e refilling of the population of a single rotational state, collisions effecting rotational relaxation are seen to operate on precisely the time scale of the experiment. Hence, a detectable amount of rotational relaxation should occur within the time of the boxcar gate.

This conjecture is born out by the 4-level double resonance (4LDR) recorded by Jensen, which appears in Fig. 9 of Appendix E. In these spectra, SF_6 was pumped in the P(33) and P(32) manifold while the probe interrogates the R(45)-R(52) manifolds. Extensive signal is seen even at "zero" delay with respect to the laser pulse; one microsecond

later, rotational relaxation has depleted the entire J=45 to J=52 region. Thus, collisions are seen to change J by 10 to 15 quanta at a very rapid rate. One must assume that relaxation within a single J manifold in the ground state, where all K are nearly degenerate, occurs on a similar time scale, if not faster.

One must be clever enough, however, to avoid the implication that relaxation out of or into levels directly pumped by the laser occurs exclusively to the nearly isoenergetic levels which are also probed. It seems more likely that relaxation occurs by exchange of energy with a rotational "heat bath" in a process like that depicted in Fig. 10 of Appendix E. This "heat bath" is composed of molecules not pumped by the laser, including the ~60% of the total room temperature population lying in hot bands, and ground state molecules having J far from the J's resonant with the pump laser. When a depleted ground state rotational level is filled, the population comes largely from the "heat bath" and not from nearby levels exclusively. Steinfeld and coworkers [5.11] used this model to explain their early work in SF_6.

A stringent test of the collisional nature of this relaxation process would be to repeat the experiments at lower temperatures, where collision rates are lower. A corresponding increase in $\tau_{3\text{-level}}$ should be observed, as well as an absolute decrease in 4LDR activity in J manifolds far from resonance. These experiments are currently under way.

5.4 DILDOR attempts in NH_3

Microwave-infrared laser double resonance [5.8] has been observed in NH_3 using the N_2O P(13) laser line at 927.739 cm^-1, which is nearly resonant with the $^{14}NH_3$ ν_2[$^qQ_-$ (8,7)] transition and the N_2O P(15) line at 925.979 cm^-1, which is 332 MHz lower than the $^{15}NH_3$ ν_2[$^qQ_-$ (4,4)] transition. This suggests that a 2-level DILDOR might be observable as well. This system has the advantage that the lineshape of a single absorption feature may be recovered without the forest of interfering structure seen in SF_6.

A Q-switched N_2O laser was resurrected with the help of Tom Anderson and pressed into service. Its configuration is nearly identical to that of the Q-switched CO_2 laser, excepting that a 4.25 m radius rotating mirror is used (instead of 10 m radius). Details of its operation have been placed in Appendix I. Since this laser operated at 50 Hz and has less gain that the CO_2 laser, the usual power meter could not be employed to measure the average pulse power. Using a Gen Tec joulemeter, the total pulse energy was estimated to be 0.1 mJ; a typical c.w. output is 2-3 W (as compared with 30 W for the CO_2 laser). From this we estimate that the average pulse intensity is about a factor of ten lower than its CO_2 counterpart.

The experimental schematic is shown in Fig. 5-3. Aside from using the N_2O laser as a pump source, all other features of the apparatus are essentially the same as for DILDOR in

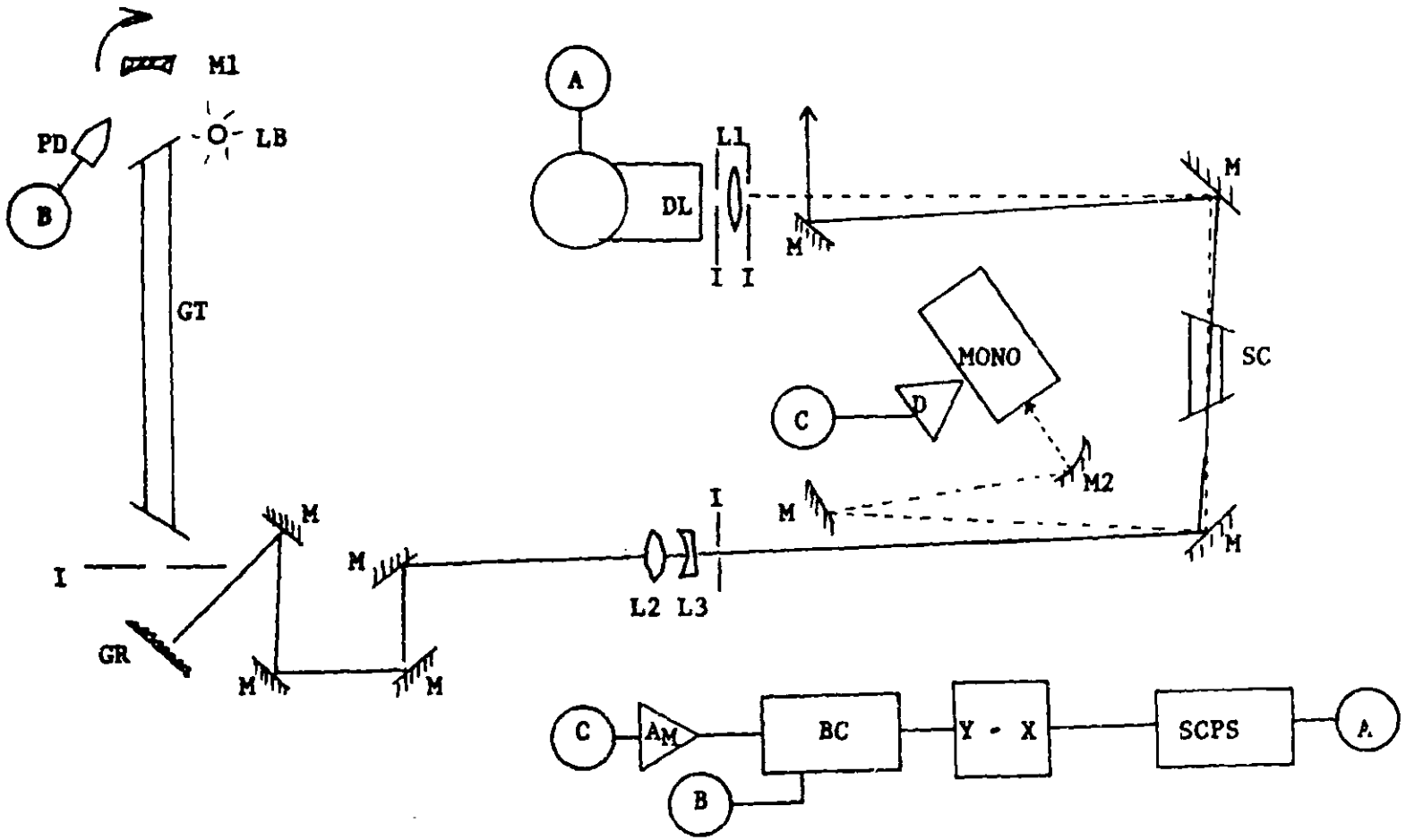

Fig. 5-3. Schematic of the apparatus used for N_2O laser-diode laser double resonance in NH_3. SCPS - scanning current power supply ; DL - diode laser; I - irises; L1 - 5 cm f.l. collimating lens; M - flat gold coated mirrors; M1 - spinning 4.25 m radius mirror; M3 - paraboloid collecting mirror; MONO - monochromator; D - Hg:Cd/Te detector; AM - amplifier; BC - boxcar integrator; Y - X denotes axes of the x-y recorder; GT - 1.5 m gain tube; GR - grating; LB - light bulb; PD - photodiode. Electrical signals: A - diode laser current supply; B - trigger pulse; C - detector output.

SF_6. Addition of collimating lenses was necessitated by the greater divergence of the N_2O laser beam. Intensities in the sample cell reached ~1 kW/cm^2.

That the N_2O P(13) line is very nearly resonant with the NH_3 (8,7) feature is clearly evident in Fig 5-4; Shimizu and Oka [5.8] estimate that the line centers are 10 MHz apart. Records of DILDOR in 1 Torr of NH_3, however, were disappointingly blank and showed no apparent signal above the noise level, as can be seen in Fig. 5-5. Several attempts were made and all met with a similar degree of success.

One may wonder why DILDOR was not successful when the microwave experiment was. A few calculations and the hindsight gained from the lineshape analysis presented in Chapter 6 can show that the DILDOR signal may be smaller than the noise recorded in Fig. 5-5. Since the dipole moment for NH_3 is 0.2 Debye [5.8] and the pump laser power is one tenth of that used for the SF experiments, we can estimate that the Rabi frequency Ω,

$$\Omega = \frac{\vec{\mu} \cdot \vec{E}}{2\sqrt{3}\,\hbar} \qquad (5\text{-}2)$$

where $\vec{E}$ is the electric field vector, was at least a factor of six smaller than in the SF_6 experiments. From the lineshape modeling of the SF spectra (detailed in Chapter 6), Ω for the NH_3 experiment should be 10-15 MHz.

An estimate of the homogeneous linewidth can be had by considering the hard-sphere collision rate [5.9] for NH_3 at 1

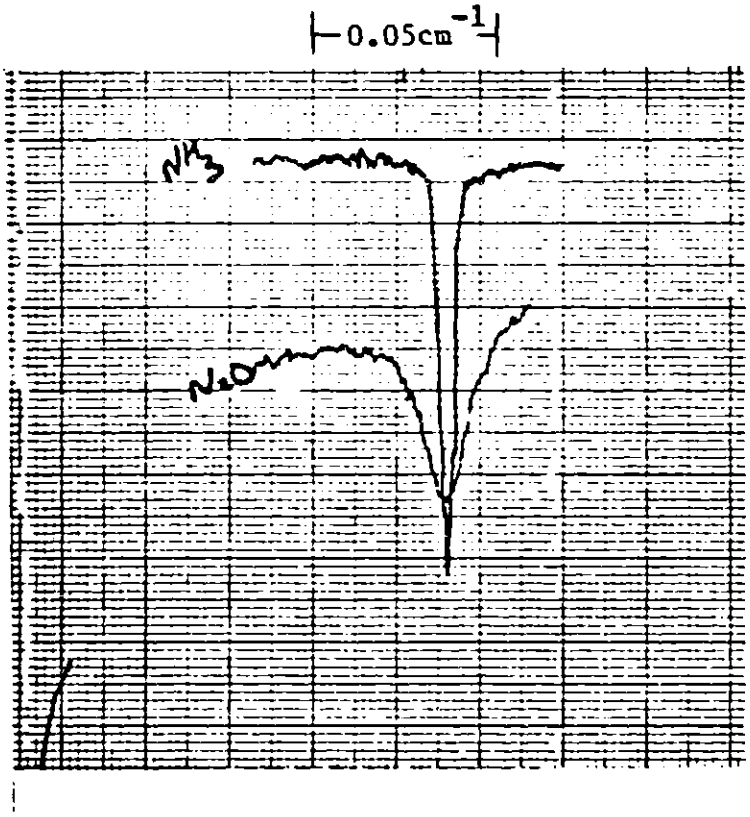

Fig. 5-4. Absorption (downward deflection) of 40 Torr N_2O in a hot cell in the region of the P(13) laser line (lower trace). Also shown is the feature $\nu_2[^qQ_-(8,7)]$ in 1 Torr of NH_3 (upper trace). Diode current and frequency increase to the right.

Fig. 5-5. DILDOR attempts in NH_3 using an N_2O laser. Absorption trace (a) was taken in 1 Torr of NH_3 over the same transition as shown in Fig. 5-4. Two DILDOR scans were then made, traces (b) and (c). Finally, trace (d) was recorded (absorption again) to indicate the amount of drift in the diode laser tuning curve. In (a) and (d), absorption is a downward deflection; in (b) and (c), downward deflections would correspond to transient transparency, or saturated absorptions.

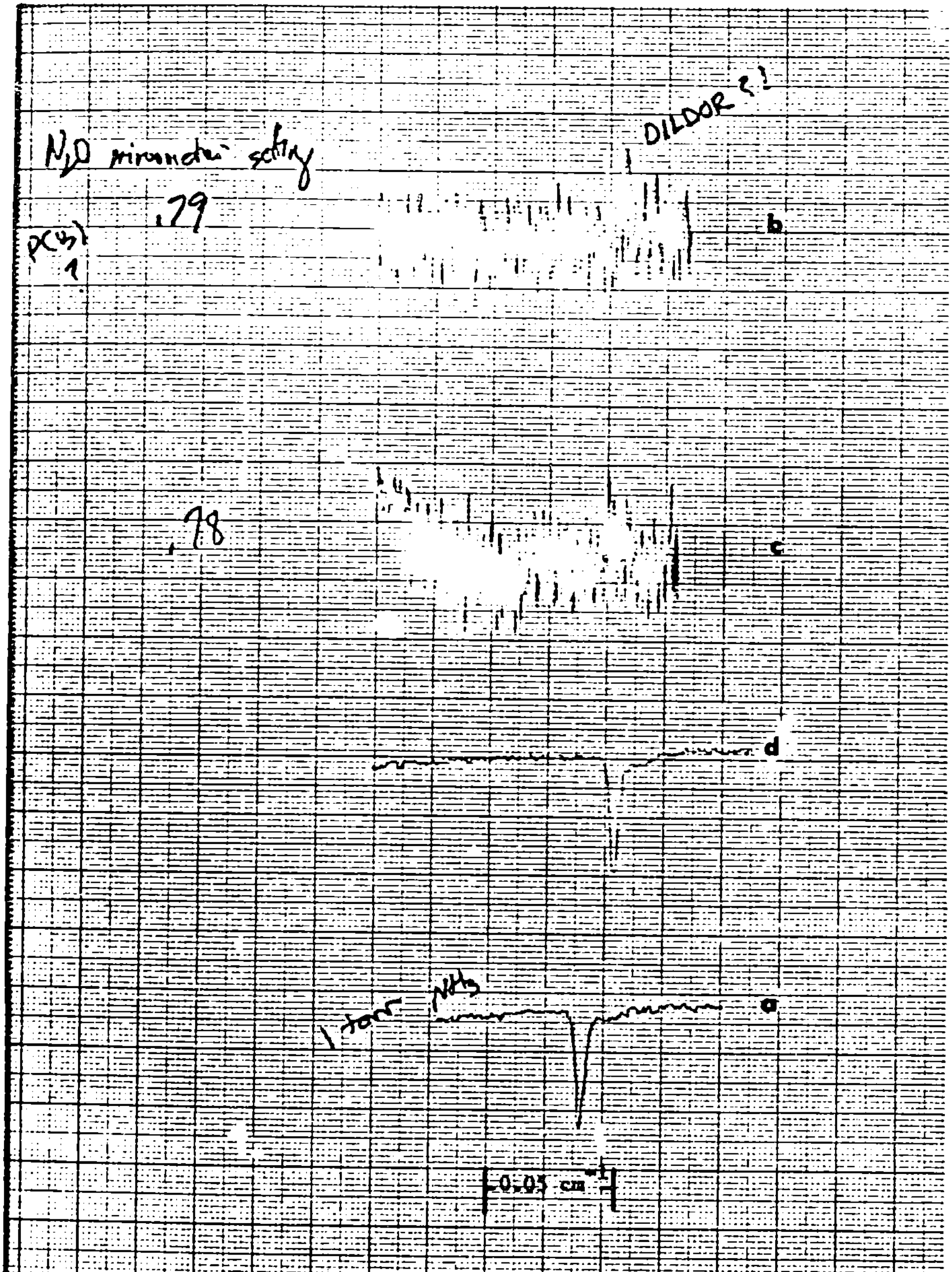
DILDOR ?!
.79
.78
b
c
d
a
1 torr NH3
0.05 cm-1

Torr,

$$z = 4d^2 \cdot \sqrt{\frac{kT}{m}} \quad \frac{N}{V} \qquad (5-3)$$

which renders, for diameter d = 4 Angstroms at room temperature,

$$z \cong 15 \text{ MHz}$$

For comparison, the Doppler width of the transition is 40 MHz FWHM [5.8]. From these estimates, we conclude that the pump laser intensity in this case is sufficient to saturate only a single velocity group of the entire Doppler contour. This velocity component is 10 MHz from line center, where the Doppler profile is down to ~60% of its peak value. Furthermore, the effective linewidth of the probe laser will be estimated in Chapter 6 to be greater than 50 MHz in some cases. It can be assumed, then, that at best only a small fraction of the entire Doppler contour was saturated and that the probe laser resolution was probably not great enough to resolve the "hole" burned into the Doppler contour. Higher pump laser power and greater probe resolution are necessary for the success of this experiment.

The microwave experiment, on the other hand, does not suffer from wide probe frequency jitter or wide Doppler contours. Since the Doppler width of the probed 3LDR transition in this case is much smaller than the pressure broadening, any saturation of the infrared transition will

appear as a decrease in the total intensity of the microwave feature being probed. The experiment was also accomplished with a c.w. laser, thus making the experimental duty cycle much more efficient and signal to noise much greater than in the DILDOR experiment.

5.5 Improvements for future experiments

Several improvements in the existing apparatus could be made at minimal cost and effort. Firstly, a new grating for the monochrometer, one blazed for 10 μ operation, would boost the throughput of the device by a factor of 2 or 3. The grating currently in use is blazed at 3 μ and is working in third order.

Determination of the polarization of the diode beam can be easily done with a pile of plates polarizer. These plates can be Brewster angle salt windows, which are inexpensive and easy to handle.

Copropagating instead of counterpropagating beams might be a preferable geometric arrangement. Using copropagating beams, the pump laser is not aimed directly into the diode laser, and the effects of the pump laser on the probe laser mentioned in section 5.2 would be minimized. This arrangement will be discussed further in the following chapter.

Gross vibration of the diode laser itself can be minimized by using a very rigid mount instead of the rotatable

mount currently in use. Vibrations of the cold head caused by the 3 Hz motion of the displacer assembly it contains cause intensity (and probably frequency) fluctuations at the detector easily seen with lock-in detection.

Major improvements in design would require a larger investment. Specifically, a fraction of the probe beam should be split off for use as a measure of incident intensity for absorption spectra. In DILDOR scans this beam could be used to monitor the frequency of the probe by recording an appropriate reference spectrum simultaneously with the DILDOR spectrum. This would minimize the effects of scan-to-scan drift in the current tuning curve of the diode laser. This configuration, of course, necessitates the use of a second detector and phase sensitive detection electronics, as well as a good quality beam splitter. A multipen recorder would be necessary to record the detectors' responses simultaneously.

An electro-optic Q-switch for the pump laser would decrease pulse-to-pulse intensity variations and trigger jitter for the boxcar integrator. Electrical pickup from the high voltage pulses necessary to drive the device might be a major problem, however. Additional optical elements may be necessary to squeeze the resonator mode through the relatively small aperture of a currently available device. Pulse rates approaching a KHz could be realized, however, thus reducing the clock time required to recover a DILDOR spectrum by a factor of 3 or so.

The TDLS-II scanning current power supply should be replaced with a unit having much less hum in the diode laser current supply, if available.

6.1 Introduction

In the last chapter, the experimental results of two types of double resonance (DR), 2-level and 3-level, were reported. Spectra were recorded for pump powers ranging from 8.8 to 11.2 kW/cm^2, and, at the highest pump power, at different times during the 700 nsec long pump pulse. The spectra exhibited structure thousands of MHz from the CO_2 laser pump frequency, and the central feature grew broader with increasing pump power. From this, a rough estimate of the dipole matrix element was made; it was found to be in reasonable agreement with the theoretical estimate of Fox [6-1].

In both the 2-level and 3-level spectra, the satellite structure appeared to be asymmetrical around the pump frequency, showing more activity to the red of the pump. In fact, all absorption features within the J manifold of the most nearly resonant line showed activity. Since this activity appeared within the first 200 ns of the pump pulse, collisional relaxation was ruled out as the cause. Instead, an unspecified off-diagonal matrix element in the full SF_6 vibration-rotation Hamiltonian was invoked, which mixes the nearly degenerate ground state K levels (clusters) [6-8]. In this manner an entire J manifold could exhibit DR structure when only a few lines are directly pumped.

In this chapter, the assertions and conclusions mentioned above will be subjected to quantitative test. In particular, we will explore all terms in the molecular Hamiltonian capable of producing K state mixing, contemplate the effects of laser polarization, utilize the lineshape expressions of Mollow [6-2, 6-3] and of Hänsch and Toschek [6-4], include double resonance of the background hotband continuum, and reconsider the effects of collisions on the lineshapes reported in Appendix E.

6.2 Lineshape expressions

6.2.1 2-level spectra

For the moment we will ignore possible mixings between SF_6 cluster states and consider what lineshapes we would expect if the observed signals were merely a series of individual 2-level systems. The theory for these lineshapes is well understood; we will use the formalism of Mollow [6-2] which has been tested experimentally [6-3] by using a sodium beam as an ensemble of 2-level atoms.

Using the same notation of [6-2], the absorption lineshape W' of probe beam is given by

$$W'(\nu) = \frac{\pi\Omega^2}{2} \frac{\kappa(\kappa'^2 + \Delta\omega^2)}{\kappa'\Omega^2 + \kappa(\kappa'^2 + \Delta\omega^2)} \frac{AC + BD}{C^2 + D^2} \qquad (6\text{-}1)$$

where

$$A = \kappa\kappa' + \Delta\nu\Delta\omega - \Delta\nu^2 + \Delta\nu\Delta\omega\Omega^2/2(\kappa'^2 + \Delta\omega^2)$$

$$B = \kappa(\Delta\omega - \Delta\nu) - \Delta\nu\kappa' + \Omega^2\Delta\nu\kappa'/2(\kappa'^2 + \Delta\omega^2)$$

$$C = \kappa\kappa'^2 + \kappa(\Delta\omega^2 - \Delta\nu^2) + \kappa'(\Omega^2 - 2\Delta\nu^2)$$

$$D = \Delta\nu(\Delta\nu^2 - \Delta\omega^2 - 2\kappa'\kappa - \kappa'^2 - \Omega^2)$$

In (6-1), Ω and Ω' are the Rabi frequencies for the pump and probe beams respectively, κ and κ' are the longitudinal and transverse relaxation rates respectively. The Doppler correction of (6-1) can be made by simply replacing the pump detuning $\Delta\omega$ and the probe detuning $\Delta\nu$ with

$$\begin{aligned} \Delta\nu &\rightarrow \Delta\nu\left(1 - \frac{v}{c}\right) \\ \Delta\omega &\rightarrow \Delta\omega\left(1 + \frac{v}{c}\right) \end{aligned} \qquad (6-2)$$

and numerically integrating over an appropriate distribution of molecular velocities:

$$W'' = \oint W'(\Delta\nu, \Delta\omega \; ; \; v) \exp(-mv^2/2kT) \, dv \qquad (6-3)$$

Note that only a one-dimensional representation of the molecular velocities need be considered, that being along the axis of propagation common to both laser beams. In (6-2) the Doppler contributions are opposite in sign due to the counterpropagating geometry of the experiment.

Since the boxcar integrator is AC coupled, it actually integrates any difference in diode beam transmittance when the gate is open. That is, the signal is proportional to the amount of change in probe beam transmittance when the pump laser fires. Hence, to model our spectra, we must subtract from (6-3) the probe transmittence lineshape with no pump field present, which is simply a series of Voigt profiles.

Many authors [6-5] have studied three-level systems similar to ours. Because of its facile adaptation to this particular case, we will follow the method of Hänsch and Toschek [6-4].

We start from Eqn. (30) of [6-4] (which contains a typographical error not preserved here),

$$\chi = \frac{|p_{bc}|^2}{\hbar} \frac{(\rho_{bb}-\rho_{cc})(\Delta_{ab}\Delta_{ac}-|\beta'|^2)-(\rho_{aa}-\rho_{cc})|\beta|^2}{\Delta_{ab}\Delta_{bc}\Delta_{ac}-\Delta_{bc}|\beta|^2-\Delta_{ab}|\beta|^2}$$

where p_{jk} is the dipole matrix element between states j and k, ρ_{kk} is the diagonal Bloch matrix element for level k, and χ is the susceptibility. The remaining variables will be explained below. We can quickly make a few simplifying assumptions appropriate to our system: 1) all $\gamma_{\alpha\beta}$, which are the relaxation rates of optical coherence, analogous to Mollow's κ', are equal; 2) all γ_α, the spontaneous decay rate of level α, are equal; 3) the probe is weak and strictly counterpropagating to the pump. Using these approximations, the probe absorption coefficient α, analagous to Mollow's W', can be expressed as

$$\alpha = \frac{\pi|k'||p_{bc}|^2}{\hbar} \frac{AR(\delta+\Delta\omega)\gamma'-B(R\{\Delta\omega\delta-\gamma'^2\}-\beta^2\{1-2R\}}{A^2+B^2} \qquad (6\text{-}4)$$

where in this case $A = -\delta(\Delta\omega\Delta s+2\gamma'^2) - \Delta\omega\beta^2$; $W = \beta^2(2\gamma'/\Delta\omega^2+\gamma'^2)$

$B = \gamma'(\delta^2-\beta^2-\Delta\omega\Delta s-\gamma'^2)$; $\delta = \Delta\omega - \Delta s$

$R = 1 - W/\gamma+2W$

It may be useful to make the following correlations between Mollow's notation and that of (6-4)

$\Delta\omega \leftrightarrow \Delta\omega$ $\qquad$ $\beta \leftrightarrow \Omega$

$\Delta s \leftrightarrow \Delta\nu$ $\qquad$ $\gamma \leftrightarrow \kappa$

$\alpha \leftrightarrow W'$ $\qquad$ $\gamma' \leftrightarrow \kappa'$

Doppler broadening can be included by use of (6-3).

6.2.3 Broadening Mechanisms

Equations (6-4) and (6-1) give theoretical lineshapes for perfect beams. In practice, many dynamic imperfections are encountered, such as variation of probe intensity with frequency (PI), "instrumental" broadening (IB) of probe linewidth and frequency jitter caused by current supply hum and temperature wiggle, pump frequency jitter (PJ), and pump power variations during the boxcar gate (PP). PJ is at most the approximately 30 MHz width of the CO_2 laser gain profile, and will not drastically affect lineshapes hundreds of MHz away. Lines close to the pump will be totally saturated at the Rabi frequencies used, hence we will disregard PJ.

Since the absolute amount of DR signal is proportional to the incident probe intensity, the probe intensity profile was fitted to a convenient function of frequency. The shape of our diode laser mode peaked in the SF_6 P(29) manifold, which tended to accentuate lines to the blue of the pump frequency.

This function was included in the integration of (6-3). The apparent asymmetry of the 3LDR spectra is caused by the shape of the mode which drops severely in intensity to the blue of the main feature.

IB contributed by far the greatest source of broadening, although none of the factors contributing to this ad hoc effect were quantitatively known. It was assumed that the "perfect" spectra, including the absorption spectrum itself, could be averaged about a particular frequency ν to find the observed signal at ν. The average was taken to be Gaussian about ν with a variable width. The need for this broadening is apparent in Fig. 3 of Appendix E, wherein the observed linewidths are much broader than the Doppler width (28 MHz FWHM) at room temperature. For comparison to spectra shown below, an unbroadened 2-level spectrum is shown in Fig. 6-1.

Pump power fluctuations during the 0.5 μsec gate can be estimated from the contour of the laserpulse, which is shown in Fig. 6 of Appendix E. Spectra were calculated for the appropriate Rabi frequencies, and added together as an approximation to the integrating effect of the boxcar. As will be seen, PP proved to be a small effect.

6.2.4 Method of calculation

Each spectrum was calculated in a three step process. First, the absorption features in the diode laser mode were catalogued, and a single resonance spectrum calculated.

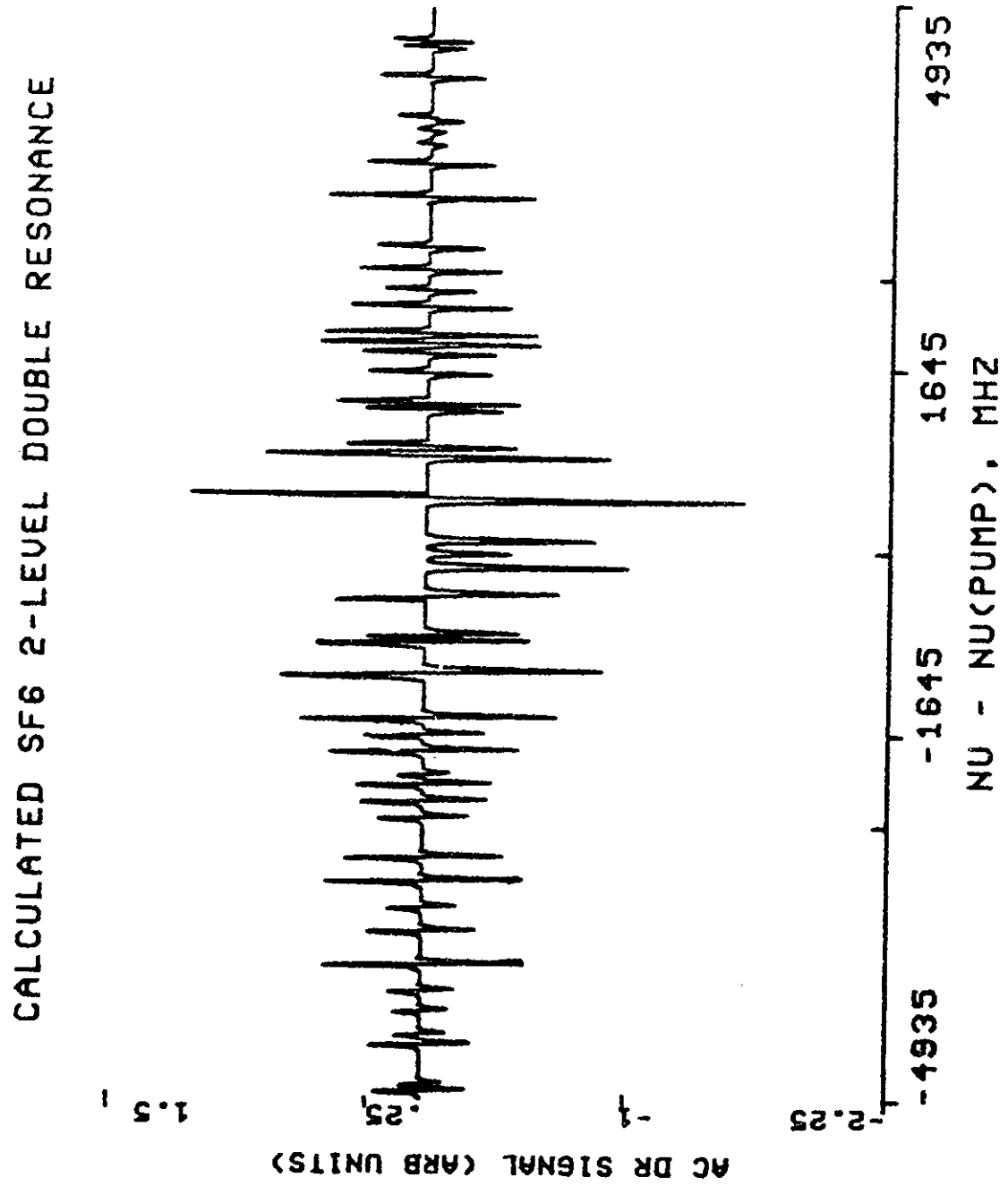

6-1. Calculated 2LDR signal in SF_6 using $\Omega = 230$, $\kappa = \kappa' = 3.6$, and Doppler width FWHM = 28 (all in MHz). No broadening has been included.

Absorption features near the CO2 P(14) laser line were similarly catalogued from published spectra [6-7]. Next, lineshapes (6-3) were calculated using the Rabi frequency as a parameter. Finally, the difference or AC spectrum was broadened according to the methods outlined above. For the 2-level case, appropriately weighted hotband lines spaced every 10 MHz were included as an approximation to the continuous background absorption. The weighting of these lines was chosen so as to predict most closely the absorption spectrum at room temperature. A portion of the calculated absorption spectrum, which includes background lines and probe intensity correction, is shown in Fig. 6-2.

Calculations were accomplished in BASIC on a DEC MINC (LSI 11/2) computer at MIT (by CR), which required large stretches of calendar time, and independently in FORTRAN at Los Alamos (by Hal Galbraith). After a spectrum was calculated, it was scaled and compared to the digitized observed spectrum. In this manner a "best" set of parameters was found for both 2-level and 3-level calculations. Finally, worthy spectra were plotted on a Houston Instruments HIPLOT digital plotter. A typical MINC run required 14 hours to compute ten spectra.

The constants κ and κ' were taken to be equal in the strong collision limit. Patel and Slusher [6-6] have found that

$$T_2' = 22 \text{ nsec} \cdot \text{Torr} \equiv 1/\kappa' \qquad (6\text{-}5)$$

6-2. Calculated SF_6 absorption spectrum near the CO2 P(18) laser line at 945.9802 cm^-1. Background absorption has been included and IB FWHM = 38 MHz.

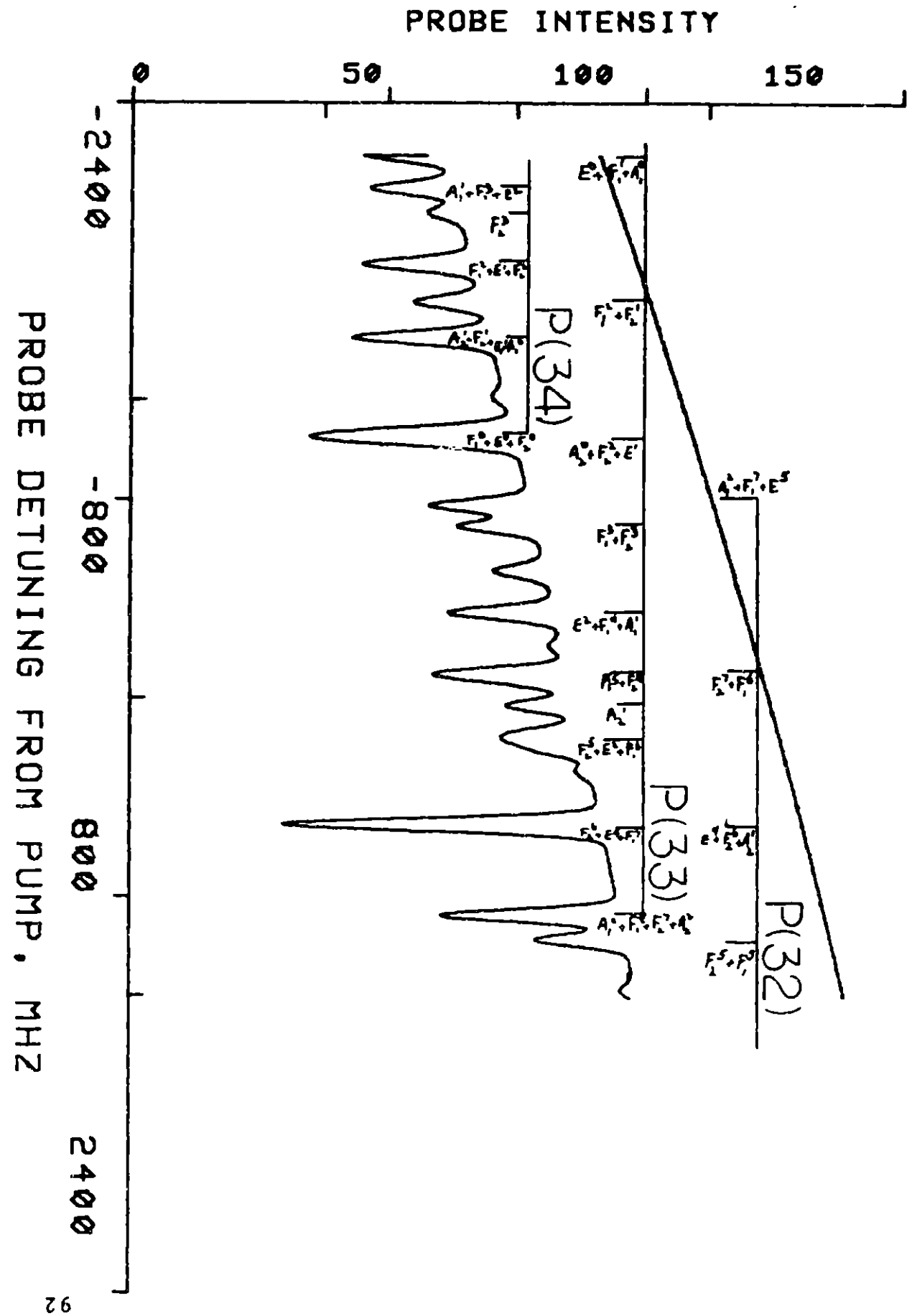
PROBE INTENSITY
0
50
100
150
-2400
-800
800
2400
PROBE DETUNING FROM PUMP, MHZ
P(34)
P(33)
P(32)

from photon echo experiments in SF6. This agrees very well with the observed time constant of the relaxation of the 2LDR signal found in Appendix E, viz.:

$$\tau = 23 \text{ nsec} \cdot \text{Torr} \equiv 1/\kappa \equiv T_1 \qquad (6\text{-}5)$$

in the strong collision limit. At 0.88 Torr, we have

$$\kappa = \kappa' = 3.6 \text{ MHz} \qquad (6\text{-}7)$$

6.3 Results

6.3.1 General features

Overall the DR lineshapes are dominated by two conceptually different processes: AC Stark shifting and saturation. When the pump laser is on, the apparent center of a line not resonant with the pump is shifted away from the pump frequency. This appears to be a "new"resonance, or an upward deflection. The "old" resonance seems to disappear, and hence produces a downward deflection. When added together, the combination produces the derivative-like signals apparent in Figs. 6-4 and 6-6.

Saturation occurs for lines relatively close to the pump frequency. Since the Rabi frequency is much greater than the Doppler width, entire lines can be saturated. The width of the hole burned in the spectrum, however, is a complex function of saturation and Stark shifting, so that the HWHM of the hole is much larger than the Rabi frequency.

6-3. 2-level DR lineshapes for background hotband lines spaced 10 MHz apart. Outer curve, Ω = 140; middle curve, Ω = 100; inner curve, Ω = 95 MHz. FWHM are 465, 285 and 235 MHz respectively. The slight baseline tilt reflects the observed hotband contour in this region.

6-4. Calculated 2LDR signal in SF_6 using Ω = 100 MHz and IB FWHM = 76 MHz (solid) and observed (dashed) for 11.7 kW/cm^2 at 0.08 Torr.

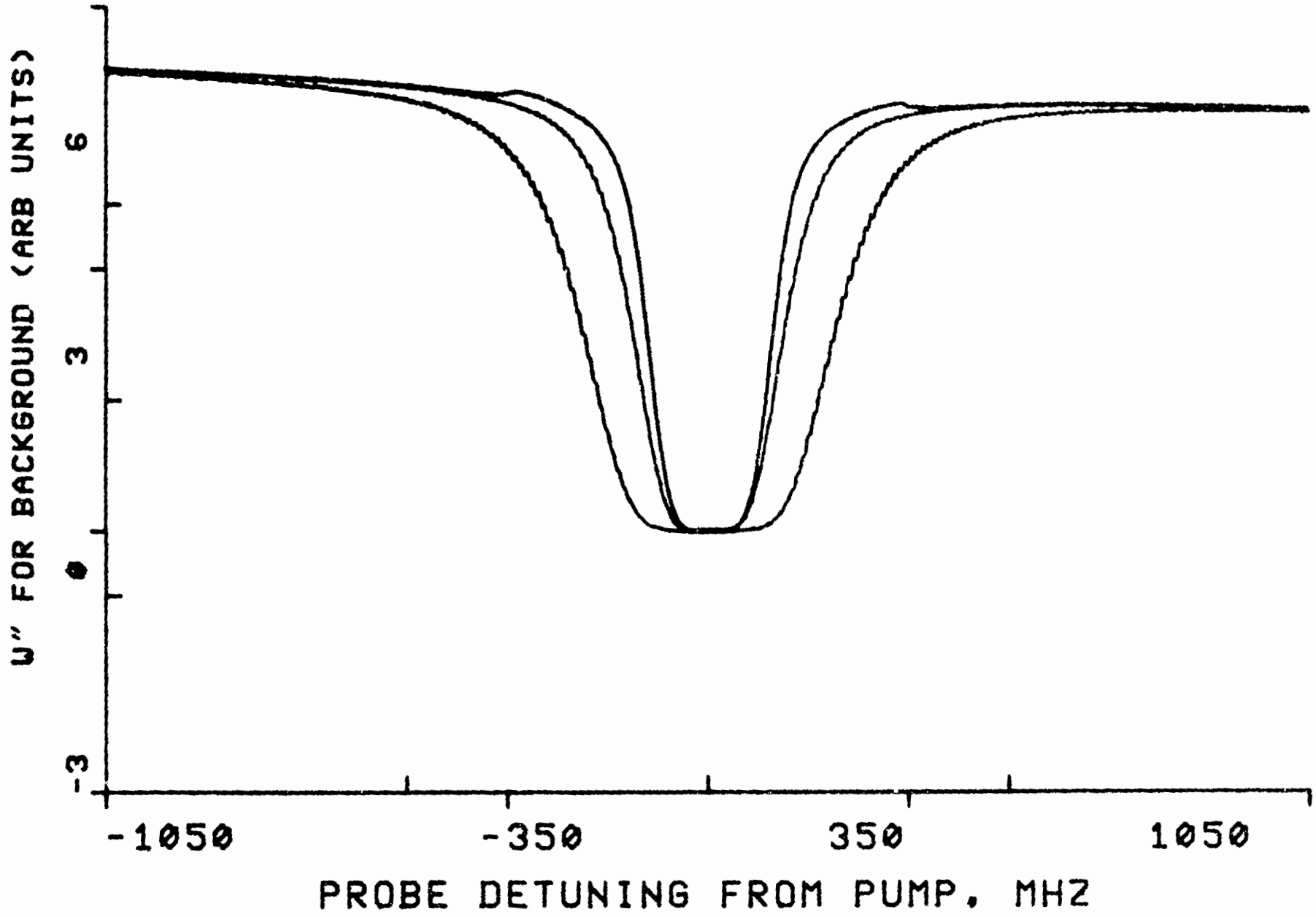
W" FOR BACKGROUND (ARB UNITS)
6
3
0
-3
-1050
-350
350
1050
PROBE DETUNING FROM PUMP, MHZ


DR SIGNAL (ARB. UNITS)
1600
0
-1600
-3200
-2400
-800
800
2400
DETUNING FROM PUMP, MHZ

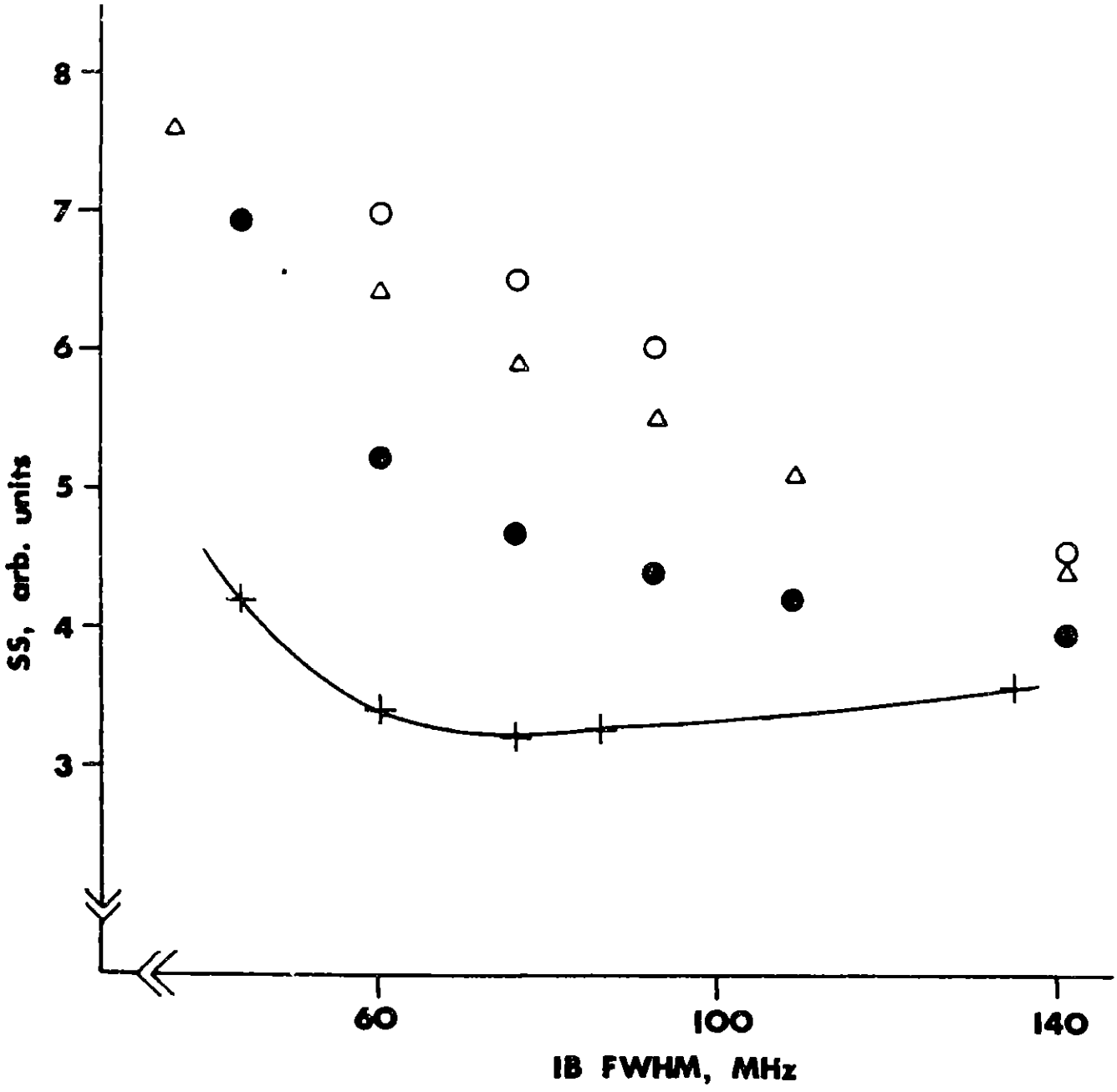

6-5. Average square deviation of calculated 2-level spectrum from observed. Rabi frequencies Ω are ○ = 80; △ = 95; + = 100; ● = 105. PI corrections and background absorption are included in these computations.

This is demonstrated in Fig. 6-3 for the "continuous" background lines. Since the lines are very dense, there is no structure far from the pump frequency where a Stark shifted resonance conceals the disappearance of a "no field" resonance. Only the saturated "hole" appears, which is symmetrical around the pump frequency.

6.3.2 Specific spectra

The closest fit to the observed 2LDR spectrum taken at 11.7 kW/cm^2 is shown in Fig. 6-4. Parameters used in its computation are Ω =100 MHz and IB FWHM = 76 MHz. The average square difference (SS) between the scaled calculated spectra and the observed spectrum are shown in Fig. 6-5; the SS minimized slowly around the values quoted above. PP broadening was not included due to its high computational overhead.

Similar plots for the 3LDR experiment are shown in Figs. 6-6 and 6-7. The fit of 3-level spectra is more strongly dependent on IB, and less on β than for the 2-level fit. In this case, best values correspond to β =65 MHz and IB FWHM = 120 MHz. When PP broadening was included, the SS was not improved but a slightly lower IB (110 MHz) was needed for best fit. Values of SS for the PP broadening are nearly identical to those for β =65 MHz. Rabi frequencies were mixed according to the profile of the average pump laser profile, 51:65:71:78::0.3:0.3:0.2:0.2.

6-6. Calculated 3LDR signal in SF_6 using β = 65 MHz and IB FWHM = 120 MHz (solid) and observed (dashed) at 0.08 Torr.

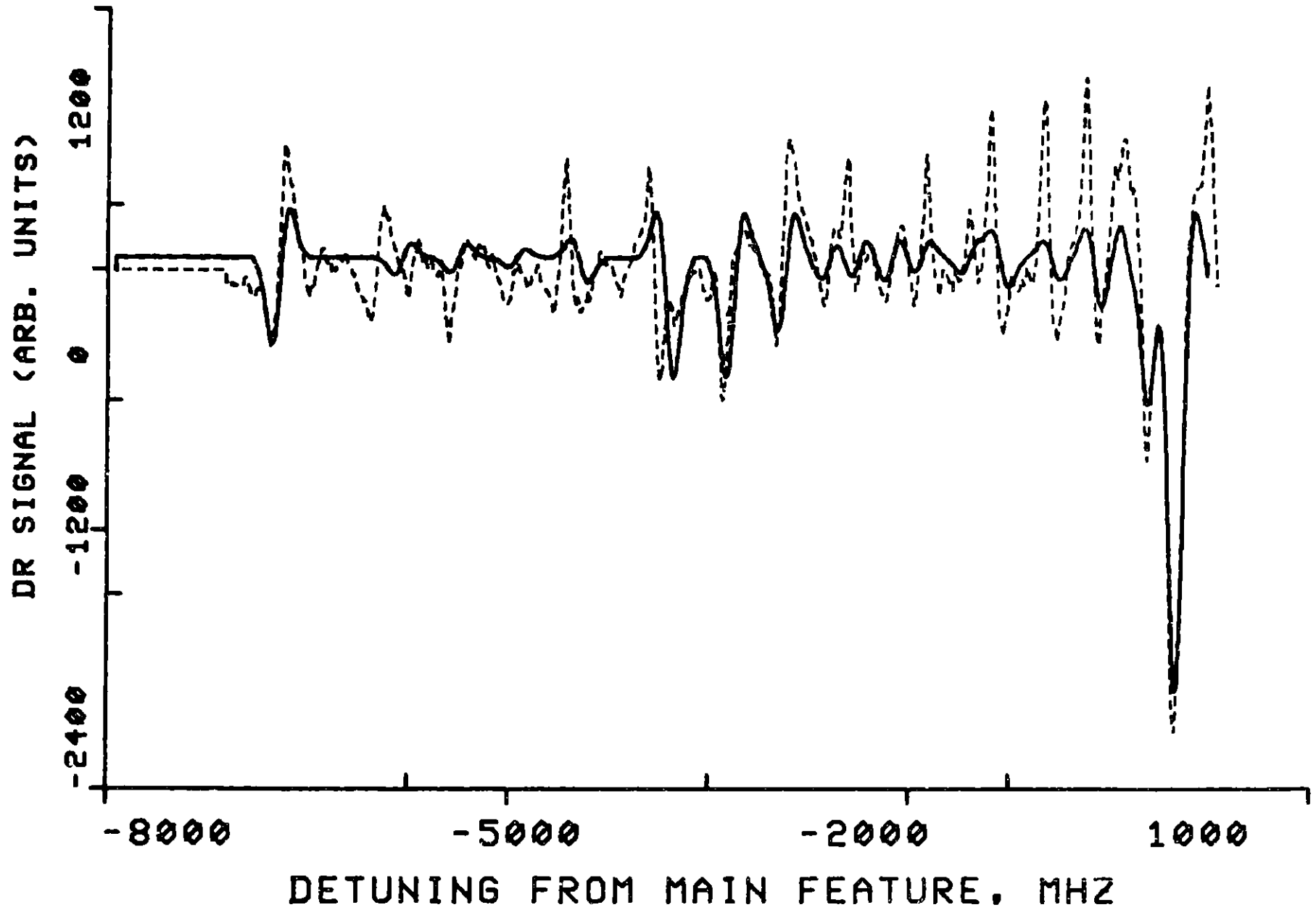
DR SIGNAL (ARB. UNITS)
1200
0
-1200
-2400
-8000
-5000
-2000
1000
DETUNING FROM MAIN FEATURE, MHZ

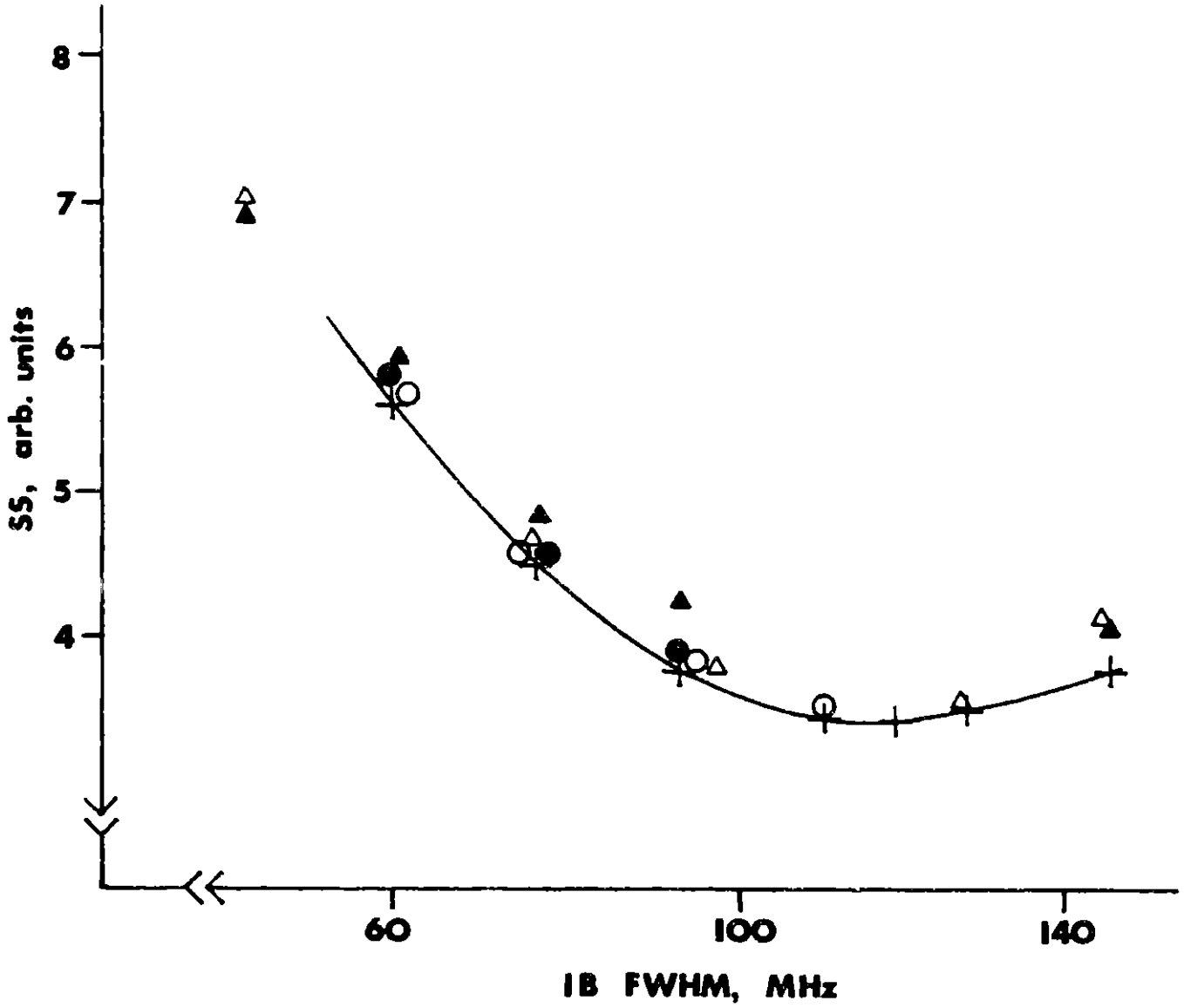

6-7. Average square deviation of calculated 3-level spectra from observed. Rabi frequencies β are o = 51; + = 65; Δ = 75; ● = 90; ▲ = 100. FI correction is included.

6.4 Discussion

6.4.1 Parameters

As can be seen in Figs. 6-4 and 6-6, the fit is surprisingly good for a two parameter calculation. All deflections are accounted for, excepting baseline drift of the boxcar. Deflections are caused primarily by Stark shifted resonances. The main features in both spectra, caused by saturation of a few transitions, are fit very well.

The parameter $\Omega \equiv \beta$ (Rabi frequency) can be calculated from theoretical estimates [6-1] of μ_{10} and the measured average intensity of the pump laser. It is important to correct the dipole moment of [6-1] for interaction with a polarized beam in a rotating-wave formalism, so that

$$\Omega = \beta = \frac{\vec{\mu} \cdot \vec{E}}{2h\sqrt{3}} \quad ; \quad \mu = 0.388 \times 10^{-18} \text{ esu·cm} \qquad (6\text{-}8)$$

Using measured values of the average pump power, beam diameter, repetition rate and pulse width, we can estimate Ω to be 81 MHz for the 2LDR experiment and 72 MHz for the 3LDR case (a slightly lower pump pulse power was used for 3LDR). The value for the 3LDR experiment is within 10% of the value used in the "best" computation; the error in its calculation from four experimentally determined quantities certainly exceeds this figure. Furthermore, since the minimum of SS is so shallow, the difference in SS for $\beta = 65$ and $\beta = 72$ is

merely a few percent. The error in digitization of the observed spectrum is certainly of comparable size. Hence, it can be confidently concluded that the two estimates of β are not significantly different in this case.

The Rabi frequency calculated for the 2LDR experiment is decidedly low, perhaps as a result of the method used to choose which calculated spectrum represents the best fit or shot to shot variations in the pump laser intensity. As was mentioned above, PP broadening was not extensively studied for the 2-level system. It does not, however, mitigate the conclusion that the theoretical estimate of μ is accurate to within 25%.

The values of IB required to fit the spectra exceed the apparent IB in the absorption spectra taken with this apparatus, which in turn is larger than that of other experiments [6-7]. It must be ascribed to electronics and technique unique to this experiment. For instance, scattered pump laser light may cause temperature fluctuations or optical pumping in the diode laser. Crossed laser beams would alleviate this problem, but the added effort in analyzing a two dimensional Doppler profile would be considerable. It may be noted that copropagating beams would produce somewhat narrower features [6-3] than counterpropagating beams.

The apparent need for different values of IB is also somewhat puzzling, although many possible explanations exist. Since the two experiments were performed in different regions

of the diode laser mode, one would expect different tuning rates per unit current $d\nu/dI$ and per degree $d\nu/dK$. The probe frequency jitter would not be equal at different frequencies in the same mode if hum and temperature jitter remain constant. Furthermore, there is no guarantee that on a particular day the diode laser was completely occluded from the pump beam, since the alignment of the pump beam was constantly tweaked. Small amounts of pump light leaking into the diode laser assembly would contribute to an apparent frequency jitter. A copropagating geometry would be less prone to these effects. Again, since the minimum in SS for 2-level fit is so shallow, the value of SS for the 2-level fit for Ω =100 at IB = 120 (the same as for minimum SS for the 3-level fit) is only 4% larger than for IB = 76. Digitization errors may well account for this difference.

6.4.2 Off-resonant pumping

A look at features to the red of the main 2LDR signal shows that the observed signals are considerably larger than those calculated here. It is tempting to ascribe this discrepancy to mixings via the molecular V-R Hamiltonian, but as is shown in Appendix H, there are no mixings sufficient to cause the added signal intensities. By default the only other processes capable of causing the effect are experimental artifacts (such as ν-dependent IB) and collisions. The repeatability and excellent signal to noise of the experiments tends to deny the importance of the former process.

In Appendix E it was concluded that since the satellite structure in the 2LDR spectra was fully developed within the first 200 ns of the pump pulse, the structure was not caused by collisional relaxation. This conclusion may have been hasty, expecially in light of the apparent lack of mixings via the molecular Hamiltonian. A collisional process operative on such a short time scale implies a cross section of about 600 A^2, which is at least three times larger than that for longitudinal (and transverse) relaxation. This is certainly a large figure, especially for a collisional process such as M-changing collisions [6.8a].

Changing the orientation of the lab-fixed component of the average dipole moment during a polarized pump laser pulse would tend to increase the unsaturated DR signals if the polarization of the probe were at right angles [6-8]. Since the polarization of the (now dead) particular diode was not determined, and in general is not known for these devices, a definitive statement cannot be made on the effects of relative polarization in this case. Double resonance experiments currently underway using lower temperatures and different geometries with a new diode laser may shed some light on this problem.

In this chapter, the results and conclusions obtained in Chapters 2 through 6 are summarized.

7.1 Laser induced chemistry

1) No entirely new reactions were observed; all LID reactions reported here have been accomplished by other methods. No mode-specific or mode-selective reactions were seen, although efforts to find reactions and conditions which might lead to mode selectivity are continuing.

2) RRKM unimolecular reaction rate theory has been used to describe the observed data quantitatively. Since the RRKM formalism is based on the assumption that energy within the molecule is distributed statistically amongst all the vibrational modes, the success of RRKM theory implies that for the conditions of these experiments (and those of many other experiments), energy absorbed from the laser field is randomized before a molecule dissociates. Thus we have an indirect answer to Question (2) of Chapter 1 (How does the energy distribute?), at least in part; apparently energy flows into all molecular modes.

More precise details, such as the role of collisions, intramolecular anharmonic, Coriolis and Fermi couplings of

modes, and field-induced effects are not elucidated by chemical evidence. The ability to perform LID in a molecular beam implies that collisions are not necessary for the absorption of an amount of energy sufficient for reaction. It must be stressed, however, that the distribution of absorbed energy amongst vibrational modes in a MIRPA experiment has not been directly probed experimentally in beam or in bulk conditions. Although research interest in this area continues, more direct answers to Question (2) than the above statement cannot be made before new spectroscopic evidence is obtained.

3) The distribution of molecules over energy has not been determined. To ascertain the true shape of the distribution of molecular energies, an appropriate spectroscopic technique is required which interrogates individual molecules undergoing MIRPA. Projects such as that begun by Burak and Quelly [7.1] and currently being extended by Mark Spencer may provide some insight.

4) Other important dynamical effects, such as the effect of the laser pulse shape on energy deposition and the effects of collisional deactivation, have not been explored in great detail. Some evidence of the time scale over which deactivation can become significant has been obtained by LID experiments done with buffer gases. In the LID of trans-dichloroethylene, for example, the presence of a few percent of the nonabsorbing "cold" cis isomer was sufficient

to quench the absorbing "hot" trans isomer before dissociation could occur. Since the TEA laser pulse has a nominal FWHM of 70 ns, the deactivation rate must be a very fast process in this example. Data of a more quantitative nature would be difficult to obtain by bulk chemistry experiments.

5) Despite the lack of dynamical information, we have shown that the chemistry produced by MIRPA can be controlled by various experimental parameters, such as pressure, focal geometry and choice of buffer gas. Proper choice can produce very selective results; for example, in the LID of CF_2CHCl, CF_2CH_2 was produced in preference to other products when hydrogen-containing buffer gas was added. By choosing a suitable parent molecule, a particularly valuable radical can be produced in large local concentrations. The astute selection of parent molecule together with appropriate experimental conditions has allowed a degree of control over the production of many transient species which cannot be had by other means [1.13].

6) Evidence reported in Chapters 2 and 3 and in Appendix B shows that the vinylidene carbene $F_2C{=}C{:}$ has been produced by LID. Evidence for the formation of the dimethyl analog, $(CH_3)_2C{=}C{:}$, is not as convincing. This may be a suitable method of producing vinylidene carbenes for spectroscopic investigation of their electronic structure.

7) Radicals produced by LID are born with some vibrational energy, which in the cases of $(CH_3)_2C{=}C{:}$ and

$H_2C{=}C{:}$ is sufficient to overcome the energy barrier to rearrangement. The observation of "hot" fragments is in concert with the data of other investigators [1.12,7.2].

7.2 Gaussian beam optics

8) It is possible to determine the average of an intensity- dependent effect, such as the average energy absorbed per molecule $\langle E \rangle$, for a small volume of species at the center of a Gaussian laser beam. This technique, Gaussian beam deconvolution, may be valuable in determining the energy centroid of the distribution discussed in (3) above. The effectiveness of the method is limited ultimately by the precision of the experimental measurements, as was shown in Chapter 4.

9) Subjecting a sample to the very wide range of fluences incurred in a focused Gaussian beam geometry tends to make the dispersion of any observed quantity look Gaussian also. This is demonstrated graphically in Fig. 3 of Appendix D. Mechanistically this effect is easily understood; the effective "dispersion" of fluences experienced by molecules in the focused beam is so much wider than the dispersion of the energy absorption function incurred at each point in the beam (that is, the width of the distribution of molecules over absorbed energy at a given fluence $P(E;\phi)$), that the geometric beam "dispersion" swamps the effect of distributions $P(E;\phi)$. This implies that observed quantities which are

averaged over the entire beam will be more sensitive to macroscopic beam shape than the microscopic dynamics of the physical process. The chemical data on the LID of trans-d_1-vinyl chloride versus focal length, depicted in Fig. 2 of Appendix A, are a striking example of this effect. In this case, the total molecular behavior was seen to be strongly dependent on beam geometry and independent of the form of distribution $P(E; \phi)$ used to model the data.

7.3 Double resonance experiments

From the modeling of 2LDR and 3LDR spectra in SF , several conclusions can be made.

10) The value of the dipole matrix element μ has been estimated accurately.

11) It was convincingly shown in Appendix H that mixings between cluster states within the same J level caused by the full vibration-rotation molecular Hamiltonian do not play a significant role in the observed 2LDR and 3LDR spectra.

12) Lineshape equations derived from two and three level Bloch equations describe individual features very accurately. An excellent fit for all features is precluded by the exclusion of collisional effects.

13) To a first approximation, however, the observed spectra can be modeled as a set of independent 2-level and 3-level systems. The dynamics of collisional coupling between

states in the same J manifold is currently under consideration by Harold Galbraith at Los Alamos. Collisions may cause population to be transferred to or from K states within the J manifold being directly pumped, and would be observed as a corresponding increase or decrease in the double resonance signals detected for these K states. This effect may be difficult to separate from the effects of AC Stark shifting, instrumental broadening and observation times long compared to the rate of collisional relaxation.

14) As a test of the hypothesis that collisions are playing a role in the observed spectra, the double resonance experiments should be repeated in SF_6 at low temperatures. At 140 K, the lowest temperature practical with SF_6, collisional relaxation rates would be decreased by a factor of $\sim \sqrt{2}$ from their room temperature values. Since a greater fraction of the molecules are in the ground vibrational state at 140 K, a decrease in number density might be affordable with no loss of signal, further decreasing the collision rate. Also, other apparent anomalies, such as the instrumental broadening, could be investigated.

15) The use of a tunable diode laser as a probe source has been an invaluable tool, enabling us to record spectroscopic details not observable by using fixed frequency probe radiation. Improvements in diode laser stability and effective linewidth must be made so that the observed instrumental broadening ceases to be the limiting factor in

the resolution of the double resonance spectra. Some suggestions to this end were put forth in Chapter 5.

REFERENCES

1.1 F. S. Klein, V. Duval, I. Glatt and J. I. Steinfeld, J. Appl. Phys. (submitted)

1.2 J. S. Haggerty and W. R. Cannon, "Sinterable Powders from Laser Driven Reactions," MIT Energy Laboratory Report MIT-EL 79-047, July 1979

1.3 T. J. Odiorne, P. R. Brooks, J. V. V. Kasper, J. Chem. Phys. 55:1980 (1971)

1.4 N. R. Isenor and M. C. Richardson, Appl. Phys. Letts. 18:224 (1971), Opt. Commun. 3:360 (1971); N. R. Isenor, V. Merchant, R. S. Hallsworth and M. C. Richardson, Can. J. Phys. 51:1282 (1973); R. S. Halsworth and N. R. Isenor, Chem. Phys. Lett. 22:283 (1973)

1.5 a) R. V. Ambartzumian, V. S. Letokhov, E. A. Ryabov, and N. V. Chekalin, JETP Lett. 20:273 (1974)
b) R. V. Ambartzumian, Yu. A. Gorokov, V. S. Letokhov and G. N. Makarov, JETP Lett. 21:171 (1975)

1.6 J. L. Lyman, R. J. Jensen, J, Rink, C. P. Robinson and S. D. Rockwood, Appl. Phys. Lett. 27:87 (1975)

1.7 Craig C. Jensen, Ph.D. Thesis, "Spectroscopy of Laser-Induced Molecular Excitation: Diode Laser Double Resonance of SF_6," M.I.T., 1979

1.8 J. I. Steinfeld, in Laser Induced Chemical Processes (Plenum Publishing Co., New York, in press)

1.9 A few review articles:
S. H. Bauer, Chem. Revs. 78:147 (1978)
M. J. Berry, Ann. Rev. Phys. Chem. 26:259 (1975)
V. S. Letokhov, Ann. Rev. Phys. Chem. 28:133 (1977)
J. Wolfrum, Ber. Bunsengesellschaft Phys. Chem. 81:114 (1977)

1.10 For a recent review of molecular beam studies of LID:
Aa. S. Subdo, D. J. Krajnovich, P. A. Schulz, Y. R. Shen and Y. T. Lee, in Multiple-Photon Excitation and Dissociation of Polyatomic Molecules, C. D. Cantrell, ed. (Springer-Verlag, Berlin, 1979)

1.11 D. F. Dever and E. Grunwald, J. Am. Chem. Soc. 98:5055 (1976); E. Grunwald and K. J. Olszyna, Laser Focus 41 (1976)

1.12 J. C. Stephenson and D. S. King, J. Chem. Phys. 69:1485 (1978), Chem. Phys. Lett. 51:48 (1977)

1.13 J. I. Steinfeld, T. G. Anderson, C. Reiser, D. R. Denison, L. D. Hartsough and J. R. Hollahan, J. Electrochem. Soc. 127:514 (1980)

1.14 W. Happer et. al., "Laser Induced Photochemistry," JASON Report JSR-78-11, Stanford Research Institute (Feb. 1979)

1.15 E. Würzberg, L. J. Kovalenko and P. L. Houston, Chem. Phys. 35:317 (1978)

1.16 P. J. Robinson and K. A. Holbrook, Unimolecular Reactions (Wiley-Interscience, New York, 1972)

1.17 F. M. Lussier and J. I. Steinfeld, Chem. Phys. Lett. 50:175 (1977)

1.18 A. Ben Reuven and Y. Rabin, "N-level Multiple Resonance," Adv. Chem. Phys. (in press)

1.19 a) J. L. Lyman, J. Chem. Phys. 67:1868 (1977)
b) E. R. Grant, P. A. Schulz, Aa. S. Sudbo, Y. R. Shen and Y. T. Lee, Phys. Rev. Letts. 40:115 (1978)

1.20 J. R. Ackerhalt and H. W. Galbraith, in Laser Spectroscopy IV: Proc. Fourth Int. Conf., H. Walther and K. W. Rothe, eds. (Springer-Verlag, Berlin, 1979) pp. 300-308

1.21 P. F. Moulton, D. M. Larsen, J. M. Walpole and A. Mooradian, Opt. Lett. 1:51 (1977); P. F. Moulton and A. Mooradian, in Proc. Conf. Laser Induced Processes in Molecules (Springer-Verlag, Berlin, 1978) pp. 37-42

2.1 L. D. Hanton and G. P. Semeluk, Can. J. Chem. 44:2143 (1962); P. M. Jeffers, J. Phys. Chem. 76:2829 (1972)

2.2 C. C. Jensen, R. D. Levine and J. I. Steinfeld, J. Chem. Phys. 69:1432 (1978)

2.3 Z. Karny, A. Gupta, R. N. Zare, S. T. Lin, J. Niemen and A. M. Ronn, Chem. Phys. 37:15 (1979)

2.4 K. King and R. Gilbert, Int. J. Chem. Kin. 11:11 (1979)

2.5 T. Anderson, J. Francisco, C. Reiser, J. Steinfeld and D. S. Frankel, Jr., 179th A.C.S. Nat'l Meeting, Houston, March 1980

3.1 A. A. Westenberg, J. H. Goldstein and E. B. Wilson Jr., J. Chem. Phys. 17:1319 (1949); E. Kloster-Jensen, J. Am. Che. Soc. 91:5673 (1969)

3.2 P. J. Stang, Accts. Chem. Research 11:107 (1978), Chem. Revs. 78:383 (1978)

3.3 see reference 1.7

3.4 W. C. Danen and J. C. Jang, in Laser Induced Chemical Processes, J. I. Steinfeld, ed. (plenum Publishing Co., New York, in press)

3.5 O. D.Judd, J. Chem. Phys. (in press); J. L. Lyman, G. P. Quigley and O. D. Judd, in Multiple-Photon Excitation and Dissociation of Polyatomic Molecules, C. D. Cantrell, ed. (Springer-Verlag, Berlin, 1979)

3.6 see reference 1.19a

3.7 see reference 1.19b

3.8 P. Carruthers and N. N. Nieto, Am. J. Phys. 33:537 (1965)

3.9 C. D. Cantrell and H. W. Galbraith, Opt. Commun. 21:121 (1977); C. D. Cantrell, A. A. Makarov and W. H. Louisell, in Advances in Chemical Physics, J. Jortner and R. Levine, eds. (Wiley, New York, 1980); C. D. Cantrell, S. M. Freund and J. L. Lyman, in Laser Handbook Vol III (North Holland Publishing, 1978)

3.10 see reference 1.20

3.11 E. Thiele, M. F. Goodman and J. Stone, Opt. Eng. 19:010 (1980)

3.12 see reference 1.12

3.13 C. E. Dykstra and H. F. Schaefer III, J. Am. Chem. Soc. 100:1378 (1978); M. D. Conrad and H. F. Schaefer, ibid., 7820

3.14 O. P. Strausz, R. J. Norstrom, A. C. Hopkinson, M. Schoenborn and I. G. Csizmaida, Theoretica Chim. Acta 29:183 (1973)

4.1 F. M. Lussier, Ph.D. Thesis, Department of Chemistry, M.I.T. 1978

4.2 A. Yariv, Quantum Electronics (John Wiley & Sons, New York, 1967)

4.3 P. Kolodner, M.S. Kwok, J. G. Black and E. Yablonovitch, Opt. Lett. 4:38 (1979)

4.4 I. P. Herman, Opt. Lett. 4:403 (1979)

4.5 J. G. Black, P. Kolodner, M. J. Schultz, E. Yablonovitch and N. Bloembergen, Phys. Rev. A 19:704 (1979)

4.6 C. Daniel and F. S. Wood, Fitting Equations to Data (Wiley-Interscience, New York, 1971)

4.7 D. R. Keefer, J. E. Allen Jr., and W. B. Person, Chem. Phys. Lett. 43:394 (1976)

5.1 I. Burak, A. V. Nowak, J. I. Steinfeld and D. G. Sutton, J. Chem. Phys. 51:2275 (1969), J. Chem. Phys. 52:5421 (1970)

5.2 K. S. Rutkovskii and K. G. Tokhadzhe, Zhur. Eksp. Teor. Fiz. 75:408 (1978);
D. S. Frankel, J. Chem. Phys. 65:1696 (1976); D. S. Frankel and T. J. Manuccia, Chem. Phys. Lett. 54:451 (1978);
W. Fuss and J. Hartman, J. Chem. Phys. 70:5468 (1979); W. Fuss, J. Hartman and W. E. Schmid, Appl. Phys. 15:297 (1978);
A. B. Peterson, J. Tiee and C. Wittig, Opt. Commun. 17:259 (1976);
T. F. Deutch and S. R. J. Bruek, J. Chem. Phys. 70:2063 (1979);
J. L. Lyman, L. J. Radziemski Jr., and A. C. Nilsson, IEEE J. Quant. Elec. (in press)

5.3 see reference 1.21

5.4 see reference 1.7

5.5 H. Weichel and L. S. Pedrotti, Electro Optical Systems Design (July 1976) p. 22

5.6 Joseph Sattler, Harry Diamond Laboratories, private communication

5.7 H. W. Galbraith, C. W. Patterson, B. J. Krohn and W. G. Harter, J. Mol. Spec. 73:475 (1978)

5.8 T. Shimizu and T. Oka, Phys. Rev. A 2:1177 (1970)

5.9 W. J. Moore, Physical Chemistry 4th ed. (Prentice Hall, Inc., Englewood Cliffs, 1972)

6.0 W. G. Harter and C. W. Patterson, Phys. Rev. Lett. 38:224 (1977)

6.1 K. Fox, Opt. Commun. 19:397 (1976); K. Fox and W. B. Person, J. Chem. Phys. 64:5218 (1976)

6.2 B. R. Mollow, Phys. Rev. A 5:2217 (1972)

6.3 F. Y. Wu, S. Ezekiel, M. Ducloy and B. R. Mollow, Phys. Rev. Lett. 38:1077 (1977)

6.4 Th. Hänsch and P. Toschek, Z. Physik 236:213 (1970)

6.5 A few papers on 3-level lineshape theory:
B. R. Mollow, Phys. Rev. A 8:1949 (1973);
M. S. Feld and A. Javan, Phys. Rev. 177:540 (1969);
B. J. Feldman and M. S. Feld, Phys. Rev. A 5:899 (1972)

6.6 C. K. N. Patel and R. E. Slusher, Phys. Rev. Lett. 20:1087 (1968)

6.7 R. S. McDowell, H. W. Galbraith, B. J. Krohn, C. D. Cantrell and E. D. Hinkley, Opt. Commun. 17:178 (1976); R. S. McDowell, H. W. Galbraith, C. D. Cantrell, N. G. Nereson, P. F. Moulton, and E. D. Hinkley, Opt. Lett. 2:97 (1978)

6.8 a) D. S. Frankel and J. I. Steinfeld, J. Chem. Phys. 62:3358 (1975)
b) see reference 5.1

7.1 T. J. Quelly, Master's Thesis, Department of Chemistry, MIT 1978; see also reference F-3.

7.2 C. R. Quick and C. Wittig, Chem Phys. 32:75 (1978), J. Chem. Phys. 69:4201 (1978)

C.1 A. N. Nesmeyanov and R. Kh. Friedlina, Chem. Abstr. 40:3451 (1946)

C.2 J. E. Francis and L. C. Leitch, Can. J. Chem. 35:348, 500 (1957)

C.3 H. C. Volger, Recl. Trav. Chem. Pays-Bas 87:501 (1968)

C.4 S. Enomoto and M. Asahina, J. Mol. Spec. 19:117 (1966)

F.1 S. Bialkowski and W. A. Guillory, Rev. Sci. Instrum. 48:1445 (1977)

F.2 E. T. Lynk, Rev. Sci. Instrum. 50:1074 (1979)

F.3 I. Burak, T. J. Quelly and J. I. Steinfeld, J. Chem. Phys. 70:334 (1979)

F.4 this reference is included herein as Appendix E

H.1 a) W. G. Harter and C. W. Patterson, J. Chem. Phys. 66:4872 (1977), J. Chem. Phys. 66:4886 (1977), Int. J. Quantum Chem. 511:445 (1977)
b) B. J. Krohn, LASL Publication (LA-6554-MS) Oct. 1976

H.2 Ch. J. Bordé, M. Ouhayoun, A. Van Lerberghe, C. Salomon, S. Avrillier, C. D. Cantrell and J. Bordé, in Laser Spectroscopy IV, Proc. Fourth Int. Conf., H. Walther and K. W. Rothe, eds. (Springer-Verlag, Berlin, 1979) p. 142; J. Mol Spec. 73:344 (1978)

H.3 H. Loete, A. Clairon, A. Frichet, R. S. McDowell, H. W. Galbraith, J. Hilico, J. Moret-Bailly and L. Henry, Comptes Rendus B285:175 (1977)

H.4 see reference 5.7

H.5 I. N. Knyazev, V. S. Letokhov, and V. V. Lobko, Opt. Commun. 35:337 (1978); I. N. Knyazev, V. V. Lobko, G. N. Makarov, and A. A. Puretzky, Appl. Phys. 19:75 (1979)

H.6 K. Fox, Opt. Lett. 1:214 (1977); H. W. Galbraith, Opt. Lett. 3:154 (1978)

H.7 J. Hilico, H. Berger and M. Loete, Can. J. Phys. 54:1702 (1976)

APPENDIX A. "Infrared Photochemistry of Halogenated Ethylenes"

C. Reiser, F. M. Lussier, C. C. Jensen and J. I. Steinfeld, J. Am. Che. Soc. 101, 350 (1979)

350 Journal of the American Chemical Society / 101:2 / January 17, 1979

Infrared Photochemistry of Halogenated Ethylenes

Christopher Reiser, Frances M. Lussier, Craig C. Jensen, and Jeffrey I. Steinfeld*

Contribution from the Department of Chemistry, Massachusetts Institute of Technology, Cambridge, Massachusetts 02139. *Received June 12, 1978*

Abstract: The infrared laser induced multiphoton reactions of mono-, di-, and trichloro-substituted ethylenes have been investigated. In all cases, the dominant mode of reaction is elimination of HCl. Free rotation around the double bond precedes elimination, leading to observable isomerization in 1,2-dichloroethylene and β-d_1-vinyl chloride. The experimental results can be represented in terms of a kinetic model with rates calculated from RRKM theory, which presupposes unhindered redistribution of vibrational energy within the molecule prior to reaction. Comparison of HCl/DCl elimination ratios between CHD=CHCl and CH_2=CDCl shows that the preferred mode of elimination is α to the chlorine atom. The pressure dependence of this product ratio is not the same for different CO_2 laser lines; however, this ability to influence the outcome of the reaction by changing the laser line is a consequence of differences in energy deposition between one line and another, and not of any mode-selective process. The preference for α-elimination suggests that the reaction may proceed by formation of vinylidenecarbene, followed by rearrangement to form acetylene.

Since the first published report of the dissociation of SF_6 by infrared multiphoton absorption,[1] chemical reactions induced by high-intensity infrared radiation have captured the imagination of a large number of both chemists and physicists. A principal reason for this interest is the apparently substantial difference between the conditions under which such reactions occur and those of normal thermal-equilibrium conditions. In the latter, molecular internal (vibrational) and external (translation/rotational) degrees of freedom are in mutual equilibrium, or very close to it; while in reactions resulting from multiple infrared photon absorption, the energy required to activate the reactive channel is, at least initially, deposited exclusively in the vibrational modes. There has even been speculation that energy could be preferentially localized in one or a few vibrational modes, thereby leading to chemical transformations which are qualitatively different from those observed under conventional conditions. In the experiments reported in this paper, we have studied a series of mono-, di-, and trichloro-substituted ethylenes in order to shed some light on the extent to which nonequilibrium effects may be reflected in overall chemical behavior.

An extensive literature has developed on these reactions in the past 2 years, which is summarized in several reviews.[2] Most of the reactions studied involve homolytic bond cleavage, as in SF_6, SiF_4, NH_3, BCl_3, $CFCl_3$, CF_2Cl_2, and similar systems. More recently, interest has turned increasingly to the types of reactions familiar from conventional thermal chemistry, but carried out under nonequilibrium excitation conditions. Typical examples include elimination of hydrogen halides:[3-5]

$$CF_3CH_2F + nh\nu \rightarrow CH_2{=}CH_2 + HF \qquad (1a)$$

$$(CH_3)_2CHCH_2Br + nh\nu \rightarrow (CH_3)_2C{=}CH_2 + HBr \qquad (1b)$$

$$CH_2{=}CHCl + nh\nu \rightarrow HC{\equiv}CH + HCl \qquad (2)$$

ring opening reactions (eq 3),

(3)

condensation to form aromatic rings[7] (eq 4),

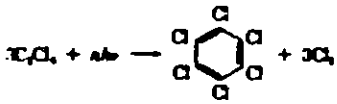

(4)

and cyclic ester pyrolysis[8] (eq 5).

$$CH_3COOCH_2CH_3 + nh\nu \rightarrow CH_3COOH + CH_2{=}CH_2 \qquad (5)$$

More complex dissociation/isomerization pathways have also been identified as having an origin in specific vibrational excitation,[9] such as eq 6. Reactions 1a and 5, in particular, have

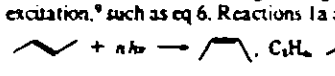

(6)

been shown to be nonthermal in origin[10] by the addition of a "chemical thermometer" to the system, which did not absorb infrared energy directly, but which underwent a reaction when the energy absorbed by a second component of the system was thermalized.[4,8] However, no evidence has been brought forward to date which implies the existence of "mode-specific" reactions, i.e., a chemical transformation resulting from localization of the vibrational energy in some part of the molecule which can be specified by the excitation procedure.[11]

We have carried out a study of reactions induced by multiple infrared photon absorption in a series of chlorine-substituted ethylenes, in order to gain information of use in elucidating the dynamics and detailed mechanisms of this process. The specific systems which have been studied can be represented by the general formula below.

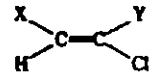

X =	Y =	
H	H	I
H	D	Ia
D	H	Ib
H	Cl	II
Cl	H	III
Cl	Cl	IV

The attractive feature of this series of molecules is that, while the primary laser-induced process is a simple HCl elimination,[5] there are also competitive channels present (such as isomerization or C–Cl bond cleavage) which provide quantitative tests of models for the dynamics of the process. The formation of stable molecular fragments, rather than reactive radicals or atoms, also simplifies the overall kinetics by avoiding secondary reactions. The reactions of the different members of the series provide information on the mechanism and stereochemistry involved, and a sufficient background on conventional thermal reactions of these species exists so that a meaningful comparison may be made between laser- and thermally induced processes. Furthermore, the vibrational spectroscopy of the parent molecules is well characterized, so that quantitative estimates may be made of energy deposition, densities of states, and other parameters required in a detailed theoretical treatment.

Experimental Section

Irradiation System. The infrared source was a Tachisto 215G CO_2 laser furnishing 0.1–1.0 J pulses on lines of the P and R branches of

the 9.6- and 10.6-μm bands. Each pulse consisted of a 40–50-ns spike containing over 70% of the energy followed by a much lower intensity tail. Transverse mode operation was constrained to TEM_{00} by an intracavity diaphragm. The beam was focused in the reaction mixture by an $f.l. = 29$ cm AR-coated Ge lens (II–IV, Inc.). For some experiments, a collimating telescope was used, consisting of a pair of AR-coated Ge lenses, giving effective apertures between $f/20$ and $f/70$. Reactions were carried out in clean Pyrex cells with NaCl end windows. Care was taken to focus the beam far from either cell walls or windows, in order to avoid the problem of heterogeneous reactions taking place at locally heated surface sites.[12]

Analytical Procedures. Most estimates of the extent of reaction were made by measurement of band intensities of characteristic parent or product molecule infrared absorptions on a Perkin-Elmer 567 spectrophotometer. These measurements were checked against gas-chromatographic analyses on a Carbowax column for the very low-pressure samples. The HCl and DCl bands were not used for quantitative analysis, since the intensities of these features are pressure dependent and are not linearly proportional to concentration under our experimental conditions. Measurement of C_2H_2/C_2HD ratios was carried out on a Hitachi RMU-6L GC–MS in the Massachusetts Institute of Technology Mass Spectrometry Facility.

Starting Materials. Vinyl chloride was obtained from a Matheson cylinder, stated purity 99.9%, and transferred to the reaction vessel by a single freeze–pump–thaw cycle.

α-d_1-Vinyl chloride (Ia) was synthesized by the method of Francis and Leitch.[13] 1,1,2-Trichloroethane was treated with $Ca(OH)_2$ in an aqueous suspension to yield vinylidene chloride (II). Deuterium bromide was added to this material at −77 °C in the presence of ultraviolet light from photoreactor Hg lamps to produce 1-bromo-2,2-dichloroethane-2-d, the composition of the latter product was verified by its NMR spectrum. Addition of the deuterated haloethane to a suspension of zinc dust in boiling ethanol resulted in the evolution of α-d_1-vinyl chloride (Ia). Deuteration at the α position was greater than 96%, based on comparison of the infrared spectrum of the product with published spectra of deuterated vinyl chlorides.[14]

trans-d_1-Vinyl chloride (Ib) was prepared by a method similar to that of Nesmeyanov et al.[15,16] A saturated solution of acetylene in 16% aqueous HCl reacted with $HgCl_2$ to form *trans*-2-chlorovinylmercuric chloride (verified by NMR). Treatment of this species with DBr in dioxane (or DBr alone) produced a gaseous product which, after treatment with $AgNO_3$ to remove acetylene, was greater than 96% CHD═CHCl. Infrared spectroscopy showed that the (*trans*-d_1)/(*cis*-d_1) ratio was approximately 9:1; this ratio degraded on storage over an extended period of time, or on attempts at further purification.

Vinylidene chloride (II) was either synthesized as described above or purchased from Aldrich Chemical Co. (stated purity, 99%).

trans-Dichloroethylene (III) was obtained from Columbia Organics. No indication of the presence of cis isomer was found in the infrared spectrum.

Trichloroethylene (IV) was Mallinckrodt AR grade.

Results

A. Vinyl Chloride (I). The infrared laser induced chemistry of vinyl chloride was reported in our preliminary communication.[5] The only products observed are HCl and acetylene, indicating a concerted elimination mechanism. The net conversion per laser pulse (CPF) *increases* somewhat over the pressure range 0.5–20 Torr; this is a consequence of increased absorption of infrared energy per molecule in the higher pressure gas. Further details, including optoacoustic measurements of energy deposition, are given elsewhere.[17]

When the infrared beam is focused to a sufficiently small diameter (f.l. of Ge lens ≤ 5 cm) to cause breakdown to occur in the vinyl chloride sample, additional products are seen. These are principally diacetylene (butadiyne),[18] carbon soot, and a noncondensable gas presumed to be H_2. The formation of such products under focused conditions has been noted by Yogev and co-workers,[9] and most probably involves reactions[19] of ethynyl radicals with the acetylene formed in the elimination step, i.e.

$$C_2H\cdot + C_2H_2 \rightarrow C_4H_2 + H\cdot \qquad (7a)$$

$$C_2H\cdot + C_4H_2 \rightarrow C_6H_2 + H\cdot \qquad (7b)$$

etc.

Thermal pyrolysis of vinyl chloride leads to a quite different set of products from that observed following infrared laser photolysis. In a flow system at 500–600 °C, dimerization to chloroprene is observed[20]

$$2CH_2{=}CHCl \rightarrow CH_2{=}C(Cl)CH{=}CH_2 + HCl \qquad (8)$$

while under static conditions at similar temperature a mixture of products is obtained[21] which includes, in addition to HCl, methane and ethylene in amounts comparable to acetylene, as well as a polymer with $C/H > 1$. Clearly, these results indicate the predominance of free-radical reactions, presumably initiated by C–Cl bond scission, which appear to be absent in the infrared laser induced process. Direct dehydrohalogenation is observed[22] behind shock waves at 1400–2000 K. These experiments[22b] provide a value of the activation energy for the elimination reaction, $E_{a,1} = (69.3 \pm 2.9)$ kcal/mol.

B. Vinylidene Chloride (II) and Trichloroethylene (IV). Vinylidene chloride and trichloroethylene also undergo elimination of HCl when subjected to intense infrared radiation at ~10 Torr, to form chlorinated acetylenes:

$$CH_2{=}CCl_2 + nh\nu \rightarrow HC{\equiv}CCl + HCl \qquad (9)$$

$$CHCl{=}CCl_2 + nh\nu \rightarrow ClC{\equiv}CCl + HCl \qquad (10)$$

Some HC≡CCl is also found in the latter system. Conventional preparations of these chlorinated acetylenes are reported[23] to have low yields, and the resulting products tend to be unstable. By contrast, the mixture containing C_2Cl_2 formed in reaction 10 appears to be stable over an extended period; the C_2Cl_2 did finally explode after repeated transfer, presumably because of leakage of O_2 into the cell.

The C_2HCl observed in the infrared photolysis of IV may have been formed by α,α-elimination or α,β-elimination of Cl_2:

$$CHCl{=}CCl_2 + nh\nu \rightarrow \left[\begin{array}{c} CHCl{=}C: \\ \text{or} \\ CH{=}CCl \\ | \\ ClC{\equiv}CH \end{array}\right] + Cl_2 \qquad (11)$$

Our experiments cannot distinguish between these two channels for this molecule. The lack of C_2H_2 among the infrared photolysis products of II indicates that α,α-elimination has not occurred for that system. Furthermore, the absence of thermal addition products, such as Cl_3CCH_2Cl, in the reaction mixture indicates that Cl_2 elimination is not a major pathway.

Sudbo et al.[24] report that IV fragments to C_2HCl_2 and Cl atoms in a beam of the parent molecules intersected by CO_2 laser pulses focused with a 25-cm focal length lens. Using similar optics and moderate pressures, we find no evidence for Cl atom production, such as the dimer $C_4H_2Cl_4$ or other recombination products. Using a 5-cm focal length lens and low sample pressures (≤0.1 Torr), Gandini et al.[25] find products resulting from C–Cl cleavage in the infrared photolysis of C_2H_3Cl/C_2H_2DCl mixtures. Again, our experiments do not show products other than those of molecular elimination. Presumably, at high fluences and low pressures used by Gandini or Sudbo, the vibrational energy content of the molecule is driven to much higher levels than in our experiments, where the rate of C–Cl bond scission (E_a ~ bond enthalpy ~ 90 kcal/mol[26]) may become faster than the lower energy molecular elimination rate ($E_a = 69$ kcal/mol).[22b]

We note that the thermal pyrolysis of IV between 385 and 445 °C results in condensation to hexachlorobenzene,[27] a reaction reminiscent of the laser-induced process in tetrachloroethylene–BCl_3 mixtures.

C. *trans*-Dichloroethylene (III). When 5 Torr of III is irradiated with the P(30) [10.6 μm] line of the CO_2 laser, the principal reaction product is *cis*-dichloroethylene. Very little elimination product (HC≡CCl or HCl) is observed. This result is in agreement with that found by Ambartzumyan et al.,[20a] Nagai and Katayama,[20b] and also Karny and Zare,[12] who report that trans → cis isomerization is the principal laser-induced reaction pathway in this system. This process is also the principal thermal reaction in the system, with an activation energy of 55 kcal mol^{-1}; a small amount of condensation to 1,2,4-trichlorobenzene is also reported,[21] which is not found in the laser-irradiated samples.

In interpreting this result, it is important to remember that measurements of product formation are made following a large number (200–2000) of infrared pulses. Initially, both isomerization and dissociation may take place (see following section), but as the irradiation proceeds, an appreciable concentration of *cis*-dichloroethylene accumulates in the cell. This species does *not* absorb CO_2 laser radiation; thus the vibrationally excited trans species is progressively diluted by cold cis molecules. Under the conditions of the experiment, this leads to rapid deactivation of the trans molecules, so that the higher energy HCl elimination channel ($E_{act} \simeq 70$ kcal/mol)[22b] is quenched while the lower energy isomerization channel ($E_{act} = 55$ kcal/mol[20]) is still able to proceed. This point is discussed in more detail in the following section.

D. α-d_1- and *trans*-d_1-Vinyl Chloride (Ia, Ib). In order to investigate the laser-induced elimination reaction in more detail, α-d_1- and *trans*-d_1-vinyl chloride were synthesized as described above and subjected to infrared photolyzing conditions. The resulting reactions were, for the α-d_1 species,

$$CH_2{=}CDCl + n\hbar\nu \rightarrow \begin{cases} C_2H_2 + DCl & (12a) \\ C_2HD + HCl & (12b) \end{cases}$$

while the trans-d_1 initially isomerized (eq 13)

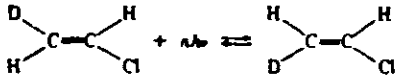

(13)

and subsequently eliminated to form acetylene (eq 14).

$$CHD{=}CHCl + n\hbar\nu \rightarrow \begin{cases} C_2H_2 + DCl & (14a) \\ C_2HD + HCl & (14b) \end{cases}$$

The product mixtures from all reactions were carefully examined for evidence of deuterium migration, but none was found; that is, no cis or trans β-d_1 species was formed when starting with the α-d_1, and no α-d_1 was formed when starting with trans-d_1.

A dilution experiment was also carried out on a 1:1 mixture of α-d_1- and h_3-vinyl chloride. The latter component was excited by infrared radiation from the 9.6-μm band of the CO_2 laser, which is not absorbed by, and has no effect on, the singly deuterated species. The dissociation yield was considerably reduced from that expected from pure vinyl chloride at the same pressure. This is attributed to rapid vibrational deactivation by the unexcited trans-d_1 species present in the mixture; similar behavior was seen in the *trans*-dichloroethylene system, which isomerizes to the nonabsorbing cis form. In a mixture in which *both* species are excited by a given infrared laser frequency, such as the *trans*- and *cis*-d_1-vinyl chloride discussed below, there was no appreciable diminution of the reaction yield.

Branching Ratio for HCl/DCl Elimination. One question we wished to explore was whether there was any preference for elimination from a particular position in the parent molecule, i.e. the branching ratios for reactions 12 and 14. This was investigated by measuring $[C_2HD]/[C_2H_2]$ ratios in the products of these reactions, using GC/MS. In order to make sure that the measured isotope ratios indeed reflected the initial branching ratios, and were not affected by subsequent H-atom exchange, a mixture of C_2D_2 (Merck Sharpe and Dohme; stated deuterium purity >99%) and HCl was analyzed over a 3-day period. This experiment demonstrated two points: (1) The absence of d_2-vinyl chloride in the infrared spectrum of the mixture showed that back-reaction between acetylene and HCl was negligible under our conditions. (2) The infrared spectrum of the acetylene[20] showed that C_2HD made up less than 3% of the total, verifying that H/D exchange also did not occur.

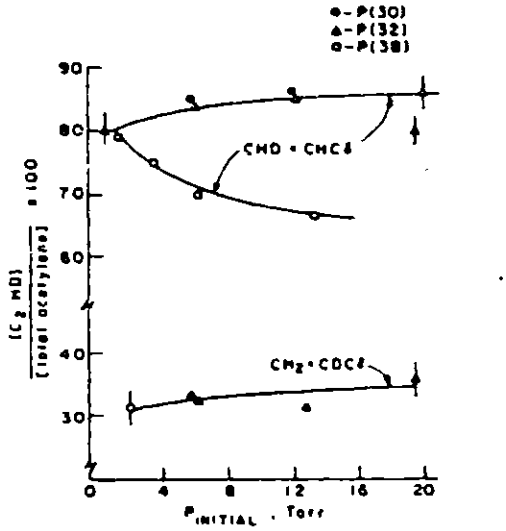

Figure 1. Effective branching ratios for HCl/DCl elimination in infrared laser pumped d_1-vinyl chloride. The CO_2 laser P(30), P(32), and P(38) [10.6 μm] lines were employed, as indicated in the figure. The precision of each determination is ±2%, as shown.

The results of the experiment are shown in Figure 1. As will be discussed shortly, cis-trans isomerization precedes HCl elimination in CHD=CHCl. Thus, the preponderance of HCl (vs. DCl) elimination in that system could be consistent with either cis, trans, or *gem* elimination. But the opposite result in CH_2=CDCl, coupled with the lack of H migration across the double bond, can be explained only by strongly favored *gem* or α,α-elimination.

The HCl/DCl elimination branching ratio also displays an interesting dependence on reactant pressure and laser line, shown in Figure 1. For irradiation by the P(32) line, this ratio is nearly constant with pressure (~80% HCl elimination from CHD=CHCl; ~30% from CH_2=CDCl). With the P(38) line, however, the HCl elimination ratio from CHD=CHCl drops from ~80% to ~65% over the pressure range 1–15 Torr. Several possible explanations for this behavior may be considered.

(1) The elimination of HCl or DCl from a particular site may be specific to the mode excited by the laser, with the mode specificity relaxed by collisions. This is considered particularly unlikely for several reasons. First, the two laser lines [P(32) and P(38)] excite different rotational states of the *same* mode of vibration in the CHD=CHCl molecule. Furthermore, all other behavior of this and many other systems is best interpreted in terms of rapid redistribution of vibrational energy within the molecule, rather than by mode-specific excitation.

(2) Some bimolecular process, such as H-atom abstraction,

may tend to make different sites equivalent. Since no radical chain products are found in any of the reaction mixtures, however, this is also considered unlikely. Furthermore, such a mechanism would not be sensitive to which laser line was used to excite the system.

(3) The most probable explanation is in terms of competing unimolecular elimination pathways for α,α- and α,β-elimination, with very similar threshold energies for the two modes of dissociation, as in the case of HX elimination from haloalkanes.[31] Energy deposition studies show that more energy is coupled into the vinyl chloride gas at higher pressures, leading to higher average vibrational excitations.[32] The energy deposition is strongly dependent on which laser line is used. This will be discussed in greater detail in the following section.

Competition between Reaction Pathways, Isomerization vs. Elimination. As noted above, infrared irradiation of *trans*-d_1-vinyl chloride always produced substantial quantities of the cis isomer along with dissociation products. In order to gain information about the competition between the isomerization pathway (reaction 13) and the elimination (reaction 14), a series of experiments was carried out at varying energy fluences through the sample. This was done by condensing the CO_2 laser beam with the two-Ge-lens telescope, which had an $f/$ number variable between $f/20$ and $f/70$. A simple treatment of the geometrical optics of the lens system[32] gives, as a first approximation to the peak intensity at the focal point of the beam,

$$I_{peak} = \frac{P_E}{f^2\lambda^2} \tag{15}$$

where P is the peak power of the laser pulse (6.7×10^8 W) and λ the wavelength (10.3 μm). Thus the intensity at the focal point varied between 3.3×10^9 W/cm^2 (at $f/70$) and 4×10^{10} W/cm^2 (at $f/20$).

The results are shown in Figure 2. At large $f/$numbers (weak focusing), no HCl or acetylene is produced, and the [cis-d_1]/[trans-d_1] ratio remains at its initial value. As the focusing is increased, isomerization is seen to take place while relatively little dissociation occurs. At the lowest $f/$number optics used, the isomerization appears to level off at a [cis]/[trans] ratio of about 1.2, while extensive dissociation occurs. The equilibrium ratio of the two isomers, calculated as the ratio of vibrational partition functions, was computed to be 0.92 at 300 K and 0.95 for temperatures exceeding 600 K. The somewhat larger experimental value may reflect preferential absorption of the infrared radiation by the trans isomer relative to the cis, leading to a greater degree of dissociation.

The basis of this behavior is the lower activation energy for isomerization relative to HCl elimination.[33] This leads to the possibility of the former reaction taking place at lower vibrational energy content in the vinyl chloride molecule than is required for dissociation.

Comparison with RRKM Theory. A. Kinetic Model. Most detailed treatments of multiphoton induced reactions[35,36] have relied on the solution of a master equation incorporating excitation, relaxation, and reaction terms. From these studies we observe several dynamic features of the population distribution over energy, $f(E)$: (a) The average energy $\langle E \rangle$ of the distribution increases only during the laser pulse. (b) A maximum $\langle E \rangle$ is reached during the pulse where up-pumping is balanced by population loss via reaction of hot molecules. (c) Very little reaction occurs after the pulse because molecules unreacted by the end of the pulse are collisionally deactivated. (d) The shape of the population distribution is nearly identical with a Poisson for $\langle E \rangle$ below the critical energy of reaction. To avoid the lengthy computation and the numerical approximations used to obtain the individual rate coefficients coupling the various energy levels, we have used these observations as the basis of a simplified kinetic model.

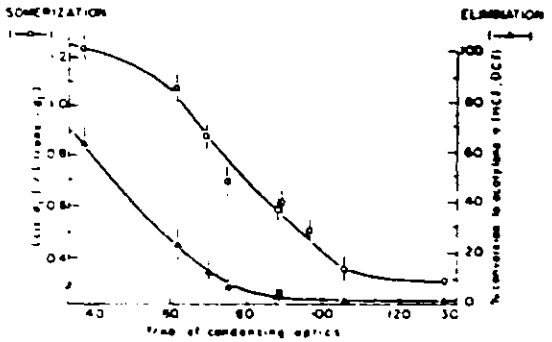

Figure 2. Competition between infrared laser induced isomerization and HCl, DCl elimination in *trans*-d_1-vinyl chloride. All experiments at an initial pressure of 3.2 Torr, 1500 pulses at 10.8 μm with 0.3 J incident energy. The $f/$number is equal to the focal length of the lens combination divided by the diameter of the Gaussian beam.

Our model is based on several assertions. (a) The population distributions are characterized by the average vibrational excitation $\langle E \rangle$ and can be expressed analytically for $\langle E \rangle$ above a few kilocalories per mole. The form of the distribution may be as narrow as a Poisson,

$$f(n) = \frac{e^{-\langle n \rangle}(\langle n \rangle)^n}{n!} \tag{16}$$

with $E = n\hbar\omega$ and $\langle E \rangle = \langle n \rangle \hbar\omega$. Although the master equation treatments predict a Poisson, this may be an artifact of using a harmonic energy grid, thus producing the same distribution as for coherently pumped harmonic oscillators.[37] The broadest distribution possible is the maximal entropy or Boltzmann-like distribution[38]

$$f(E) = \frac{N(E)\, e^{-\gamma E}}{Q} \tag{17}$$

where $N(E)$ is the Whitten-Rabinovitch expression for the density of states,[39]

$$Q = \int_0^\infty N(E) e^{-\gamma E}\, dE \tag{18}$$

and γ is a temperature-like parameter determined from

$$\langle E \rangle = \frac{\int_0^\infty E N(E) e^{-\gamma E}\, dE}{Q} \tag{19}$$

(b) When reaction occurs, the form of the distribution is not greatly affected. For the 3.2 Torr *trans*-d_1-vinyl chloride system used in this model, very little reaction occurs for each pulse. Only the highest energy molecules, comprising a small fraction of the total distribution, react.

(c) In the 1-s interval between laser shots, the products from the reaction zone mix, by diffusion, into the rest of the unreacted cell volume.

(d) Using assertions (a)-(c), the net reaction can be approximated by a continuous process analogous to placing all the brief intervals of reaction back to back. The total time of reaction is then the total number of laser pulses times the reaction time per pulse. This time was chosen as 10^{-7} s/pulse, to include the full laser pulse and to allow for two or three collisions (at 3.2 Torr) during each pulse.

(e) Since the $\langle E \rangle$ of the population distribution is static (observation (b)) during this interval, a constant reaction rate for a particular reaction j can be calculated using RRKM unimolecular reaction rates[40] averaged over the proper population distribution:

Table I. Vibrational Frequencies of Deuterated Vinyl Chlorides and Transition-State Configurations (cm^{-1})

	trans-d_1-vinyl chloride				*cis*-d_1-vinyl chloride			
mode[a]	molecule	isom t.s.	β-elim t.s.	α-elim t.s.	molecule	isom t.s.	β-elim t.s.	α-elim t.s.
(a′) 1	3114	3000	3000	2200	3090	3000	2200	2200
2	3066	3000	2500	3000	3047	3000	3000	3000
3	2231	2200	2200	2030	2210	2200	2500	2200
4	1608	1300	1800	1800	1580	1300	1800	1800
5	1308	1300	1308	1300	1315	1300	1315	1300
6	1237	1237	1240	1130	1328	1328	1320	1250
7	909	700	750	r.c.	909	700	750	r.c.
8	678	650	r.c.	490	710	680	r.c.	490
9	385	350	280	280	368	350	280	280
(a″) 10	947	r.c.[b]	1500	1500	927	r.c.	1500	1500
11	798	700	800	750	790	720	800	750
12	515	515	515	515	543	543	540	540

[a] Number of normal modes in accordance with standard assignment; see ref 29a and 38. [b] r.c. = reaction coordinate.

$$k_j = \int_{E_0}^{\infty} k_j^{RRKM}(E) f(E)\, dE \qquad (20)$$

The energy-dependent rates $k_j^{RRKM}(E)$, incorporating the Whitten-Rabinovitch density of states function, are given by

$$k^{RRKM}(E) = h^{-1} \frac{\sigma_r^{\dagger}}{\sigma_r} \frac{(E - E_0 + \alpha^{\dagger} E_z^{\dagger})^{s-1}}{(E + \alpha E_z)^{s-1}} \times \frac{\prod_{i=1}^{s} \omega_i \; 1 - \beta^{\dagger} \frac{dW^{\dagger}(E^{\prime\dagger})}{dE^{\prime\dagger}}}{\prod_{i=1}^{s-1} \omega_i^{\dagger} \; 1 - \beta \frac{dW(E')}{dE'}} \qquad (21)$$

with

$$\alpha = 1 - \beta W(E')$$

$$\beta = \frac{s-1}{s} \frac{(\omega^2)}{(\omega)^2}$$

$$W(E') = \exp[-2.4191(E')^{0.25}]$$

and $E' = E/E_z$. The ω's are the normal-mode vibrational frequencies, and E_z is the zero-point vibrational energy, for the parent molecule or the transition state (denoted by †). There are $s = 12$ normal modes for the vinyl chloride molecule, and the rotational symmetry numbers $\sigma_r = \sigma_r^{\dagger} = 1$. The vibrational frequencies for the parent *cis*- and *trans*-d_1-vinyl chloride were taken from published analyses of the infrared spectrum,[41] and those for the transition states estimated by standard methods.[42] These frequencies are listed in Table I.

Using these assertions, we can approximate the reaction kinetics of the α-d_1-vinyl chloride system as a set of parallel first-order reactions:

$$(\text{trans-}d_1) \xrightarrow{k_1} (\text{cis-}d_1) \qquad (22a)$$

$$(\text{trans-}d_2) \xrightarrow{k_2} C_2H_2 + DCl \qquad (22b)$$

$$(\text{trans-}d_1) \xrightarrow{k_3} C_2HD + HCl \qquad (22c)$$

and

$$(\text{cis-}d_1) \xrightarrow{k_4} (\text{trans-}d_1) \qquad (23a)$$

$$(\text{cis-}d_1) \xrightarrow{k_5} C_2H_2 + DCl \qquad (23b)$$

$$(\text{cis-}d_1) \xrightarrow{k_6} C_2HD + HCl \qquad (23c)$$

where the k_j are determined only by (E) and the choice of distribution in eq 20. In this system, k_1 and k_4 are the rates for cis ⇌ trans isomerization. The trans-elimination rate from the trans isomer is k_2; this is set equal to zero, since it is equivalent to isomerization followed by cis elimination. Both β(cis) and α(*gem*) elimination can contribute to k_3. Similarly, k_5 is the rate for β(cis) elimination from the cis isomer, and k_6 is the rate for (*gem*) elimination. Equations 22 and 23 lead, in turn, to a set of coupled equations for the concentrations of *cis*- and *trans*-d_1-vinyl chloride:

$$\frac{d}{dt}[\text{trans-}d_1] = -(k_1 + k_2 + k_3) f [\text{trans-}d_1] + k_4 f [\text{cis-}d_1] \qquad (24a)$$

$$\frac{d}{dt}[\text{cis-}d_1] = k_1 f [\text{trans-}d_1] - (k_4 + k_5 + k_6) f [\text{cis-}d_1] \qquad (24b)$$

The factor f is the fraction of molecules in the cell which are pumped to high vibrational excitation by the focused laser beam. We estimate f to be $\sim 5 \times 10^{-5}$, which is the approximate volume encompassing the reacting molecules[5] divided by the total cell volume (214 cm^3). Variations of f by ±50% affected the calculated results by only 1-2%.

We find the eigenvalues of eq 24, from the usual determinantal procedure, as

$$r^{\pm} = \frac{1}{2}\{-f(p+q) \pm f[(q-p)^2 + 4k_4k_1]^{1/2}\} \qquad (25)$$

with

$$q = k_1 + k_2 + k_3 \qquad (26a)$$

and

$$p = k_4 + k_5 + k_6 \qquad (26b)$$

The concentrations after an irradiation time t are given by

$$\begin{pmatrix} [\text{trans-}d_1] \\ [\text{cis-}d_1] \end{pmatrix}_t = c_1 \begin{pmatrix} 1 \\ \gamma^+ \end{pmatrix} e^{r^+ t} + c_2 \begin{pmatrix} 1 \\ \gamma^- \end{pmatrix} e^{r^- t} \qquad (27)$$

In eq 23

$$\gamma^{\pm} = \frac{r^{\pm} + qf}{k_4 f} = \frac{k_1 f}{pf + r^{\pm}} \qquad (28)$$

The total reaction time was 1.5×10^{-4} s, as mentioned above.

The coefficients c_1 and c_2 are found from the initial conditions, $[\text{trans-}d_1]_{t=0} = c_1 + c_2 = 0.78$ for the sample we used, and

$$[\text{cis-}d_1]_{t=0} = c_1\gamma^+ + c_2\gamma^- = 0.22 \qquad (29)$$

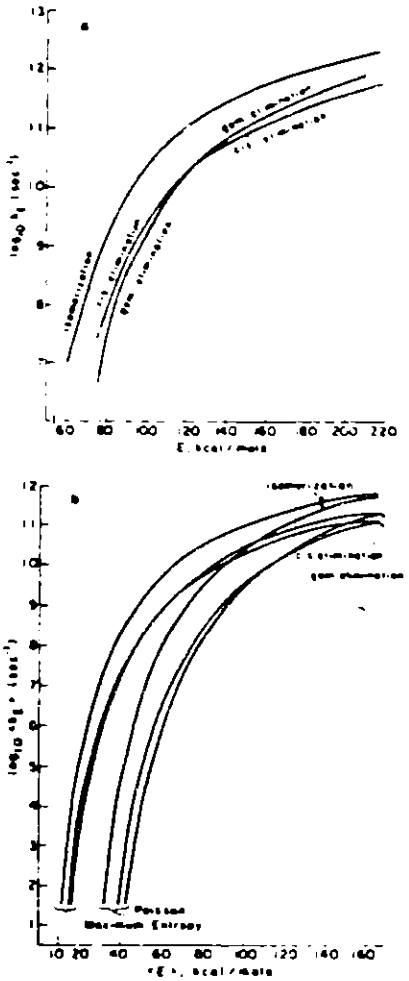

Figure 3. (a) Calculated RRKM rates for (i) cis-trans isomerization, (ii) β(cis)-elimination, and (iii) α-elimination, using the frequencies listed in Table II for *trans*-d_1-vinyl chloride. Activation energies were 61 kcal/mol for isomerization, 69 kcal/mol for β-elimination, and 73 kcal/mol for α-elimination. (b) Averages of these rates over Poisson (eq 31) and maximal-entropy (eq 32) energy distributions, as a function of mean energy $\langle E \rangle = \int E f(E)\, dE$.

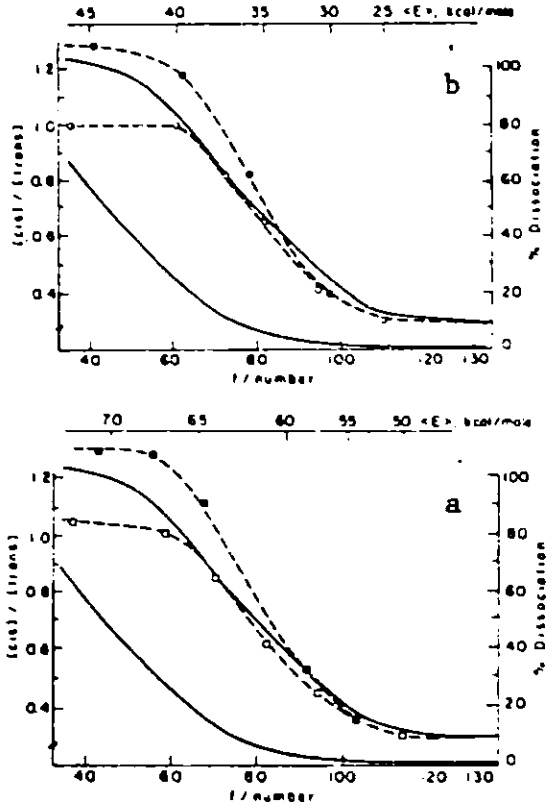

Figure 4. Dissociation (right-hand scale) and isomerization (left-hand scale) yields as a function of f (number and mean energy. The solid curves are experimental data, taken from Figure 2. The dashed curves are the results of the calculations described in this section. Open symbols, $\langle E \rangle_{\mathrm{exp}} = \langle E \rangle_{\mathrm{calc}}$; solid symbols, $\langle E \rangle_{\mathrm{exp}} = \langle E \rangle_{\mathrm{calc}} + 1$ kcal/mol. (a) Calculation with Poisson distribution, eq 31. The values of E_0 are 63, 70, and 69 kcal/mol for isomerization, cis elimination, and *gem* elimination, respectively. (b) Calculation with Boltzmann-like maximal-entropy distribution, eq 32. The corresponding values of E_0 are 61, 69, and 73 kcal/mol.

The rates of formation of the two isotopic varieties of acetylene are

$$\frac{d}{dt}[C_2H_2] = fk_2[\text{trans-}d_1] + fk_5[\text{cis-}d_1] \qquad (30a)$$

$$\frac{d}{dt}[C_2HD] = fk_3[\text{trans-}d_1] + fk_6[\text{cis-}d_1] \qquad (30b)$$

Inserting the precursor concentration (27) in eq 30 leads to the solutions

$$[C_2H_2]_t = w(e^{x't} - 1) + x(e^{z't} - 1) \qquad (31a)$$

and

$$[C_2HD]_t = y(e^{x't} - 1) + z(e^{z't} - 1) \qquad (31b)$$

with

$$w = \frac{c_1 f}{r^+}(k_2 + k_5\gamma^+) \qquad (32a)$$

$$x = \frac{c_2 f}{r^-}(k_2 + k_5\gamma^-) \qquad (32b)$$

$$y = \frac{c_1 f}{r^+}(k_3 + k_6\gamma^+) \qquad (32c)$$

and

$$z = \frac{c_2 f}{r^-}(k_3 + k_6\gamma^-) \qquad (32d)$$

B. Competition between Isomerization and Dissociation. Figure 3 shows a set of calculated RRKM rates for the isomerization, α,α-elimination and α,β-elimination channels, along with averaged rates using both Poisson and maximal entropy distribution functions. For a given mean excitation level $\langle E \rangle$, the value of the averaged rate constant for the Poisson distribution can be many orders of magnitude lower than for the Boltzmann-like distribution. This is a consequence of the more extended "tail" of the latter distribution which, even for low values of $\langle E \rangle$, extends to energies where the k^{RRKM} become large (see ref 38). As noted by Grant et al.,[39] appreciable reaction occurs with a narrow Poisson distribution only at $\langle E \rangle$ close to the E_0 of reaction.

In Figure 4 we show the comparison of relative isomerization/dissociation yields, calculated from the kinetic model [illegible]

the RRKM rate theory described in the preceding section, with the experimental data. For each limiting form of the vibrational energy distributions, and at several values of incident energy flux Φ (determined from the focal length of the beam condensing optics by eq 15), we found a value of $\langle E \rangle$ which gave the proper percent dissociation of the vinyl chloride into acetylene and HCl. This value was then used to calculate the expected [cis]/[trans] ratio at that energy flux.

As can be seen from Figure 4, either form of the distribution is capable of reproducing the observed yields. The difference is that at any given flux Φ, the value of $\langle E \rangle$ which is required is about twice as high for the narrower Poisson distribution (eq 16) than for the maximal-entropy, or Boltzmann-like, distribution (eq 17). This is just what would be expected from the behavior of the energy-averaged RRKM rates shown in Figure 3b. We also tested the effect of small variations in the activation energies, E_0, for the isomerization and two dissociation channels, within the stated experimental uncertainties for these quantities (±1-2 kcal/mol); the values listed for the curves in Figures 3 and 4 gave the best agreement with the data. The effect of allowing a small amount of differential excitation between cis and trans molecules is also shown in Figure 4; increasing $\langle E \rangle_{trans} - \langle E \rangle_{cis}$ from zero to only 1 kcal/mol causes the limiting [cis]/[trans] ratio at high energy fluxes to increase from 1.05 to 1.25. Since the absorption coefficients for the particular laser line employed are certainly different for the two isomers, such a small amount of differential excitation is quite reasonable, and satisfactorily accounts for the observed ratio.

The principal conclusion from these results is that a statistical, non-mode-specific model provides an excellent description of the laser-induced chemistry taking place in this system. The internal energy distributions are characterized only by a mean energy ($\langle E \rangle$), and RRKM rates, which presuppose a free flow of energy throughout the molecule, are employed. It is not possible, however, to specify a unique form of the distribution function without an independent measurement of the absolute amount of energy deposited by the laser field.

C. Stereochemistry of the Elimination Reaction. The preceding calculation also gives α/β elimination ratios which are in agreement with the experimental results shown in Figure 1, namely, 80-90% C_2HD (HCl elimination) from CHD=CHCl and 30-40% C_2HD from CH_2=CDCl. The former ratio *decreases*, and the latter increases, as the mean excitation ($\langle E \rangle$) in the system is raised. This ($\langle E \rangle$) dependence could explain the pressure dependence found for the P(38) line: increasing vinyl chloride pressure often has the effect of *increasing* the mean excitation of the molecules, since pressure broadening of the absorption lines helps to overcome local saturation effects.[17] The magnitude of this effect would, of course, vary from one line to another, thus accounting for the different behavior following excitation with the P(32) and the P(38) lines. We have, in this case, the ability to influence the outcome of a reaction by selective excitation with one or another laser line. This is *not* a result of any mode-specific excitation, however; in fact, it is just the opposite, since the result is predicted by a statistical (RRKM) model. The effect of changing laser lines is, instead, a more subtle one of varying the amount of energy deposited in the system, which in turn depends on such factors as saturation, frequency matching, and pressure broadening. Clearly, any relationship between excitation frequency and reaction product distribution, which is taken to be evidence for a mode-specific process, must be carefully evaluated in terms of energy deposition in the system before such evidence can be accepted.

The predominant mode of elimination in these systems is seen to be *cis*- or *gem*-elimination. Precedents in the literature for this type of reaction are sparse; a general comment that "elimination reactions of halo-olefins to acetylenes ... proceed best with the elements to be eliminated are located *trans*"[4] is based on a small number of examples, none involving hydrogen halide elimination. Haloalkanes dehydrohalogenate via α,α and α,β channels,[31] but their stereochemistry need not resemble that of the haloolefins. Lee and co-workers[32] have observed *cis*-elimination from CO_2-laser-excited CF_2=CHCl in a molecular beam, and find no energy barrier in the exit channel for this reaction.

The large fraction of α,α-elimination found in these systems raises the question of whether products characteristic of the possible carbene intermediate could be isolated. Alkylidene carbenes are known in solution,[33,34] but only the difluoro species has been observed in the gas phase.[35] It is possible, though, that with a parent molecule in which the rearrangement to the acetylene were inhibited, the gas-phase carbene could be produced by laser-induced dehydrohalogenation, and that its products could be isolated.

Straus and co-workers[36] have shown that the mercury-photosensitized reactions of substituted ethylenes proceed with free rotation about the C-C bond and α-elimination to produce the carbene. Recent observations of intersystem crossing induced by multiple infrared photon absorption,[37] along with the similarity of the mercury-photosensitized and infrared-multiple photon pathways in this case, suggest that, when the energy content of the molecule is of the order of 100 kcal/mol, vibronically induced singlet-triplet mixing may occur. This suggests not only that the vibrational energy is freely redistributed among all available modes, but that even the distinction between electronic and vibrational energy may break down.

Acknowledgments. This work was supported by the Office of Advanced Isotope Separation, Department of Energy, under Contract EY-76-S-02-2793. We also thank Professors Klaus Biemann and George Whitesides for providing GC, MS analyses.

References and Notes

(1) R. V. Ambartzumyan, Yu. A. Gorokhov, V. S. Letokhov, and G. N. Makarov, *J. Exp. Theor. Phys. Lett.*, 21, 375 (1975).
(2) (a) R. V. Ambartzumyan and V. S. Letokhov in "Chemical and Biochemical Applications of Lasers", Vol. III, C. B. Moore, Ed., Academic Press, New York, N.Y., 1977, pp 167-316. (b) C. D. Cantrell, S. M. Freund, and J. L. Lyman in "Laser Handbook", Vol. III, North-Holland Publishing Co., Amsterdam, 1978.
(3) W. Braun and W. Tsang, *Chem. Phys. Lett.*, 44, 354 (1976).
(4) T. H. Richardson and D. W. Setser, *J. Phys. Chem.*, 81, 2301 (1977).
(5) F. M. Lussier and J. I. Steinfeld, *Chem. Phys. Lett.*, 50, 175 (1977).
(6) A. Yogev and R. M. J. Benmair, *Chem. Phys. Lett.*, 48, 290 (1977).
(7) Reaction 4 is reported to take place only in the presence of BCl_3 as an added sensitizer; C_2Cl_4 itself does not absorb the infrared radiation used to induce the reaction, according to H. R. Bachmann, R. Rinck, H. Noth, and F. L. Kompa, *Chem. Phys. Lett.*, 45, 169 (1977).
(8) W. C. Danen, W. D. Munslow, and D. W. Setser, *J. Am. Chem. Soc.*, 99, 6961 (1977).
(9) A. Yogev and R. M. J. Loewenstein-Benmair, *J. Am. Chem. Soc.*, 95, 8487 (1973).
(10) In the sense that the vibrational excitation of the reacting molecule is not significantly distributed among translational degrees of freedom, or to other molecules present in the system.
(11) S. Mukamel and J. Ross, *J. Chem. Phys.*, 66, 5235 (1977), and I. Shamah and G. Flynn, *J. Am. Chem. Soc.*, 99, 3191 (1977), have suggested that energy may indeed localize in a particular normal mode of vibration as a result of redistribution via V-V inelastic collisions. However, which modes are likely to accept vibrational energy is a property of the molecule itself and not of which mode may have been initially excited by the infrared pumping. In addition, the RRKM theory of unimolecular reactions, which we employ in the ensuing discussion, assumes that vibrational energy can localize in the reactive part of a molecule, as one of many possible configurations available to a system in which the energy is statistically distributed over all internal degrees of freedom.
(12) Z. Karny and R. N. Zare, *Chem. Phys.*, 23, 321 (1977).
(13) J. E. Francis and L. C. Leitch, *Can. J. Chem.*, 35, 348, 500 (1957).
(14) S. Enomoto and M. Asahina, *J. Mol. Spectrosc.*, 19, 137 (1966).
(15) A. N. Nesmeyanov and R. Kh. Freidlina, *Chem. Abstr.*, 40, 3451 (1946).
(16) H. C. Volger, *Recl. Trav. Chim. Pays-Bas*, 87, 501 (1968).
(17) F. M. Lussier, J. I. Steinfeld, and T. F. Deutsch, *Chem. Phys. Lett.*, 58, 277 (1976).
(18) Identified by infrared bands at 630, 1240, and 3330 cm^{-1}: A. V. Jones, *Proc. R. Soc. London, Ser. A*, 211, 285 (1952).
(19) C. F. Cullis, D. J. Hucknall, and J. V. Shepherd, *Proc. R. Soc. London, Ser.*

A, 338, 525 (1973).
(20) J. H. Dunn, C. M. Herter, and P. W. Trotter, U.S. Patent 2 635 122 (1953).
(21) M. J. Molera and E. Ariza, *An. R. Soc. Esp. Fis. Quim.* **54**, 389 (1958).
(22) (a) P. Cadman and W. J. Engelbrecht, *Chem. Commun.*, 453 (1970); (b) F. Zabel, *Int. J. Chem. Kinet.* **9**, 651 (1977).
(23) (a) A. A. Wessenberg, J. H. Goldstein, and E. B. Wilson, Jr., *J. Chem. Phys.* **17**, 1319 (1949); (b) E. Kloster-Jensen, *J. Am. Chem. Soc.*, **81**, 5673 (1959).
(24) Aa. S. Sudbø, P. A. Schulz, E. R. Grant, Y. R. Shen, and Y. T. Lee, *J. Chem. Phys.*, **68**, 1306 (1978).
(25) A. Gandini, C. Wilks, and R. A. Back, 13th Informal Conference on Photochemistry, Clearwater Beach, Fla., Jan. 1978.
(26) S. W. Benson, "Thermochemical Kinetics", Wiley, New York, N.Y., 1968.
(27) A. M. Goodall and K. E. Howlett, *J. Chem. Soc.*, 2599 (1954).
(28) (a) R. V. Ambartzumyan, N. V. Chekalin, V. S. Doljikov, V. S. Letokhov, and V. N. Lokuman, *J. Photochem.*, **6**, 55 (1976); (b) K. Nagai and M. Kobayama, *Chem. Phys. Lett.*, **51**, 329 (1977).
(29) (a) L. C. Hanson and G. P. Semeluk, *Can. J. Chem.*, **44**, 2143 (1962); (b) P. M. Jeffers, *J. Phys. Chem.*, **76**, 2823 (1972).
(30) (a) G. Herzberg, "Molecular Spectra and Molecular Structure. II. Infrared and Raman Spectra of Polyatomic Molecules", Van Nostrand, Princeton, N.J., 1945, pp 288–293; (b) W. F. Coney, *Phys. Rev.*, **47**, 368 (1935); (c) F. Stitt, *J. Chem. Phys.*, **8**, 56 (1940).
(31) (a) K. C. Kim, D. W. Setser, and B. E. Holmes, *J. Phys. Chem.*, **77**, 307 (1973); (b) K. C. Kim and D. W. Setser, *ibid.*, **78**, 2166 (1974).
(32) D. R. Keefer, J. E. Allen, Jr., and W. B. Person, *Chem. Phys. Lett.*, **43**, 364 (1976).
(33) The activation energy for cis–trans isomer ration of 3-d₁-vinyl chloride is not known, but should be intermediate between that of ethylene-d_2 (62 kcal/mol[34]) and 1,2-dichloroethylene (55 kcal/mol[35]). In any case, it must be less than that for HCl elimination (69 kcal/mol[17]).
(34) J. E. Douglas, B. S. Rabinovitch, and F. S. Looney, *J. Chem. Phys.*, **23**, 315 (1955).
(35) J. L. Lyman, *J. Chem. Phys.*, **67**, 1868 (1977).
(36) E. R. Grant, P. A. Schulz, Aa. S. Sudbø, Y. R. Shen, and Y. T. Lee, *Phys. Rev. Lett.*, **40**, 115 (1978).
(37) P. Camuthers and N. N. Nieto, *Am. J. Phys.*, **33**, 537 (1965).
(38) C. C. Jensen, R. D. Levine, and J. I. Steinfeld, *J. Chem. Phys.*, **69**, 1432 (1978).
(39) G. Z. Whitten and B. S. Rabinovitch, *J. Chem. Phys.*, **38**, 2466 (1963).
(40) P. J. Robinson and K. A. Holbrook, "Unimolecular Reactions", Wiley-Interscience, New York, N.Y., 1972.
(41) (a) S. Nanba, S. Ichinoka, and S. Enomoto, *J. Chem. Phys.*, **31**, 1151 (1959); (b) G. Varsanyi, *Acta Chim. Hung.*, **35**, 81 (1963).
(42) H. E. O'Neal and S. W. Benson, *J. Phys. Chem.*, **71**, 2903 (1967); see also E. Tschuikow-Roux and S. Kodama, *J. Chem. Phys.*, **50**, 5304 (1969).
(43) E. Eliel, "Stereochemistry of Carbon Compounds", McGraw-Hill, New York, N.Y., 1962, p 348.
(44) Aa. S. Sudbø, P. A. Schulz, Y. R. Shen, and Y. T. Lee, *J. Chem. Phys.*, **69**, 2312 (1978).
(45) P. J. Stang, *Acc. Chem. Res.*, **11**, 107 (1978); *Chem. Rev.*, in press.
(46) H. D. Hartzler, in "Carbenes", Vol. II, R. A. Moss and M. Jones, Jr., Ed., Wiley-Interscience, New York, N.Y., 1975, pp 43–100.
(47) P. J. Stang, J. Davis, and D. P. Fox, *J. Chem. Soc., Chem. Commun.*, 17 (1975).
(48) (a) O. P. Strausz, R. J. Norstrom, D. Saluhub, R. K. Gosavi, H. E. Gunning, and L. G. Cazmaschi, *J. Am. Chem. Soc.*, **92**, 6395 (1970); (b) R. J. Norstrom, H. E. Gunning, and O. P. Strausz, *ibid.*, **88**, 1454 (1978).
(49) I. Burak, T. J. Quelly, and J. I. Steinfeld, *J. Chem. Phys.*, to be published.

APPENDIX B. "Formation of Vinylidenecarbene Intermediates in Multiple Infrared Photon Elimination Reactions"

C. Reiser and J. I. Steinfeld, J. Phys Chem. 84, 680 (1980)

[Reprinted from the Journal of Physical Chemistry, 84, 680 (1980)]

Formation of Vinylidenecarbene Intermediates in Multiple Infrared Photon Elimination Reactions

Publication costs assisted by the U.S. Department of Energy

Sir: Multiple infrared photon excitation (MIRPE) of α-chloro olefins ($R_2C{=}CHCl$) by intense CO_2 laser pulses has been found to lead to elimination of HCl.[1-3] Deuterium labeling studies[3] have shown that the reaction proceeds mainly via a 3-center elimination. This result suggests that vinylidenecarbene ($R_2C{=}C{:}$) may be formed during the dehydrohalogenation. Such species are well-known in solution;[4] however, the only other gas-phase reaction in which they are formed appears to be mercury-photosensitized 1,1 eliminations.[4,5] Carbenes, such as $:CF_2$, have often been observed in laser-induced multiple-photon dissociation.[6]

In the MIRPE of vinyl chloride (R = H, D), acetylene is the sole hydrocarbon product, suggesting that rearrangement of the carbene is extremely rapid, if not concerted with the elimination. This behavior is consistent with expectations[4,5] that the barrier to the rearrangement

$$H_2C{=}C{:} \rightarrow HC{\equiv}CH \qquad (1)$$

is extremely low. We have extended our previous work[3] on these systems to substituted vinyl chlorides (R = CH_3, F) in order to see whether the rearrangement could be slowed down sufficiently to permit the vinylidenecarbene to exist as a long-lived intermediate.

1-Chloro-2-methylpropene (Aldrich) and 2-chloro-1,1-difluoroethylene (PCR) were used as received except for transfer under reduced pressure to the reaction cell. Infrared spectra prior to MIRPE showed no major impurities to be present. The compounds were photolyzed with the 9.6-μm P(16) or P(18) and 10.6-μm R(18) CO_2 laser lines, respectively, either alone at pressures of 4–5 torr or in the presence of added gases. The gaseous product mixtures were collected and analyzed by GC/MS (H/P 5990 A or Hitachi RMU-6L).

The MIRPE of $(CH_3)_2C{=}CHCl$ leads to HCl (observed in the product infrared spectrum) and butadiene as major products, with smaller amounts of allene, 2-butyne, and diacetylene. Photolysis in the presence of CH_3OH, H_2O, NH_3, H_2S, or D_2S vapor yielded no additional products. These results suggest that the $(CH_3)_2C{=}C{:}$ formed by loss of HCl rearranges extremely rapidly, either by methyl migration across the double bond (eq 2) or by intramolecular insertion (eq 3).

Since the acetylenic form is ~30–40 kcal/mol more stable than the carbene,[7] the resulting 2-butyne, if formed, would contain a large amount of excess vibrational energy. Some of this could be stabilized by collisional relaxation,

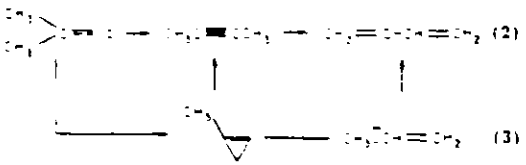

(2)

(3)

but the principal route seems to be further rearrangement to the still more stable butadiene. The same products could be derived from the methylcyclopropene since the ring can open to form the butenic diradical of the butadiene by way of the 2-carbene.[7] A possible test of this proposed mechanism would be to deactivate collisionally these intermediates and quench further rearrangement by adding an inert buffer gas. It must be remembered, however, that increased collisions can also influence the MIRPE process itself[1,2] and thus the mean excitation in the products. It may be noted that allene is also found when CF_2Cl_2 is photolyzed in the presence of $(CH_3)_2C{=}CH_2$ and results from secondary multiphoton excitation of $CH_3(CH_3)C{=}CH_2$.[8] Diacetylene appears to be a ubiquitous side product in reactions of this type.[1,2,5]

The behavior of $CF_2{=}CHCl$ under the same conditions is quite different. Aside from HCl, the principal products are C_2F_4 (67%) and C_2F_3H (33%). No C_2F_2 is observed. In the presence of added H_2S or CH_3OH, the products are $C_2F_3H_3$ (82%),[11] C_2F_3H (12%), and C_2F_4 (6%). It seems clear that, in this system, the $F_2C{=}C{:}$ species is long-lived, with essentially no rearrangement taking place to the acetylene. In the presence of labile hydrogens, the dominant reaction path seems to be H abstraction to form stable olefins. A possible mechanism to form the C_2F_4 would be secondary MIRPE of the vinylidenecarbene to form $:CF_2$ plus free carbon, a small amount of soot formation in the pure $CF_2{=}CHCl$ is consistent with this possibility. When the photolysis is carried out in the presence of D_2S, the principal product is C_2F_3HD, with a lesser amount of $C_2F_3D_3$ and small amounts of the previously mentioned products. The presence of $C_2F_3D_3$ confirms the existence of $F_2C{=}C{:}$, the large amount of C_2F_3HD suggests that a C–Cl homolysis channel, to form C_2F_3H, is also important in this system.[12] The chemistry of this system is, indeed, quite complex, since several dissociation channels following MIRPE are available.

These results demonstrate that, not surprisingly, difluorovinylidene does not undergo rearrangement and can readily be trapped by hydrogen donors, whereas isobutylidene undergoes rearrangement more rapidly than it can be trapped. Since $(CH_3)_2C{=}C{:}$ can be trapped in solution,[4] the activation barrier to rearrangement must be no less than 10–15 kcal/mol or so. In the case of $H_2C{=}C{:}$, Schaefer and co-workers[13] have predicted a barrier to rearrangement of 8.6 kcal/mol. For the rearrangement

$$F_2C{=}C{:} \rightarrow FC{\equiv}CF \qquad (4)$$

however, a semiquantitative MO calculation[14] gives an activation barrier ~50–60 kcal/mol higher than that for reaction 1. The greater vibrational complexity of $(CH_3)_2C{=}C{:}$, as compared with $H_2C{=}C{:}$ or $F_2C{=}C{:}$, will lead to a partitioning of absorbed infrared energy into internal modes of the first named species, thus providing sufficient energy to surmount the barrier.[15] For the parent or difluoro species, the lower degree of vibrational excitation is sufficient to permit reaction 1 to occur, but not reaction 4, with its appreciably higher barrier.

This work illustrates how the MIRPE process may be of value in chemical investigations by permitting the preparation of primary dissociation products or unstable intermediates at a high instantaneous concentration in the presence of cold diluents. Spectroscopic characterization of species such as vinylidenecarbenes, which have hitherto not been directly observed, may be possible in this way.

Acknowledgment. This work was supported by the Office of Advanced Isotope Separation Technology, U.S. Department of Energy (Contract EY-76-S-02-2793), and the Air Force Office of Scientific Research (Grant 78-3725). Professors G. Whitesides and K. Biemann provided GC, MS instrumental facilities. We also thank Professor P. J. Stang and E. R. Grant, and earlier referees, for valuable suggestions.

References and Notes

(1) F. M. Lussier and J. I. Steinfeld, *Chem. Phys. Lett.*, **50**, 175 (1977).
(2) C. Reiser, F. M. Lussier, C. C. Jensen, and J. I. Steinfeld, *J. Am. Chem. Soc.*, **101**, 350 (1979).
(3) Analogous results have been observed in fluorinated ethylenes by C. R. Quick and J. Wittig, *J. Chem. Phys.*, **69**, 4201 (1978).
(4) P. J. Stang, *Acc. Chem. Res.*, **11**, 107 (1978); P. J. Stang, *Chem. Rev.*, **78**, 383 (1978).
(5) O. P. Strausz, R. J. Norstrom, D. Salahub, R. K. Gosavi, H. E. Gunning, and I. G. Csizmadia, *J. Am. Chem. Soc.*, **92**, 6395 (1970); R. J. Norstrom, H. E. Gunning, and O. P. Strausz, *ibid.*, **88**, 1454 (1976).
(6) J. J. Ritter, *J. Am. Chem. Soc.*, **100**, 2441 (1978).
(7) J. H. Davis, W. A. Goddard III, and L. B. Harding, *J. Am. Chem. Soc.*, **99**, 2919 (1977).
(8) I. M. Bailey and R. Walsh, *J. Chem. Soc., Faraday Trans. 1*, 1146 (1978).
(9) E. J. York, W. Dittmar, J. R. Stevenson, and R. G. Bergman, *J. Am. Chem. Soc.*, **95**, 5680 (1973).
(10) A. Yogev and R. M. J. Loewenstein-Benmair, *J. Am. Chem. Soc.*, **95**, 6467 (1973).
(11) The GC–MS analysis did not permit us to distinguish between the two possible isomers, $CFH{=}CFH$ and $CF_2{=}CH_2$.
(12) Aa. S. Sudbø, P. A. Schulz, Y. R. Shen, and Y. T. Lee, *J. Chem. Phys.*, **69**, 2312 (1978); Aa. S. Sudbø, P. A. Schulz, E. R. Grant, Y. R. Shen, and Y. T. Lee, *ibid.*, **68**, 1306 (1978); Aa. S. Sudbø, P. A. Schulz, E. R. Grant, Y. R. Shen, and Y. T. Lee, *ibid.*, **70**, 912 (1979).
(13) C. E. Dykstra and H. F. Schaefer III, *J. Am. Chem. Soc.*, **100**, 1378 (1978); M. D. Conrad and H. F. Schaefer III, *ibid.*, **100**, 7820 (1978).
(14) O. P. Strausz, R. J. Norstrom, A. C. Hopkinson, M. Schoenborn, and I. G. Csizmadia, *Theor. Chim. Acta*, **28**, 183 (1973).
(15) Using an impulsive-half-collision model and the data on translational energy release following MIRPE of $F_2C{=}CHCl$,[1] we estimate a vibrational excitation of 15–20 kcal/mol in the $(CH_3)_2C{=}C$ fragment but only 2–5 kcal/mol for $H_2C{=}C{:}$ or $F_2C{=}C{:}$. To the extent that one can trust such a rough estimate, this result suggests that the barrier calculated[13] for rearrangement 1 may still be too high.

Department of Chemistry
Massachusetts Institute of Technology
Cambridge, Massachusetts 02139

Christopher Reiser
Jeffrey I. Steinfeld*

Received August 30, 1979

Two isomers of d_1-vinyl chloride were prepared, trans-d_1-vinyl chloride [C.1] and α-d_1-vinyl chloride [C.2].

C.1 trans-d_1-vinyl chloride

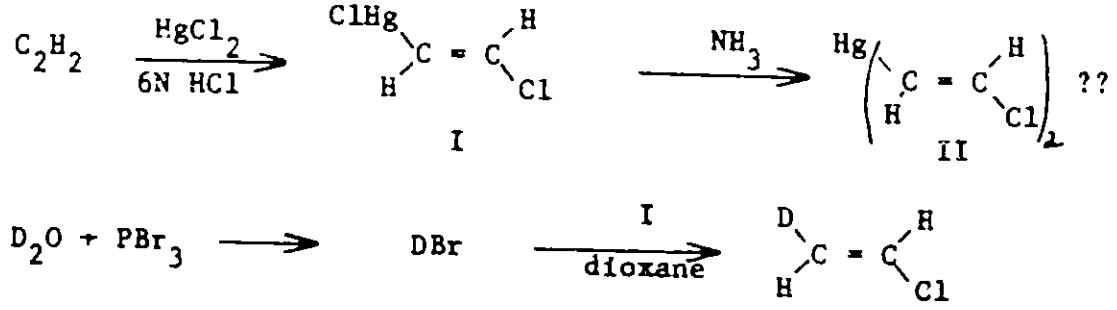

A 6N HCl solution was prepared by adding 60 ml conc. HCl to 40 ml boiled distilled water in a 250 ml flask. 96 g $HgCl_2$ were added and dissolved with ease. Welding grade acetylene was bubbled into the solution with a sintered glass bubbler; the excess gas was bubbled through water to prevent backstreaming of air. After 2 hours a white soapy precipitate began to form.

The precipitate was filtered off every 20 min or so to avoid clogging the bubbler, and continued to form for several hours. It was difficult to dry even in a vacuum desiccator. The precipitate can be recrystallized to fluffy white needles from benzene and showed an NMR doublet at δ6.28, δ6.34, affirming its identity as trans-chlorovinyl mercury chloride (I) [C.3].

Attempts at synthesizing trans-dichlorovinyl mercury (II) from I failed. A 40 ml sample of benzene saturated with I was placed in a dropping funnel. Upon addition of 40 ml ammonia a sticky dense white precipitate formed. The precipitate was difficult to collect and dissolved when washed with water. The remainder dried to a hard white solid which resisted attempts at dissolution.

DBr was synthesized by adding fresh D_2O dropwise to fresh boiling PBr_3. The gas was collected through a water condenser and an ice-cooled trap into a LN_2 cooled flask. Its IR spectrum showed at least 95% isotopic purity. The DBr was admitted to a 250 ml Erlenmeyer flask containing 25 ml of dioxane; the flask was shaken for one hour. The dioxane was then added to 26 g of I in a 3-necked RB flask sitting in a 50°C oil bath. Gas was collected by slowly flowing dry N_2 over the dioxane with continuous stirring. The N_2 stream passed through an ice cooled trap and two LN_2 traps. After one hour the contents of the two LN_2 traps were collected through a $KOH/CaCl_2$ filled tube into a gas flask. Its IR spectrum compared favorably with that published [C.3] for trans-d_1-vinyl chloride, showing about 96% isotopic purity with traces of moisture and acetylene. The ratio of trans to cis isomers was about 9:1.

Acetylene was cleaned from the mixture with a simple procedure. A solution of 10 ml water and 5 ml conc. nitric acid was saturated with silver nitrate. This solution was

frozen in a small flask with a ground glass neck. The gas mixture was then frozen into the flask. The contents were allowed to thaw, then were shaken for 30 minutes, during which a small amount of a white precipitate (presumably silver acetylide) formed. The gas in the flask was then frozen into a second flask containing loose P_2O_5 as a drying agent. Finally, the gas was frozen into a storage bulb. Its spectrum showed no trace of acetylene or moisture.

C.2 α -d_1-vinyl chloride

$$C_2HCl_3 \xrightarrow[H_2O]{CaO} \underset{\text{III}}{CH_2CCl_2} \xrightarrow[\text{(cold)}]{DBr,\ UV} \underset{\text{IV}}{CH_2BrCDCl_2}$$

$$\text{IV} \xrightarrow[EtOH]{Zn} \begin{matrix} H \\ H \end{matrix}\!\!>\!C=C\!<\!\begin{matrix} D \\ Cl \end{matrix}$$

1,1-dichloroethene (vinylidene chloride, III) was prepared from 1,1,2-trichloroethane by refluxing 30 ml in 120 ml water and 18 g CaO for 4 hours. The alkene was distilled off at 1 atm (bp = 32°) and redistilled using a Vigreaux column. The yield was 17 mls or 66%; the product was identified by IR and NMR and stored over hydroquinone to prevent polymerization. III is also commercially available.

DBr was synthesized as described in the preceeding section.

1,1-dichloro-2-bromoethane-1-d_1 (IV) was synthesized in a quartz flask fitted with a dry ice and acetone cooling collar.

15 mls of III were distilled into the flask in vacuo, followed by 20 ml of DBr, using LN_2 cooling. The contents melted upon removal of the LN_2 and refluxed from the dry ice/acetone cooled portion of the flask. A UV photoreactor (courtesy of the undergraduate laboratory) utilizing 15 Hg lamps was then employed to irradiate the reactants for 2 hours. The coolant was removed from the collar and excess reactant pumped off. The product (IV) was washed from the quartz flask with methylene chloride, treated with a saturated solution of sodium bicarbonate, dried over $CaCl_2$ and distilled (bp = 90° at 140 Torr). NMR revealed a broad peak at δ4.2. Recovery was 12 mls, or about 46% yield.

Six ml of IV was added over a 50 min. period to a refluxing suspension of Zn dust in 40 ml of ethanol. The evolved gas passed through two ice traps and was collected in a LN_2 cooled trap. The gas was passed four times over dry $CaCl_2$ in bulb to bulb distillations, after which no trace of EtOH was seen in the IR spectrum. The spectrum agreed well with that of [C.4] with excellent isotopic purity. About 2.6 g were recovered.

APPENDIX D. "Energy deposition in molecules resulting from multiple infrared photon absorption"

C. Reiser and J. I. Steinfeld, Opt. Eng. 19, 002 (1980)

Energy deposition in molecules resulting from multiple infrared photon absorption

Christopher Reiser
Jeffrey I. Steinfeld

Department of Chemistry
Massachusetts Institute of Technology
Cambridge, Massachusetts 02139

Abstract. The most important factor determining the response of systems to high-intensity infrared radiation is the quantity of vibrational energy deposited in the absorbing molecules. Determination of this quantity is complicated by spatial nonuniformities in the infrared radiation fluence and by distributions over energy in the system. In this paper, we obtain expressions for the infrared fluence distribution in a focused Gaussian beam. This is combined with an empirical model for the excitation function $\langle n \rangle(\Phi)$ to calculate energy deposition for a range of parameters. These results are compared with available experimental data on dissociation yields for sulfur hexafluoride, and also to various approximate results. Finally, we consider the advantages and limitations of several possible experimental approaches to determining the absolute excitation level of molecules and microscopic energy distributions in the focal volume of the laser beam.

Key Words: laser/chemistry, multiphoton effects, molecular decomposition, Gaussian beams.
Optical Engineering 19:1:002-009 (January/February 1980).

INTRODUCTION

In any experiment which measures the overall response of a system caused by irradiation of a sample, such as energy deposition, absorption cross section at the irradiation wavelength, or net dissociation yield, determination of the intensity distribution of the radiation is of fundamental importance. Physical theories which explain the effect must account for the intensity dependence of its magnitude or extent. In principle, parameters characteristic of the radiation field, such as intensity or fluence (integrated intensity), should be precisely determinable with the use of an appropriately calibrated transducer. However, variations in intensity throughout the sample may make it difficult to relate a measured effect to a particular value of the intensity. While the necessary procedures may be relatively straightforward for well-collimated beams, it is often necessary to employ strongly focused beams, especially for the dissociation of small molecules. Thus, some procedures must be used to link the measured effect, the overall beam intensity, and the focusing optics used in the experiment. In this paper, we will consider the technique for dealing with beams of Gaussian cross section appropriate for laser applications, such as the problem of multiple infrared photon absorption in gases.

Several authors[1-6] have used various approximations to model their particular optical geometries. In most multiple photon experiments, the exact beam cross-section function is not known, especially if the experiments utilize a focused beam. It is therefore difficult to separate those effects which are caused by the wide range of intensities intercepted by the sample from those which are caused by the fundamental microscopic dynamics. The data must be corrected for the geometrical form of the beam before the empirical results can be compared with a physical model. Since the geometry of Gaussian beams is well characterized,[7-10] extraction of purely dynamical effects becomes fortuitously analytic, as has been demonstrated.[11] We wish to present a consistent approach here, to consider the implications of the beam geometry for various types of Gaussian beams, and to illustrate the shortcomings of "deconvoluted" data.

Original manuscript LC-101 received August 3, 1979.
Accepted for publication Sep. 13, 1979.

DEFINITIONS

Whenever possible, we will adhere to the notation found in Yariv,[7] including the following definitions:

- $z(0)$ – location of focal plane on propagation (Z) axis
- ω_0 – spotsize at focal point; radius to e^{-1} point of field
- $\omega(z)$ – spotsize at axial point z
- $R(z)$ – radius of curvature at z
- z_0 – $\pi\omega_0^2/\lambda$
- Φ – energy fluence; for pulsed beams, $\Phi = \int (\text{intensity})\, dt$
- $V(\Phi)$ – volume in beam experiencing fluence Φ or greater
- $v(\Phi)$ – change in $V(\Phi)$ per unit fluence
- ϱ – molecular density
- λ – wavelength of radiation

PROPERTIES OF THE BEAM

We will consider "TEM_{oo}" Gaussian beams, for which the intensity I follows:

$$I(r,z) = E^*E = I_0 \frac{\omega_0^2}{\omega^2(z)} \exp\left(\frac{-2r^2}{\omega^2(z)}\right) \qquad (1)$$

where

$$\omega(z) = \omega_0 \left[1 + \frac{z^2}{z_0^2}\right]^{1/2}. \qquad (2)$$

The fluence $\Phi(r,z)$, which is of great importance in multiple

photon chemistry,[13-14] has the same form as the intensity; Eq. (3) therefore describes $\Phi(r,z)$ as well. Subscripts x and y will be used to denote orthogonal transverse directions. To avoid confusion, we will define circular beams as those for which $\omega_0 = \omega_{0x} = \omega_{0y}$ occurring at z(0), elliptic beams those for which $\omega_x(z) = \omega_{0y}$ = constant $\neq \omega_{0x}$ occurring at z(0)*, and finally elliptic confocal beams as those having $\omega_{0y} \neq \omega_{0x}$ but $z_{0y} = z_{0x}$. The generic term elliptical refers to elliptic or elliptic confocal beams.

One can characterize the light beam by specifying the complex beam radius q(z) at some point z,

$$\frac{1}{q(z)} = \frac{1}{R(z)} - i\frac{\lambda}{\pi\omega^2(z)} \tag{3}$$

where

$$R(z) = z\left(1 + \frac{z_0^2}{z^2}\right). \tag{4}$$

For our purposes it will be of greater use to know the spotsize ω'_0 and its location z'(0), such as the waist inside a stable resonator, through distances and optics whose combined ray transfer matrix elements are [abcd], and finally a distance ℓ to z(0). The total ray transfer matrix $\underset{\sim}{M}$ for propagation from z = 0 to z(0) is

$$\underset{\sim}{M} = \begin{bmatrix} 1 & \ell \\ 0 & 1 \end{bmatrix} \times \begin{bmatrix} a & b \\ c & d \end{bmatrix} = \begin{bmatrix} A & B \\ C & D \end{bmatrix} \tag{5}$$

Using the ABCD law of Gaussian beam propagation,[7] we find q(z(0)) from q(z'(0)) and matrix $\underset{\sim}{M}$:

$$q(z(0)) = \frac{Aq(z'(0)) + B}{Cq(z'(0)) + D} \tag{6}$$

At z(0), R(z(0)) = 0. Combining Eqs. (4) and (6), we can express ω_0 as

$$\omega_0 = \frac{\omega'^2_0}{d^2 - c^2}. \tag{7}$$

The distance ℓ at which the spotsize reaches ω_0 can also be found from the condition that R(z(0)) = 0; straightforwardly one obtains

$$\ell = -(db + caz'_0)/(c^2z'_0 + d^2). \tag{8}$$

Thus, by knowing the location and size of a beam waist, and all optics from that point to the region of interest, one can easily compute the location and size of the second waist.

In practice, however, a pure "TEM_{00}" mode may be difficult to obtain from a pulsed laser and some spatial filtering[15] may be necessary to exclude unwanted beam components. For such systems the location and size of the beam waist can be determined empirically, using simple measurements and tools, such as a scanning pinhole or variable aperture. Since the beam is most intense at z(0) and may cause a plasma at obstructing surfaces, direct measurement of the beam waist may be difficult. Sufficiently far from z(0), however, the beam expands asymptotically to the cone whose half apex angle is

$$\Theta = \tan^{-1}\left(\frac{\omega_0}{z_0}\right). \tag{9}$$

If the spotsize of the beam is measured at two points z_1 and z_2, we have

$$\tan\Theta = \frac{\omega(z_2) - \omega(z_1)}{z_2 - z_1}. \tag{10}$$

*Such a beam would be produced, for example, by a cylindrical focusing lens.

Equation (10) combined with Eq. (6) yields

$$\omega_0 = \frac{\lambda}{\pi}\frac{z_2 - z_1}{\omega(z_2) - \omega(z_1)}. \tag{11}$$

Since the apex of the cone defines z(0), we find z(0) simply:

$$z(0) = z_1 - \omega(z_1)\cot\Theta = z_2 - \omega(z_2)\cot\Theta. \tag{12}$$

Thus from two measurements of the beam cross section one can easily find the location and size of the beam focus.

Equations (4)–(12) are valid for circular as well as elliptical beams, and allow the relative magnitude of the fluence to be specified in the region of interest. The absolute magnitude of the fluence can be found using a joulemeter, which measures the total pulse energy E_T

$$E_T = \int_0^\infty \Phi(r,z)2\pi r dr \tag{13}$$

where it is assumed that the dimension of the joulemeter face is much larger than $\omega(z)$. For convenience, we evaluate Eq. (13) at z = z(0), so that for circular beams

$$E_T = \int_0^\infty \Phi_0 \exp(-2r^2/\omega_0^2)2\pi r\, dr = \Phi_0\frac{\pi\omega_0^2}{2}. \tag{14a}$$

For elliptical beams, Cartesian coordinates are suitable variables of integration:

$$E_T = 4\int_0^\infty\int_0^\infty \Phi(x,y,z(0))\, dxdy = \frac{\pi}{2}\Phi_0\,\omega_{0x}\,\omega_{0y}. \tag{14b}$$

The correspondence in Eqs. (14a), (14b) between E_T and total power, and between Φ_0 and peak intensity, can be seen easily.

DETERMINATION OF CRITICAL VOLUMES

Of critical interest in our analysis is the number of particles intercepted by the beams. If the particle density ρ is given, a suitable volume inside the beam can be found which contains the particles under study. Many authors[1-5] have derived expressions for volumes pertinent to their respective applications; Keefer et al.[4] obtained an expression for the volume enclosed by an isointensity (iso-fluence) surface in a Gaussian beam,

$$V(\Phi) = -\frac{\pi^2\omega_0^3}{\lambda}\int_0^{U'}(1 + U^2)\ln[K(1 + U^2)]dU \tag{15}$$

where

$$K = \Phi/\Phi_0$$
$$U' = (1/K - 1)^{1/2}$$
$$U = (z - z(0))/z_0.$$

Eq. (15) can be evaluated exactly, yielding

$$V(\Phi) = \frac{4}{3}\lambda z_0^3\left(U - \tan^{-1}U' + \frac{U^3}{6}\right) \tag{16}$$

where U = U'. Equation (16) reduces to Keefer's result when all terms are dropped but the last, proportional to U^3. A similar expression can be obtained for the corresponding volume in an elliptic beam,

$$V(\Phi) = 8\int\int\int dxdydz \tag{17}$$

where each integral extends between zero and the appropriate upper bound:

$$x' = \left[\frac{\omega_x^2(z)}{2}\left\{\ln\left(\frac{\omega_{ox}}{K\omega_x(z)}\right) - \frac{2y^2}{\omega_{oy}^2}\right\}\right]^{1/2} \tag{18a}$$

$$y' = \left[\frac{\omega_{oy}^2}{2}\ln\left(\frac{\omega_{ox}}{K\omega_x(z)}\right)\right]^{1/2} \tag{18b}$$

$$z' = z_{ox}\left(\frac{1}{K^2} - 1\right)^{1/2}. \tag{18c}$$

After two integrations of Eq. (17), we obtain

$$V(\Phi) = \pi\omega_{ox}\omega_{oy}\int_0^{z'} \ln\left(\frac{\omega_{ox}}{K\omega_x(z)}\right) dz \tag{19}$$

$$= \frac{\pi^2}{\lambda}\omega_{ox}^2\omega_{oy}(m - \tan^{-1} m) \tag{20}$$

where m is analogous to U in the circular beam case,

$$m = \left(\frac{1}{K^2} - 1\right)^{1/2}.$$

For the elliptic coniocal case, evaluation of Eq. (17) is more difficult. The upper bounds are given by

$$x' = \left[\frac{\omega_x^2(z)}{2}\left\{\ln\left(\frac{\omega_{ox}\omega_{oy}}{K\omega_x(z)\omega_y(z)}\right) - \frac{2y^2}{\omega_y^2(z)}\right\}\right]^{1/2} \tag{21a}$$

$$y' = \left[\frac{\omega_y^2(z)}{2}\ln\left(\frac{\omega_{ox}\omega_{oy}}{K\omega_x(z)\omega_y(z)}\right)\right]^{1/2} \tag{21b}$$

$$z' = \frac{\pi}{2\lambda}\left\{-(\omega_{oy}^2 + \omega_{ox}^2) + (\omega_{oy}^4 + \omega_{ox}^4 + \omega_{ox}^2\omega_{oy}^2[4m-2] + \omega_{ox}^4)^{1/2}\right\}^{1/2}. \tag{21c}$$

After two integrations, we obtain

$$V(\Phi) = \pi\int_0^{z'} \omega_x(z)\omega_y(z)\ln\left(\frac{\omega_{ox}\omega_{oy}}{K\omega_x(z)\omega_y(z)}\right) dz \tag{22}$$

which must be evaluated numerically. Values of $V(\Phi)$ for a range of K and $(\omega_{ox}/\omega_{oy})$ are given in an Appendix.

For values of Φ small with respect to Φ_o, $K \ll 1$. In this limit, from Eq. (16), $V(\Phi) \propto \Phi_o^{3/2}$ for circular beams. From Eq. (20), $V(\Phi) \propto \Phi_o$ for elliptic beams. Figure 1 shows the dependence of $V(\Phi)$ on K, where the quantity V' plotted is the dimensionless quantity in parentheses in Eq. (16) or (20).*

The differential volume, or change in volume per unit change in Φ,

$$v(\Phi) = \frac{dV(\Phi)}{d\Phi} \tag{23}$$

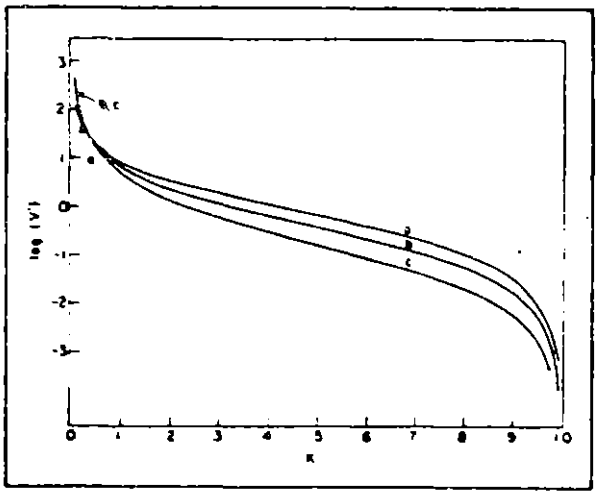

Figure 1. Behavior of $V(\Phi)$ with parameter $K = \Phi/\Phi_o$. V' is given by the expression in parentheses in (a) Eq. (20) (elliptic), (b) Eq. (18) (circular). Curve (c) retains only the last term of Eq. (18), valid for $\Phi \ll \Phi_o$ as in Ref. 4.

can be found easily from Eqs. (16) and (20). They are, for circular beams,

$$v(\Phi) = -\frac{4\pi_o^2}{3}\left(\frac{U(2K+1)}{\Phi_o K^2}\right) \tag{24}$$

and for elliptic beams,

$$v(\Phi) = -\frac{\pi^2}{\lambda}\omega_{ox}^2\omega_{oy}\left(\frac{m}{\Phi}\right) \tag{25}$$

Equation (24) is equivalent to Eq. (18) of Ref. 3. We will use these formulas in the following section for the deconvolution of experimental data.

Usually the spotsize of the beam can be chosen by proper selection and placement of optics. In some situations one may wish to maximize $V(\Phi)$ for some particular value of Φ, for instance the threshold fluence Φ_R for dissociation in multiple photon chemistry experiments.[4] It would be valuable, therefore, to know at what ω_o it is that $V(\Phi_R)$ maximizes, or for what ω_o

$$\frac{\partial V(\Phi_R)}{\partial \omega_o} = 0. \tag{26}$$

Straightforwardly differentiating Eq. (13) with respect to ω_o, one obtains

$$\frac{\partial V(\Phi)}{\partial \omega_o} = \frac{2\pi^2\omega_o^3}{9\lambda}(15U - 24\tan^{-1} U + U^3) \tag{27}$$

which vanishes at $U = 1.323406\ldots$, implying $\Phi_o = 2.751403\,\Phi_R$. Thus, for given parameters E_T and Φ_R, $V(\Phi_R)$ maximizes when

$$\omega_o = \left(\frac{E_T}{2.7514\pi\Phi_R}\right)^{1/2} = 0.481\left(\frac{E_T}{\Phi_R}\right)^{1/2}. \tag{28}$$

For elliptic beams, we have

$$\frac{\partial V(\Phi)}{\partial \omega_{ox}} = \frac{\pi^2}{\lambda}\omega_{oy}\omega_{ox}^2(2m - 3\tan^{-1} m) \tag{29}$$

*Note that the approximation used in Ref. 4 is valid only for $K = \Phi/\Phi_o \lesssim 0.1$.

which vanishes at $m \approx 1.451104\ldots$, implying $\Phi_0 = 1.762\,\Phi_R$, and thus for E_T, Φ_R and ω_{oy},

$$\omega_{ox} = \frac{E_T}{2.768\,\omega_{oy}\Phi_R}. \tag{30}$$

$V(\Phi_R)$ increases monotonically with decreasing ω_{oy} in this case. Also, it can be shown that there is no elliptic configuration which renders a larger $V(\Phi_R)$ than the circular case when Eq. (25) holds, with constant E_T and Φ_R.

TREATMENT OF EXPERIMENTAL DATA

In an experiment in which a net quantity is measured from the irradiation of a sample with a Gaussian beam, various portions of the sample experience vastly different fluences (intensities). The net quantity is thus the sum of the response of the system over all portions of the beam used. Interesting physical theories, however, describe a system's response at a particular value of the fluence, and not over the whole beam simultaneously. Therefore, it would be of value to extract the system's response at particular fluences from experimental data (deconvolution) and to describe an experimental result using a physical theory (convolution). For collimated Gaussian beams, Kolodner et al.[1] have already demonstrated the technique of deconvolution. Briefly, the total response C_T per unit length of beam used is expressed as the weighted average of the system's response function $g(\Phi)$ over the beam area

$$C_T = \frac{\ell}{E_T}\int_0^\infty g(\Phi)\Phi(r)2\pi r\,dr \tag{31a}$$

$$= \frac{\ell}{E_T}\int_0^{\Phi_0} g(\Phi)\frac{\pi\omega_0^2}{2}\,d\Phi. \tag{31b}$$

Taking the derivative of Eq. (31) with respect to Φ at Φ_0 and recalling Eq. (14a), we have

$$g(\Phi_0) = \frac{E_T}{\ell}\frac{dC_T}{dE_T}. \tag{32}$$

Equation (24) holds for circular beams as well as elliptical unfocused beams.

For other beam shapes, however, the change of variables between Eq. (31a) and (31b) cannot be made, but the general scheme can still be applied. For a general beam type we use as a starting point,

$$B_T = \frac{\ell}{E_T}\int_0^{\Phi_0}\Phi g(\Phi)\,v(\Phi)\,d\Phi \tag{33}$$

where B_T is the total response. Taking the derivative of Eq. (33) with respect to Φ and evaluating at some fluence Φ_1, we obtain

$$g(\Phi_1) = \frac{E_T}{\ell\Phi_1 v(\Phi_1)}\left(\frac{dB_T}{dE_T}\right) \tag{34}$$

which is a general deconvolution equation. For focused beams, $v(\Phi_0)$ diverges so that a convenient Φ_1 must be chosen, such as

$$\Phi_1 = k\Phi_0,\ k < 1. \tag{35}$$

For focused circular and elliptic beams respectively, Eq. (34) becomes

$$g(\Phi_1) = \frac{1}{\ell v(\Phi_1)}\left(\frac{\pi\omega_0^2}{2k}\right)^2\left(\frac{dB_T}{dE_T}\right) \tag{36a}$$

or

$$g(\Phi_1) = \frac{1}{\ell v(\Phi_1)}\left(\frac{\pi\omega_{ox}\,\omega_{oy}}{2k}\right)^2\left(\frac{dB_T}{dE_T}\right). \tag{36b}$$

In Eqs. (36) the derivatives are merely the local slope of the B_T vs. E_T graph. Taking small differences between large numbers of finite precision produces a noisy derivative; smoothing[14] may be necessary.

Convolution of the empirically or theoretically derived $g(\Phi)$ function can be accomplished by numerical evaluation of an integral equation such as Eq. (30). As an example, let $g(\Phi)$ be the absorption cross-section function. The energy absorbed E_D in a cell of length 2ℓ and radius r much greater than the beam radii, centered at z(0), could be modeled via

$$E_D = 8\ell\int_0^{\ell}\int_0^{r}\int_0^{r} g(\Phi)\,\Phi(x,y,z)\,dx\,dy\,dz. \tag{37}$$

The value of such a convolution lies in the freedom to choose the limits of integration to conform to the physical volume of interest in the experimental apparatus. A serious shortcoming of the technique lies in the nature of its formulation and in the experimental method. When a value for $g(\Phi)$ is found, it must be the average response function for all molecules experiencing fluence Φ. It is therefore a first moment of the microscopic distribution of molecules over response, and may not lead directly to descriptions of other responses which are sensitive to the shape or temporal behavior of the microscopic distribution.

Taking energy deposition again as an example, the response function $g(\Phi)$ is actually the average cross section for absorption over whatever distribution of molecules over absorbed energy. $P(E;\Phi)$ is formed when an ensemble of molecules is subjected to fluence Φ:

$$g(\Phi) = \langle g(\Phi)\rangle = \frac{\int_0^\infty EP(E;\Phi)dE}{\Phi\int_0^\infty P(E;\Phi)dE} \tag{38a}$$

$$= \frac{\langle E\rangle}{\Phi}. \tag{38b}$$

The distribution function $P(E;\Phi)$ reflects the dynamical physics of the absorption process, but is not determined by measurements which detect only averages over $P(E;\Phi)$, such as absorption.

Example: multiple photon absorption

To highlight such difficulties, and to illustrate the effects of the range of fluences in a focused circular Gaussian beam, we consider the problem of multiple infrared photon absorption and consequent dissociation of SF_6. Although much data has been published for this molecule,[15] the data taken using beams of well-characterized Gaussian cross section are scarce. Dissociation experiments typically utilize TEA lasers operating in a multimode or unstable resonator configuration; the actual fluences at all points in these beams are not known exactly. The convolution of a dissociation cross-section function with some model of the fluence distribution becomes at best only approximate.

For energy absorption, many careful measurements have been made.[16-44] The data of Ambartzumian et al.[18] and of Black et al.[23] extend to $\sim 10\,J/cm^2$ and are depicted in Figure 2 along with an arbitrary fit used for ease in computation. For Ref. 22, the fit used is

$$\langle n\rangle(\Phi) = 8.333\Phi \qquad 0 \le \Phi < 1.5$$
$$10.475(\Phi + 0.161)^{1.2} + 0.23 \qquad 1.5 \le \Phi \tag{39}$$

and for Ref. 23,

$$\langle n\rangle(\Phi) = 9.15\Phi \qquad 0 \le \Phi < 2.55$$

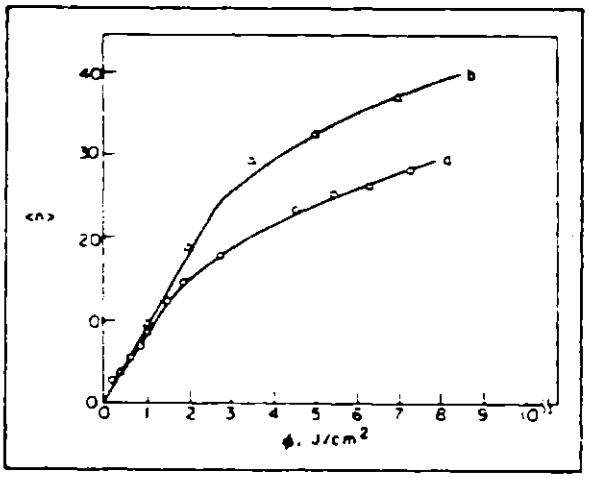

Figure 2. Mean CO_2 laser photon absorption in SF_6, <n>(Φ), taken from (a) Ref. 22, and (b) Ref. 23. Lines correspond to arbitrary fits given by Eqs. (39) and (40).

$$14.1(\Phi + 0.084)^{1/2} + 0.51 \qquad 2.55 \leq \Phi \tag{40}$$

where <n>(Φ) is the average number of photon energies (λ = 10.7 μm, ν = 940 cm^{-1}) absorbed per SF_6 molecule at fluence Φ, for pulse length of approx. 10^{-7} sec. The fit in Eq. (40) is made to the deconvoluted data of Ref. 23; in Ref. 22, only a rough estimate of the fluence was made for fluences between 1 and 10 J/cm^2. Using these data, an estimate of the total energy absorbed in a beam of arbitrary shape can be computed.

To model dissociation of SF_6 molecules, however, more dynamical information must be obtained. The shape of the distribution of molecules over absorbed energy at a particular average absorbance P(E;<E>) must be specified. This shape of P(E;<E>) has not been determined, but may be narrower[21,31] or broader[32] than a thermal distribution at the same <E>. There is some evidence[30,31] that a Boltzmann-like distribution itself can model multiple photon absorption fairly well. The shape of the nonequilibrium distribution may also depend on <E>,[33] for instance, being proportionately broader at high <E> than at low <E>. For lack of dynamical information, however, and because we wish to avoid the dynamical details of the multiple photon absorption process, we will assume that the distribution is Boltzmann-like,

$$P(E|\langle E\rangle) = \frac{N(E)\exp[-\gamma(\langle E\rangle)E]}{\int_0^\infty N(E)\exp[-\gamma(\langle E\rangle)]dE} \tag{41}$$

where P(E|<E>) is the particular form of P(E;<E>) corresponding to the maximal-entropy assumption.[33] In Eq. (42), N(E) is the density of vibrational states per unit energy at vibrational energy E, and $\gamma(\langle E\rangle)$ is a parameter analogous to $(kT)^{-1}$. Details of the computation of the Whitten-Rabinovitch function[34] for N(E) and of the RRKM rates[35] used below can be found in Ref. 25; a description of $\gamma(\langle E\rangle)$ is in Ref. 33.

Computationally the influence of P(E;<E>) on the total distribution p(E) of all molecules in the beam can be easily seen. When P(E;<E>) is summed over all values of <E> resulting from the Gaussian dependence of the fluence, the spatially averaged distribution p(E) can be expressed as

$$p(E) = \phi \int_{\Phi_m}^{\Phi_0} P(E;\langle E\rangle)\nu(\Phi)d\Phi \tag{43}$$

where Φ_m is a convenient lower bound, which is 0.5 J/cm^2 in these computations, and <E> is given as a function of Φ by Eq. (39) or (40). Figure 3 shows p(E) when P(E;<E>) is a delta function at E = <E> and when it is expressed by Eq. (42). Over a large range of

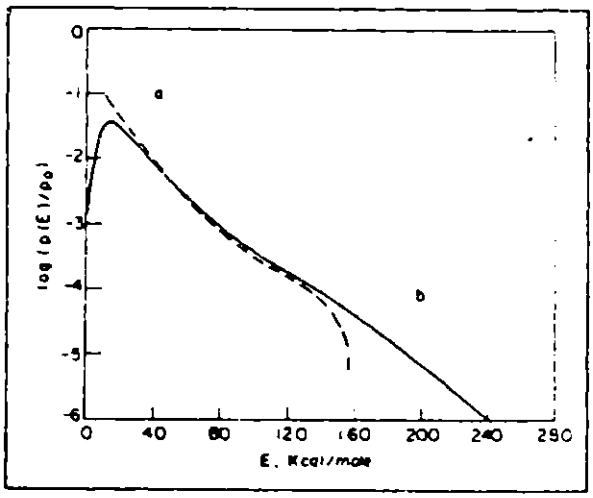

Figure 3. Normalized distributions p(E) for a circular Gaussian beam using $\omega_0 = 8.03 \times 10^{-3}$ cm, $E_T = 0.1$ J and Eq. (39) for <E>(Φ). The expressions for P(E;<E>) used are (a) (dashed), a delta function at E = <E>, and (b) a Boltzmann-like distribution, P(E;<E>), given by Eq. (42).

vibrational energies, the two curves are determined largely by the beam shape. At high energies, the thermal "tails" of distribution Eq. (42) are manifest as that part of p(E) extending beyond E = $h\nu\langle n\rangle(\Phi_0)$.

Decreasing the spotsize of the beam increases the peak fluence and hence the number of molecules reaching very high energies. Using Eq. (39) as a model of absorption [even though the ex-

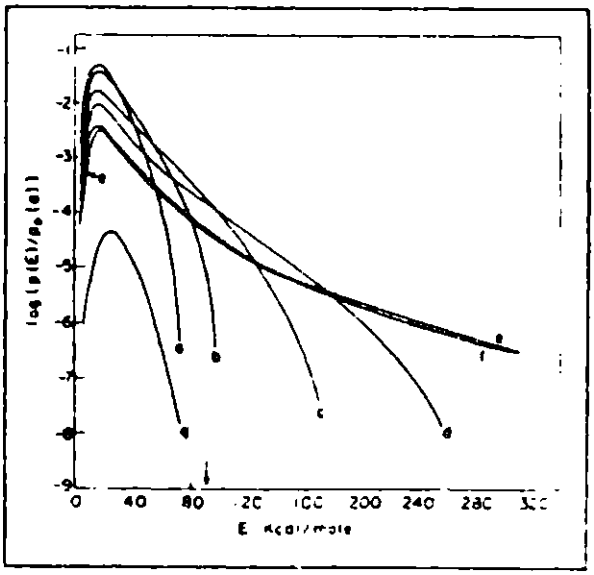

Figure 4. Distributions p(E) normalized to distribution (a) using ω_0 = 0.1 J and Eqs. (39) and (42), while varying ω_0 (in cm): (a) 0.2, (b) 0.15, (c) 0.09, (d) 0.05, (e) 0.02, (f) 0.018. Curve (g) is a plot of Eq. (42) scaled by 10^{-3} with <E> = 25.5 kcal/mole, which is the <E> for curve (d).

perimental points do not extend beyond ~ 10J/cm²] and disregarding dissociation, we show in Figure 4 the effect on p(E) of decreasing ω_0 while keeping E_T and Φ_m constant. Even though the average number of photons absorbed per molecule does not change greatly, the fraction extending beyond ~ 10^4 Kcal/mole increases dramatically with Φ_0. For comparison, curve (g) is $P(E|<E>) \times 10^{-3}$ for $<E> = 25.5$ Kcal/mole, the average energy in distribution (d).

In the absence of a detailed dynamical model which describes simultaneous absorption and dissociation, using distributions such as those in Figure 4 to model dissociation is a crude approximation to the actual dynamical process. If two conditions are met, however, the model becomes more tenable. These are that (1) the pumping be much faster than the V → T relaxation rate and that (2) at fluences near the threshold fluence for reaction Φ_R (see below) the values of $<n>(\Phi)$ be well known. Condition (1) is met using $\tau_{pulse} = 10^{-7}$ sec and $k_{relax} = 10^6$ sec^{-1}, which are reasonable parameters.[34] Condition (2) specifies that for those values of <E> where significant portions of the microscopic distribution $P(E,<E>)$ contribute to dissociation, the function $h\nu<n>(\Phi) = <E>$ should be accurate. For sufficiently high fluences, <E> approaches and exceeds the activation energy of the reaction E_a and the exact magnitude of <E> need not be known as accurately.

We will use a method similar to that of Black et al.[23] for computing the fraction of molecules f(E) dissociated at internal energy E

$$f(E) = \frac{k_{RRKM}(E)}{k_{RRKM}(E) + k_{RELAX}(E)} \qquad (44)$$

In Eq. (44), k_{RELAX} will be held constant at 10^6 sec^{-1} and $k_{RRKM}(E)$, the RRKM microscopic rate at energy E, are computed exactly as in Ref. 23. The total number of molecules dissociated divided by the molecular density yields the equivalent volume V_R of particles dissociated.

$$V_R = \frac{1}{\rho}\int_0^\infty f(E)\,p(E)\,dE \qquad (45a)$$

$$= \int_{E_a}^{E'} f(E) \int_{\Phi_m}^{\Phi_0} P(E|<E>)\,v(\Phi)\,d\Phi\,dE \qquad (45b)$$

where the integral over E need not be evaluated below E_a, where f(E) is zero, or above a convenient E′, where $P(E|<E>)$ becomes very small. The order of integration can be reversed in Eq. (45b).

$$V_R = \int_{\Phi_m}^{\Phi_0} v(\Phi) \int_{E_a}^{E'} f(E)\,P(E|<E>)\,dE\,d\Phi \qquad (46)$$

so that the integrals over E need to be evaluated only once for each <E>. The volume V_R is analogous to the reaction volume of Keefer et al.[4]

Figure 5(b) shows the dependence of V_R on ω_0 as computed from Eq. (45b), for both functions of $<n>(\Phi)$, i.e. Eqs. (39) and (41). The resemblance to Figure 5(a) is undeniable, indicating that the dissociation follows the geometry of the beam even when the dispersion $P(E|<E>)$ is included. In other words, the net dissociation is determined largely in the region of E where the two curves of Figure 2 are very close. Moreover, the curves in Figure 5(b) maximize at the ω_0 predicted by Eq. (28) (indicated by an arrow) when Φ_R is taken from Figure 6 (see below). This indicates that the fluence threshold model of Keefer et al.[4] may be a valid description of the system for values of K larger than originally supposed.

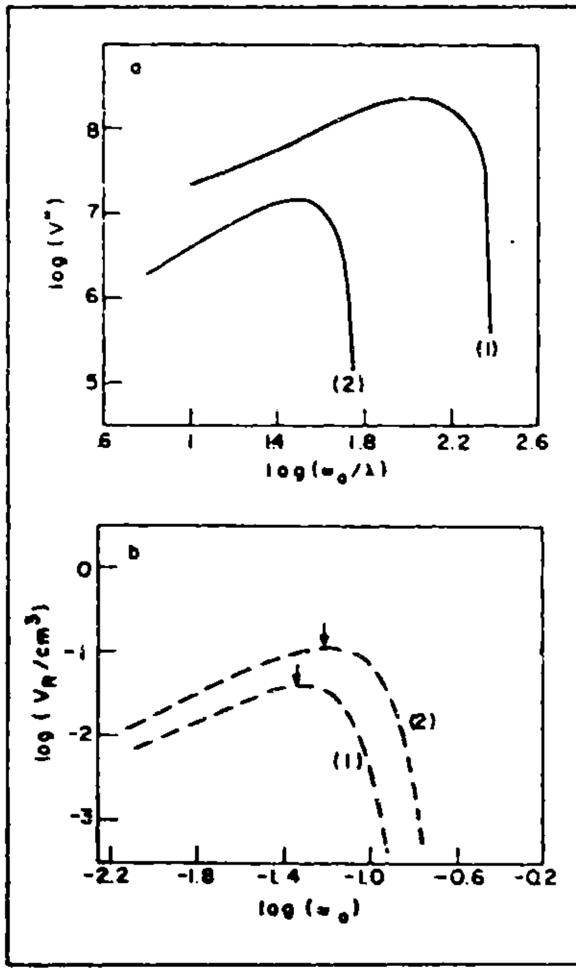

Figure 5. (a) Reduced volumes $V'(\Phi)$ for $\Phi = 1$ J/cm², $E_T = 0.1$J, $\lambda = 10.7$ μm, for (1) circular beams, $V' = (\omega_0/\lambda)^2 (U - \tan^{-1} U + U^3/6)$ and (2) elliptic beams, $V' = (\omega_{0x}/\lambda)^2 (\omega_{0y}/\lambda)(m - \tan^{-1} m)$ using $w_{0y}/\lambda = 10^2$. (b) Equivalent volume V_R of dissociated SF_6 as a function of ω_0 in a circular beam for $<n>(\Phi)$ given by (1) Eq. (39) and (2) Eq. (40), and $k_{RELAX} = 10^6$ sec^{-1}.

Using Eq. (16) one may find the fluences Φ_R for which $V_R = V(\Phi_R)$. These are plotted in Figure 6. At large ω_0, $V_R \to 0$ as $\Phi_R \to \Phi_0$. At smaller ω_0, however, a fluence threshold is reached, which depends greatly on the model of $<n>(\Phi)$ and weakly on k_{RELAX}. Using Eq. (39), the threshold is attained at $\Phi_R \approx 11$J/cm², where the data become least accurate. The data of Black et al.[23] are less uncertain in the region of $\Phi_R \approx 6$J/cm², but agreement with the empirically determined[1,4] $\Phi_R \approx 1$J/cm² is not achieved.

The failure of these calculations to replicate the fluence threshold can be attributed to several sources. The main weakness in the model lies in condition (2), that is, in the region of fluence of the assumed Φ_R and somewhat above, the calculation of Φ_R is very sensitive to $<n>(\Phi)$ for <n> up to ~ 30 = $E_a/h\nu$. Furthermore, the original data for $<n>(\Phi)$ have a finite uncertainty, within which the extrapolated function $<n>(\Phi)$ and hence Φ_R may fluctuate considerably. Also, the form of the distribution $P(E;<E>)$ may actually be broader than the Boltzmann-like

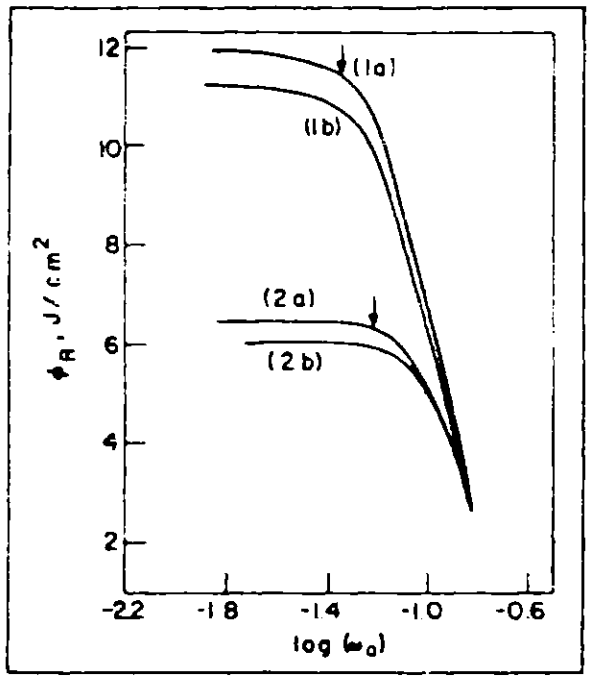

Figure 6. Threshold fluence Φ_R vs ω_0 for the data of Figure 5(b), where Φ_R is the fluence for which $V(\Phi_R) = V_R$ using Eq. (18). Curves (1) use $\langle \sigma(\omega)\Phi \rangle$ of Eq. (29) and (2) use Eq. (40). Curves (a) use $k_{RELAX} = 10^6$ sec^{-1}, and (b) use $k_{RELAX} = 10^8$ sec^{-1}.

distribution used, in which case molecules experiencing lower fluence contribute to dissociation and thereby lower Φ_R. This may not be unreasonable if, as suggested in Ref. 22, a fraction of molecules in volume element $v(\Phi)$ do not participate in the absorption process, leaving the remaining particles to absorb more energy apiece. Overall, the need is seen for a dynamical model to describe the time evolution of the absorption and dissociation process at a particular fluence, rather than the simple kinetics conventionally used.

The experimental determination of the distribution $P(E;\langle E \rangle)$ requires interrogation of individual molecules rather than measurement of a fully averaged effect. We have seen that measurement of any one such observable, such as net energy deposition, net dissociation yield or single-frequency cross section, is not sufficient to uniquely specify the distribution. Parameters such as effective threshold fluence, Φ_R, are themselves functions of the focusing geometries. Spectroscopic methods will be required to get at this information in detail. When applicable, laser-induced fluorescence[24] will be a viable technique for these measurements. In other cases, double-resonance absorption can be used to probe such distributions.[27,28] The problem is that the detailed spectroscopy of any polyatomic molecule for vibrational states much above the first few levels is really not well known. While analyses of such highly excited systems have begun to appear,[29,30] much more spectroscopy will have to be carried out before these methods can be used to provide unambiguous information about the multiple-photon absorption process.

ACKNOWLEDGMENTS

This work was supported by the Office of Advanced Isotope Separation Technology, U. S. Department of Energy (Contract EY-76-S-02-2793) and the Air Force Office of Scientific Research (Grant 78-3725).

APPENDIX: EVALUATION OF CRITICAL VOLUMES FOR ELLIPTIC CONFOCAL BEAMS

Equation (22), which expresses the volume $V(\Phi)$ for elliptic confocal beams as a function of K, ω_{ox}, and ω_{oy} can be recast as a function of a dimensionless variable $S = z/z_{ox}$:[12]

$$V(\Phi) = -\left(\frac{\pi^2}{4k}\right)^{1/2} \omega_{ox}^{-1}\omega_{oy} \int_0^{S'} (1+S^2)^{1/2} \times$$

$$(1+dS^2)^{1/2} \ln[K^2(1+S^2)(1+dS^2)]\, dS \qquad \text{(A1)}$$

where

$$d = \left(\frac{\omega_{ox}}{\omega_{oy}}\right)^2$$

and

$$S' = z'/z_0 .$$

The two parameters d and K in Eq. (A1) range from 0 to + 1. Eqs. (15) and (19) are special cases of Eq. (A1), for which $d = 1$ (circular) and $d = 0$ (elliptic), respectively. We have evaluated the integral in Eq. (A1) numerically for various values of d and K; the results are shown in Figure 7, where the quantity plotted is

$$V' = V(\Phi)/\left(\sqrt{\frac{\pi^3}{k}}\, \omega_{ox}^{-1}\omega_{oy}\right). \qquad \text{(A2)}$$

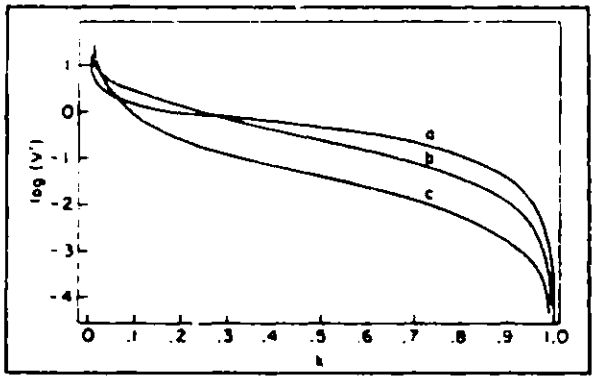

Figure 7. Behavior of V' with parameters K and d for elliptic confocal beams. (a) $d = 0.999$ (b) $d = 5 \times 10^{-2}$ (c) $d = 10^{-2}$.

In Figure 7, curve (a) corresponds to a very nearly circular beam, i.e. $d = 0.999$, and curve (c) corresponds to a nearly elliptic or cylindrically focused beam, i.e. $d = 10^{-2}$. Note that the behavior remains very similar to the circular case until quite small values of d are reached.

REFERENCES

1. J. L. Lyman, S. D. Rockwood, S. M. Freund, J. Chem. Phys. 67, 4545 (1977).
2. J. L. Lyman and K. M. Leary, J. Chem. Phys. (1979) in press.
3. W. Fuss and T. P. Cotter, Appl. Phys. 12, 265 (1977).
4. D. R. Keefer, J. E. Allen Jr., W. B. Person, Chem. Phys. Lett. 43, 394 (1976).
5. S. Speiser and J. Jortner, Chem. Phys. Lett. 44, 399 (1976).
6. M. N. R. Ashfold, G. Hancock, G. Ketley, Faraday Disc. 67, 1979 (in press).
7. A. Yariv, *Quantum Electronics*, John Wiley & Sons, Inc., New York, 1967.
8. L. W. Casperson, Appl. Opt. 12, 2434 (1973).
9. H. Kogelnik, Appl. Opt. 4, 1562 (1965).
10. P. E. Tiee, J. P. Gordon, J. R. Whinnery, Proc. IEEE 53, 129 (1965).

11. P. Kolodner, M. S. Kwok, J. C. Black, E. Yablonovitch, Opt. Lett. 4, 38 (1979).
12. J. L. Lyman, J. W. Hudson, S. M. Freund, Opt. Comm. 21, 112 (1977).
13. P. Kolodner, C. Winterfeld, E. Yablonovitch, Opt. Comm. 20, 119 (1977).
14. R. L. Woodin, D. S. Bomse, J. L. Beauchamp, J. Am. Chem. Soc. 100, 3248 (1978).
15. D. A. B. Miller and S. D. Smith, Appl. Opt. 17, 3804 (1978).
16. C. Daniel and F. S. Wood, *Fitting Equations to Data*, Wiley-Interscience, New York, 1971.
17. For a general review of multiple photon chemistry see (a) R. V. Ambartsumyan and V. S. Letokhov, in Chemical and Biochemical Applications of Lasers, Vol. III, C. B. Moore, ed., Academic Press, New York, N.Y. 1977, pp. 167-316; (b) C. D. Cantrell, S. M. Freund, J. L. Lyman, in "Laser Handbook," Vol. III, North Holland Publishing Co., Amsterdam, 1978.
18. J. L. Lyman, R. G. Anderson, R. A. Fisher, B. J. Feldman, Opt. Lett. 3, 238 (1978).
19. D. O. Ham and M. Rothschild, Opt. Lett. 1, 28 (1977).
20. T. F. Deutsch, Opt. Lett. 1, 25 (1977).
21. M. Stafast, W. E. Schmid, K. L. Kompa, Opt. Comm. 21, 121 (1977).
22. R. V. Ambartsumyan, Yu. A. Gorokhov, V. S. Letokhov, G. N. Makarov, Sov. Phys. JETP 42, 993 (1975).
23. J. G. Black, P. Kolodner, M. J. Shultz, E. Yablonovitch, N. Bloembergen, Phys. Rev. A 19, 1164 (1979).
24. J. L. Lyman, R. J. Jensen, J. Rink, C. P. Robinson, S. D. Rockwood, Appl. Phys. Lett. 27, 87 (1975).
25. J. L. Lyman, J. Chem. Phys. 67, 1868 (1977).
26. E. R. Grant, P. A. Schulz, As. S. Sudbø, Y. R. Shen, Y. T. Lee, Phys. Rev. Lett. 40, 115 (1978).
27. P. Carruthers and M. M. Nieto, Am. J. Phys. 33, 537 (1965).
28. J. G. Black, E. Yablonovitch, N. Bloembergen, S. Mukamel, Phys. Rev. Lett. 38, 1131 (1977).
29. K. D. Hänsel, Chem. Phys. Lett. 57, 619 (1978).
30. C. Reuser, F. M. Lussier, C. C. Jensen, J. I. Steinfeld, J. Am. Chem. Soc. 101, 350 (1979).
32. J. R. Ackerhalt and H. W. Galbraith, in *Laser Spectroscopy IV*, H. Walther and K. W. Rothe, eds.), Proc. 4th Intl. Conf., Rottach Egern (1979), Springer Series in Optical Science, Springer-Verlag, Heidelberg, pp. 300-306.
33. C. C. Jensen, J. I. Steinfeld, R. D. Levine, J. Chem. Phys. 69, 1432 (1978).
34. C. Z. Whitten and B. S. Rabinovitch, J. Chem. Phys. 38, 2466.
35. P. J. Robinson and K. A. Holbrook, Unimolecular Reactions, Wiley-Interscience, New York, N.Y. 1972.
36. C. C. Jensen, Ph.D. Thesis, Massachusetts Institute of Technology, 1979.
37. J. I. Steinfeld, C. C. Jensen, C. Reuser, and T. Anderson, J. Chem. Phys. (in press).
38. W. Fuss and J. Hartmann, pp. 129-130, *Laser-Induced Processes in Molecules* (K. L. Kompa and S. D. Smith, eds.), Springer Series in Chemical Physics No. 6, Springer Verlag, Berlin, 1979; W. Fuss and J. Hartmann, J. Chem. Phys. 70, 5468 (1979).
39. K. D. Hänsel, pp. 143-145, *Laser-Induced Processes in Molecules* (op. cit.), K. D. Hansel, Chem. Phys. 33, 35 (1978).

APPENDIX E. "Infrared double resonance of SF_6 with a tunable diode laser"

C. C. Jensen, T. G. Anderson, C. Reiser and J. I. Steinfeld, J. Chem. Phys. 71, 3648 (1979)

Infrared double resonance of SF_6 with a tunable diode laser

C. C. Jensen,[a] T. G. Anderson, C. Reiser, and J. I. Steinfeld

Department of Chemistry, Massachusetts Institute of Technology, Cambridge, Massachusetts 02139
(Received 14 June 1979; accepted 17 July 1979)

Double resonance spectroscopy has been carried out on the ν_3 band of SF_6 using a CO_2 laser pump and a tunable diode laser probe. Power broadening of the pumped transition is observed, and a value for the transition moment $\mu_{12} \simeq 0.3 \times 10^{-18}$ esu cm is obtained. Off-resonant pumping of all symmetry components in the J manifold coupled to the pump laser is observed; this is attributed to field-induced mixing of nearly degenerate fine-structure levels in the vibrational ground state of the molecule. From the decay of the double resonance signals, we measure relaxation times $P\tau = (24 \pm 3)$ msec Torr for 2-level signals and $P\tau = (43 \pm 11)$ msec Torr for 3-level signals, corresponding to an effective cross section of 17 Å^2. Excited-state transitions corresponding to $2\nu_3 - \nu_3$ with $J = 32$ are observed. The implications for multiple infrared photon excitation models are considered.

I. INTRODUCTION

Once the collisionless, multiple infrared photon induced dissociation of molecules such as SF_6 by intense CO_2 laser pulses was found to be both an efficient and an isotope-selective process,[1,2] a great deal of attention was directed toward understanding this phenomenon.[3] Of a number of questions which have been raised about the nature of this process, one which is not yet settled concerns the nature of the initial excitation steps, that is, the route by which a molecule absorbs the first two to five photons, prior to reaching its vibrational "quasicontinuum."[4] This problem arises because the anharmonicity of the vibration will tend to displace $(n+1)\nu_3 - n\nu_3$ bands to successively longer wavelengths, and thus out of resonance with the single-frequency pump laser.

Several suggestions have been put forward for achieving the required anharmonic compensation, but each has been found untenable in the light of subsequent experimental developments. Bloembergen *et al.*[4] initially showed that a classical, driven anharmonic oscillator could be coherently pumped, via multiphoton absorption, to the required vibrational excitation level. However, the observed threshold for dissociation (~ 50 kW/cm^2)[1] is too low for the classical approximation to be valid. Ambartzumian *et al.*[5] suggested a "P–Q–R" compensation scheme, in which a single laser line pumps first a $P(J)$ line in the SF_6 $\nu_3 - 0$ band, then a $Q(J-1)$ line in the $2\nu_3 - \nu_3$ band (which happens to occur at just the same frequency), followed by an $R(J-1)$ line in the $3\nu_3 - 2\nu_3$ band, at which point the molecule is presumed to have reached the quasicontinuum. Clearly, such a coincidence of frequencies would be highly fortuitous at any one laser line, let alone applying to all the CO_2 laser lines [$P(12)$ to beyond $P(30)$] which can be used for dissociating SF_6. Further consideration of the SF_6 ν_3 mode led to the realization that for $n \geq 2$, the degenerate $n\nu_3$ levels will be split by anharmonic coupling. These splittings were calculated,[7] and appeared to offer a nearly resonant pathway for CO_2 laser photon absorption up through $n = 5$. However, the calculated splittings are not consistent with recent observations on the $3\nu_3 - 0$ overtone absorption spectra.[8] Recently, Ackerhalt and Galbraith[9] have suggested that Coriolis interactions in the excited vibrational levels of SF_6 produce a distribution of transition frequencies adequate to account for the observed multiple infrared photon excitation behavior. We will return to this model later in this paper.

To decide among these various models, we need some definite information on the location of levels in $2\nu_3$, such as frequencies of assigned transitions in $2\nu_3 - \nu_3$.[10] One way of obtaining such information is by means of infrared double-resonance (IRDR) spectroscopy, in which the sample is pumped by a high-intensity CO_2 (or other) laser, and probed with a lower-intensity beam at another IR frequency. A variety of information can be obtained from such experiments,[11] including:

(a) *2-level IRDR*, in which the pump and probe beams are at the same nominal frequency. Power broadening of the saturated transitions is observed, and a T_1-type decay time can be determined.

(b) *3-level IRDR*. Ground-state depletion (GSD) can be observed at frequencies remote from the pump line, providing verification of the assignments of the pumped levels. Excited-state absorption (ESA) provides direct information on the frequencies of transitions originating in the vibrationally excited state (ν_3, in this case).

(c) *4-level IRDR*, in which signals are observed at transitions not directly coupled to the pumping field, provides information on collisional relaxation pathways among the levels.

IRDR was first carried out on SF_6 using two CO_2 lasers (Q switched and cw).[12] A "red"-shifted transient absorption was observed, which was attributed to a superposition of absorptions from vibrationally excited levels following V–V relaxation out of the initially pumped ν_3 level. Ambartzumian *et al.*[5] have supported their P–Q–R anharmonic compensation model with the observation that the absorption curve measured in Ref. 12 is nearly coincident with the curve of SF_6 dissociation efficiency vs CO_2 laser line frequency.[3,5] However, the transient absorption observed in IRDR corresponds

[a] Present address: Joint Institute for Laboratory Astrophysics, Boulder, CO.

 0021-9606/79/213848-10$01.00

to a much lower level of excitation than in the collision-free multiple-photon excitation experiments; the absorption profile can be well represented by that of shock-heated SF_6[12] at 550 °K, while various models for the multiple-photon excitation require effective temperatures of 1700 to 2200 °K.[14]

The IRDR method has been extended to lower sample temperatures,[11] to shorter (~nsec) time scales with the use of mode-locked CO_2 lasers,[16] and also to higher excitation levels ($\nu_3 \sim 5$) by means of pump pulse-probe pulse experiments.[17] Recent experiments[18] using a CO_2 TEA laser pump/cw CO_2 laser probe have extended this range to $\nu_3 \sim 10$. In all of these experiments, however, the system could be probed at only a limited number of discrete frequencies, dictated by the available CO_2 laser lines. To observe finer details of the transient IRDR spectrum, it is necessary to use a tunable probe source, as in the work reported here, in which the probe is a tunable diode laser.[18] Similar experiments, employing a CO_2 laser pump source and a tunable diode laser probe source in a configuration somewhat different from that described here, have also been carried out by Moulton and Mooradian at the M.I.T. Lincoln Laboratory.[19,21]

II. EXPERIMENTAL

A. Instrumentation

The general scheme of the apparatus used in these experiments is similar to that described in Refs. 12 or 19, namely, a high-intensity Q-switched CO_2 laser beam is made to overlap with a low-intensity, tunable, cw laser beam in a sample of SF_6. We measure changes in the transmittance of the cw beam which are correlated with the pump beam pulses.

The pulsed CO_2 laser is a spinning-mirror (150 Hz) Q-switched continuous discharge with a dispersive cavity. The 2 mJ pulses, collected from a higher order diffraction of the intracavity grating, are 400 nsec long (FWHM) with a low-intensity tail extending to 1 μsec. The beam wavefront was measured with a variable aperture and found to have a Gaussian profile with a radius of 0.255 cm, corresponding to an effective area of 0.2 cm^2. The pulse is collected by three gold coated flat mirrors which direct it to a fourth mirror located just in front of the gas sample cell. The pulse is reflected at an angle such that the CO_2 laser pulse and the diode laser probe beam overlap throughout the region of the cell. The pump beam, which is counter-propagating relative to the probe beam, exits the gas sample cell at a small angle (~1°) with respect to the probe beam and intersects a mirror which finally directs the pump beam away from the apparatus to reduce scattered light.

The diode laser is a Laser Analytics Model SDL-30 PbSnSe element mounted in a Model TCR closed-cycle refrigerator, which is temperature stabilized to ±0.001 °C over the operating range 14–100 °K. Current to the diode is provided by an Arthur D. Little TDLS-II power supply, which is current stabilized to ±0.0001 A over the range 0.5–2.0 A. This combination provides tunable infrared output over the range 930–960 cm^{-1} in a series of modes from 0.2 to 1.0 cm^{-1} in width, with 1–2 cm^{-1} gaps between modes. The modes can be shifted in frequency to a limited extent by varying the temperature set point of the closed-cycle cooler. Multimode power output is 0.1 to 1.0 mW. The linewidth was not measured directly, but is certainly far less than the Doppler width of individual SF_6 lines, which is ~30 MHz, or 0.001 cm^{-1}. The diode laser mode profiles are reproducible as long as the diode is maintained at a suitably low temperature (typically 15–25 °K). Since the diode power is very low, there are no saturation effects produced by the probe beam.

The diode laser radiation is collimated by a 5 cm f.l. IRTRAN® lens and reflected through the sample cell by a gold coated mirror. Two additional mirrors direct the beam to a 25 cm f.l. paraboloidal focusing mirror and thence to the entrance slit of a Bausch and Lomb 0.25 m monochromator equipped with a 300 l/mm grating blazed at 3 μm and operated in third order. The monochromator is used to separate the longitudinal modes of the diode laser beam, as well as to attenuate scattered radiation from the Q-switched CO_2 laser. An Arthur D. Little Hg:Cd/Te infrared detector in a home-built liquid nitrogen dewar is mounted at the exit slit of the monochromator. The signal is preamplified, ac coupled to a Tektronix 1121 amplifier (gain variable from 1 to 100), and sent to a PAR Model 160 Boxcar Integrator. The Boxcar Integrator is triggered 10 μsec before the Q-switched laser emits a pulse. This is accomplished by an amplified signal from a photodiode positioned near the rotating mirror of the Q-switched laser such that the rotating mirror reflects the light from a small white light lamp onto the diode before achieving maximum Q for the laser cavity during its rotation. The signal is sampled with a 0.5 μsec gate either coincident with the Q-switched laser pulse or at a selected delay following the pulse. The output of the Boxcar Integrator is coupled to the y axis of an x–y recorder (MFE Corporation, Model 815 M). The x scale signal is provided by an output voltage of the diode laser power supply which is proportional to the current output to the diode laser element. For the relaxation time measurements, the Boxcar Integrator is replaced by a Biomation 620 Transient Recorder. The entire apparatus is diagrammed in Fig. 1.

B. Calibration

In working with the tunable diode laser, it is necessary to have a frequency calibration accurate to ±0.0001 cm^{-1} within each individual mode. This is accomplished by measuring reference spectra along with each double resonance spectrum. To record these spectra, the diode laser beam is chopped at 100 Hz and the signal from the detector is coupled to a PAR Model 120 lock-in amplifier, and thence to the x–y recorder. Scans of SF_6 absorption profiles, recorded in this way, are included in the double resonance spectra shown in the following sections.

The primary frequency markers are the P-branch lines themselves of the 00°1 – 10°0 transition of "hot"

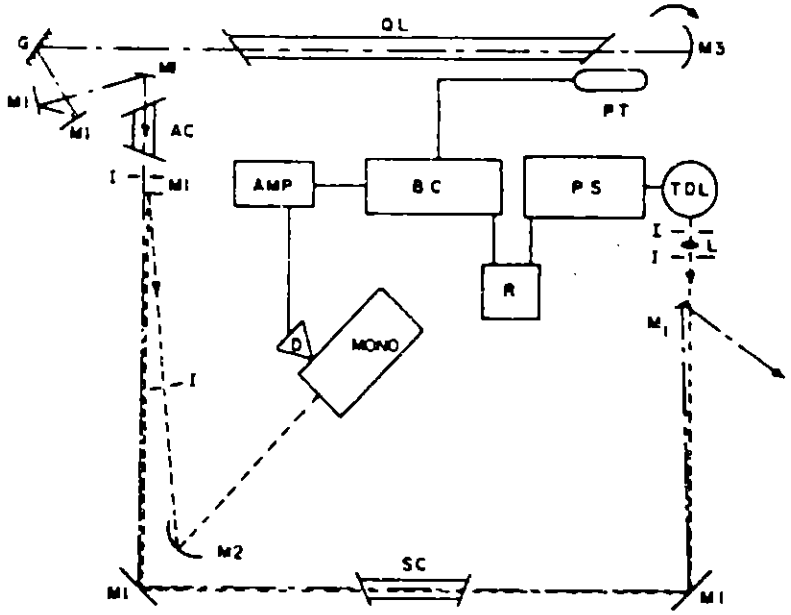

FIG. 1. Double resonance experiment with closed cycle cooled tunable diode laser. ---, diode laser beam. — — —, Q-switched CO_2 laser beam. TDL, closed cycle cooled tunable semiconductor diode laser. M1, flat gold coated mirror. SC, gas sample cell (NaCl windows, Pyrex walls, 3.2 cm o.d.). M2, ½ m f.l. gold coated mirror. MONO, ½ m monochromator. D, Hg:Cd/Te IR detector. AMP, × 100 amplifier. BC, Boxcar integrator. R, x–y recorder. PS, TDL power supply. PT, pretrigger assembly. M3, rotation (Q switching) gold coated (10 m f.l.) mirror. G, grating, blazed at 10 μm. L, 5 cm f.l. lens (collimating). AC, attenuation cell. I, iris diaphragm.

CO_2. The SF_6 absorption features in the neighborhood of these lines have all been assigned by McDowell and co-workers, for the CO_2 $P(14)$, $P(16)$, and $P(20)$ lines,[22] the $P(12)$ and $P(22)$ lines,[23] and in the congested region around the $P(16)$ line.[24] In other regions of the spectrum, we could use lines of the $00°1 - 10°0$ transition in N_2O,[25] or ammonia lines measured between 942 and 956 cm^{-1} by Nereson.[26] To interpolate between these discrete frequencies, we used a 1 in. solid Ge etalon with a free spectral range of 0.0499 cm^{-1}. Interference fringes, recorded in the same manner as an absorption spectrum, were counted to provide the frequency difference from a standard feature and a desired spectroscopic feature at an unknown frequency. Finally, a fairly extensive "map" of the SF_6 10 μm absorption spectrum was made available to us by Los Alamos Scientific Laboratory,[27] from which most of the absorption features could be readily identified.

C. Artifacts

In carrying out these experiments, it is essential to keep scattered pump-beam light from interfering with the desired signals. The Q-switched CO_2 laser intensity is ~10 kW/cm^2, while that of the diode laser is ~0.1 mW/cm^2; thus, a rejection ratio of 10^8 between the two beams is required. This is accomplished by extensive spatial filtering, using iris–diaphragm apertures, along the beam path, by angling the cell windows to avoid direct backward reflections, and especially by using the monochromator as a very narrow-band filter to isolate the diode mode from the CO_2 pump line. If such precautions are not taken, a portion of the CO_2 laser pulse reaches the diode itself, inducing severe frequency and amplitude fluctuations in the diode laser output. Since this output passes through the SF_6 absorber before being detected, the resulting signal will display all of the structure of the original absorption spectrum, and can easily mask the desired double-resonance signals.

III. RESULTS

A. 2-level IRDR

The line shape of a saturated transition may be studied by tuning a probe field across a transition which is simultaneously irradiated by a pump field and monitoring the signal change of the probe. We have carried out such measurements at the CO_2 $P(18)$ and $P(22)$ lines, which pump in the $P(33)$ and $P(84)$ manifolds of SF_6, respectively.[11,12] In both cases, there is a strong "hole burning," or induced transparency, in the absorption spectrum at the frequency of the pumped transition. The double resonance signal at the $P(18)$ pump line is shown in Fig. 2. One sees, in addition to the expected saturated line, a series of weaker satellite signals to the "red" of that line. The strongest features can be identified with the other symmetry components of the $P(33)$ manifold, which are not directly pumped by the CO_2 $P(18)$ line; the reason for their appearance will be considered shortly. The addition of a foreign gas, such as Ar [Fig. 2(b)], results in enhancement of the intensity of these satellite lines, and appearance of additional, weaker signals in the $P(32)$ manifold, corresponding to a change in J'' of one quantum of rotational angular momentum. Further addition of foreign gas, or observation of the spectrum after a ~1 μsec delay, shows a residual population depletion at the pumped transition, while the rest of the rotational fine structure appears to show a nonspecific, overall decrease in intensity [Fig. 2(c)].

In Fig. 3, we show the appearance of the two-level double resonance spectrum at pump laser intensities

between 0.8 and 11.2 kW/cm^2. Two observations are especially noteworthy: first, the "satellite structure" appears rather abruptly between ~1 and ~3 kW/cm^2 applied intensity; second, the strong central feature appears to broaden as the intensity is increased. We shall return to the first point in the ensuing discussion.

The linewidth at half-height of a power-broadened transition is given by[28]

$$\delta\omega_{1/2}=\frac{1}{T_2}\left[1+T_1T_2\left(\frac{\mu_{12}\mathcal{E}_0}{\hbar}\right)^2\right]^{1/2}. \quad (1)$$

where μ_{12} is the transition dipole moment and $\mathcal{E}_0$ is the electric field associated with a beam of intensity I.[29] If the Rabi frequency $(\mu_{12}\mathcal{E}_0/\hbar)$ is much larger than $(T_1T_2')^{-1/2}$, Eq. (1) may be simplified to

$$\delta\omega_{1/2}=\left(\frac{T_2}{T_1}\right)^{1/2}\left(\frac{\mu_{12}\mathcal{E}_0}{\hbar}\right). \quad (2)$$

If we make the further reasonable[30] assumption that $T_1=T_2'$, we obtain

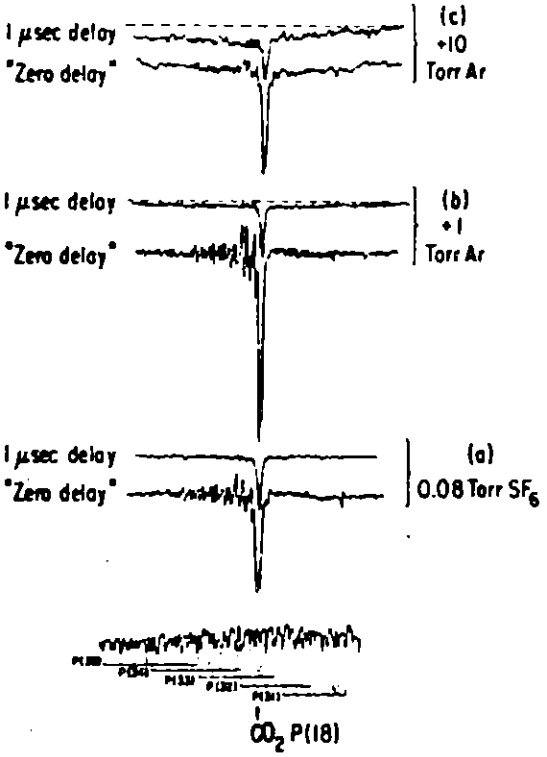

FIG. 2. Two-level infrared double resonance in SF_6. The bottom trace is the normal absorption spectrum of SF_6 in the vicinity of 945.98 cm^{-1} [CO_2 $P(18)$ line], with the $P(31)-P(35)$ transitions identified. Successive scans show the double resonance effect in 0.08 Torr SF_6 with 0, 1.0, and 10.0 Torr Ar added. In the "zero delay" trace, the 0.5 μsec gate is set coincident with the CO_2 laser pulse; the delayed trace corresponds to ~1 μsec following the pulse. Note that absorption is "down" on the normal spectrum, while induced transparency is down on the double resonance spectrum.

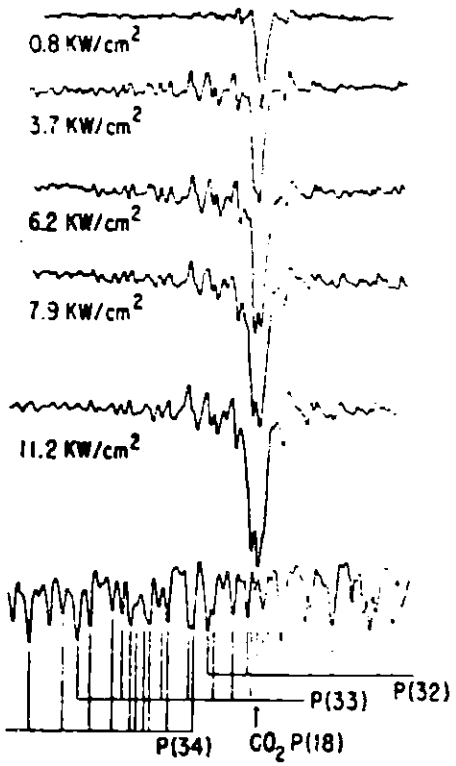

FIG. 3. Power broadening of the two-level infrared double resonance in 0.08 Torr SF_6. The bottom trace is an expanded version of the absorption spectrum shown in Fig. 2, near the $P(33)$ manifold. Successive scans shows the double resonance effect at peak laser intensities of 0.8 to 11 kW/cm^2.

$$\delta\nu_{1/2}=\frac{\delta\omega_{1/2}}{2\pi}=\frac{\mu_{12}\mathcal{E}_0}{h}; \quad (3)$$

thus, the measured half-width should be proportional to the square root of the intensity. A plot of these quantities is shown in Fig. 4; the expected relationship appears to be reasonably well fulfilled. A theoretical estimate of the proportionality factor, obtained by using the value of $\mu_{12}=0.388\times10^{-18}$ esu cm,[31] is $\delta\nu_{1/2}/I^{1/2}=117$ MHz/(kW/cm^2)$^{1/2}$, which compares favorably with the measured slope of 74 MHz/(kW/cm^2)$^{1/2}$. Similar values are also obtained in the two-level double resonance experiments at the CO_2 $P(12)$[29] and $P(22)$[25] lines. At an applied intensity of 23 MW/cm^2, at which single-frequency multiphoton dissociation becomes appreciable[1-9], Eq. (3) would predict a power-broadened "hole" width of 11 GHz or ~0.35 cm^{-1}; at 1 GW/cm^2, which is attainable with focused TEA laser beams, the width would increase to ~2.5 cm^{-1}, which is an appreciable fraction of the inhomogeneously broadened infrared band.

Figure 5 shows the time development of the double resonance signal during and immediately following the pump laser pulse. For this experiment, the boxcar integration gate was set at 100 nsec; the "zero delay"

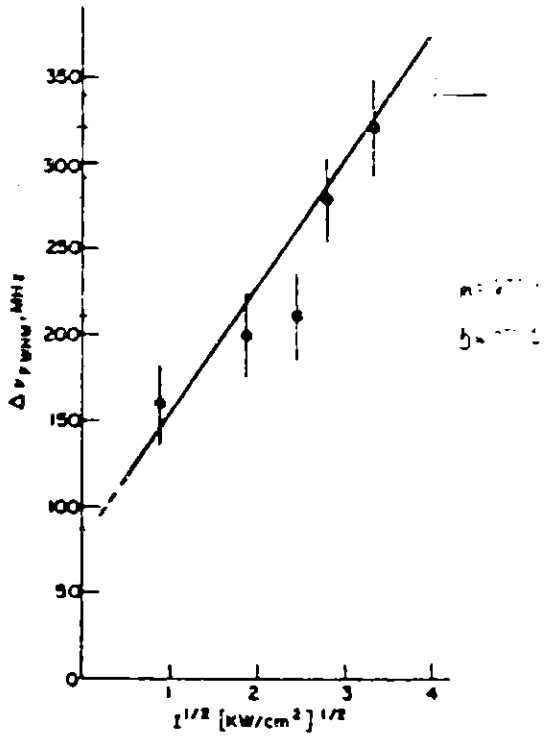

FIG. 4. Plot of power-broadened line width (FWHM) of two-level double-resonance signal vs square root of pump laser intensity.

scan is coincident with the leading edge of the pump laser pulse, and successive scans are incremented by 100 nsec each. Note that the satellite structure appears as soon as the pump pulse reaches an appreciable fraction of its peak intensity. The time development of the strong saturation signal is shown in Fig. 6. From four separate determinations at 0.05 to 0.12 Torr SF_6, we obtain a value for the relaxation time $p\tau = (24 \pm 3)$ nsec Torr.

Double resonance spectra were also recorded in the presence of He, Ar, and CH_3F as added buffer gases; the results are discussed below, in Sec. III C.

B. 3-level IRDR

Three-level double resonance signals were observed upon pumping SF_6 with the CO_2 $P(14)$, $P(16)$, and $P(18)$ laser lines. The $P(16)$ line pumps in the dense Q branch of the molecule, and produces a complex IRDR spectrum covering the $R(45)$ through $R(52)$ lines (this is shown in Fig. 8); Q-branch lines corresponding to these J values may be found within ± 260 MHz of the CO_2 pump line,[24] in agreement with the power-broadening arguments presented earlier. A much simpler DR spectrum is obtained on pumping with either the $P(14)$ or $P(18)$ CO_2 lines; an example of the former is shown in Fig. 7. The strongest feature corresponds to the $A_1^0 + F_2^1 + F_1^1 + A_1^0$ symmetry components of the $P(28)$ manifold at 946.308 cm^{-1},[27] resulting from ground-state depletion of the $A_1^0 + A_2^0 + F_1^1 + F_2^1$ symmetry feature of the $R(28)$ manifold, which is pumped by the CO_2 laser $P(14)$ line at 949.479 cm^{-1}.[25] As in the case of the two level double resonance, the other symmetry components of the $P(28)$ manifold appear as satellite structure around the main line. Conspicuously *absent*, however, is an IRDR signal corresponding to the $A_2^1 + F_2^1 + F_1^1 + A_1^0$ components of the $P(30)$ manifold. The reason for this is quite straightforward: the R branch transitions couple only to the $F^{(+)}$ levels, while the P branch transitions couple only to the $F^{(-)}$ levels.[26] Thus, the $R(28)$ and $P(30)$ manifolds possess no upper level in common, and no 3-level IRDR signal of this type should be expected.

The relaxation time of the 3-level IRDR signal was measured in a manner similar to that described in the previous section. The measured value of $p\tau$ was (43 ± 11) nsec Torr; this is significantly longer than that measured for the 2-level IRDR signal. The reason for this difference will be discussed shortly.

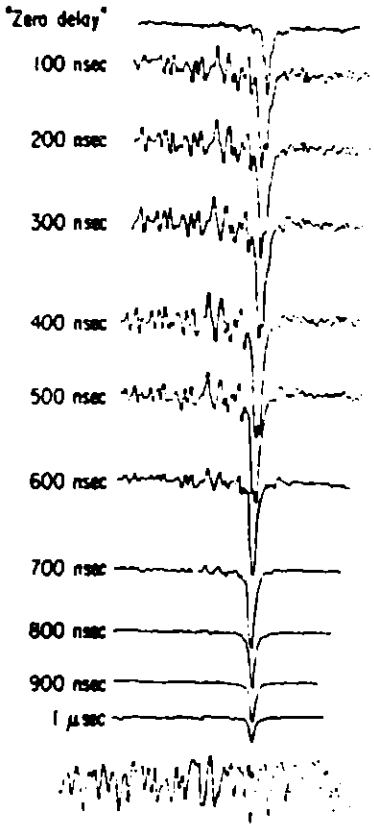

FIG. 5. Development of the two-level infrared double resonace signal in 0.08 Torr SF_6 as a function of time. In the "zero-delay" scan, the 100 nsec sampling gate is set to the leading edge of the CO_2 laser pulse. The gate is then incremented by 100 nsec intervals in the successive scans between 0 and 1.0 μsec. The small arrow in the lower absorption trace indicates the position of the CO_2 $P(18)$ line, as in Fig. 4.

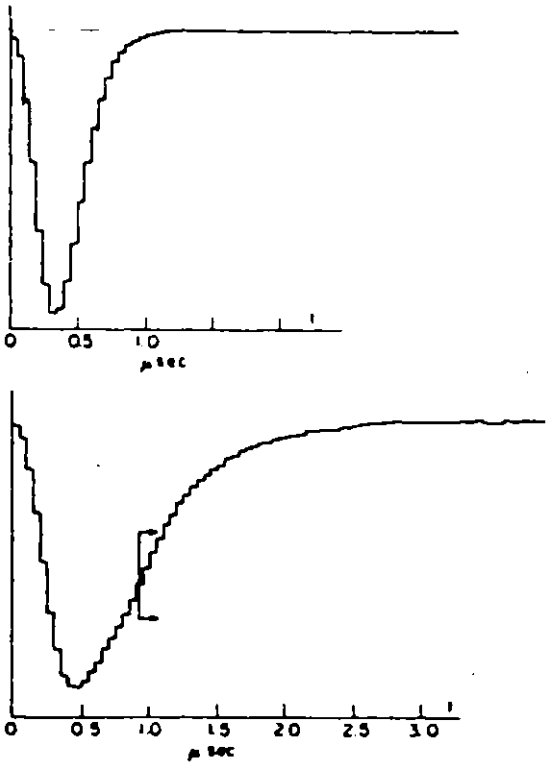

FIG. 6. Relaxation of two-level double resonance signal in 0.063 Torr SF_6. Upper trace; CO_2 laser pulse profile. Lower trace: diode transmission signal. The relaxation time (470 nsec) is obtained by fitting to the signal at times longer than 0.9 μsec, i.e., after the end of the pump pulse

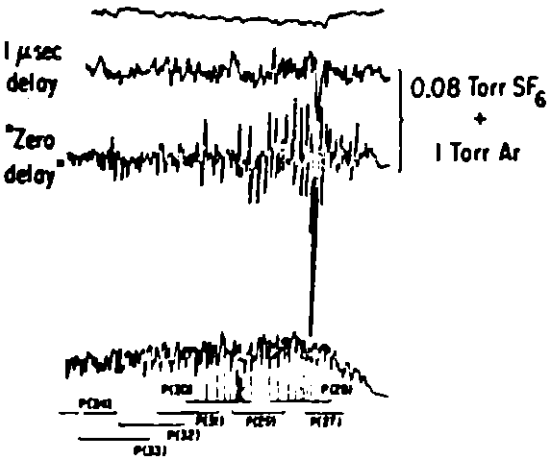

FIG. 7. Three-level infrared double resonance in 0.08 Torr SF_6 + 1.0 Torr Ar. The diode scans across the $P(27)-P(33)$ manifolds in the 946.0–946.4 cm^{-1} region; the laser pump line is the CO_2 $P(14)$, at 949.45 cm^{-1}, which coincides with the $A_1+A_2+F_1+F_2$ component of the SF_6 $R(28)$ manifold.[22] Top trace is background signal with both beams present but no SF_6 in the cell.

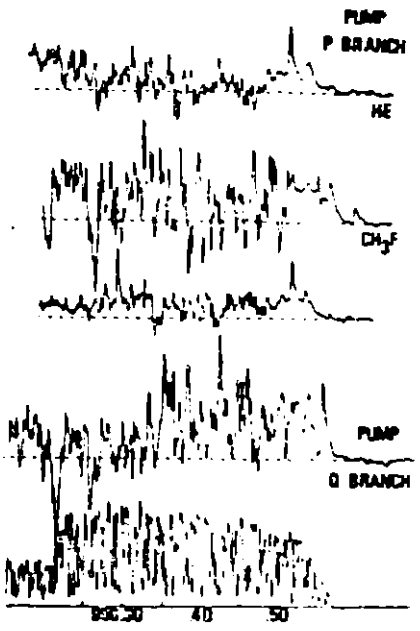

FIG. 8. Three- and four-level infrared double resonance spectra. The bottom curve is a diode laser absorption spectrum of 0.08 Torr SF_6 in the $R(45)-R(32)$ region. Above this is an IRDR scan in the same spectral region, pumping with the CO_2 $P(18)$ line at 947.75 cm^{-1}. The top three traces are the same region, pumping with the CO_2 $P(19)$ line at 945.980 cm^{-1}. Middle to top: 0.08 Torr SF_6 alone; 1 Torr CH_3F added; and 1 Torr He added. All spectra taken with 0.5 μsec gate coincident with the pump laser pulse.

In addition to ground-state-depletion signals, excited-state-absorption signals may be seen arising from pumped levels in ν_3, corresponding to $2\nu_3-\nu_3$ transitions.[20] An example of such signals, observed in this work, may be seen in the third trace in Fig. 8. Two new absorption features are observed at 950.300 and 950.508 cm^{-1}, on pumping with the CO_2 $P(18)$ line at 945.980 cm^{-1}.

C. 4-level IRDR

When collisions transfer populations from rotational levels directly pumped by the CO_2 laser to others, not directly coupled to the pump field, four-level double resonance spectra may be observed. In general, these spectra are more complex than the 2- and 3-level IRDR signals. Examples of collision-induced structure may be seen in Figs. 2 and 7; a clearer example is shown in Fig. 8, in which we observe in the $R(45)$-$R(52)$ region, while pumping with the CO_2 laser $P(18)$ line. This line pumps $J''=33$ (and some 32) in SF_6, and no 3-level IRDR signals are observed in a low-pressure SF_6 sample. Addition of He produces little additional signal, but addition of a similar amount of CH_3F produces numerous IRDR signals, both ground-state depletion and excited-state absorption. This implies collisional changes in J of 10 to 15 quantum units of angular mo-

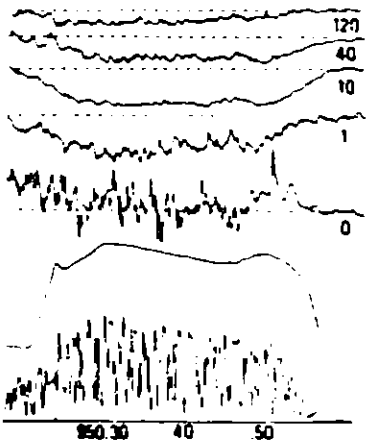

FIG. 9. Time dependence of four-level double resonance spectra. Lower curve is diode laser spectrum (950.223–950.560 cm^{-1}) of an R-branch region of 0.08 Torr SF_6 plus 1 Torr He. Upper curves are double resonance spectra [$P(18)$ CO_2 laser line pump field] at successive 0.5 μsec time gate delays labeled in μsec.

mentum. From analysis of these and other[25] 4-level IRDR signals, we conclude that there is apparently no restriction on changes in symmetry quantum number in a rotationally inelastic collision. It should be noted that in a dipole transition, these symmetry species are unchanged.

The long-time relaxation behavior in this region is shown in Fig. 9. After several μsec, the specific DR transitions are smeared out into an overall depletion of rotational state population, with the profile being simply a reflection of the diode mode shape. A similar, though less pronounced, population depletion may be seen in curve (c) of Fig. 2. The decay of this depletion is uniform across its frequency profile, and simply corresponds to the V–T relaxation process originally measured in Ref. 12.

IV. DISCUSSION

The principal observations from this work are: Off-resonant symmetry components of a given J level are pumped, at least to some extent, by a laser line resonant with only a single component, the spectroscopic assignments in the SF_6 $\nu_3 - 0$ band are confirmed in detail, and several lines from the $2\nu_3 - \nu_3$ band are observed; and collisional relaxation times for the laser-pumped levels are determined, with no apparent restrictions on symmetry changes in such collisions. We will discuss each of these points briefly, and conclude by considering the implications for our understanding of multiple infrared photon dissociation processes.

A. Coupling of ground-state manifolds: Collision or field induced?

As can be seen in Figs. 2, 3, and 5, the 2-level IRDR hole-burning signal is accompanied by satellite structure corresponding to the entire symmetry manifold of a given J level. This structure is essentially fully developed after 100 nsec, at an SF_6 pressure of 0.08 Torr (see Fig. 5). If collisional relaxation within the J manifold were responsible, the cross section for such collisions would have to be in excess of 1100 $Å^2$. This is a situation reminiscent of that in Ref. 16, in which collisionless relaxation processes had to be invoked to account for the rapid (~nsec) decay of the pumped levels. Unlike Ref. 16, however, we are not in a regime of a high density of states, so that a purely intramolecular mechanism can be ruled out. Instead, we consider the mixing of near-degenerate symmetry components in the ground vibrational state, brought about by field-induced perturbations associated with the pump laser field.

The splittings in the ground-state J manifold are of the order of a few MHz,[27] while the power broadening at 1 kW/cm^2 and above is several hundred MHz (see Fig. 3). Thus we expect these components to be strongly mixed by second-order Stark effects. The dominant mixing will be between sublevels of the same symmetry designation (A_1, ..., F_2). From Fig. 3, we see that the satellite structure appears rather sharply between 0.8 and 3.7 kW/cm^2, a range over which the Rabi frequency increases from ~100 to ~200 MHz (see Fig. 4). At the lower end of this range, the pump laser field interacts only with the $P(33)$ A_1^1 line, while at Rabi widths of 200 MHz and above, $P(33)$ F_1^1, F_2^1, F_1^4, F_1^3, and E^1, in addition to $P(32)$ $F_1^4 + F_2^1$ features, become involved.[27] Thus, all symmetry components of the $J = 33$ manifold (and some in $J = 32$) become accessible via the mixing process. The A_1 component is not coupled in this mechanism, but this would not be noticed, since a pure A_1 line does not appear in the spectrum.

The matrix elements appearing in the mixing coefficients are off-diagonal in the pure rotational angular momentum operator R by a one quantum unit. These matrix elements are also responsible for the "weak (R nonconserving) transitions" in SF_6,[28] which have been suggested as an important part of the multiple photon absorption process.[29] Calculations of the mixing coefficients, and comparison with these experimental results, which are currently in progress, should provide information on both the centrifugal splittings in the ground-state rotational manifold and on the strengths of the weak transitions. More exact calculations of the details of the power-broadened off-resonant line shapes will require the methods developed by Mollow[30] and by Wu *et al.*[31]

B. SF_6 ν_3 spectroscopy

In the case of SF_6, a thorough analysis of the vibration–rotation spectrum is available,[32–37] so that the 2- and 3-level IRDR spectra serve merely to confirm the these assignments, as well as to validate the method itself. From the excited-state-absorption transitions (Sec. III B, Fig. 8) we may obtain at least an estimate of the $2\nu_3 - \nu_3$ band profile. Pumping at $P(18)$ produced an apparent R-branch line at ~950.5 cm^{-1}; the 2-level IRDR (Sec. III A) confirmed that we are pumping in the $J'' = 33$ level. We consider a highly simplified approximation in which we treat the $2\nu_3 - \nu_3$ band as having a

single origin at 945.5 cm^{-1}, an effective Coriolis constant ζ_3 and a rotational constant identical to that of the fundamental. Considering the line position of the $R(32)$ transition at 950.5 cm^{-1}, we obtain from the line position equation for a spherical top,[36]

$$B[(1-\zeta_3)+(1-\zeta_1)]J = \Delta\nu \,, \tag{4}$$

where $\Delta\nu = 5$ cm^{-1} is the displacement of the $R(32)$ line from the assumed band center for the $2\nu_3 - \nu_3$ transition, $J = 32$ is the rotational quantum number, $\zeta_1 = 0.67$ is the Coriolis constant for ν_3, and $B = 0.09$ cm^{-1} is the rotational constant of ν_3. Substituting these values into Eq. (4) we obtain $\zeta_3 = -0.41$.[42] Since $B_{eff} = B(1-\zeta)$, the $2\nu_3 - \nu_3$ band would be much wider than the fundamental. Clearly, a much larger number of excited-state transitions will have to be identified before any more detailed analysis can be attempted.

C. Collision-induced relaxation

These experiments represent the first direct observation of relaxation from individual rotational levels in a spherical top. The standard technique of microwave double-resonance spectroscopy[43] cannot be applied to such molecules, since they do not possess a permanent dipole moment[44]; laser-excited infrared fluorescence[45] is also not applicable, since the intensity-limited resolution is insufficient to resolve rotational features.

The exponential decay constant for the double resonance signals was found to be (24 ± 3) nsec Torr for the 2-level IRDR (Sec. III A), but (43 ± 11) nsec Torr for the 3-level IRDR (Sec. III B). The reason for this difference may be understood by reference to Fig. 10. First, it is necessary to note that the observed double resonance signal is proportional to the difference between the transmitted diode intensity at the observation time t and that at a time $\bar{t}$ when the intensity is no longer changing. The former is proportional[38] to the instantaneous population difference $(n_0 - n_1)$ between ground and excited vibrational states, respectively, while the latter is proportional to the equilibrium value of this difference, $\bar{n}_0 - \bar{n}_1$. Thus, the observed signal $S\propto[(n_0 - n_1) - (\bar{n}_0 - \bar{n}_1)]$. The relaxation behavior will be given by

$$\frac{dS}{dt} = \frac{d}{dt}[(n_0 - n_1) - (\bar{n}_0 - \bar{n}_1)]$$

$$= \frac{d(n_0 - \bar{n}_0)}{dt} - \frac{d(n_1 - \bar{n}_1)}{dt}$$

$$= \gamma_0(n_0 - \bar{n}_0) - \gamma_1(n_1 - \bar{n}_1) \tag{5a}$$

$$= -\frac{1}{\tau}S(t) \,, \tag{5b}$$

where γ_0 is the relaxation rate in the ground vibrational state, γ_1 that in the excited vibrational state, and τ is the observed phenomenological relaxation time. If the 3-level system we are observing [case (a)] is fully saturated, then $(n_0 - \bar{n}_0)_{t=0} = -(n_1 - \bar{n}_1)_{t=0}$, and

$$1/\tau_{(3\text{-level})} = \gamma_0 + \gamma_1 = 2\gamma_{rot} \tag{6}$$

if we take $\gamma_0 = \gamma_1 = \gamma_{rot}$, as Moulton's experiments indicate.[38] On the other hand, in the 3-level system [case (b)], the upper level of the probed transition does *not* suffer a change in population, so $(n_1 - \bar{n}_1)_{t=0} = 0$, and

$$1/\tau_{(2\text{-level})} = \gamma_0 = \gamma_{rot} \,. \tag{7}$$

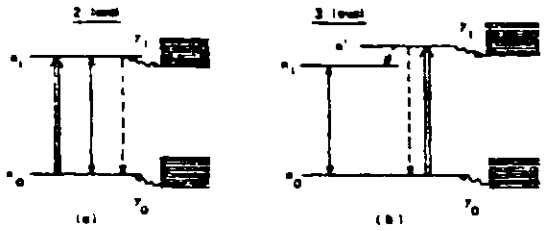

FIG. 10. Relaxation pathways in (a) two- and (b) three-level infrared double-resonance experiments.

This simple consideration predicts that the relaxation time for the 2-level IRDR should be half that for the 3-level IRDR, which is essentially what is observed. The measured $p\tau_{(2\text{-level})}$ is also in good agreement with the values reported by Moulton[38] and Fuss,[17] both of whom obtain (36 ± 3) nsec Torr. The effective cross section for the rotational relaxation process, $\sigma_{eff} = \gamma_{rot}/n\bar{v}$, is 170 $Å^2$, in reasonably good agreement with a theoretical estimate of 230 Å based on a dipole–dipole interaction model.[51]

There appear to be no restrictions on which symmetry components may be coupled in a rotationally inelastic collision, for all the collision partners studied. This is in marked contrast to dipole selection rules for photon absorption or emission, in which the pure rotational angular moment R, the "cluster momentum" K_R, and the symmetry designation (A_1, A_2, E, F_1, or F_2) are unchanged while $\Delta J = 0$ or ± 1. Indeed, even with the limited tuning ranges available from most diode lasers, far too many data can be generated than can be sensibly dealt with on a "state-to-state" level. It is preferable to employ a grouping procedure for the molecular rotational levels which will permit the significant features of the energy transfer process to be recognized, such as the "cluster analysis" developed by Harter *et al.*[52–57]

During the 0.5 μsec time gate width, the SF_6 molecules, at 0.06 Torr, have experienced approximately one collision. Little rotational relaxation appears to occur on this time scale. After 1 μsec (an average of 3–5 collisions per molecule), $\Delta J \geq \pm 1$ transfer may be seen. When rotational state changes do occur, all symmetry components are accessible. Physically this is reasonable when one considers the SF_6 molecule to be a "soft," spherically symmetric particle. Collisions among such particles would not be expected to result in much torque compared with perturbations of a soft body fixed frame.

Addition of a spherically symmetric collision partner, such as He or Ar, results initially in population of neighboring J levels (see Figs. 2 and 7), but *not* in large J changes (e.g., from $J = 32$ to ~ 50, see Fig. 8). Addition of a polar collision partner, such as CH_3F, on the other hand, leads to the extensive J changes observed in Fig. 8. Thus, even though the rate of gas-

kinetic SF_6–CH_2F collisions ($\sim 1\times10^7$ sec^{-1} at 300 °K, 1 Torr) is half that of SF_6–He collisions (2.2×10^7 sec^{-1}),[38] energy transfer in the SF_6–He mixture is considerably less efficient than in the SF_6–CH_2F mixture. The SF_6–SF_6 or He–SF_6 collision interaction can be characterized by a dispersion force with a $1/r^6$ dependence, where r is the distance between collision partners. The collision interaction for CH_2F–SF_6 is expected to be dominated by a dipole-induced dipole force with a $1/r^4$ dependence. The longer range interaction of the CH_2F–SF_6 collision interaction is expected to be more efficient in energy transfer than the He–SF_6 collision interaction, as is evidenced by these results.

At longer times (Fig. 9), much of the detailed spectral structure is lost, indicating that all probed levels are nearly equally involved in the relaxation process.

D. Implications for multiple infrared photon absorption processes

The results obtained in this work can help to clarify the mechanism of the initial absorption steps in the multiple infrared photon induced dissociation process. The model which adheres most closely to our observation is that of Ackerhalt and Galbraith,[9] in which rotational compensation is the dominant method of overcoming anharmonicity. Field-induced mixing of symmetry components within a J manifold appears to make an important contribution to initiating multiple absorption ladders, at least in spherical-top molecules. It is worth noting that we did not observe any "weak ($\Delta R \neq 0$) transitions," which have been proposed by Knyazev *et al.*[39] as a way of obtaining anharmonic compensation.

Power broadening of the absorption line shape can be very important in multiple infrared photon excitation of light molecules, in which the absorption spectrum is sparse relative to the CO_2 laser line spacing. This will lead to the nonlinear intensity dependence of energy deposition and dissociation yield observed in such systems as vinyl chloride.[39] This effect may combine with pressure broadening to cause a significant increase in yield with added buffer gas pressure, e.g., in vinyl fluoride[40] and CDF_3.[41] We plan to explore these effects in greater detail, using diode-infrared laser double resonance. At higher pressures, the rotational relaxation effects observed in this work will also contribute importantly to multiple-photon absorption via parallel excitation ladders.

The IRDR spectra confirm in detail the assignments made for the well-studied[42–47] ν_3 fundamental of SF_6. For spectra which are not as well interpreted, however,[48] this method will be a useful technique in carrying out the analysis. For example, from the 3-level IRDR signal (Sec. III B), we obtain a measurement of the $J=28$ combination difference, $\Delta\nu(R-P)=949.479-946.308=3.071$ cm^{-1}, from which a value for $B\zeta_3$ could be obtained directly. For measurements in excited vibrational states, the IRDR technique is essential. In this connection, use of a tunable infrared pump, instead of a CO_2 laser at fixed frequencies, would be particularly desirable.

ACKNOWLEDGMENTS

This work was supported by the Office of Advanced Isotope Separation Technology, U. S. Department of Energy, under Contract EY-76-S-02-2793. The tunable diode laser system was provided by instrumentation grants from the National Science Foundation. We thank Drs. R. McDowell and H. Galbraith (Los Alamos Scientific Laboratory) and P. Moulton and A. Mooradian for helpful discussions and for making available data in advance of publication.

[1] R. V. Ambartzumian, Yu. A. Gorokhov, V. S. Letokhov, and G. N. Makarov, JETP Lett. 21, 171 (1975).
[2] J. L. Lyman, R. J. Jensen, J. Rink, C. P. Robinson, and S. D. Rockwood, Appl. Phys. Lett. 27, 87 (1975).
[3] A recent review (with 122 references) is that of R. V. Ambartzumian and V. S. Letokhov, in *Chemical and Biochemical Applications of Lasers*, Vol. III, edited by C. B. Moore (Academic, New York, 1977), pp. 167–316.
[4] N. Bloembergen, Opt. Commun. 15, 416 (1975); D. M. Larsen and N. Bloembergen, *ibid.* 17, 254 (1976); N. Bloembergen, C. D. Cantrell, and D. M. Larsen, in *Tunable Lasers and Applications*, edited by A. Mooradian, T. Jaeger, and P. Stokseth (Springer–Verlag, Berlin, 1976), pp. 162–175.
[5] R. V. Ambartzumian, Yu. A. Gorokhov, V. S. Letokhov, G. N. Makarov, A. A. Puretzkii, and N. P. Furzhikov, JETP Lett. 23, 217 (1976); R. V. Ambartzumian, N. P. Furzhikov, Yu. A. Gorokhov, V. S. Letokhov, G. N. Makarov, and A. A. Puretzkii, Opt. Commun. 18, 517 (1976).
[6] R. V. Ambartzumian, Yu. A. Gorokhov, V. S. Letokhov, G. N. Makarov, and A. A. Puretzkii, JETP Lett. 23, 26 (1976).
[7] C. D. Cantrell and H. W. Galbraith, Opt. Commun. 18, 513 (1976); C. C. Jensen, W. B. Person, B. J. Krohn, and J. Overend, *ibid.* 20, 275 (1977).
[8] H. Kildal, J. Chem. Phys. 67, 1287 (1977); J. R. Ackerhalt, H. Flicker, H. W. Galbraith, J. King, and W. B. Person, *ibid.* 68, 1461 (1978).
[9] J. R. Ackerhalt and H. W. Galbraith, J. Chem. Phys. 69, 1200 (1978); H. W. Galbraith and J. R. Ackerhalt, Opt. Lett. 3, 152 (1978).
[10] Indeed, from knowledge of the $2\nu_3$ levels alone, we can deduce the splitting constants G_{21} and T_{33}, and thence the structure of the entire ν_3 manifold.
[11] J. L. Steinfeld and P. L. Houston, in *Laser and Coherence Spectroscopy*, edited by J. I. Steinfeld (Plenum, New York, 1978), pp. 1–123.
[12] I. Burak, A. V. Nowak, J. I. Steinfeld, and D. G. Sutton, J. Chem. Phys. 51, 2275 (1969); J. I. Steinfeld, I. Burak, D. G. Sutton, and A. V. Nowak, J. Chem. Phys. 52, 5421 (1970).
[13] A. V. Nowak and J. L. Lyman, J. Quant. Spectrosc. Radiat. Transfer 15, 945 (1975).
[14] J. G. Black, E. Yablonovitch, N. Bloembergen, and S. Mukamel, Phys. Rev. Lett. 38, 1131 (1977); E. R. Grant, P. A. Schulz, Aa. S. Sudbø, Y. R. Shen, and Y. T. Lee, Phys. Rev. Lett. 40, 115 (1978).
[15] K. S. Rutkovskii and K. G. Tokhadzhe, Zhur. Eksp. Teor. Fiz. 75, 406 (1978).
[16] D. S. Frankel, J. Chem. Phys. 68, 1696 (1978); D. S. Frankel and T. J. Manuccia, Chem. Phys. Lett. 54, 451 (1978).
[17] W. Fuss and J. Hartmann, J. Chem. Phys. 70, 5468 (1979). W. Fuss, J. Hartmann, and W. E. Schmid, Appl. Phys. 15, 287 (1978); A. B. Peterson, J. Tiee, and C. Wittig, Opt. Commun. 17, 259 (1976).
[18] T. F. Deutsch and S. B. J. Brueck, J. Chem. Phys. 70, 2063 (1979), which includes a summary of earlier IRDR ex-

periments on SF_6.

[8] A preliminary account of this work was given by J. I. Steinfeld and C. C. Jensen, in *Tunable Lasers and Applications*, edited by A. Mooradian, T. Jaeger, and P. Stokseth (Springer-Verlag, Berlin, 1976), pp. 190–192.

[9] P. F. Moulton, D. M. Larsen, J. N. Walpole, and A. Mooradian, Opt. Lett. 1, 51 (1977).

[10] P. F. Moulton and A. Mooradian, "High Resolution Double Resonance Spectroscopy of SF_6," in *Proc. Conf. Laser Induced Process in Molecules* (Springer-Verlag, Berlin, 1979), pp. 37–42.

[11] R. S. McDowell, H. W. Galbraith, B. J. Krohn, C. D. Cantrell, and E. D. Hinkley, Opt. Commun. 17, 178 (1976).

[12] R. S. McDowell, H. W. Galbraith, C. D. Cantrell, N. G. Nereson, P. F. Moulton, and E. D. Hinkley, Opt. Lett. 2, 97 (1978).

[13] R. S. McDowell, H. W. Galbraith, C. D. Cantrell, N. G. Nereson, and E. D. Hinkley, J. Mol. Spectrosc. 68, 288 (1977).

[14] R. G. Whitford, K. J. Siemsen, H. D. Riccius, and G. R. Hanes, Opt. Commun. 14, 70 (1975).

[15] N. G. Nereson, J. Mol. Spectrosc. 68, 489 (1978).

[16] R. S. McDowell (private communication).

[17] L. Allen and J. H. Eberly, *Optical Resonance and Two-Level Atoms* (Wiley-Interscience, New York, 1975), p. 140.

[18] The conversion factor (in rationalized MKS units) is $I(W/m^2) = (\epsilon_0/\mu_0)^{1/2} |\mathcal{E}_0|^2$, where $(\epsilon_0/\mu_0)^{1/2} = (377\ \text{ohm})^{-1}$ is the permittivity of free space. A convenient approximate relationship is $\mathcal{E}_0\,(\text{statvolts/cm}) = 2U,\ (\text{kW/cm}^2)^{1/2}$.

[19] The homogeneous relaxation times T_1 and T_1' have been found to be experimentally equal in a variety of molecular systems, such as NH_3[20] and OCS.[12] Theoretical analyses[21] indicate that their ratio should, in any case, lie between 1.0 and 0.5 for a two-level system.

[20] G. M. Dobbs, R. H. Micheels, J. I. Steinfeld, J. H.-S. Wang, and J. M. Levy, J. Chem. Phys. 63, 1904 (1975).

[21] J. C. McGurk, R. T. Hofmann, and W. H. Flygare, J. Chem. Phys. 60, 2922 (1974); H. Mader, J. Ekkers, W. E. Hoke, and W. H. Flygare, J. Chem. Phys. 62, 4380 (1975).

[22] W. K. Liu and R. A. Marcus, J. Chem. Phys. 63, 272, 290 (1975).

[23] K. Fox, Opt. Commun. 19, 397 (1976).

[24] C. C. Jensen, Ph. D. thesis, Massachusetts Institute of Technology (January, 1979).

[25] G. Herzberg, *Molecular Spectra and Molecular Structure II. Infrared and Raman Spectra of Polyatomic Molecules* (Van Nostrand, Princeton, 1945), pp. 446–458.

[26] The centrifugal distortion coefficient for SF_6 has been measured to be 6 Hz, or 2×10^{-10} cm^{-1} (Ch. Bordé, Fourth Intl. Laser Spectroscopy Conf., Rottach-Egern, 1979). Thus, the total spread of each J'' manifold will not exceed $DJ^4 \sim 2\times10^{-4}$ cm$^{-1} \sim 6$ MHz.

[27] R. W. Galbraith, C. W. Patterson, B. J. Krohn, and W. G. Harter, J. Mol. Spectrosc. 73, 475 (1978).

[28] I. M. Kayazev, V. S. Letokhov, and V. V. Lobko, Opt. Commun. 23, 337 (1978); R. V. Ambartzumyan, I. N. Knyazev, V. V. Lobko, G. N. Makarov, and A. A. Puretzky, Appl. Phys. 19, 75 (1979).

[29] B. R. Mollow, Phys. Rev. A 5, 2217 (1972).

[30] F. Y. Wu, S. Ezekiel, M. Ducloy, and B. R. Mollow, Phys. Rev. Lett. 38, 1077 (1977).

[31] M. Johnston and D. M. Dennison [Phys. Rev. 48, 868 (1935)] predict $\zeta_1 = -\zeta_1$ for the ν_3 vibration of a spherical top, but Herzberg[25] points out that this is only an approximation which does not take into account Coriolis interaction with other vibrational sublevels. Nevertheless, the closeness of the value found for ζ_1 to the theoretical estimate is encouraging.

[32] T. Oka, Adv. Atom. Mol. Phys. 9, 127 (1973).

[33] Infrared–radiofrequency double-resonance has been used to observe pure rotational transitions in the $\nu_3 = 0$ and 1 states of methane,[34–36] but no relaxation measurements were reported.

[34] R. F. Curl, Jr., T. Oka, and D. S. Smith, J. Mol. Spectrosc. 46, 518 (1973).

[35] R. F. Curl, Jr., J. Mol. Spectrosc. 48, 165 (1973).

[36] M. Takami, K. Uehara, and K. Shimoda, Jap. J. Appl. Phys. 12, 824 (1973).

[37] R. F. Curl, Jr., and T. Oka, J. Chem. Phys. 36, 4908 (1973).

[38] E. Weitz and G. Flynn, Ann. Rev. Phys. Chem. 25, 275 (1974).

[39] At the low SF_6 pressures used in these experiments, we can take a linear approximation to the transmittance $= \exp[-k_{ss} \times (n_s - n_s)] \approx 1 - k_{ss}(n_s - n_s)$.

[40] M. M. Mkrtchyan and V. T. Platonenko, Sov. J. Quantum Electron. 6, 1187 (1978).

[41] W. G. Harter and C. W. Patterson, J. Chem. Phys. 66, 4872 (1977).

[42] C. W. Patterson and W. G. Harter, J. Chem. Phys. 66, 4886 (1977).

[43] W. G. Harter and C. W. Patterson, Int. J. Quantum Chem. S11, 445 (1977).

[44] W. G. Harter, C. W. Patterson, and F. da Paixo, Rev. Mod. Phys. 50, 37 (1978).

[45] W. G. Harter, H. W. Galbraith, and C. W. Patterson, J. Chem. Phys. 69, 4888 (1978).

[46] W. G. Harter, C. W. Patterson, and H. W. Galbraith, J. Chem. Phys. 69, 4696 (1978).

[47] We use hard-sphere collision diameters $\sigma(He) = 2.6$ Å, $\sigma(CH_3F) = 4.0$ Å, $\sigma(SF_6) = 5.5$ Å.

[48] F. M. Lussier, J. I. Steinfeld, and T. F. Deutsch, Chem. Phys. Lett. 58, 277 (1976).

[49] C. B. Quick, Jr., and C. Wittig, J. Chem. Phys. 69, 4201 (1978).

[50] L. P. Herrmann and J. B. Marling, Livermore Report UCRL-52341 (1978).

[51] For example, portions of the diode laser absorption spectrum of vinyl chloride have been recorded (J. E. Melzer, S. M. Thesis, Massachusetts Institute of Technology (1977)], but a complete analysis has not been carried out.

F.1 Introduction

In recent years, the low cost of laboratory microprocessors and minicomputers has enabled many laboratories to obtain digital processors for signal recovery and analysis and for computation. Concurrently, transient digitizers have become popular, but leave the experimenter the task of linking the digitizer to his processer. Although successful interfacing designs have been reported [F-1, F-2] they are not straightforwardly adaptable to other processors or digitizers. In this paper we report interface designs suitable for linking many different Biomation transient recorder models to the Digital Equipment Corporation PDP 8 and LSI 11 families. Specifically, our devices have linked a Biomation Model 828 to a MINC (LSI 11/2) and a PDP 8/L processer.

A block diagram for the interfaces is shown in Fig. F-1. In both cases, most of the interface is contained on a single general-purpose interface card available from DEC. A few extra gates are necessary to adapt the general interfaces to the 828. In both cases a multiconductor ribbon cable connects the 828 to the interface, which is located in the processer cabinet.

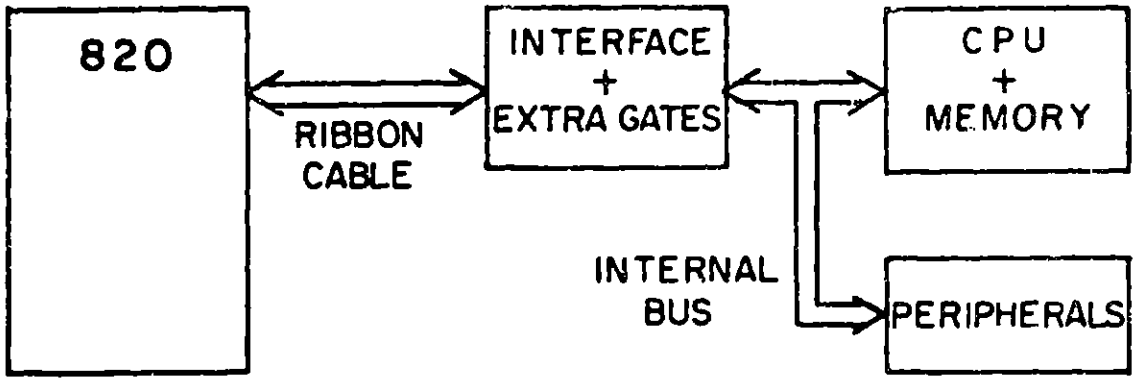

F-1. Block diagram for Biomation 820 interfaces.

Since the 820 and other Biomation models use only two active "handshaking" signals, COM and FLG, to gate the transfer of digitized records to the computer, these interfaces should be useful for a variety of transient recorder models. The present systems also provide for computer control of the transient recorder, or computer-to-820 datum transfer, although maximum transfer rates are attained when the digitizer runs in AUTO DIGITAL, or automatic transfer mode.

F.2 MINC Interface

The DRV11-B DMA interface used for the Biomation-MINC link required three extra TTL chips to be mounted on the interface card itself. One, a 74121 monostable, was placed in convenient predrilled holes. The other two, a 7410 NAND buffer and a 74367 tri-state buffer, were glued to the back side of the interface card. The only other modification of the DRV11-B board was to remove the copper artwork connecting pins K and L of connecter J2 (output connecter) so that pin K could be used to route the signal COM from the extra 74367 chip to the 820. The schematic for the entire interface is shown in Fig. F-2.

Communication between the DRV11-B and the 820 is accomplished via a 40-conductor 26 AWG ribbon cable approx. 26 meters in length. Every other wire in the cable is ground

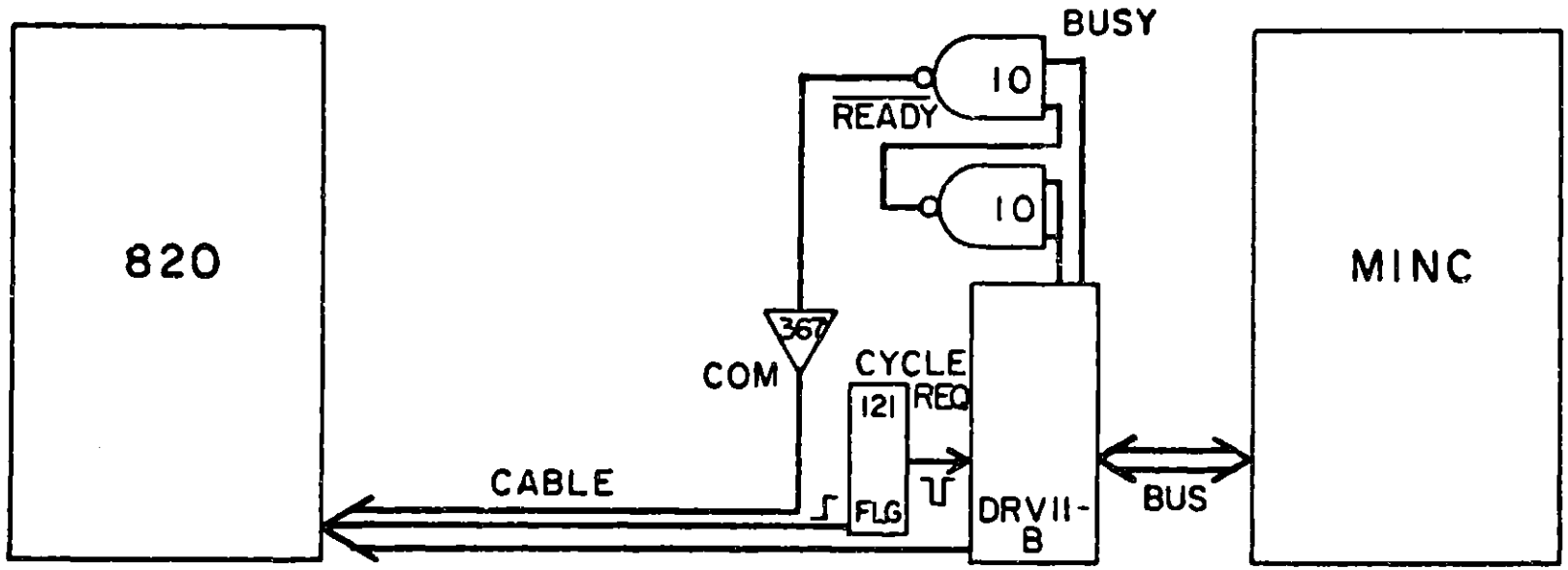

F-2. Circuit diagram for MINC interface. Not shown are the following constant logic levels: Hi to 820 pins 19, 24, 25; J1 pin J; J2 pins F, J, T. Lo to 820 pins 14-16, 20-23; J1 pins K, R, BB, CC; J2 pins D, N, DD-VV.

to minimize crosstalk. Voltages necessary to specify constant logic levels at the DRV11-B were routed from the 820 connecter through the cable to the DRV11-B connecters. Specifically, the DMA interface was wired for burst mode or synchronous transfer to insure maximum transfer rates, although single cycle or asynchronous transfer was also used successfully. Thus, once the 820 intitiates transfer, all data are transfered at the maximum rate, which is determined by the MINC bus cycle time. Also, logic specifying DATO or DRV11-B to 820 transfers was hard wired, even though some exchanges may actually pass Input Control data to the 820, as explained below.

Operation of the interface is straightforward. First, under software control, the word count register (WCR) in the DRV11-B is loaded for the desired number of data words to be transfered. For Input Control or Output Status transfers, only one word is transfered. For transfer of a digitized record, any number up to 2K words can be chosen. Next the bus address register (BAR) is loaded with the location to which transfer is desired in MINC memory. The bit pattern corresponding to the desired Biomation 820 operater/operand command is then placed in the DRV11-B output data buffer register (ODBR), where it will stay throughout the data transfer. Note that if Bit 12 is hi in the ODBR, the 820 will interpret the command as an Input Control command even though the DRV11-B has been wired for 820-to-DRV11-B data transfers. Finally, the GO bit in the control/status register (CSR) is

written hi, activating the interface.

As shown in the timing diagram, Fig. F-3, when the GO bit turns hi, the READY line goes lo, asserting COM (lo). The 820 interprets this as a command transition and interprets the command word in the ODBR. FLG goes lo while the 820 is busy, and when it rises the monostable (121) is triggered. On the rising edge of the monostable CYCLE REQ pulse, the DRV11-B latches data from the 820 into the input data buffer register (IDBR). Busy goes hi, forcing COM hi, and a DMA cycle is performed to pass the data word to MINC memory. If more than one word is to be transfered, BUSY goes lo at the end of the DMA cycle while READY stays lo, thus causing another COM pulse and subsequent data transfer. After the required number of words are transfered, READY goes hi, BUSY remains hi, and the DRV11-B makes an interrupt request if the interrupt enable bit in the CSR is on. Using a program similar to the one below, data transfer rates of greater than 50 full 2K records/sec was accomplished with an 820 recording timebase of 0.05 microseconds:

```
        MOV     #INTH,124       ; LOAD INT VECTOR HANDLER
        MOV     #-4000,WCR      ; LOAD WCR FOR FULL REC XFER
        MOV     #BUF,BAR        ; DATA STASHED IN BUF BUFFER
        MOV     CDAT,ODBR       ; LOAD DATA OUT COM INTO ODBR
        MOV     GO,CSR          ; TURN DRV11-B ON
        WAIT                    ; WAIT FOR INTERRUPT=DONE
                                ; INTERRUPT OCCURS
        RTS     PC              ; EXIT FROM SUBROUTINE
INTH:   RTI                     ; NO 'HANDLING' NECESSARY
CDAT:   .WORD   4000            ; CATA OUT COMMAND
GO:     .WORD   101             ; DRV11-B GO COM W INTERRUPT
BUF:    .BLKW   4000            ; RESERVE 2K WORD BUFFER
```

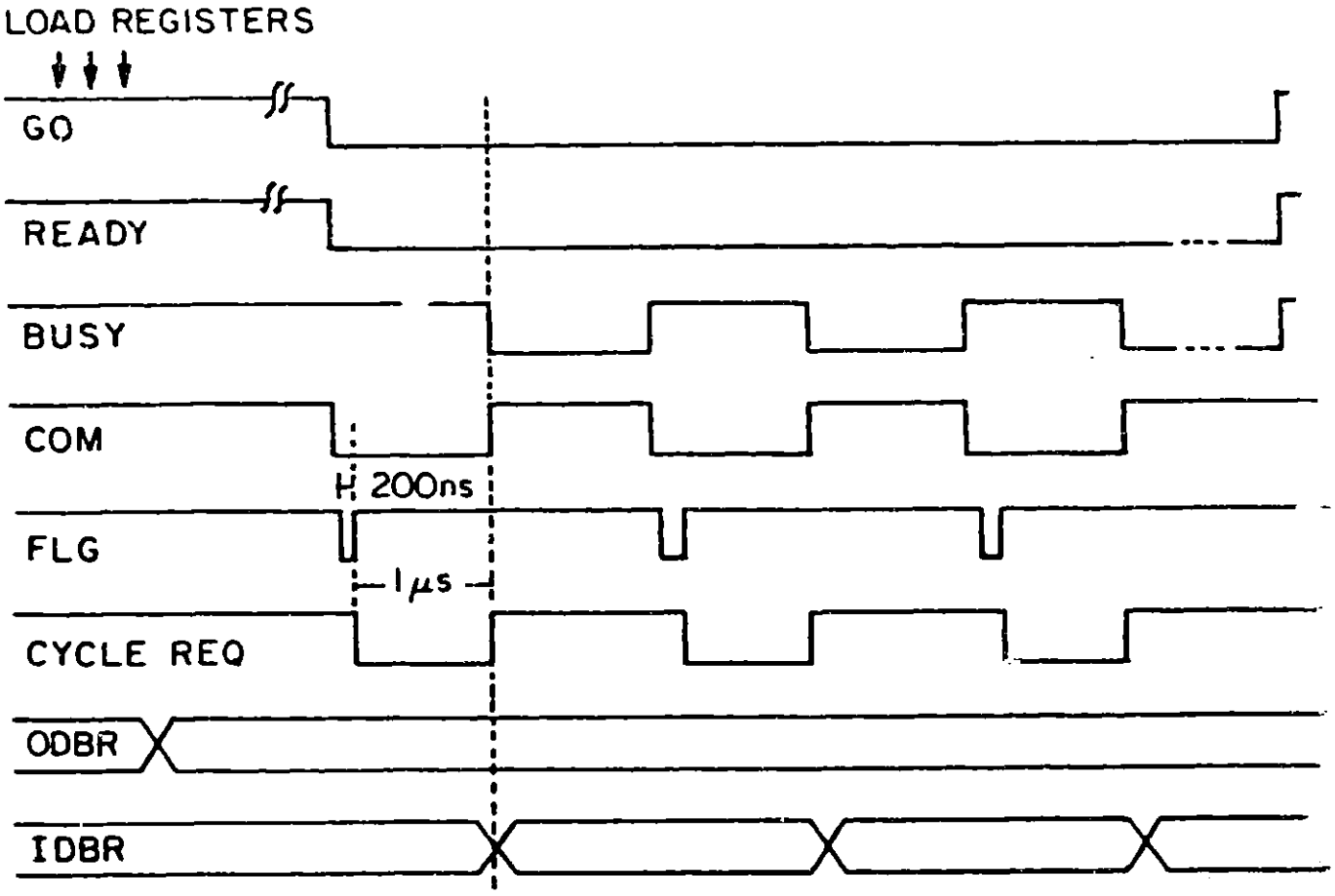

F-3. Timing diagram for DRV11-B burst mode word transfers.

No errors in data transfer were detected even though the ribbon cable exceeds the recommended maximum length of 50 feet (17 meters). Programs similar to the one above have been written as generalized FORTRAN-callable subroutines.

Although it was not implemented in our interface, the highest three bits of the ODBR may be used to address more than one 820 unit. In this manner a single DRV11-B could transfer data from several units, one at a time, via a parallel bus cable connecting them.

F.3 PDP 8/L Interface

Unlike the MINC interface, the device chosen to effect transfer from the 820 to our PDP 8/L was a program data transfer module M735. This device is considerably slower than a DMA interface, but for the PDP 8 family, a DMA interface is not available on a single card. Thus, for simplicity in circuit design and ease in programming, a wordwise program transfer module was chosen.

The schematic for the 820 to 8/L link is shown in Fig. F-4. Data from the M735 output data buffer (ODB) is routed through OC inverters with resistive pullup to a cable identical to the one used for the MINC link. The lowest eight bits of the ODB are connected in parallel with the corresponding bits in the input data buffer (IDB) for half-duplex operation. Other extra logic elements create

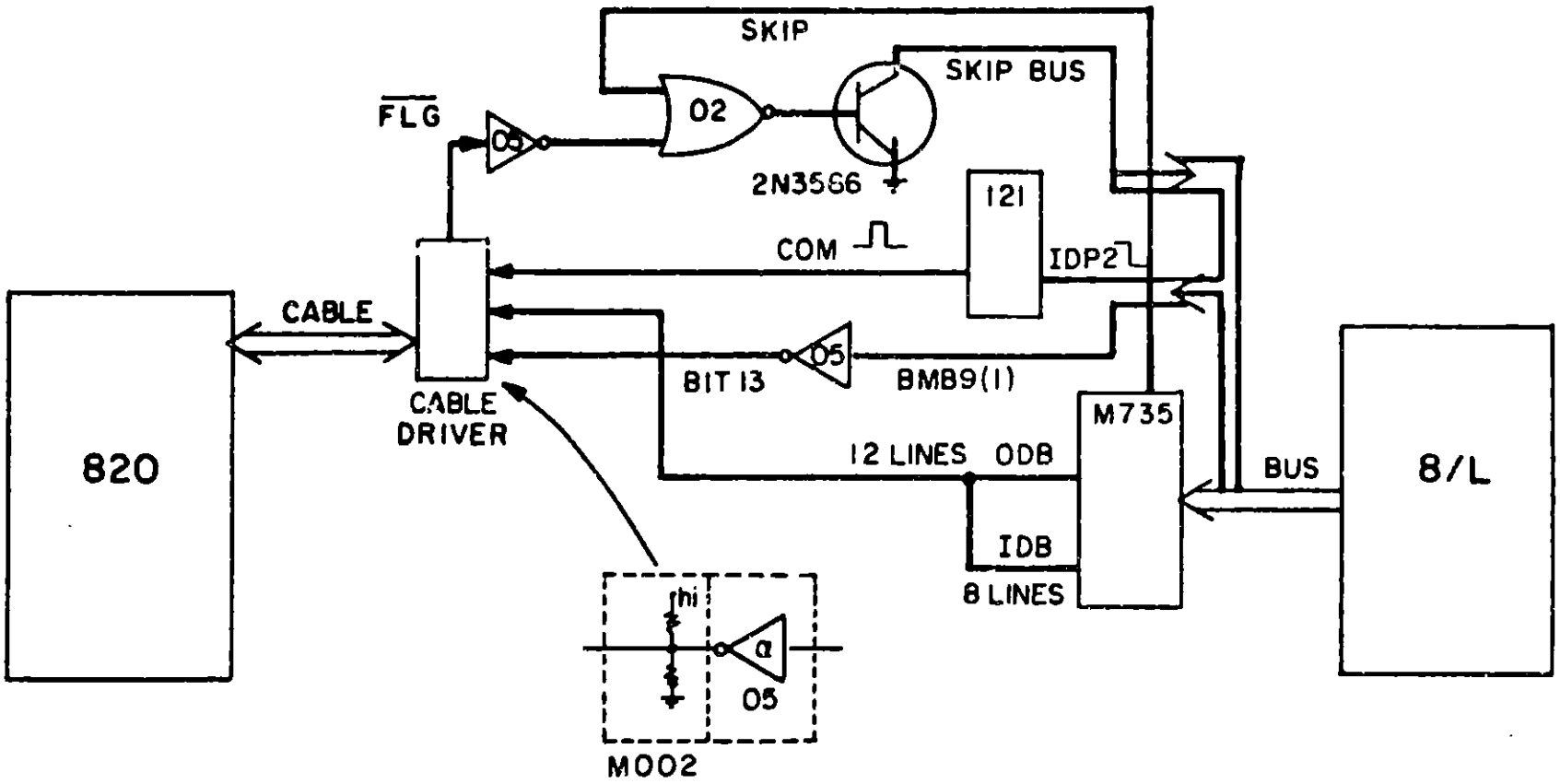

F-4. Circuit diagram for PDP 8/L interface. Not shown are the following constant logic levels: Hi to 820 pin 23. Lo to 820 pins 14-16, 19-22, 24, 25.

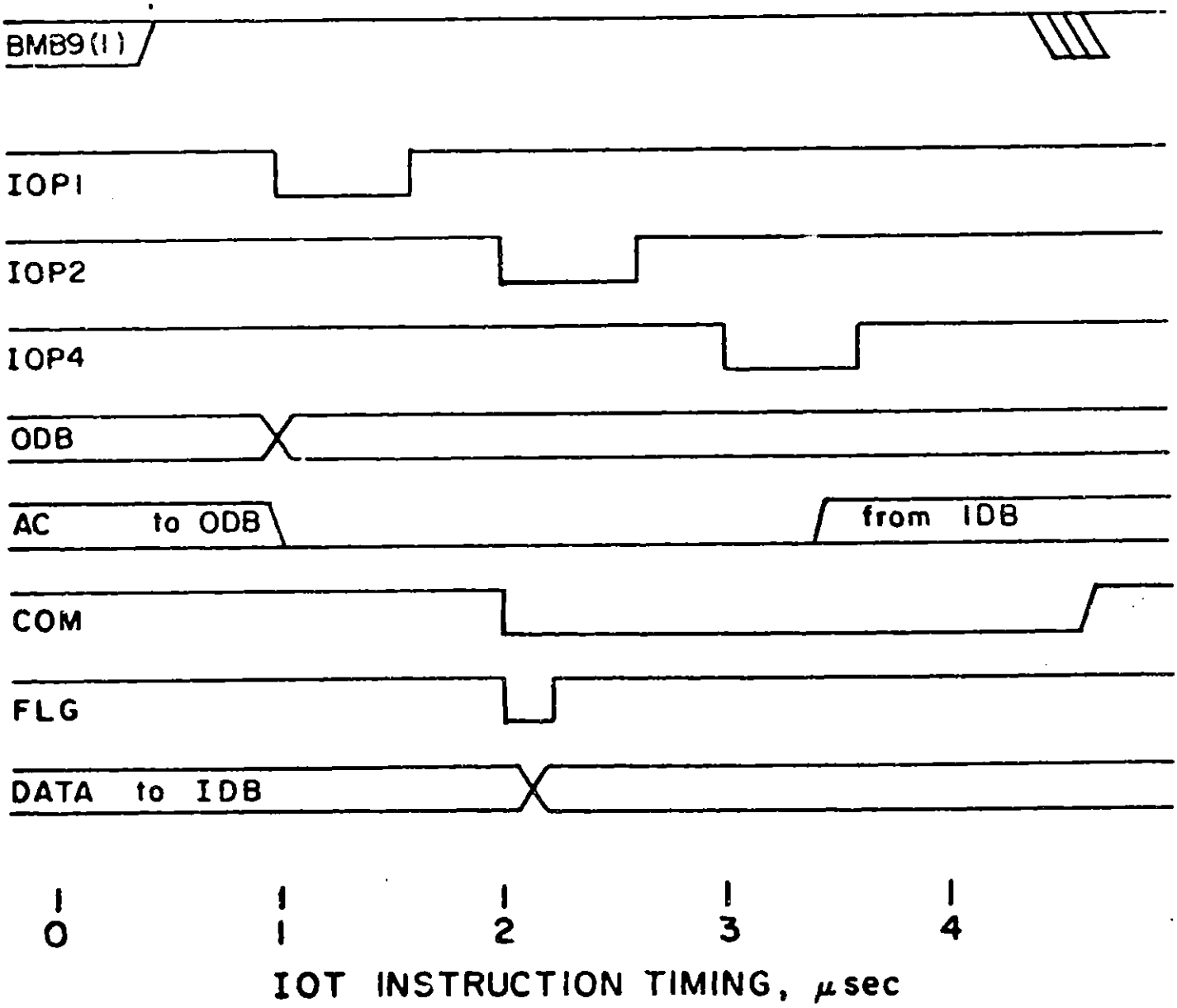

F-5. Timing diagram for program data transfers using the M735 interface on the PDP 8/L.

command pulses and provide for sensing FLG. Constant logic levels are implemented by daisy-chain wiring in the 820 connector plug and at the wire-wrappable connecter block in the 8/L cabinet where the M735 and other modules are inserted.

Three events, independently specifiable by the lowest three bits in the IOT microinstruction, can occur in one program data transfer cycle, as shown in Fig. F-5. At IOP1, the ODB is loaded from the accumulater (AC). IOP2 triggers a 74121 monostable, which is sent to the 820 as a command pulse. The monostable times out after IOP4, when data can be strobed through the input data buffer (IDB) into the AC.

Any combination of IOPn events can be chosen to occur in the same instruction. For Output Status operations, all three events are chosen; at the end of the IOT cycle the AC contains the eight bit status word from the 820. For Input Command operations, only IOP1 and IOP2 are chosen.

Because the operator/operand structure of the 820 requires 13 bits and the 8/L is a 12-bit processer, an extra bit is needed to specify whether Input Control or Output Status is desired. This bit is Bit 9 in the IOT instruction, which specifies whether or not an IOP4 transfer will occur. It is available on the PDP 8 bus as BMB9(1). Thus Bit 9 in the IOT microinstruction is set for Output Status, an left off for Input Control.

This arrangement works well for all operations except

DATA OUT, for which some additional software scale timing must be considered. Once the 820 has been placed in Digital Output mode by the B/L and the first DATA OUT operater applied, a period of time passes before the 820 produces the first datum. The program can sample FLG until it goes hi, signaling the readiness of the 820. Data can then be strobed out of the 820 under program control without further delay at maximum rate, which is determined chiefly by the software routine execution time. Using a program similar to the one below, data transfer rates of about 10 full 2K records/sec was effected using a recording timebase of 0.05 microseconds on the 820:

```
        TAD     TRDATC  / GET DIGITAL OUT COMMAND
        6373            / GIVE TO 820; M735 IN LOC 37
        TAD     N2K
                / GET NUMBER -2K FOR FULL RECORD XFER
        DCA     TRCNTR  / DEPOSIT IN COUNTER
        DCA     10      / CLEAR AUTOINCREMENT REG 10;
                / DATA BEGIN IN LOC 0, DATA FIELD 1
        TAD     TRDOUT  / GET DATA OUT COMMAND
        6373            / GIVE FIRST DATA OUT TO 820
        6371            / IS 820 READY?
        JMP     .-1     / NO -- ASK AGAIN
        CDF1            / YES - CHANGE TO DATA FIELD 1
FTR5A,  6376            / TAKE THIS DATA WORD
        DCA I   10      / DEP IN CURRENT LOC, INC 10
        ISZ     TRCNTR  / TAKEN ENOUGH WORDS?
        JMP     FTR5A   / NO -- GO BACK FOR ANOTHER
        CDF0            / YES - RETURN TO DATA FIELD 0
        TAD     TRDAT2  / GET TRUNCATE DIGITAL OUT COM
        6373            / GIVE TO 820
        JMP I   EFUN3I  / SUBROUTINE EXIT
TRDATC, 3420            / CONSTANTS IN OCTAL; DIG OUT
N2K,    -4000           / =-2048 DECIMAL
TRCNTR, 0               / WORD TRANSFER COUNTER
TRDOUT, 4000            / DATA OUT COMMAND
TRDAT2, 3401            / TRUNCATE DIGITAL OUT COM
```

F.4 IMPLEMENTATION

Successful implementation of this digital signal recovery system has been reported in double resonance spectroscopy experiments. The curious experimenter is invited to read references [F-3] and [F-4] for further details.

F.5 Acknowledgment

This work has been supported by the Office of Advanced Isotope Separation Technology, U. S. Department of Energy, under Contract EY-76-S.02-2793.

Appendix G. Program Listings

In this Appendix, programs in machine language (PAL-III for the PDP-8/L and MACRO-11 for the MINC) for use with the Biomation 820 interfaces described in Appendix F are listed. Also included are two files used to prepare this thesis.

FORTRAN callable MACRO subroutines are simple to cons uct. Arguments are passed from the MAIN program to the subroutine using R5. When control reaches the subroutine, R5 points to a list in core. The first word on the list is the number of arguments in the subroutine CALL statement. The next word in the list is the address of the first argument; the next word is the address of the second argument, etc. Once the MACRO subroutine has been typed in, it is compiled with the RT-11 MACRO command. The OBJect file created can be directly linked to a compiled FORTRAN program.

In FOCAL the arrangement is more complex. A version of 4K FOCAL called "FOKAL for TR" has been produced which includes a PAL-III function FCOM for communication with the 820. To load the entire package, one must first load the FOCAL and FOCAL modifications portion of the FOKAL for TR tape, then start at address 200. After the initial dialogue the * appears. Loading the FCOM function can then be done in the same manner as loading FOCAL. Routines for running the ARDS can be loaded optionally. Finally, FOCAL must be

restarted at location 200 as usual.

Since the FCOM function accepts only one record from the 820, recovery of many records may be slow. Another function, FLOG for TR, was written to maximize the transfer rate between the 8/L and the 820. This function can be overlaid into FOKAL for TR; it uses the space normally occupied by the FLOG function. Several features available using FCOM are not available using FLOG, so that it is recommended that if FLOG for TR is needed, FCOM should also be loaded.

FOKAL reserves the higher 4K of the 8K 8/L memory for storing data from the 820. Two words are used for one "cell", or 24 bits per cell. Since the precision of the 820 is eight bits, 2^16 or 64K records can be accumulated with no loss of precision. The 4K words of memory used for storing the 2K data cells are unavailable for use as program space, so that program space is considerably smaller than for 8K FOCAL. When the ARDS routines are loaded, program space becomes very small.

The following are brief descriptions of the programs listed in this Appendix:

TR1.MAC - MACRO subroutine for taking one variable length record from the 820. CALL TR1(NCELLS,NREC(I),ISTAT) performs a one record transfer from the 820 to the MINC. The transfer occurs when the status of the 820 equals ISTAT. The transfer of NCELLS individual points is made into consecutive words in

core starting with NREC(I). NREC should be a regular FORTRAN integer vector.

STATUS.MAC - MACRO subroutine for recovering the status of the 820.

USETR1.FOR - FORTRAN example of the use of STATUS and TR1.

OUTPUT.BAS - program used under MINCSYS to print this thesis ON the LA34 DECWRITER IV.

RUNCOM.TXT - command file for RT11 RUNOFF program provided by DEC. RUNOFF is a text formatting program which reads a text file which contains original text and commands, and outputs a finished document. A typical command to RUNOFF would be:

*SY1:CHAP3.DOC<RUNCOM.TXT,CHAP31.TXT,CHAP32.TXT/F

FCOM - function for transient recorder communication to the 8/L. FCOM us called from a FOCAL program as follows:

FCOM(1,X)	returns value of cell X
FCOM(2,X,Y)	sets cell X to the value Y
FCOM(3,X)	sends a COMmand the 820 whose Input Control Command decimal value is X
FCOM(4,X)	returns status of 820 as requested by the Output Status Command whose decimal value is X
FCOM(5,X,Y)	takes X data points from the 820 and

adds then into consecutive cells starting with cell Y

FLOG - fast 820 interface function.

FLOG(A,B,C,D) takes C records with A data points per record from the 820. Each record is added into consecutive cells starting with cell B. D is the "ready" status of the 820.

PEAKAVG - FOCAL program illustrating the use of FCOM. This program takes 400-cell records from the 820. In each record, the peak of the signal is found. If the peak value exceeds a minimum value M, it is averaged until C peaks above the minimum are recorded.

```
                TR1.MAC
.TITLE  TR1  QUICKIE 820 RECORD TAKER
;               TAKES VARIABLE LENGTH RECORD ONCE
;               WHEN 820 IS 'READY'
;
        DWCR = 172410           ; WORD COUNT REGISTER
        DBAR = 172412           ; BUS ADDRESS REG
        DCSR = 172414           ; CONTROL/STATUS REG
        DIDBR= 172416           ; INPUT DATA BUFFER READ ONLY
        DODBR= 172416           ; OUTPUT "    "     WRITE ONLY
;
        DIV = 124               ; INTERRUPT VECTOR
;
TR1::   ADD     #6,R5           ; MOVE TO 3RD ARG
        MOV     CSTAT,DODBR     ; LOAD STATUS COMMAND
        MOV     #INTH,DIV       ; SET INT ADDRESS
        CLR     DIV+2           ;NEW PSW = 0
TRY:    CLR     R1
        CLR     BUF2            ; CLEAR PREVIOUS TRY
        MOV     #BUF2,DBAR      ; LOAD BUS ADDR
        MOV     #-1,DWCR        ; 1 WORD TRANSFER
        MOV     GO,DCSR         ; LET'S HAVE IT
W3:     NOP
        NOP
        NOP
        NOP
        NOP                     ; TREAD WATER
        TST     R1              ; STATUS IN YET?
        BEQ     W3              ; IF NO, WASTE TIME
        CMPB    @(R5),BUF2      ; SAME AS WANTED STATUS?
        BNE     TRY             ; ASK AGAIN IF NO
        SUB     #4,R5           ; RESTORE POINTER TO 1 ARG
;
TAKE:   MOV     @(R5)+,R1       ; GET RECORD LENGTH
        NEG     R1              ; FORM NEGATIVE
        MOV     R1,DWCR         ; LOAD WORD COUNTER
        CLR     R1              ; CLEAR SWITCH
        MOV     (R5),DBAR       ; MOVE LOCATION TO BUS ADDR
        MOV     CDAT,DODBR      ; LOAD DATA OUT COM
        MOV     GO,DCSR         ; LET IT RIP
W2:     TST     R1
        BEQ     W2              ; BACK IF NOT
;
;               INTERRUPT OCCURS
;
        RTS     PC              ; GO HOME AFTER SHORT WAIT
;
INTH:   INC     R1
        RTI                     ; POP PSW, PC
;
BUF1:   .WORD   0
BUF2:   .WORD   0
CSTAT:  .WORD   3400            ; STATUS COMMAND
```

```
CDAT:   .WORD   4000            ; DATA OUT COMMAND
CSTOP:  .WORD   13401           ; STOP DATA
GO:     .WORD   101             ; DRV11-B GO COMMAND NO INT
        .END
```

STATUS.MAC

```
.TITLE  STATUS  FOR GETTING BIOMATION STATUS
;
        WCR = 172410
        BAR = 172412
        CSR = 172414
        DBR = 172416
        DIV = 124
;
STATUS::
        TST     @(R5)+          ; MOVE OVER OARG
        MOV     CSTAT,DBR
        MOV     #INTH,DIV
        MOV     #BUF2,BAR
        MOV     #-1,WCR
        MOV     GO,CSR
        TST     R5
        TST     R5
        TST     R5
        TST     R5
        TST     R5
        TST     R5
        MOV     BUF2,@(R5)
        RTS     PC
;
INTH:   RTI
;
BUF2:   .WORD   0
CSTAT:  .WORD   3400
GO:     .WORD   101
        .END
```

USETR1.FOR

```
C       USETR1 -- PROGRAM TO USE MACRO ROUTINE TR1
C       30 JAN 80 BY CHRIS REISER
C
      INTEGER NEWREC(2048)
C
C       NEWREC FOR NEW RECORDS, ACCUMULATED INTO IACC
C
      CALL STATUS(ISTAT)
      TYPE 102, ISTAT
6     ACCEPT 102,NSHOTS
  102 FORMAT (I6)
C
C       ACCEPT 10 RECORDS
C
      DO 10 NSHOT=1,NSHOTS
      CALL TR1(2048,NEWREC(1),ISTAT)
C
C       TAKE 2048 CELLS FROM 820 (THE WHOLE RECORD), PUT THEM
C       IN CONSECUTIVE MEMBERS OF NEWREC STATRING WITH
C       NEWREC(1), WHEN 820 HAS STATUS OF ISTAT
C
C
   10 CONTINUE
C
C       USER CAN DO ANYTHING WITH DATA HERE
C       OR GO BACK FOR MORE
C
      GOTO 6
  101 FORMAT (10I9)
      END
```

```
  *5040
FLØØ,   NØP      /NAST TRANSIENT RECØRDER NUNCTIØN
        /10.78 BY C REISER
        INT      /# DATA
        CIA
        DCA      NDATA
        PUSHJ
        EVAL-1
        INT      /CELL #
        CLL RAL  /X2
        TAD      N3       /ADD ØNFSET
        DCA      FCELL
        PUSHJ
        EVAL-1
        INT      /# RECØRDS
        CIA
        DCA      RCNTR    /RECØRD CØUNTER
        PUSHJ
        EVAL-1
        INT      /TR READY STATE
        CIA
        DCA      NRDY
SETUP,  TAD      NDATA
        DCA      DCNTR    /DATA CØUNTER
        TAD      FCELL
        DCA      10
        TAD      10
        DCA      11
ASK,    TAD      STASK
        6377
        TAD      NRDY
        SZA      CLA
        JMP      ASK
        TAD      TRDATC   /HERE WHEN READY
        6373     /START DATAØUT
        TAD      TRDØUT
        6375     /LØAD BUFFER
        6371
        JMP      .-1      /TREAD TILL FLAG
        CLA CLL
        CDF1
REC,    6376     /TAKE DATUM
        TAD      I        10
        DCA I    11       /ADD IN
        TAD I    10       /HØRD
        SZL
        IAC CLL  /INC IF ØNLØ
        DCA I    11
        ISZ      DCNTR
        JMP      REC      /BACK TILL EØR
```

```
          CDFO
          TAD       DØFF
          6373      /TURN ØFF DATA
          ISZ       RCNTR
          JMP       SETUP    /BACK FØR MØRE RECØRDS
          JMP I     EFUN3I   /BYE
/
/
NDATA,    0
N3,       -3
FCELL,    0
NRDY,     0
RCNTR,    0
DCNTR,    0
STASK,    3400
TRDATC,   3420
TRDØUT,   4000
DØFF,     3401
//
/
EFUN3I=0136
CDFO=6201
CDF1=6211
PUSHJ=4540
INT=JMS I 0053
EVAL=1613
/
$
```

FCOM

```
 *FNTABF+15
        XFTR
*0035
        XFTR-1
*4400-21
  FNTABF=0374
  INT=JMS I 0053
  PUSHA=4542
  GETC=4545
  EVAL=1613
  P0PA=1413
  EFUN31=0136
  L3RD=0046
  H0RD=0045
  EXP=0044
  PUSHJ=4540
XFTR,           /FUNCTI0N F0R TRANSIENT REC0RDER
                /10.77 BY CHRIS REISER
        INT             /MAKE 1ST ARG INT
        PUSHA           /ST0RE
        PUSHJ
        EVAL-1          /GET NEXT AR0
        CLA
        P0PA            /REC0VER FCN #
        TAD     FTRA    /ADD JMP I
        DCA     .+1     /SET UP JMP
        0               /THIS WILL BE A JMP I
FTRA,   JMP I   .       /JMP T0 LIST
        FTR1
        FTR2
        FTR3
        FTR4
        FTR5
FTR3,   INT             /GET DATUM
        6373            /0IVE T0 TRANSIENT REC
        JMP I   EFUN31          /AND THATS ALL
FTR1,   JMS     FTRADD  /RETURNS CELL X ADD
        CDF0=6201
        CDF1=6211
        CDF1            /CHANGE DF
        DCA     TRCURAD
        TAD I   TRCURAD /PUT CUR ADD & TAKE L0RD
        CDF0
        DCA     L0RD    /PUT IN L0RD
        CDF1
        TAD I   TRCURAD /PICK UP H0RD
        CDF0
        DCA     H0RD    /PUT IN H0RD
        JMS     TRFL0T  /CHNG T0 FLTING PT
        JMP I   EFUN31          /D0NE
TRBEG,  -3              /STARTS DATA AT L0C 0
        TRCURAD=0010
TRFL0T, 0       /CHNG 2W0RD INT T0 FLT PT
```

```
        DCA     EXP     /CLEAR EXP
        TAD     HØRD
        SZA CLA
        JMP     TR2F    /HØRD NØT 0
        TAD     LØRD
        SNA CLA
        JMP I   TRFLØT  /NUMBER=0
TR2F,   TAD     LØRD
        CLL RAL         /BEGIN SHIFT
        DCA     LØRD    /PUT BACK FØR NØW
        TAD     HØRD    /GET HØRD WØRD
        RAL             /RØTATE, LINK IN
        SZL             /DØNE RØTATING IF L=1
        JMP     TR2FL   /FINISH
        DCA     HØRD    /PUT BACK LØRD
        ISZ     EXP     /WILL NEVER BE 0
        JMP     TR2F
TR2FL,  JMS     TR2FLA  /WHICH RØTATES RIGHT
        TAD     HØRD    /READY FØR ANØTHER
        JMS     TR2FLA
        TAD     EXP     /GET EXP
        CIA
        TAD     TR24    /ADD 24 DEC
        DCA     EXP     /THE REAL EXP
        JMP I   TRFLØT  /RETURN
TR24,   0030            /24 DECIMAL
TR2FLA, 0
        RAR
        DCA     HØRD    /PUT IT BACK
        TAD     LØRD    /PICK UP LØRD
        RAR             /RØTATE LINK IN
        DCA     LØRD
        JMP I   TR2FLA  /RETURN
FTRADD, 0
        INT             /CELL # AND INT
        CLL RAL         /MUL BY 2
        TAD     TRBEG   /ADD ØFFSET
        JMP I   FTRADD  /RRETURN
FTR4,   INT             /GET DATUM
        6377            /GIVE, RECEIVE DATA
        DCA     LØRD    /LD INTØ LØRD
        DCA     HØRD    /FAKE LIKE ITS 2WØRD INT
        JMS     TRFLØT
        JMP I   EFUN3I          /DØNE
FTR5,   TAD     TRDATC
        6373            /START DATAØUT
        INT
        CIA             /FØRM -# ØF CELLS
        DCA     TRCNTR  /CØUNTER
        PUSHJ
        EVAL-1
        JMS     FTRADD  /GET CELL ADD
        DCA     TRCURAD /CURRENT ADD
```

```
          TAD     TRCURAD
          DCA     TRCUR2  /FORM IDENTICAL PNTR
          TAD     TRDOUT
          6375            /SET UP DATOUT
          CLA CLL         /CLEAR '
          CDF1
          TRCUR2=0011
          TRCNTR=0004
FTR5A,    6376            /GET A DATUM
          TAD I   TRCURAD /ADD TO CUR LORD
          DCA I   TRCUR2  /REPLACE IT
          TAD I   TRCURAD /GET HORD
          SZL             /DONT INC UNLESS OFLO
          IAC CLL             /ADD ONE TO HORD
          DCA I   TRCUR2  /REPLACE HORD
          6371
          JMP     .-1     /TREAD WATER TILL READY
          ISZ     TRCNTR  /DONE YET?
          JMP     FTR5A   /NO
          CDF0            /YES
          TAD     TRDT2
          6373            /TURN OFF DATAOUT
          JMP I   EFUN3I          /FINISH
TRDOUT,   4000          /COM FOR DATA
TRDATCOM,       3420 /DATOUT START
TRDT2,          3401 /DATOUT STOP
FTR2,     JMS     FTRADD  /GET ADRESS OF CELL
          DCA     TRCURAD /LOAD IT
          PUSHJ
          EVAL-1          /GET Y
          JMS     TRINT   /CHNG TO 2WORD INT
          CDF1
          DCA I   TRCURAD /LD LORD
          CDF0
          TAD     HORD
          CDF1
          DCA I   TRCURAD /LD HORD
          CDF0
          JMP I   EFUN3I          /DONE
TRINT,    0               /FLT PT TO 2WD INT
          CLA
          TAD     HORD
          RTL             /FIND A 1?
          SNL             /CHECK FOR IS
          JMP I   TRINT   /#=0
          CLA
          TAD EXP
          TAD     TR23    /ADD -23 DEC
          SNA
          JMP I   TRINT   /NO SHIFT CASE
          DCA     EXP
TRINT1,   TAD     HORD
          CLL RAR         /START SHIFT
```

```
          DCA     HØRD
          TAD     LØRD
          RAR             /RØT L IN
          DCA     LØRD
          ISZ     EXP     /DØNE YET?
          JMP     TRINTI
          TAD     LØRD
          JMP I   TRINT
TR23,     7751            /=-23 DECIMAL
$
```

PEAK AVG-

```
C-FØKAL,1977

01.01 C AVG PULSE HEIGHTS FRØM T.R.
01.10 S C=0;S H=0;A "# PULSES",N,"  MIN HEIGHT "M
01.20 F I=200,300;S Z=FCØM(2,I,0)
01.30 I (144-FCØM(4,1792))1.3,1.5,1.3
01.50 S Z=FCØM(5,400,1);D 3;I (C-N)1.2
01.60 T "MAX = "H" AFTER "C" PULSES; H/C = "H/C
01.70 Q

03.10 S Z=0;F I=250,300;I (Z-FCØM(1,I))3.25,3.15,3.15
03.15 C SHITMØUSE
03.21 S Z=Z-FCØM(1,201);I (Z-M)3.22;S H=H+Z;S C=C+1
03.22 R
03.25 S Z=FCØM(1,I)

31.10 S Z=FNEW(2);S Z=FNEW(3,40);W A;T "*",I
31.20 Z=FNEW(3,200);S Z=FNEW(1)
```

OUTPUT.BAS

```
1 REM -- OUTPUT - TEXT SPITTER FOR ALLIGNING LP: PAPER
2 REM    14 MAR 80 BY C REISER
10 PRINT 'Source File'; \ INPUT S$
20 OPEN S$ FOR INPUT AS FILE #1
30 OPEN 'LP:' FOR OUTPUT AS FILE #2
40 L%=0% \ P%=1%
50 IF END #1 THEN CLOSE #1,#2 \ STOP
60 LINPUT #1,L$ \ L%=L%+1%
70 PRINT #2,L$
80 IF L%=66% THEN L%=0% \ P%=P%+1%
85 IF P%=2% THEN P%=1% \ GOSUB 95
90 GO TO 50
95 CLOSE #2 \ OPEN 'LP:' FOR OUTPUT AS FILE #2
96 PRINT 'OK For more'; \ INPUT A$ \ RETURN
100 END
```

RUNCOM.TXT

```
.PS 60
.SP 2
.UC
.NJ
.LM 13
.RM 75
.ND
.NNM
.TS 21 29 37 45 53 61 69 77
```

Appendix H. Consideration of some aspects of the SF6 Hamiltonian

In this appendix we will consider tensor terms in the SF6 vibration- rotation Hamiltonian which are capable of mixing clusters. If such mixing exists, intensity of strongly pumped transitions may be borrowed by clusters mixed to them, giving rise to anomalously large DR signals. These considerations have been provided by Dr. Harold W. Galbraith of the Los Alamos Scientific Laboratory.

H.1 Hyperfine interactions

Although the resolution of our experiment was not sufficient to resolve individual symmetry components of a cluster, the splittings within a cluster and between clusters in the ground vibrational state can be calculated [H-1]. Specifically, the matrix elements for the inter- cluster splitting in the ground state is given by

$$T_{044}(J,J)_{\alpha\alpha} = (2^3 3^3 5)^{\frac{1}{2}}(2J+1)\, \|T_v(0)\| \cdot \|T_J(4)\| \begin{Bmatrix} 1 & 1 & 0 \\ J & J & 4 \\ J & J & 4 \end{Bmatrix} \times (-1)^J F^{(4JJ)}_{A_1\alpha\alpha}\, {}^0t_{044} \qquad \text{(H-1)}$$

$$= (-1)^J F^{(4JJ)}_{A_1\alpha\alpha} \frac{\sqrt{3}}{\sqrt{28}} \{(2J-3)(2J-2)(2J-1)2J(2J+1) \times (2J+2)(2J+3)(2J+4)(2J+5)\}^{\frac{1}{2}}\, {}^0t_{044} \qquad \text{(H-2)}$$

Recently Borde et. al. [H-2] have estimated that ${}^0t_{044} \doteq 6$ Hz from very high resolution saturation spectroscopy. Using this value, calculation of (H-2) for J = 33 renders

$$T_{044}(JJ)_{\alpha\alpha} = -F^{(4,33,33)}_{A_1\alpha\alpha} \times 322 \text{ MHz} \qquad \text{(H-3)}$$

Using the expressions of Krohn [H-1b] for the F^4 coefficients in (H-3), the ground state cluster spacing is approximately 5.7 MHz for 4-fold axis clusters and 4.8 MHz for 3-fold axis clusters.

As Borde et. al. point out [H-2], symmetry states within a cluster are mixed by spin-rotation and spin-spin interactions. Spectroscopically, they have shown mixing of the E^0 and F_1^0 states of Q(38) as "crossover peaks" occuring between the E^0 and F_1^0 peaks. These transitions violate the $\Delta C = 0$ selection rule by virtue of tensor spin-spin interactions which are off-diagonal in the cluster approximation. The crossover peak intensities, which are proportional to the square of the mixing, are at best 10%.

The ground state splitting between these two symmetry components can be calculated from (H-3) to be ~ 4 kHz. Since, in our case, the intercluster splitting is about 5 MHz, the intercluster mixing will be down by a factor of 10^3. Hence hyperfine interactions are far too weak to perturb DR intensities between clusters, and may be eliminated as a mechanism for transferring intensity.

H.2 Centrifugal distortion

The only other ground state molecular mixing process to be considered is due to the sixth rank tensor centrifugal distortion operator, given for 4-fold axis clusters by

$$g = {}^{0}t_{044}\,\frac{1}{8}\,[V_0^6 - (\tfrac{7}{2})^{\frac{1}{2}}\,(V_4^6 + V_{-4}^6)] \qquad \text{(H-4)}$$

This operator mixes states of $\Delta K = 0, \pm 4$ (and $\Delta K = 0, \pm 3$ for 3-fold axis clusters). Evaluation of this expression provides, for $J = 33$,

$$g = \frac{{}^{0}t_{066}}{64}\left(\frac{14\cdot4}{11\cdot9}\right)(2J+1)^{-1}(2J+7)(2J+6)\cdots(2J-5)\,,^{1/2}\begin{Bmatrix} J & 6 & J \\ 27 & 4 & -31 \end{Bmatrix} \qquad \text{(H-5)}$$

$$= 1.3 \times 10^{8}\ {}^{0}t_{066} \qquad \text{(H-6)}$$

for ${}^{0}t_{066}$ expressed in Hz.

In the 2-level experiment, the sixth-rank tensor interaction couples the $F_1^5 + F_2^4$, $K = 27$ cluster, which is nearly resonant with the pump field, with the $F_1^2 + F_2^1$, $K = 31$ cluster. Evaluating the appropriate F^4 coefficients to find the splitting between these two clusters in the ground state, we find via (H-3) that this splitting δ is

$$\delta = (3.5 - (-1.8)) \times 10^{2} \approx 322 \text{ MHz} \qquad \text{(H-7)}$$

$$\approx 17 \text{ MHz}$$

This is the energy difference over which the perturbation interaction of (H-6) must apply. The extent of mixing is

given, in a simple perturbative approach, by

$$\text{mixing} \simeq \frac{g}{\delta} = \frac{1.3 \times 10^{8}\ {}^{0}t_{066}}{1.7 * 10^{7}} \qquad \text{(H-8)}$$

$$= 7.6\ {}^{0}t_{066}$$

Hence for 10% mixing we require that ${}^{0}t_{066} > 10^{-2}$ Hz.

Although a measurement of ${}^{0}t_{066}$ has not been made, its size can be obtained by standard vibration-rotation ordering. We assert that

$$\frac{t_{224}}{B} \simeq \frac{{}^{0}t_{066}}{{}^{0}t_{044}} \qquad \text{(H-9)}$$

where B is the rotation constant, since both ratios are taken between parameters which differ by two orders in J. Using best values [H-3] for the known constants in (H-9), we find that

$${}^{0}t_{066} \simeq \frac{{}^{0}t_{044}t_{224}}{B} \simeq \frac{6 \times 3.8 \times 10^{-5}}{10^{-1}} \qquad \text{(H-10)}$$

$$\simeq 2 \times 10^{-3}\ \text{Hz}$$

We conclude that although this is a possible source of mixing, it would take an unusually large molecular constant ${}^{0}t_{066}$ to give appreciable mixing of ground state clusters and hence is unlikely.

H.3 "Weak" transitions

In the excited vibrational state mixings must occur over

even larger detunings than for ground state misings. The primary such mixing is due to the second order Coriolis tensor t_{224}, which mixes different R (pure rotation) values of the same J. This mixing leads to the "weak transitions" of Galbraith et. al. [H-4], which have been suggested [H-5] to be important in the multiphoton absorption process. According to [H-4], weak transitions to the same upper state belong to lower states having different J values. The energy difference δ between the ground states can be simply estimated by

$$\delta \simeq B_o J(J+1) - B_o (J+1)(J+2) \simeq 6 \text{ cm}^{-1} \qquad \text{(H-11)}$$

The very large size of δ in this case indicates that mixings of this type would not be observable in this experiment.

H.4 Optical mixing

The final class of possible mixings are optical, or molecule-pump field coupling. We will consider only dipolar and ignore higher n-pole and magnetic interactions.

In the standard treatment [H-6] the molecular dipole is expanded in normal coordinates in a Taylor's series. In the lab frame it is a permutationally invariant vector, and hence is a double tensor of indices $(1,A_{1g})$. The molecule-fixed components are related to the laboratory- fixed components by a $D^{(1,1)}$ rotation matrix. We can write [H-7]

$$\mu_{LAB}^{(1,A_{1g})} = \{D^{(1,1)} \times (\mu_0 q_3^{(0,1)} + \{q_3 \times q_3 \times q_3\}^{(0,1)} \mu_2^a + \{q_3 \times q_3 \times q_3\}^{(0,3)} \mu_3^b + \cdots)\}^{(1,A_{1g})} \qquad \text{(H-12)}$$

From (H-12) two kinds of terms arise, T_{110} and T_{314}, which are scalars and fourth rank tensors of A_{1g} symmetry, respectively. Since the T_{314} tensor has a vibrational rank of 3 it cannot connect 0 ν_3 states with 1 ν_3 states, hence no mixing via this operator occurs. Furthermore, T_{110} is a scalar in R and cannot mix clusters to any order. Hence, mixing by optical dipole interactions can be ruled out also, leaving no terms in the dressed molecular Hamiltonian which appreciably mix clusters in a given J level.

I.1 TAC II CO_2 TEA laser

Aligning the optical cavity of the TAC II laser follows a procedure similar to that used for aligning other infrared lasers in the laboratory. The output coupler must be removed by unbolting its gimbal mount and removing the entire mount. Next, the brewster angle ZnSe windows must be replaced by pinholes machined into round aluminum stock, made specially for this job. A HeNe laser can then be directed by means of a micrometer-mounted mirror through the two pinholes. The beam should strike the grating in the center.

Alignment of the grating can be checked by turning the "tuning" micrometer handle to insure that successive diffraction orders of the HeNe beam fold back into the pinholes. The vertical tilt micrometer can be tweaked accordingly. Once the HeNe beam and grating are aligned, the windows and output coupler can be replaced. The output coupler is then adjusted until the reflection of the HeNe beam from the outside surface of the coupler folds back into the HeNe laser itself. In this manner one is assured that the output coupler is perpendicular to the optical axis of the TEA laser cavity.

Final tweaking of the grating may be tedious. The best chance for lasing occurs when the front surface of the grating

is parallel to the back plate of its gimbal mount. When the laser is finally turned on, the grating must be slowly tuned until lasing occurs on some random line. The front mirror can then be tweaked. The calibration of the tuning thumbscrew on the grating can be checked against the CO_2 laser spectrum analyzer. Adjustment of the tuning calibration can be done by temporarily loosening the set screws on the tuning micrometer sleeve, turning the outside thumbscrew to the desired digit while holding the micrometer handles still, then tightening the sleeve set screws.

The calibration of the Optical Engineering CO_2 laser spectrum analyzer can also be checked with a HeNe laser. By shining the HeNe directly into the analyzer, three diffraction orders should be visible on the analyzer screen. The middle spot, the sixteenth order spot, is very nearly coincident with the R(40) 10.6 micron laser line; the calibrated screen can be adjusted accordingly.

I.2 N_2O laser secrets

Much useful information on the operation of the Q-switched N_2O laser was found in Joel Levy's research notebooks. The comments below may also be of use in its operation.

1) The 1.5 cm bore Q-switched CO_2 laser will not lase with N_2O presumably because of the large bore (poor cooling) and long residence time of the gas in the tube.

2) In the N_2O laser, discharge is difficult to sustain with no CO (carbon monoxide) in the mixture. CO turns the discharge blue. The three lead power supply having 100K resistive ballasts in the high voltage leads is necessary to maintain discharge in both arms of the tube.

3) The N_2O laser lases well using CO_2 as a gain medium. Thus CO_2 can be used to align the optics with ease, then replaced with N_2O.

4) Best lasing with N_2O was had with a mixture of N_2O:CO:N_2:He of 1:0.5:1:3.5 Torr, with minimum current necessary to sustain discharge. It was necessary to reduce the total pressure in the tube to below one Torr to ignite the discharge, after which the pressure was increased slowly to an operating pressure of about 6 Torr.

5) Q-switched lasing is impossible in the 1 cm bore tube with a 10 or 20 meter radius mirror. Q-switched lasing was obtained using a flat mirror at one end, and a rotating 20 meter radius mirror and a 4.25 m radius stationary mirror at the other end. The current configuration utilizes a 4.5 meter radius rotating mirror and a plane grating.

6) Maximum repetition rate for the N_2O laser is about 50 Hz. Care must be taken to avoid frequencies close to line current, lest the beat note between the laser repetition frequency and line frequency be detected by sophisticated electronics.

I.3 Boxcar settings for DILDOR

Typical settings of the PAR Model 160 boxcar integrator for DILDOR experiments are as follows (? means does not matter):

Trig mode - EXT	Time base - .1 msec
O.T.D. - ?	S/D - as needed
Slope - negative	Scan rate - 1 min
Threshhold -as needed	DELAY
D.O. - DELAY	Ap. Time - .1 sec, min dial
Repeat - ?	blue TC - ?
Input - 100K	red TC -.1 msec
Prefilter - .005 MHz	Zero - as needed
Coupling - AC	Memory - OFF
In. sens. - 50 mV	In. offset - OFF
rear panel: ext. gate - OUT	

I.4 PDP-8/L to MINC link

Characters can be transfered from the PDP-8/L to the MINC with the cable diagramed in Fig. I-1. This cable plugs into an SLU port on the MINC. To effect transfer, output from the 8/L is transferred to the ARDS by executing an FNEW(5) function. A program such as PDP8IN (listed below) must be running on the MINC. This program accepts any characters typed on the ARDS, line by line, as input and stores them on diskettes. In this fashion a FOCAL program can write data on the ARDS and effect data transfer; FOCAL programs can be transferred with a WRITE ALL command.

With a minor modification to the FOCAL operating system, the PDP-8/L can be used as a paper tape reader for the MINC. In this mode, a tape is not read into 8/L memory, but is merely transfered to the MINC as it is read. The instructions

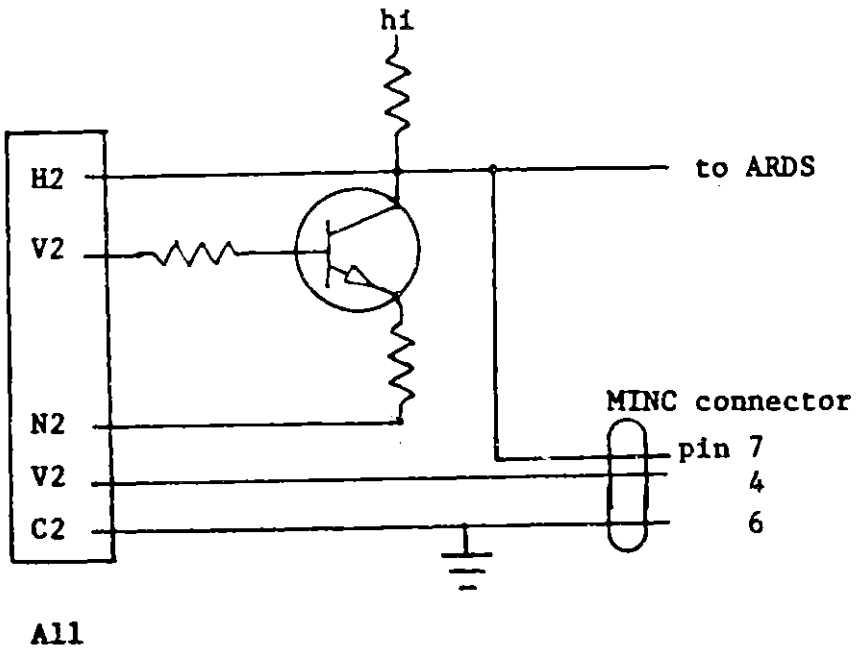

Fig. I-1. PDP-8/L to MINC link. A three conductor ribbon cable was connected to the existing board in the 8/L which is used for communication to the ARDS.

are:

1. Load FOCAL
2. Execute FNEW(5) so that output goes to ARDS
3. RUN PDP8IN on MINC
4. STOP the 8/L
5. Load these two locations with instructions:

location	instruction	
2030	4355	READC = JMS 2155
2031	5230	JMP .-1

6. Place tape in LSR
7. Start 8/L at location 2030
8. Start LSR
9. That's all

When the entire tape is read, stop the LSR. PDP8IN can be stopped with two CTRL/C's.

PDP8IN.BAS

```
1 REM -- stop pgm with ^C^C then type 'CLOSE #1'
4 PRINT "Filename for data"; \ INPUT F$
5 OPEN F$ FOR OUTPUT AS FILE #1
10 CIN('retrieve',S$)
20 IF ASC(SEG$(S$,1,1))=138 THEN S$=SEG$(S$,2,100)
30 PRINT #1,S$ \ GO TO 10
50 OPEN F$ FOR INPUT AS FILE #1
60 FOR I=1 TO 3 \ INPUT #1,S$ \ PRINT S$ \ NEXT I
70 CLOSE #1
100 END
```

I.5 TEA laser pulse counter

A small digital pulse counter was built in 1977. The wiring for this counter is shown in Fig. I-2. Separate switches control power, reset and count direction (up/down).

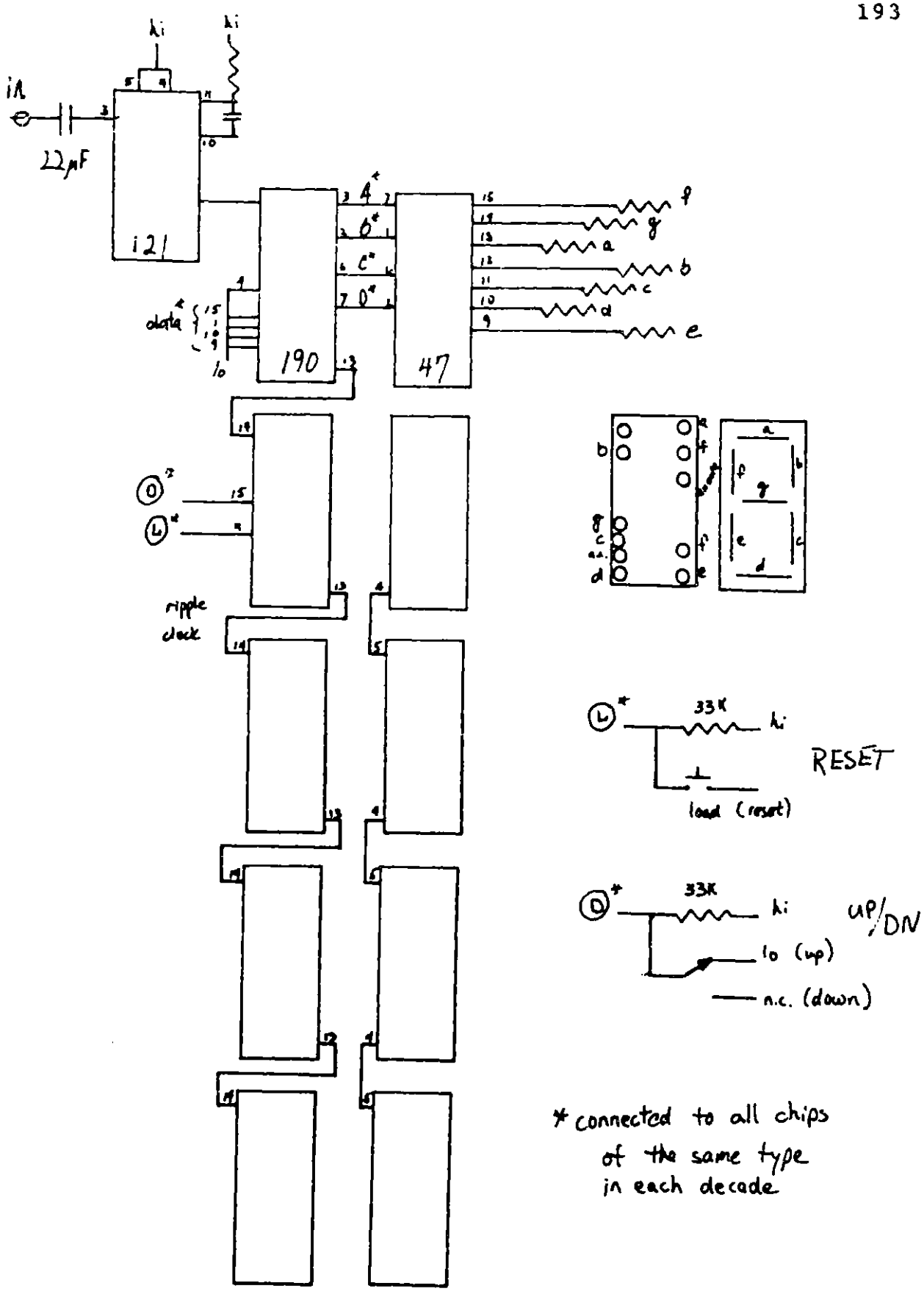

Fig. I-2. Circuit diagram for TAC II pulse counter.

Connection is made by simple BNC cable to the SYNC OUT connector on the TAC II laser, although the counter may work in other applications as well.

APPENDIX J. Laboratory Report: Studies of SiH_4 using CO_2 lasers

In 1978, J. Haggerty and R. Cannon (and coworkers) discovered that sinterable powders of silicon nitride (Si_3N_4) could be produced in an atmospheric pressure flow of silane and ammonia when irradiated with approximately 100 W/cm^2 of c.w. CO_2 laser radiation [1.2]. Many details of the process were unknown, such as the detailed gas phase chemical mechanisms, absorption cross sections as a function of temperature and pressure, the possibility of multiple photon absorption, etc. A collaboration between that Energy Laboratory group and Prof. Steinfeld's group was initiated with the hopes of investigating the possibility of multiple photon heating of silane and silane/ammonia mixtures, and of obtaining accurate values of the absorption coefficients of those gases for the various CO_2 laser frequencies. The absorption coefficients were needed for modeling the energy deposition in the c.w. experiments, and to ascertain which laser line would be most efficient in heating the mixtures. It was hoped that multiple photon induced dissociation of silane would help to unravel the complex gas phase chemical mechanisms by which the powders were formed, but these experiments proved to be disappointing. This Appendix was submitted to Haggerty and Cannon at the conclusion of several months of work, and is contained in their final program report, Reference 1.2.

Experimental

Two types of experiments were performed: low pressure, high intensity irradiation with a pulsed CO_2 laser, and simple measurement of the attenuation of c.w. CO_2 laser lines. In both sets of experiments, silane was used from the tank after many freeze-pump-thaw cycles; NH_3 was treated similarly. Cl_2 used in one experiment was obtained from an ultra high purity lecture bottle.

Typical pulses from the Tachisto Model 215G CO_2 TEA laser contain 0.3J with a FWHM of about 50 ns. Usually 1500 pulses were used for each sample at a rate of 1 Hz. Figure 1 shows the apparatus used for the irradiation; joulemeters (9 and 11 in diagram) allow the percent transmittance of the sample to be measured to $\pm$ 5%. Two lenses were employed to vary the focal geometry of the beam and thereby to control the peak fluences at the focal point of the beam. For an effective focal length for the telescope of 67 cm, the beam radius at the focus is 0.66 mm; with .3J/pulse, the fluence at the focus would be 22 J/cm^2. Similarly, with a focal length of 28 cm, the fluence would be increased to 1.5×10^3 J/cm^2. In this manner the peak fluence could be adjusted from a relatively weak value to the point where dielectric breakdown occured in the sample.

Reagent pressures were read from an MKS 2000A pressure transducer with a 0.1-1000 torr stated range although the head was found to be sensitive to 10^{-2} torr. The response of the transducer was checked against a dibutylphthalate manometer. Mixtures of gases were prepared by successively freezing known quantities of gas into a cold finger in the cell. After irradiation, the products were characterized by their

infrared spectrum, taken on a Perkin-Elmer 567 IR spectrophotometer. A variety of laser lines, sample pressures, and sample mixtures were investigated, as can be seen in Table I1.

Two methods were used to obtain the absorption coefficients of SiH_4 and NH_3, differing slightly in technique as dictated by the availability of equipment. The apparatus in Figure I2a was employed for all but a few data points; it employs two choppers to modulate the sample and reference beams at different frequencies, allowing two lock-ins to detect the sample and reference intensities independently while using the same detector. When only one chopper was available, it was positioned to modulate the two beams at a relative phase of 90°, again allowing independent measurement with one detector.

The laser itself consists of a 1m gain cell with a rotatable grating and a 5 m radius mirror forming the cavity; the beam emerges via a small hole in the mirror, which is mounted on a piezoelectric crystal. The stabilization network depicted in Figure I3 minimizes output intensity drift caused by thermal expansion of the aluminum girder supporting the optical elements. By modulating the mirror position by $\pm$ 0.5 micrometers, the frequency of the cavity resonance is modulated under the CO_2 gain curve. A lock-in detects the slope of the gain curve at the cavity mode frequency by demodulating the very slight ripple in the laser output and applies an error voltage to the pzt to bring the cavity mode to the peak of the gain profile.

Two cells were employed with 1.73 cm and 9.97 cm lengths fitted with perpendicular NaCl windows. When possible, sample pressures of about 130 torr were used; for very strongly attenuated lines, it was necessary to employ lower pressures. Again, the MKS 2000A pressure

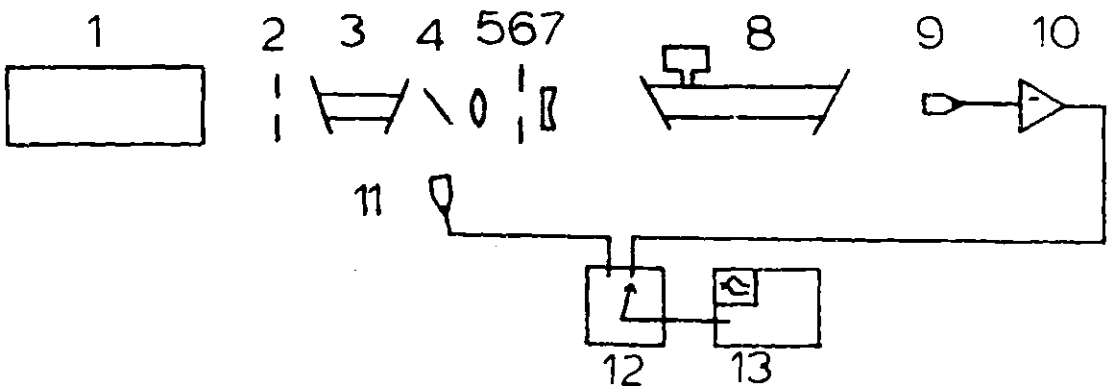

Fig.31. Apparatus for TEA laser experiments. 1, Tachisto Model 215G laser; 2,6 - irises; 3 - attenuation cell; 4 - beamsplitter; 5,7 - telescope lenses; 8 - sample cell with pressure head; 9,11 - joulemeters; 10 - inverting differential amplifier; 12 - signal alternater; 13 - Biomation digital scope.

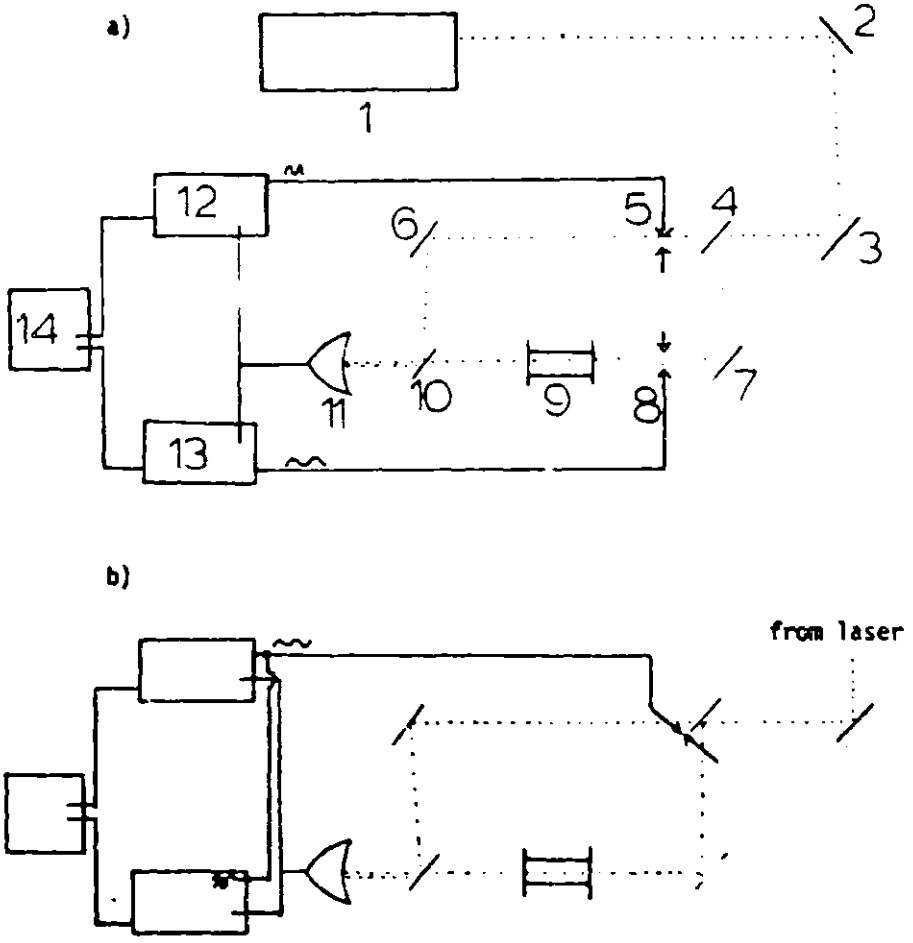

Fig.32. Apparatus for absorption measurements. a) two chopper method. 1 - laser; 2,3,6,7 - mirrors; 4,10 - ZnSe beamsplitters; 5,8 - choppers; 9 - sample cell; 11 - pyroelectric detector; 12 - reference channel lock-in; 13 - sample channel lock-in; 14 - PDP 8/L computer. b) single chopper method; lockin 13 is set to 90° relative phase.

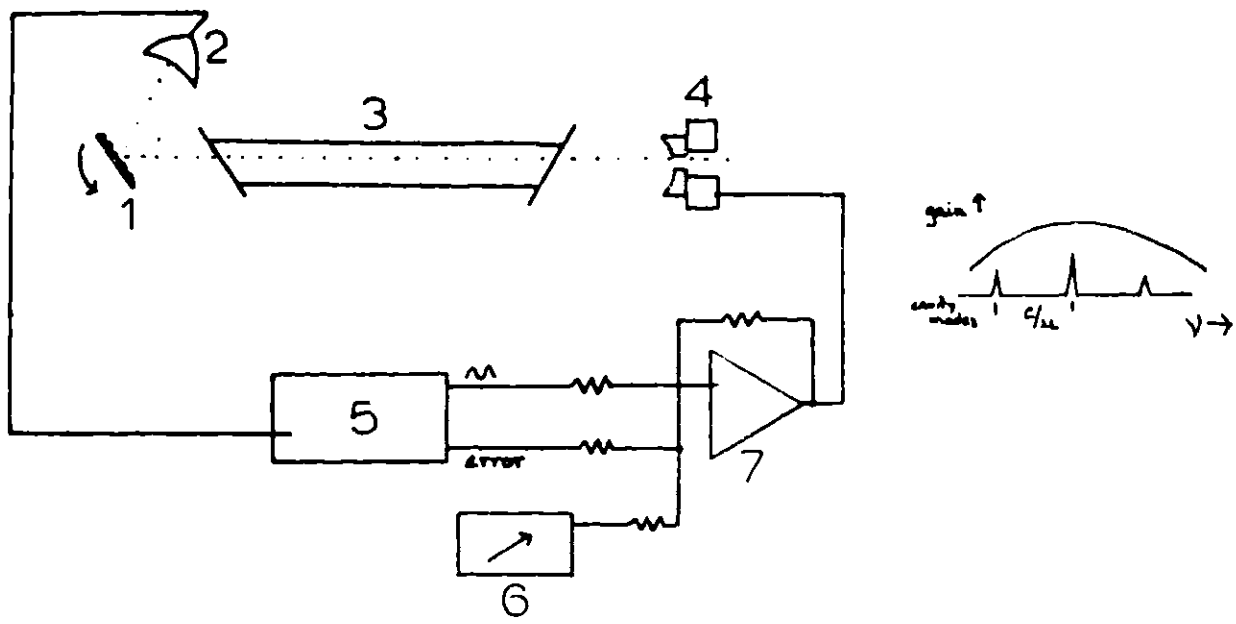

Fig. 3. Stabilized CO_2 laser used in absorption measurements. 1 - rotatable grating; 2 - detector; 3 - 1m gain tube; 4 - pzt mounted mirror; 5 - lock-in; 6 - manual dc offset; 7 - high voltage op amp. Depiction of cavity resonances under a Doppler-broadened gain profile is shown at right.

head was used after calibration against a mercury manometer.

The procedure for measuring the attenuation of a sample is straightforward. The laser was tuned to the desired line, and the stabilization network activated. With the sample frozen into a cold finger in the cell, the ratio of the sample and reference lockins' signals was averaged for approximately one minute (about 400 samples) by a PDP 8/L computer. The sample was then thawed and the ratio again averaged for one minute. The laser was then tuned to the next line, etc. The transmittance, T, is given by

$$T = \frac{I/I_0 \text{ (sample unfrozen)}}{I/I_0 \text{ (sample frozen)}} \qquad (J\text{-}1)$$

where I and I_0 are actually the voltages from the sample and reference lock-ins respectively. Typically the 67% confidence limits of T were $\pm$ 3%. The extinction coefficient α can be calculated from T and the known sample pressure p and cell length ℓ via

$$\alpha = \frac{-1}{p\ell} \ln T \qquad (J\text{-}2)$$

All measurements were taken at room temperature. During the course of a measurement the samples did not absorb enough power to raise the temperature of the cell noticeably.

Results

Table J1 contains a summary of results for the TEA laser experiments. No reaction was noted for conditions which did not produce dielectric breakdown inside the cell, which is evidenced by a blue-white spark. The

breakdown threshhold is sensitive to sample pressure and peak intensity; for silane pressures above 2 torr, breakdown always occurred for fluences of 1.5×10^3 J/cm^2. For fluences below 100 J/cm^2, however, breakdown did not occur for pressures up to approximately 5 torr. For conditions where no breakdown occurred, no incondensible gas (i.e. H_2) was observed in the cell after irradiation and no change in the reagent IR spectrum occurred. One attempt was made to trap any H_2 which may be produced by adding Cl_2; even a mixture of one torr each was sufficient to cause breakdown using the 28 cm focal length optics. Lower pressures in this case would produce quantities of products too small to detect with our apparatus, hence this experiment was abandoned.

Several attempts were made to induce reaction in mixtures of silane and ammonia. These experiments were marked by difficulty similar to the silane-only experiments. For a given pressure of gas a long focal length produced no reaction but a short focal length caused breakdown.

Table 2 exhibits the extinction coefficients α for NH_3 and SiH_4 for laser for laser lines in the 10.6 micrometer CO_2 laser band. Good agreement with the results of Patty et al. (Appl. Opt. 13, 2850 (1974)) is seen for the ammonia absorptions. For very strong attenuations, it was necessary to decrease the sample pressure; values for α are noted in parentheses where the uncertainty in I/I_0 (with sample) exceeded 25%, due to the opacity of the gas at the particular laser line.

Discussion

Failure of the TEA laser experiments is disappointing. Since pyrolysis of silane can be accomplished with long pulses or c.w. radiation at a few tenths of an atmosphere, we know that a dissociation channel is available to sufficiently hot molecules. Apparently for these

Table 1. TEA Laser Experiments Performed on Silane

Silane only: line	p(torr)	lens f.l. (cm)	# of shots	results
P(20)	4.6	80	2000	no change in p or spectrum; no powder
	1.21	28	2200	slight brown powder
	5.4	28	400	heavy powder; p increase; breakdown
	2.2	28	500	light powder; p increase
	2.4	66	1000	no changes
	2.4	28	1500	breakdown on first pulses
P(24)	2.0	28	2200	slight powder, p increase; breakdown
	3.57	28	700	powder, breakdown
	0.54	28	2000	no change
	1:1 torr Cl_2	28	1500	breakdown on first 250 shots
	Silane/ ammonia			
	0.6/1.2	67	2300	no changes
	0.6/1.2	28	1000	no changes
	1.4/3.7	67	1000	no changes
	1.4/3.7	28	1000	breakdown; slight power, p increase

Table12. Absorption coefficients $(atm\text{-}cm)^{-1}$ for the 10.6 μm band of the CO_2 laser. $\alpha = -1/p\ell\ \ell nT$.

	NH_3			SiH_4			
(J)	R		P	R	P		
40			1.0				
38	.044		1.02	1.68	1.05		
36	.01 (not measured)		1.8	.27	18.1		
34	.0072		3.5	(small)	5.01		
32	.0065		13.6	.19	3.79		
30	.047		.87	.96	6.46		
28	.057		.35	2.68	(24.4)	8.94	
26	.059		.42	.70	7.42		
24	.056		.16	.31	(34.5)	10.7	
22	.071		.13	1.36	(28.9)	8.17	
20	.12	.22	.30	1.61	(43.0)	12.9	
18		7.25	.18	.87	11.8		
16	.24		.41	1.14	.96		
14	.47	.50	.83	.79	1.94		
12	21.5		.65	.23	3.95		
10			.16	.34	.50		
8			.35	.007	2.70		
conditions:	E	A B	A E	C	C	D	

A: 136 $\pm$ 2 torr 10 cm cell
B: 130 " 1.7 "
C: 53 $\pm$ 1 " 1.7 " ; $\alpha > 20$ untrustworthy
D: 11 " 1.7 "
E: 25 " 1.7 " single chopper method

conditions, individual silane molecules do not absorb sufficient photons to overcome the dissociation reaction energy barrier. If we assume this barrier is the Si-H bond enthalpy (approx 70 kcal/mole) a molecule must absorb at least 26 photons with λ = 10.6 micrometers before dissociation could occur. Presumably silane molecules absorb on the average for fewer than 26 photons, even at the focal point of the beam.

The possibility of a multiple photon dissociation of silane cannot be precluded, however, for fluences much higher than those used here. To utilize fluences greater than 2×10^3 J/cm^2, sample pressures must be much below a torr. Our methods of analysis require more product than this would afford; typically these experiments are performed with an *in situ* mass spectrometer. Also, production of powder at such low pressure seems implausible.

Agreement between the data of Patty *et al.* and this work is not surprising. Patty and co-workers prepared ammonia samples in parts-per-million concentrations in one atmosphere of air; one would expect a somewhat larger pressure broadening than for these conditions. This pressure broadening causes NH_3 absorption features to overlap the spectral bandwidth of the CO_2 laser employed; greater pressure or laser bandwidth will cause greater absorption. It should be noted that for neither Patty's measurements nor these is the laser bandwidth accurately known, although the lasers are of similar construction.

A dramatic effect on the absorptivities is seen for very strongly attenuated lines for both ammonia and silane: in all cases a decrease in α is observed for a decrease in pressure. Presumably this reflects the broadened nature of the individual absorption features, which are not in exact resonance with the laser lines until pressure broadening causes some spectral overlap between the molecular absorption and laser emission

lineshapes. Since the exact positions of the absorption features, their relative intensities, and pressure-broadening parameters are not known for silane, it would be impossible to calculate the extinction coefficients for this molecule at a given pressure. If these parameters were known, the qualitative behavior of the absorptionties may be predicted for particular laser lines, but a more lucrative approach would be direct measurement of the attenuations at the pressures of interest.

BIOGRAPHICAL NOTE

Chris Reiser was born to Dr. Howard G. and Joanne E. Reiser at 10:17 P.M. on June 1, 1954, whereupon he was heard to say, "It was cooler in heaven." A life of academics was forecast for him at the age of seven, when his teacher at the St. Paul the Apostle Elementary School predicted that his handwriting would never be legible. Forsakin a career as a Latin linguist, he entered the arena of college science at the College of St. Francis in Joliet, IL, before graduating at the top of his class from Joliet Catholic High School in 1972. Shortly after matriculation into Lawrence University in Appleton, WI, he disappeared into Science Hall and is rumored to have lived from vending machine food alone until graduating magna cum laude in honors and in course in 1976 with a B.A. in chemistry-physics. Despite his shortcomings (he was a computer programmer), he was elected to Phi Beta Kappa.

Some say that Reiser's life really began in the fall of 1976 when he entered the Chemistry graduate program at MIT. His liveliness was recognized when he received the Graham S. Arnold Most-living-places-in-shortest-time Traveling Trophy, having had five separate addresses in a three year span. After dissertating under Jeff Steinfeld, he received his Ph.D. in chemical physics in the spring of 1980; his degree did not seem to improve his squash game, quarter-mile race time, or archery score. He maintains that the only academic award he has received is the American Legion Good Citizenship Medal for his outstanding performance as an eighth grader.